Bulletin
of
The Geological Society of America

VOLUME 66 October 1955 NUMBER 10

CONTENTS

Pages

Welded tuffs of Chiricahua National Monument, Arizona. By Harold E. Enlows 1215–1246

Precambrian monazite and zircon from the Mountain Pass rare-earth district, San Bernardino County, California. By Howard W. Jaffe 1247–1256

Experimental deformation of Hasmark dolomite. By John Handin and H. W. Fairbairn 1257–1274

Experimental study of the strength of rocks. By Eugene C. Robertson 1275–1314

Short Notes

Pony-Cherry Creek age relations in southwestern Montana. By Rolland R. Reid 1315–1316

Pony-Cherry Creek age relations in southwestern Montana—a reply. By Robert Scholten 1317–1318

Permian glaciation in northern Mexico? By William E. Humphrey 1319–1324

Use of indicators in the determination of ice-movement directions in Alberta. By C. P. Gravenor and L. A. Bayrock 1325–1328

Subscription $15.00 per year.

Printing Office: Mt. Royal & Guilford Aves., Baltimore 2, Md.

Communications for publications should be addressed to The Geological Society of America, Dr. H. R. Aldrich, Secretary, 419 West 117 Street, New York, N. Y.

Please give notice of change of address 4 weeks in advance. Claims for non-receipt of the Bulletin of a given month must be sent to the Secretary of the Society before the end of the second succeeding month.

Entered as second-class matter at the Post Office at Baltimore, Md., under the Act of Congress of July 16, 1894.
Accepted for mailing at special rate of postage provided for in Section 1103 Act of October 3, 1917, authorized on July 8, 1918.

PAPERS IN PRESS FOR FORTHCOMING ISSUES

Origin of Playa Stone Tracks, Racetrack Playa, Inyo County, California. By George M. Stan

Geology of the Blue Ridge near Harpers Ferry, West Virginia. By Richard P. Nickelsen

Biogeographic and Geologic Indications of Unglaciated Areas in Scandinavia during the Glac Ages. By Eilif Dahl

Geophysical Investigations in the Emerged and Submerged Atlantic Coastal Plain. Part Continental Slope and Continental Rise South of the Grand Banks. By Charles Bent and J. Lamar Worzel

Zones of Regional Metamorphism in the Precambrian of Northern Michigan. By Harold James

Directional-Current Structures from the Prealpine Flysch, Switzerland. By John C. Crowe

Sequence of Alluviation along the Loup Rivers, Valley County Area, Nebraska. By Robert Miller and Glenn R. Scott

Delta-Front Valleys Bordering the Mississippi Distributaries. By Francis P. Shepard

Uranium-Lead Method of Age Determination. Part I: Lake Athabasca Problem. By W. R. Ech mann and J. L. Kulp

Stratigraphic Sequence in the Eagle Rock Volcanic Area near American Falls, Idaho. By Har T. Stearns and Andrei Isotoff

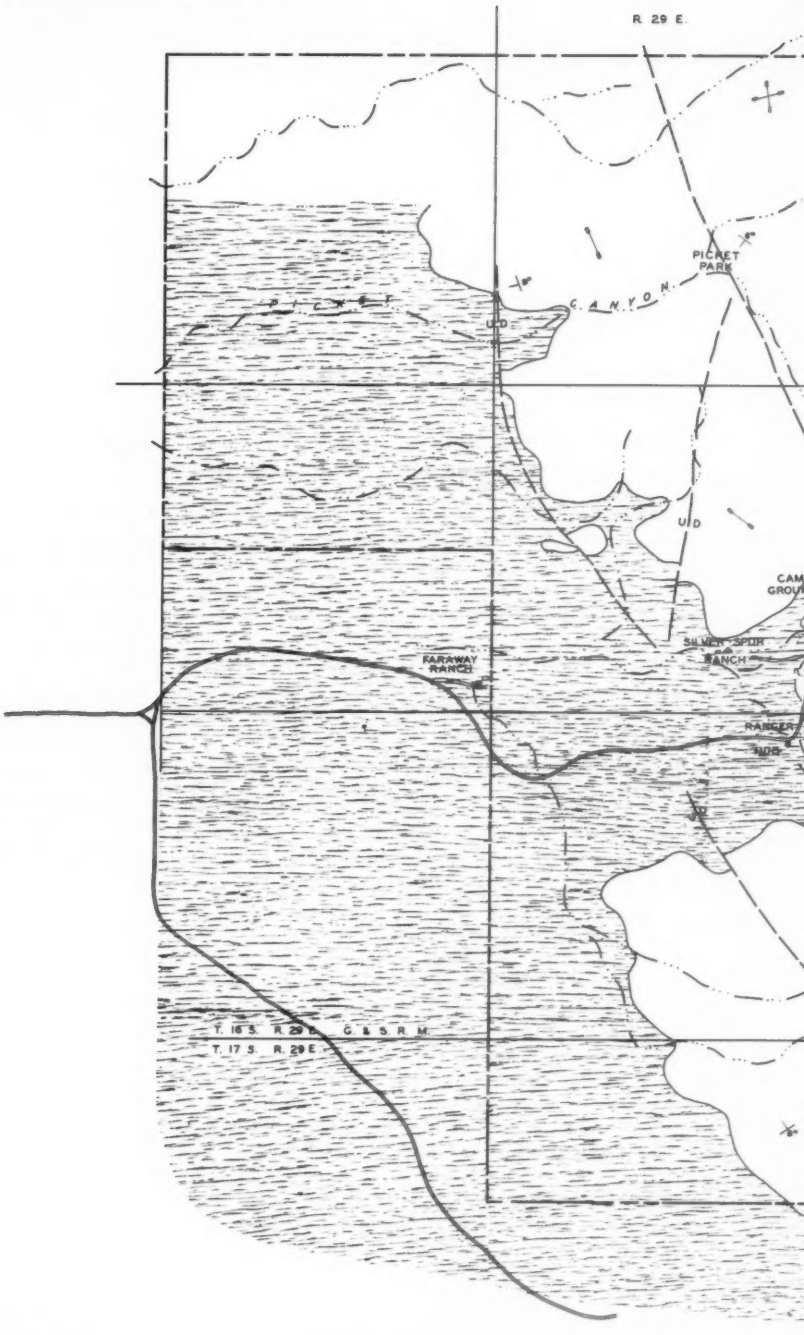
R. 29 E.
PICKET
CANYON
PICKET PARK
UCD
UCD
FARAWAY RANCH
SILVER SPUR RANCH
RANGER
T. 16 S. R. 29 E. G & S R M.
T. 17 S. R. 29 E.

GEOLOGIC MA

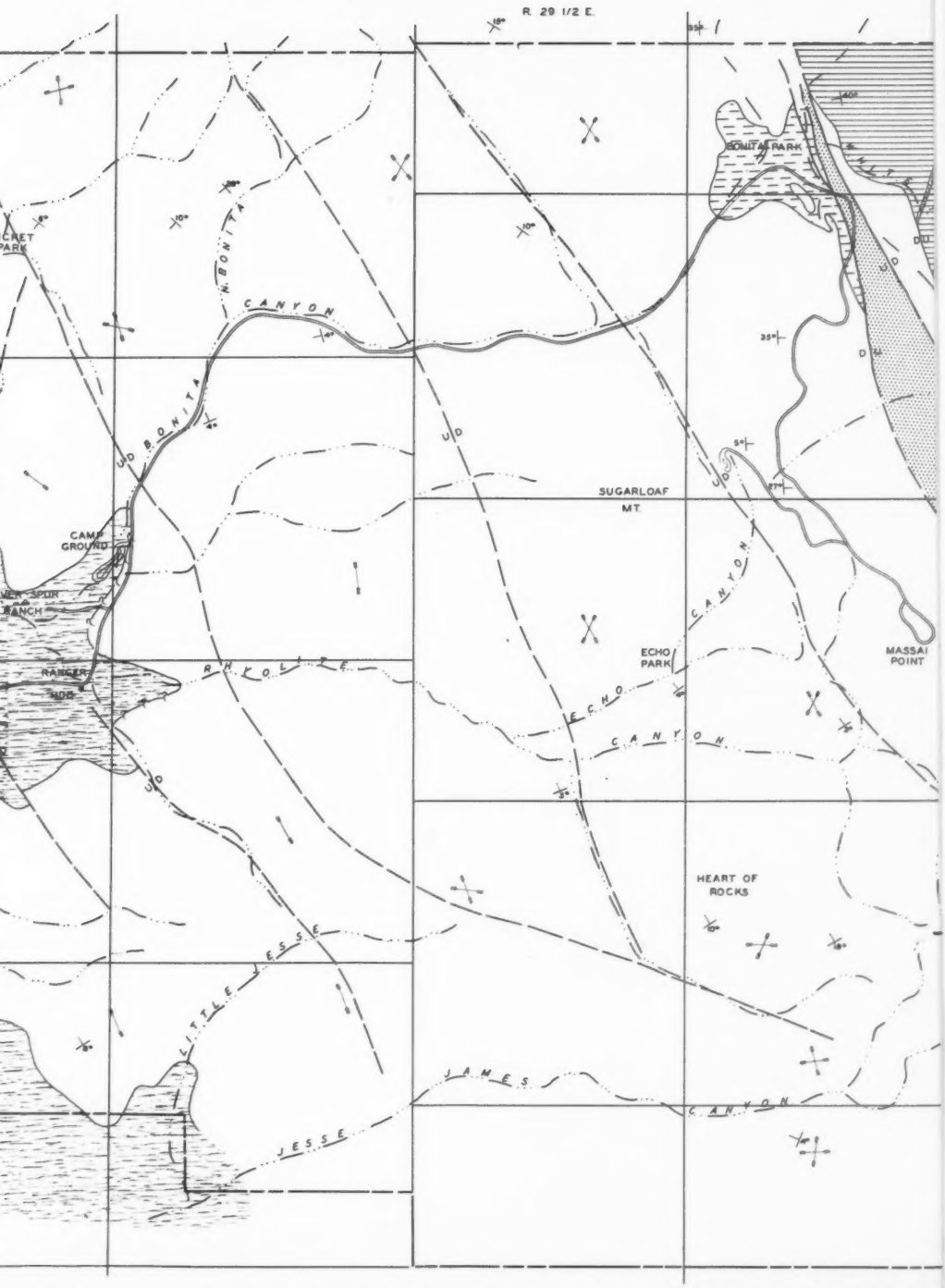

OGIC MAP OF CHIRICAHUA NATIONAL MONUMENT, ARIZONA

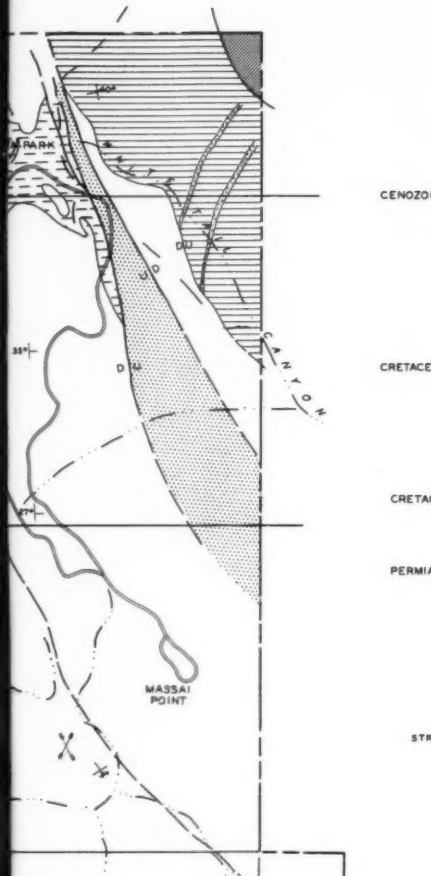

EXPLANATION

CENOZOIC	RHYOLITE CANYON FORMATION
	FARAWAY RANCH FORMATION
	BONITA PARK FORMATION
CRETACEOUS ?	BASALT
	RHYOLITE PORPHYRY
CRETACEOUS	BISBEE GROUP
PERMIAN	CHIRICAHUA LIMESTONE

FAULT

D

DOWNDROPPED SIDE OF FAULT

STRIKE AND DIP OF BEDDING OR EUTAXITIC STRUCTURE

STRIKE OF VERTICAL JOINTS

GEOLOGY BY HAROLD E. ENLOWS

1953

SCALE

0 1/4 1/2

IN MILES

T, ARIZONA

BULLETIN OF THE GEOLOGICAL SOCIETY OF AMERICA
VOL. 66, PP. 1215-1246, 6 FIGS., 5 PLS. OCTOBER 1955

WELDED TUFFS OF CHIRICAHUA NATIONAL MONUMENT, ARIZONA

BY HAROLD E. ENLOWS

ABSTRACT

Chiricahua National Monument, Arizona, and much of the western part of the Chiricahua Mountains contain extensive bedded rhyolite deposits of Cenozoic age heretofore termed flows. Most of these volcanic rocks, however, are more correctly classified as welded rhyolite tuff or ignimbrite, the result of many eruptions of *nuées ardentes*. These deposits are characterized by vertical gradation from a coherent, nonporous base exhibiting prominent eutaxitic structure to a less coherent, porous top. By following vertical joints of tectonic origin and the eutaxitic structure developed by flattening and aligning of blocks of pumice in the deposit, weathering has developed spectacular columns and balanced rocks.

Study of the petrography, structure, conditions of deposition, and origin of this unusually thick section of rock permits an evaluation of features which have been termed characteristic of welded tuffs, and facilitates identification of this important rock type.

CONTENTS

TEXT

	Page
Introduction	1216
Geography	1216
Topography	1216
Sedimentary rocks	1216
Igneous rocks	1217
Structure	1218
Acknowledgments	1218
Petrography of Rhyolite Canyon formation	1218
General features	1218
Member 1	1221
Member 2	1222
Member 3	1224
Member 4	1225
General description	1225
Upper ashy phase	1225
Basal firmly welded phase	1227
Member 5	1228
Member 6	1229
General description	1229
Upper ashy phase	1229
Basal firmly welded phase	1229
Unusual features	1230
Chemical composition and classification	1232
Member 7	1234
Member 8	1234
Member 9	1235
General description	1235
Constituents	1235
Origin	1236
Structure of Rhyolite Canyon formation	1237
Attitude of the beds	1237
Faults	1237
Joints	1237
Origin	1239
Source of material	1242
Summary	1242
Analyses of characteristic features of the welded-tuff variety of *nuées ardentes* deposits	1243
References cited	1245

ILLUSTRATIONS

Figure	Page
1. Index map showing the location of Chiricahua National Monument	1219
2. Graph showing the variation of density with depth in members 2 and 8	1220
3. Graph showing the variation of porosity with depth in members 2 and 8	1220
4. Application of a northwest–southeast shear diagram to faults and joints in the Rhyolite Canyon formation	1238
5. Cross section of a typical deposit of *nuée ardente* origin	1240
6. Section through Chiricahua National Monument from the northeast corner to Bonita Canyon near Ranger Headquarters	1241

Plate	Facing page
1. Geologic map of Chiricahua National Monument	1215

	Following page
2. Welded tuffs, Chiricahua National Monument	1222
3. Characteristic outcrops of welded-tuff members	
4. Photomicrographs of welded tuffs	
5. Photomicrographs of welded tuffs	

TABLES

Table	Page
1. Summary of exposed rock formations in Chiricahua National Monument	1216
2. Sequence of volcanic rocks at Chiricahua National Monument	1221
3. Chemical analyses and calculated norms for two samples of member 6	1233
4. Chemical analysis and calculated norm for member 9	1236

Introduction

Geography

The Chiricahua Mountains lie in Cochise County in the southeastern part of Arizona. They strike about N. 15° W., and are 40 miles long and 20 miles wide at their broadest part. They extend from 109°05′ to 109°30′ N. Lat., and from 31°35′ to 32°10′ W. Long. Two peaks in the range rise above 9000 feet, while many exceed heights of 8000 feet. The mountains are flanked by the San Simon Valley to the east and the Sulphur Springs Valley on the west.

Chiricahua National Monument lies in the northwest portion of the Chiricahua Mountains, and consists of 10,964 acres in Ts. 16 and 17S., Rs. 29, 29½, and 30 E. It is best reached by following state highway 181 northeastward from U. S. 666, 8 miles east of Pearce, Arizona.

Topography

Chiricahua National Monument is dominated by a conical peak named Sugarloaf Mountain located in its east central portion. High ridges trending N. 20° W. and S. 20° E. from this peak form the backbone of the Chiricahua Range in this area. Drainage from the eastern slope of these ridges is largely diverted into Whitetail Canyon which runs about S. 50° E. from its point of origin 1½ miles northeast of the top of Sugarloaf Mountain. Two westerly trending canyons, Bonita to the north and Rhyolite to the south of Sugarloaf, drain most of the Monument area, coalescing to form the broad, flat valley in the west-central part of the Monument.

Table 1.—Summary of Exposed Rock Formations in Chiricahua National Monument

Age	Formation	Thickness (feet)	Description
	Rhyolite Canyon formation	1897	Rhyolite welded tuff with minor ash-shower tuffs and a capping flow of rhyodacite
	Unconformity		
Cenozoic	Faraway Ranch formation	800+	Rhyolite tuff and breccia, basalt breccia, and dacite flows
	Unconformity		
	Bonita Park formation	300+	Red beds and some associated rhyolite tuff
	Unconformity (?)		
Lower Cretaceous (?)	Basalts and rhyolite porphyry		Basalts, apparently flows and perhaps a portion of the upper part of the Bisbee group or Outlaw formation, now found in a fault block; thin rhyolite porphyry dikes intruding the Bisbee group
Lower Cretaceous	Bisbee group	2500±	A basal conglomerate with limestone boulders followed by maroon to green sandstones and grits
	Unconformity		
Lower Permian	Chiricahua limestone	600±	A basal quartzite followed by light-gray limestone

Sedimentary Rocks

The oldest rocks exposed in Chiricahua National Monument crop out in the extreme northeastern corner. The prominent quartzite mentioned by Stoyanow (1926, p. 318–319) lies at the base of the Permian Chiricahua limestone. Above the quartzite is the carbonate section of the Chiricahua limestone, succeeded first by a thick section of the Lower Cretaceous Bisbee group with recognizable Glance conglomerate at the base, and in turn by a section of what appears to be the Morita formation. This sequence of Lower Cretaceous rocks is

apparently similar to G. T. Raydon's Outlaw formation (1953, M. S. thesis, Univ. of Calif., p. 79) described from the area east of Paradise. Above the Bisbee group lies a sequence of red beds associated with tuff which Maxwell (1941, unpublished report, Natl. Park Service, Region III, p. 9) terms lake beds of Cenozoic age. Waller (1952, M. S. thesis, Univ. of Tulsa, p. 17–44) has described these in detail, and terms them the Bonita Park formation. The Bonita Park formation may possibly be equivalent to some of the volcanic sediments of Raydon's (1953, M. S. thesis, Univ. of Calif., p. 91) Blacktail formation, although his descriptions suggest little lithologic similarity. Lying upon the Bonita Park formation, and probably in part contemporaneous with it, is a series of volcanic rocks.

Igneous Rocks

A badly faulted, basaltic mass is in contact with the Bisbee group, the Bonita Park formation, and the volcanic rocks. Maxwell (1941, unpublished report, Natl. Park Service, Region III, p. 17) terms this an intrusion; but Waller (1952, M. S. thesis, Univ. of Tulsa, p. 55) considers it a fault block of flow basalt, probably older than the Bonita Park formation and younger than the Bisbee group. It seems reasonable to identify this basalt with the basic rocks forming the upper part of Raydon's (1953, M. S. thesis, Univ. of Calif., p. 86) Outlaw formation, which would place it in the Lower Cretaceous. Lasky (1938, p. 11) describes 2000 feet of augite basalt flows of Comanchean age in the Lordsburg mining district a few miles east of the Chiricahua Mountains.

The Bisbee group has been intruded by at least two dikes of acid igneous rock, consisting of a very-light-gray, porphyritic material termed syenite by Maxwell (1941, unpublished report, Natl. Park Service, Region III, p. 18). Petrographic analysis shows an abundance of quartz, both in the aphanitic groundmass and as phenocrysts, and suggests classification as rhyolite porphyries.

Most of Chiricahua National Monument is underlain by a thick sequence of volcanic rocks separated into two major subdivisions by an angular unconformity. Differences in the attitudes of the beds and in lithology readily distinguish these two major subdivisions. The lowermost group is termed the Faraway Ranch formation from prominent outcrops near that ranch on lower Bonita Canyon (Enlows, 1951, p. 106). This formation consists of at least 800 feet of coarse rhyolite tuff and breccia, basalt breccia, and flows of biotite dacite. It rests upon the Bonita Park formation in the Hands Pass region just east of the Monument. This group of volcanic rocks is probably a correlative of the thick section of andesitic and dacitic lavas, breccias, and tuffs studied by Raydon (1953, M. S. thesis, Univ. of Calif., p. 91) in the Portal area, which he has named the Blacktail formation. No evidence leading to precise dating of these rocks has been found in the Chiricahua Mountains, but their stratigraphic position indicates an Upper Cretaceous or Cenozoic age. Lavas, breccias, and tuffs of rhyolite, andesite, and quartz latite in the Lordsburg mining district are thought by Lasky (1938, p. 16–17) to have covered a wide area and to be of Miocene (?) age. A tentative age of Cenozoic is given to these rocks.

The Faraway Ranch formation is unconformably overlain by a series of gently dipping, stratified, volcanic rocks some 1900 feet thick. Well-developed vertical joints and a eutaxitic or pseudo-bedded structure formed by flattened, porous inclusions have served as channels for weathering agents, leading to the development of pinnacles, balanced rocks, and other weirdly sculptured masses for which the Monument is famous. Within the Monument this rock sequence is best exposed in Rhyolite Canyon, and hence is named the Rhyolite Canyon formation (Enlows, 1951, p. 106). It can be traced southward into the main portion of the Chiricahua Mountains, and apparently crops out all along the central and western part of the range, extending eastward into the Portal area. Raydon (1953, M. S. thesis, Univ. of Calif., p. 95) has named 4500 feet of rhyolitic tuffs and welded tuffs which cap the section in the Cave Creek area the Cave Creek formation, and states that they are probably correlative with those of Chiricahua National Monument. These rocks are also probably related to the Miocene volcanic rocks described by Lasky

(1938, p. 16) from the Lordsburg and Santa Rita districts and the Little Hatchet Mountains of southwestern New Mexico. The Rhyolite Canyon formation in Chiricahua National Monument is composed chiefly of rhyolite masses (which prior to this report have been generally referred to as flows) interstratified with beds of incoherent tuff.

Structure

The stratified rocks of the Monument dip westward, forming a monoclinal block. The sedimentary beds in the northeast corner dip 25°–40° in a S. 40°–75° W. direction, a much steeper dip than that of the overlying volcanic rocks. The welded tuffs dip northwest or southwest at gentle angles, forming a broad syncline plunging toward the west at 3°–4°.

Anomalous dips are noted in the Faraway Ranch formation. The coarse tuffs and breccia appear to dip S. or SE. 20°–40°; but dips to the southwest and north were noted, varying widely over short distances. Too little information is available on the Faraway Ranch formation to warrant a structural analysis.

The stratified volcanic and sedimentary rocks dip 30°–40° E. along the fault zone parallel to Whitetail Canyon. One quarter mile west of this the normal westerly dip is again established, which may indicate that drag along the fault zone caused these unusual dips.

The rocks of the Monument are cut by a number of faults striking generally S. 30° W. The fault planes appear to be almost vertical, and the northeastern block is generally downthrown. The most prominent faulting, however, is in an elongate zone parallel to upper Bonita and Whitetail Canyons striking S. 20°–30° E. The welded tuffs, the underlying Bonita Park formation, and the basalt mass are all badly broken and exhibit abundant slickensides along this zone. One large block of welded tuff has been downdropped and lies as a graben bordered by basalt and rocks of the Bisbee group. Although details of the movement of the fault blocks are obscured by talus, valley detritus, and a multiplicity of faults, the topographically high position of the stratigraphically low sedimentary beds indicates that the block east of the fault zone, now composed principally of the sedimentary rocks, has been upthrown with respect to the block west of the fault zone, now composed principally of welded tuff.

Acknowledgments

Superintendents Frank Fish and Clair Cooke of Chiricahua National Monument placed their equipment and staff at my disposal. Naturalists Natt Dodge and Leslie Arnberger were of great assistance in procuring aerial photographs and maps, and in obtaining chemical analyses of Chiricahua rocks from the U. S. Geological Survey. Mrs. Margaret Patty of the staff of McFarlin Library went far beyond the mere performance of her duty in obtaining reference books, and Mr. G. T. Raydon very generously made available the manuscript of his unpublished paper on the geology of the northeastern Chiricahua Mountains.

Petrography of Rhyolite Canyon Formation

General Features

With the exception of the uppermost member, which caps Sugarloaf Mountain and which has been classified as a rhyodacite, all members of the Rhyolite Canyon formation are rhyolites.

The beds of very-light-gray or pinkish-gray tuff[1] turn yellowish gray or light brown upon exposure. They are porphyritic, containing phenocrysts of quartz and sanidine in a groundmass of loosely packed glass shards and fragmental pumice, quartz, sanidine, and magnetite. The tuff commonly grades into a coherent, well-cemented, rhyolitic mass that rings under the hammer.

Most of the Rhyolite Canyon formation comprises beds of tough, compact rhyolite, heretofore referred to as flows. They are pale brown to pinkish gray, darkening to pale brown or grayish red on exposure. All are porphyritic containing phenocrysts of quartz and sanidine in a grayish-pink to grayish-red, aphanitic groundmass. Light-gray inclusions of porous pumice are common, and toward the base of a

[1] Color designations used in this paper are those of the Rock-Color Chart prepared by the National Research Council.

bed they become flattened and lenticular. A eutaxitic or pseudo-bedded structure is formed by these many porous, discontinuous lenses included in the grayish-red, aphanitic groundmass, with the plane of maximum flattening of the inclusions parallel to the base of the formation. Prominent vertical joints follow a rectangular pattern in all of these beds.

The tough, compact beds of rhyolite are separated by intervening beds of incoherent tuff. The contact between the hard rhyolite and the overlying tuff is gradational, while the contact at the base of the hard rhyolite is very sharp. Several units of the hard rhyolite are noted, ranging in thickness from 1 to 800 feet.

The tuff grading into the underlying, dense, compact rhyolite forms a familiar unit which has been termed a welded tuff or ignimbrite. In the Chiricahua area there have been several eruptions of hot ash, each giving rise to a separate layer of welded tuff. These layers are of varying thickness, but each grades through a lithologic sequence, as follows:

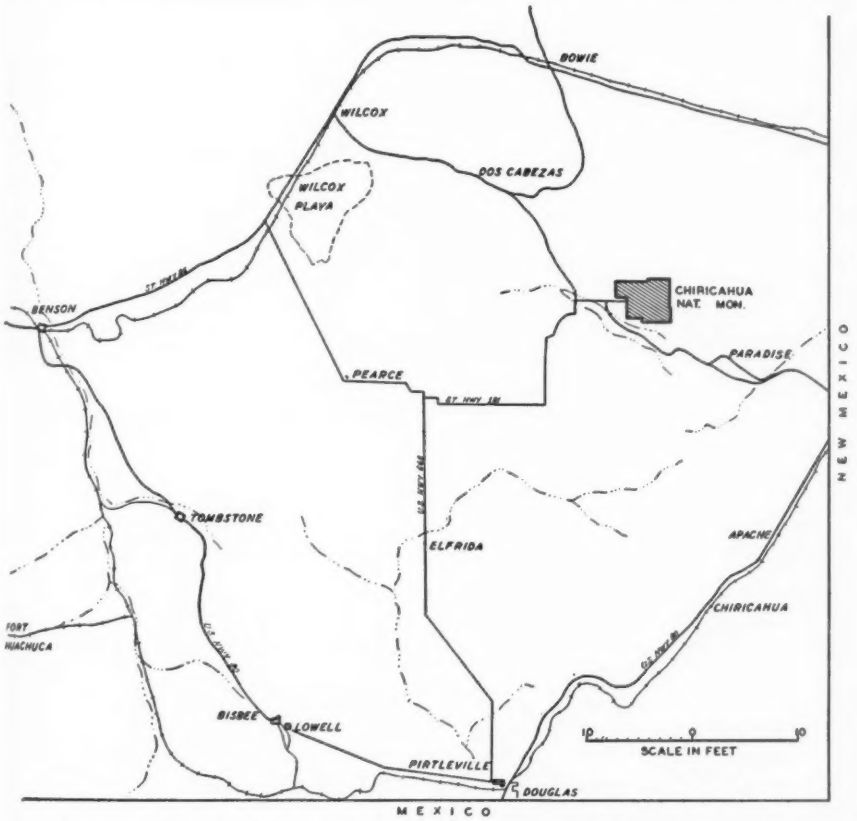

FIGURE 1.—INDEX MAP SHOWING THE LOCATION OF CHIRICAHUA NATIONAL MONUMENT

Soft, poorly welded, porous, very-light-gray tuff, low in phenocrysts and magnetite, with a uniform structure and composed of glass fragments which are extensively devitrified; very few inclusions of lapilli size;

Grades downward into hard, thoroughly welded, pale-brown tuff, low in porosity, with much of the glass still vitreous, and an increasing number of phenocrysts; many flattened inclusions of lapilli and bomb size give a eutaxitic structure to the rock, while flattening and aligning of the finer fragments develop a microscopic eutaxitic structure.

Two welded-tuff units were chosen as rep-

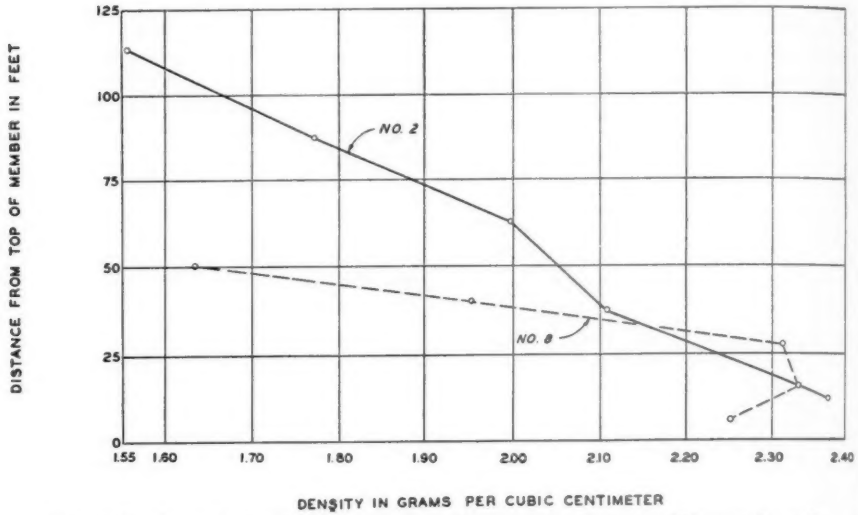

FIGURE 2.—GRAPH SHOWING THE VARIATION OF DENSITY WITH DEPTH IN MEMBERS 2 AND 8

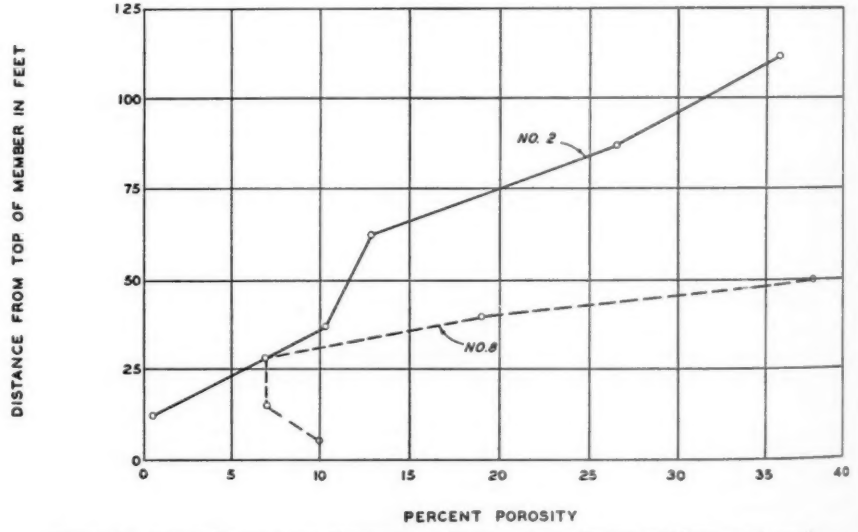

FIGURE 3.—GRAPH SHOWING THE VARIATION OF POROSITY WITH DEPTH IN MEMBERS 2 AND 8

resentative of this type of sequence and were sampled at regular intervals from top to bottom. Both porosity and density were determined for these samples. (*See* Figs. 2, 3.)

The gradation in porosity and density in member 2 is as would be expected with increasing overburden. The abnormal results obtained in the two lowest samples of member 8 may be due to fractures, pores opened by weathering, or to original inequalities in porosity. Chilling, as postulated by Marshall (1935, p. 339), might account for the increased porosity at the base.

Density measurements were made on the

thicker members of the Rhyolite Canyon formation, but not in the systematic fashion in which members 2 and 8 were studied. A general pattern was noted in all cases, however. Density increased uniformly downward until values near 2.3 were reached, at which point no further increase was noted. In these thicker members the maximum value for density was reached at depths of 25–100 feet from the top. Rocks collected near the base of member 6, under 880 feet of overburden, show densities between 2.29 and 2.33. No uniform tendency for a decrease of density at the very base of the members was observed.

TABLE 2.—SEQUENCE OF VOLCANIC ROCKS AT CHIRICAHUA NATIONAL MONUMENT

Formation	Member	Thickness (feet)	Field Description
	9. Rhyodacite	220	Black to medium dark gray, vesicular, probably a flow
	8. Welded rhyolite tuff	50	Soft light-gray tuff at top, grading down into pale-brown, coherent, brittle rock, cliff-forming at times
	7. Rhyolite tuff	10	Fairly coherent, light-gray tuff probably owing to an ash shower or small *nuée ardente*
	minor unconformity		
	6. Welded rhyolite tuff	880	Rather incoherent light-gray tuff, in places showing bedding, grading down into poorly welded light-gray tuff which grades down into coherent, brittle, light-brownish-gray, vertically jointed rock exhibiting well-developed eutaxitic structure; the principal scenic rhyolite of the Monument
Rhyolite Canyon	5. Welded rhyolite tuff	2½	Dark, glassy rhyolite grading up into soft gray tuff
	4. Welded rhyolite tuff	275–0	Top of soft light-gray tuff containing seams of strongly welded, grayish-red rhyolite and a bed of accretionary lapilli; grades down into coherent, brittle, pinkish-gray rhyolite with strong vertical joints
	3. Welded rhyolite tuff	190–0	Firmly welded, dusky-red rhyolite with many prominent inclusions; Grades abruptly into overlying member 4
	2. Welded rhyolite tuff	270–0	Soft, light-gray top grading into grayish-red, brittle rhyolite showing few inclusions and no pronounced vertical joints
	minor unconformity		
	1. Welded rhyolite tuff	30	Brittle, dark gray, very firmly welded, weathers to a loose granular mass
	major unconformity		
Faraway Ranch	Rhyolite tuff	20–0	Soft, gray to pink ash-shower tuff
	Lapilli tuff	200±	Crudely bedded, coarse, appears rhyolitic, probably of ash-shower origin
	Basalt breccia	175±	Very coarse, boulders up to 12 inches in diameter
	Biotite dacite	400+	Grayish-red to brownish flows, some exhibiting pahoehoe structure

Member 1

This is a homogeneous, dark-gray rock exhibiting laths of sanidine and grains of quartz up to 2 mm in diameter included in a glassy groundmass. The rock is brittle, and when broken develops conchoidal fractures. Weathering produces a granular mass of loosely cemented phenocrysts and glass granules.

Member 1 is found only in Picket Canyon below Picket Park and to the north of this toward West Whitetail Canyon. It rests upon the tilted and eroded surface of the lapilli tuff of the Faraway Ranch formation, and is overlain by the very thick member 6 of the Rhyolite Canyon formation.

Although the eutaxitic structure in members 1 and 6 is parallel, their contact is rough and might well be an erosion surface. The vesicular base of member 6 might indicate rapid cooling at a contact with cool basement rocks. Since the gradational or conformable contacts of members 2, 3, 4, 5, and 6 indicate continuous depositions member 1 must have preceded these other members. Because member 1 is undoubtedly a welded tuff and lies with angular unconformity on the Faraway Ranch formation, it is included in the Rhyolite Canyon formation.

Phenocrysts and occasional cindery inclusions make up 10–15 per cent of the rock, the phenocrysts consisting of about equal numbers of sanidine and quartz grains, occasional magnetite grains, and very occasional hornblende grains. The mineral and angular rock fragments are all included in a brownish-black, vitroclastic groundmass which exhibits unusually good microscopic eutaxitic structure. Not only have the glass fragments been molded about the phenocrysts and rock fragments, but they have also shown complete accommodation in the adjustment of one fragment to the other, with the result that all have been flattened and pore spaces almost completely eliminated. No devitrification is noted in the glassy matrix. The quartz and feldspar phenocrysts have corroded and embayed borders.

The rock fragments or inclusions in the glassy matrix are pale brown and exhibit phenocrysts of quartz and plagioclase in a glassy groundmass which does not show the microscopic eutaxitic structure of the typical welded tuff.

No chemical analysis of the rock was run, but the silica content can be judged approximately from the index of refraction of the glass. The measured index of refraction of 1.496, when fitted to the curve developed by George (1924, p. 365) to show the relation of the index of refraction to the silica content in natural glasses, indicates approximately 73 per cent silica. This index is very close to the value of 1.492 quoted by George for the average index of refraction for obsidian or rhyolite glass. The presence of about equal amounts of quartz and feldspar phenocrysts, according to Vogt (1921, p. 346), indicates an especially acid porphyry with more than 75 per cent silica.

Member 2

Except in the Picket Canyon outcrop where it is missing, member 2 forms the base of the Rhyolite Canyon formation and rests with angular unconformity upon the Faraway Ranch formation. Member 2 is 130 feet thick in lower Rhyolite Canyon just above Ranger Headquarters and 100 feet thick above the Silver Spur Ranch, but reaches its maximum thickness of 270 feet in the section at the mouth of Little Jesse James Canyon. The upper 30 feet of the member consists of porous, poorly consolidated tuff containing an unusually high proportion of fragments of lapilli size; the next 20 feet is transitional; and the basal portion is firmly welded. This member is a typical welded-tuff unit in that it shows gradation from a loosely cohering, porous, ashy top downward into a firmly welded rock mass of low porosity which rings under the hammer. It is atypical in that it exhibits two anomalous textural features. The incoherent upper portion is just as vitreous as the basal, more firmly welded part, and it contains a higher proportion of inclusions than does the firmly welded base.

The upper portion of this member is very light gray, but changes to a pinkish gray or light brownish gray downward. It has a very porous, aphanitic groundmass which contains occasional quartz and sanidine phenocrysts and a great many inclusions of pumice lapilli, some as large as 2 cm in diameter. The lapilli inclu-

PLATE 2.—WELDED TUFFS, CHIRICAHUA NATIONAL MONUMENT

FIGURE 1.—LOOKING EASTWARD UP BONITA CANYON FROM FARAWAY RANCH (Nat. Park Ser. Photo)

FIGURE 2.—LOOKING NORTHEASTWARD FROM THE HEART OF ROCKS AREA (Nat. Park Ser. Photo)

PLATE 3.—CHARACTERISTIC OUTCROPS OF WELDED-TUFF MEMBERS

FIGURE 1.—VIEW IN RHYOLITE CANYON SHOWING MEMBERS 4 TO 6, RHYOLITE CANYON FORMATION

FIGURE 2.—WEATHERING FOLLOWING THE EUTAXITIC STRUCTURE

FIGURE 3.—VERTICAL JOINTS IN MEMBER 6, RHYOLITE CANYON FORMATION

FIGURE 4.—WEATHERING FOLLOWING VERTICAL JOINTS AND EUTAXITIC STRUCTURE TO FORM A ROCK PINNACLE (Nat. Park Ser. Photo)

FIGURE 1

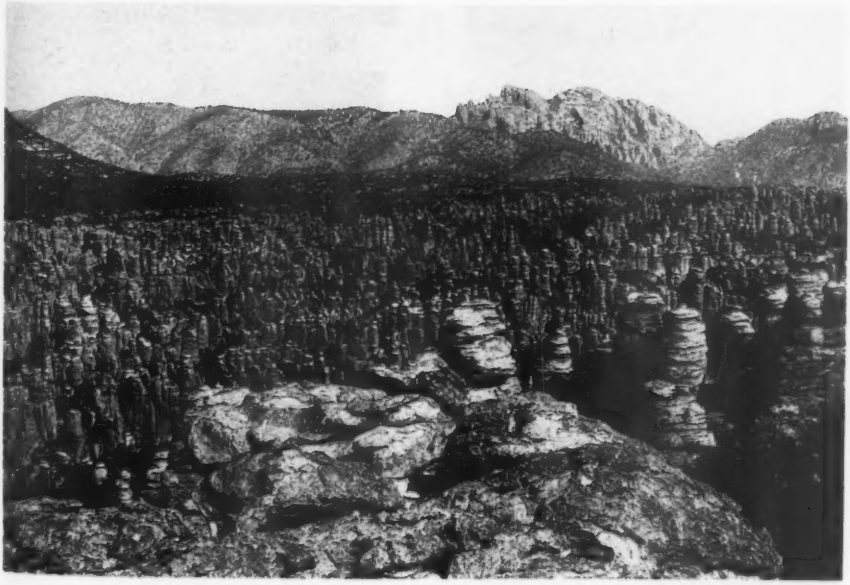

FIGURE 2

WELDED TUFFS, CHIRICAHUA NATIONAL MONUMENT

FIGURE 1

FIGURE 2

FIGURE 3

FIGURE 4

CHARACTERISTIC OUTCROPS OF WELDED-TUFF MEMBERS

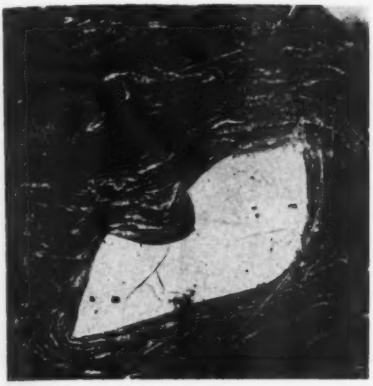

FIGURE 1

FIGURE 2

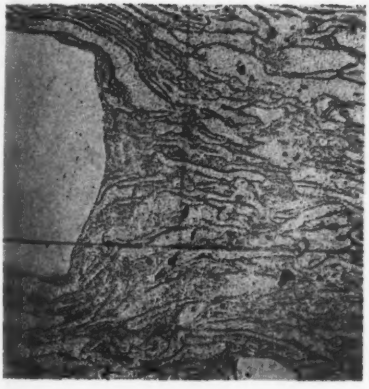

FIGURE 3

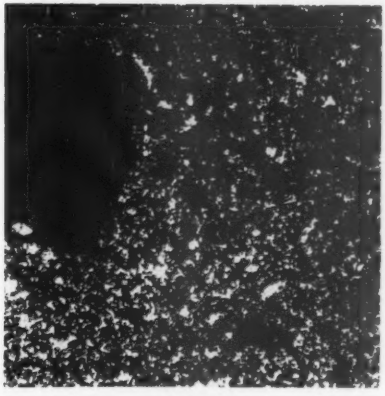

FIGURE 4

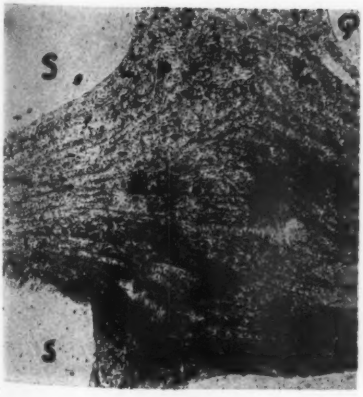

FIGURE 5

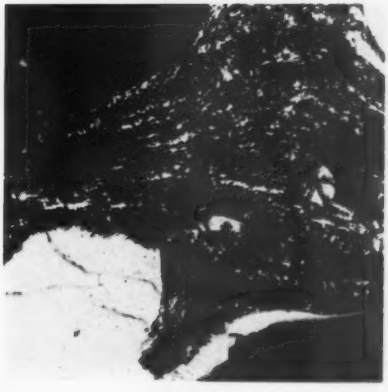

FIGURE 6

PHOTOMICROGRAPHS OF WELDED TUFFS

FIGURE 1

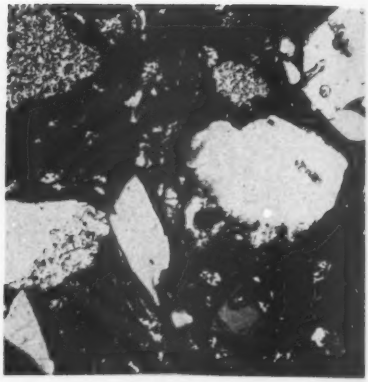

FIGURE 2

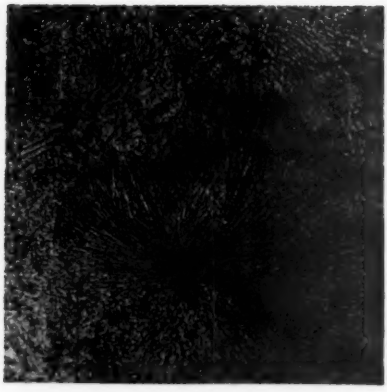

FIGURE 3

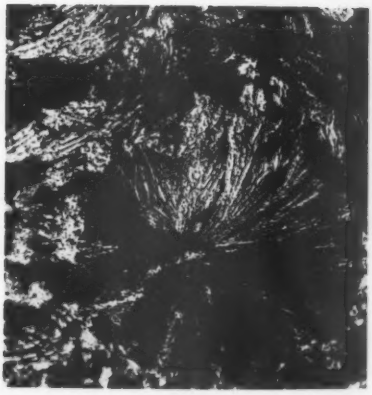

FIGURE 4

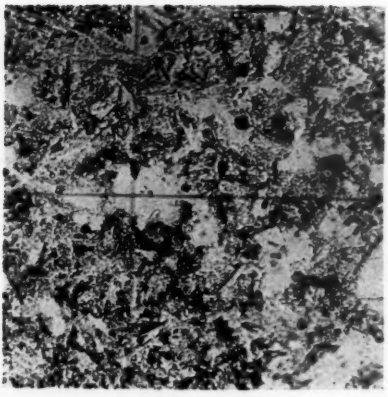

FIGURE 5

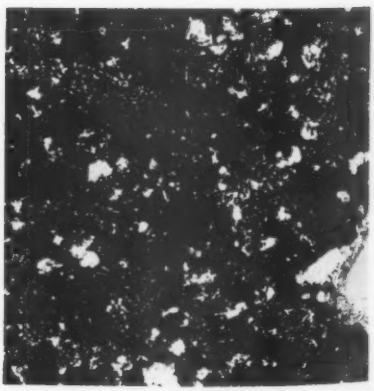

FIGURE 6

PHOTOMICROGRAPHS OF WELDED TUFFS

sions are darker than the ashy matrix, usually a medium gray or grayish brown, and may form as much as 15 per cent of the rock. No particular orientation of the inclusions can be seen.

The aphanitic groundmass consists of a porous mass of pumice dust and glass shards which show very little devitrification. The groundmass makes up 80–85 per cent of the rock, while the other 15–20 per cent is made up of the following inclusions:

(1) Laths of sanidine and rounded grains of quartz up to 2 mm in diameter, often exhibiting corroded borders

(2) Magnetite grains from dust size up to 0.5 mm in diameter

(3) Many tiny, angular grains of quartz and feldspar, and an occasional flake of biotite

(4) Lapilli—porous pumice fragments showing no evidence of crushing; some of unaltered glass, some partially devitrified, and many with phenocrysts of quartz and sanidine; apparently of rhyolitic composition.

This upper phase of member 2 is about 80 per cent glass and 20 per cent crystal fragments.

When typically developed the lower phase of member 2 consists of a grayish-red, aphanitic matrix containing a few gray inclusions and sparse phenocrysts of sanidine laths and rounded quartz grains. Near the top of this phase the inclusions are undeformed, but they become flattened and form lens-shaped streaks toward the base. The eutaxitic structure caused by the flattened inclusions is not well marked, and occasionally the rock exhibits a very homogeneous texture almost unbroken by inclusions.

The aphanitic groundmass, which forms 95 per cent of the rock, is largely glassy or cryptocrystalline, and composed of pumice fragments and glass shards firmly pressed together and exhibiting little porosity. Rather poor axiolites, spherulites, and microscopic eutaxitic structure are present in the generally glassy groundmass, along with occasional masses of xenomorphic quartz and sanidine grains. An occasional dusky red or porous, light-gray inclusion is noted. The red inclusions are of a cryptocrystalline texture, while the gray show a xenomorphic granular texture and are composed of quartz and sanidine grains up to 0.5 mm in diameter.

Phenocrysts of sanidine and quartz, generally corroded and embayed and up to 1.5 mm in

PLATE 4.—PHOTOMICROGRAPHS OF WELDED TUFFS

FIGURE 1.—MICROSCOPIC EUTAXITIC STRUCTURE IN GLASSY GROUNDMASS OF MEMBER 1
Nicols parallel, ×75

FIGURE 2.—SAME VIEW AS FIGURE 1
Nicols crossed

FIGURE 3.—MICROSCOPIC EUTAXITIC STRUCTURE IN MEMBER 5
Specimen taken from the basal 16 inches; nicols parallel, ×75

FIGURE 4.—SAME VIEW AS FIGURE 3
Nicols crossed

FIGURE 5.—MICROSCOPIC EUTAXITIC STRUCTURE IN MEMBER 6
Quartz and sanidine phenocrysts labeled Q and S, nicols parallel, ×75

FIGURE 6.—SAME VIEW AS FIGURE 5
Nicols crossed

PLATE 5.—PHOTOMICROGRAPHS OF WELDED TUFFS

FIGURE 1.—PHENOCRYSTS AND LITHIC INCLUSIONS IN THE GLASSY GROUNDMASS OF MEMBER 3
A poor microscopic eutaxitic structure is seen but no distortion of rock fragments, nicols parallel, ×25

FIGURE 2.—SAME VIEW AS FIGURE 1
Nicols crossed

FIGURE 3.—SPHERULITIC GROWTH IN THE DEVITRIFYING GLASSY GROUNDMASS OF MEMBER 6
Nicols parallel, ×75

FIGURE 4.—SAME VIEW AS FIGURE 3
Nicols crossed

FIGURE 5.—VITROCLASTIC STRUCTURE AND HIGH PROPORTION OF PORE SPACE SEEN IN THE UPPER, LESS COHERENT PHASE OF MEMBER 8
Nicols parallel, ×75

FIGURE 6.—SAME VIEW AS FIGURE 5
Nicols crossed

diameter, occasional magnetite grains up to 0.5 mm in diameter, and rare biotite laths form the other 5 per cent of the rock.

Member 3

This unit has a sharp but conformable contact with the underlying member 2 and grades abruptly into the overlying member 4. The soft, ashy layer commonly separating the welded tuff members in this area is missing between members 3 and 4; the gradational contact might indicate that member 4 is a basal phase of member 3 if it were not for the profound difference in the texture of the two members. The changes noted in the field, as one goes downward from member 4 into member 3 may be summarized as follows:

(1) The color changes from grayish red to dusky red, the characteristic hue of the lower member.

(2) The horizontal eutaxitic structure of the upper member, imparted by streaks of porous, gray material, is not clear in the lower member. In certain places a very rude, horizontal structure is seen in the orientation of the long axes of the sanidine laths, but inclusions are haphazardly oriented and show no tendency to be flattened parallel to the base of the formation. The inclusions are of two types; porous, very-light-gray cinders which form an overwhelming majority of the inclusions, and dense, very dusky-red cinders. Their angular shapes make them much more apparent than the flattened inclusions in the rocks above. The inclusions comprise, on the average, 1–5 per cent of the volume of the rock, but in some cases may make up as much as 20 per cent. Most are no more than 7 cm in diameter, but some may be as large as 15 cm.

(3) There is no tendency to form columns. The outcrops in Rhyolite Canyon show two sets of vertical joints, striking N. 17° E. and N. 30° W.; but the joint planes are very closely spaced, thus breaking the rock up into many small blocks rather than into large columns.

This member reaches its maximum thickness of 190 feet below the intersection of Rhyolite and Sara Deming canyons, and thins westward to a thickness of only 50 feet on the slope above Silver Spur Ranch. In the Picket Canyon outcrop this member is missing.

The porous, light-gray inclusions consist of a soft, vesicular matrix containing laths of feldspar and grains of rounded quartz. The inclusions vary in size from mere grains about 1 mm in diameter to fragments 15 cm in diameter, and most are angular.

The pore space varies from 25–35 per cent. Phenocrysts of sanidine laths and rounded quartz grains up to 2 mm in diameter, generally corroded and embayed, form about 15 per cent of the mineral matter. A few magnetite grains as large as 1 mm in diameter are noted. The matrix is a mixture of xenomorphic grains of quartz and sanidine up to 0.05 mm in diameter, and cryptocrystalline material in a ratio of 75 per cent cryptocrystalline material to 25 per cent xenomorphic quartz and feldspar grains. Both axiolitic and spherulitic structures are present, but no microscopic eutaxitic structure is apparent.

Angular inclusions of a very dusky to dusky-red color, ranging in size from 1 mm to bombs 10 cm in diameter, are sparingly scattered through member 3. A groundmass of glass, cryptocrystalline material consisting of microlites which are probably quartz and feldspar, and much iron oxide make up most of these inclusions. The iron oxide consists of both magnetite and hematite, commonly in very tiny grains, but some grains reaching 1 mm in diameter. Included in the groundmass are a few xenomorphic grains of quartz and sanidine 0.05–0.1 mm in diameter. No preferred orientation was noted in either the microlites or the xenomorphic grains. Although somewhat vesicular, this type inclusion is far more dense than the more common light-gray inclusion.

The major portion of member 3 consists of a homogeneous, firmly welded tuff of dusky-red color. It contains sanidine laths and rounded quartz grains in an aphanitic matrix. At some places the phenocrysts align themselves in rough layers parallel to the base of the formation, but more often their orientation appears to be haphazard.

The aphanitic groundmass consists of reddish-brown glass (index less than balsam) stained by many tiny grains of hematite. Many small grains of magnetite can be observed partially altered to hematite. Very good microscopic eutaxitic structure is noted, marked by oriented strings of iron oxide grains with

the long axes parallel to the borders of inclusions or phenocrysts. The glass is partially devitrified, and contains axiolites along with nests of xenomorphic quartz and feldspar grains. The long axes of the axiolites commonly parallel the microscopic eutaxitic structure. The usual phenocrysts of rounded quartz grains and sanidine laths, with a few large grains of magnetite, are noted; but the rock is unusual in that the phenocrysts make up 40 per cent of the total rock material. The maximum diameter for phenocrysts is 3 mm.

An explanation of the lack of a porous, rather incoherent top and of the prominent eutaxitic structure, found in typical welded tuff members, is based upon variables in *nuées ardentes*. If several eruptions follow one another quite closely the fine material of the great black cloud or upper part of the *nuée ardente* may have no time to settle, and a considerable thickness of the lower and coarser, or avalanche portion of the *nuée* would accumulate. If composed of the same type of material, the deposits from the different avalanches might be confused; but if the deposit of one particular *nuée* contained distinctive inclusions, or had a distinctive color, it might well be separated from the rest of the accumulation.

It is likely that the temperature of the material furnished by the various avalanches would differ. If a deposit were hot, thorough welding would probably result, along with collapse of the pumice fragments, and a very coherent rock with prominent eutaxitic structure would form. If, however, the temperature were lower, the smaller fragments might weld themselves into a coherent groundmass containing pumice fragments and other inclusions too cool and strong to collapse, and thus eutaxitic structure would not appear. Eutaxitic structure would also be held to a minimum if unusually large quantities of cool, or already solidified, fragments were included within the avalanche of the *nuée ardente*.

The first of a series of *nuées* might clear the vent of much solid material and thus might be far richer in solid inclusions than succeeding ones.

It is postulated that two *nuées* of different temperature and composition were erupted, one closely following the other. The more solid avalanche material of the first formed member 3. The second *nuée* followed so quickly that it swept away the great black cloud of the first before the cooler more finely divided material could settle out. Thus, the avalanche portion of the second *nuée* directly overlies that of the first, and member 3 grades upward into member 4 with no incoherent tuff portion to separate them.

Member 4

General description.—This member reaches its maximum thickness of 275 feet in Rhyolite Canyon, but thins rapidly to the west and northwest. On the slope above Silver Spur Ranch it has thinned to 125 feet, at the mouth of Little Jesse James Canyon it is 130 feet thick, and in Picket Canyon near the western boundary of the Monument it is missing. Most outcrops of this member show a typical welded-tuff unit, consisting of a porous, poorly consolidated, light-gray upper portion grading into a dense, brittle, grayish-red base which exhibits eutaxitic structure and rings under the hammer. The upper contact with member 6 or 5 is sharp, while at the base it grades abruptly into member 3.

Upper ashy phase.—At most exposures the poorly consolidated, upper portion of member 4 appears to be the normally developed, upper phase of a welded-tuff unit. However, on a steep slope just to the left of the highway at the downstream entrance to Bonita Park the following section is exposed:

Top obscured	
Light-gray, porous, rather incoherent tuff	25 feet
Grayish-red, firmly welded tuff lens	8 inches
Light-gray, porous, rather incoherent tuff	2 feet
Small lenses of grayish-red, firmly welded tuff 1–2 inches thick and 2–3 feet long, embedded in light-gray, incoherent tuff	1 foot
Light-gray, porous, rather incoherent tuff	20 feet
Base obscured	

The 8-inch layer of firmly welded, grayish-red tuff grades into the light-gray, less coherent tuff at both its top and bottom contact. Traced laterally in one direction it is obscured by talus; but in the other direction it becomes thinner,

grayer, and less coherent, and finally fades into the even slope of the soft, light-gray tuff. Two other lenses of coherent, grayish-red rock were noted in the same horizon. One was similar to the first, a lens 20 feet in length and 8 inches thick. Several feet below this second 8-inch lens was a zone containing many small, irregular lenses of hard, grayish-red rock, each small lens being 2–3 feet long and only an inch or so thick.

On the Rhyolite Canyon trail, between its intersection with Hunt Canyon and Echo Canyon trails, there is a second unusual outcrop of the upper, ashy phase of member 4. It comprises a thick layer of accretionary lapilli, or chalazoidites. The outcrop extends from a point 1600 feet west of the intersection of the trails to a point some 700 feet to the west. Both the upper and lower portions of the mass are obscured, but it appears to be lens-shaped, at least 700 feet long, 15 feet thick, and of unknown breadth. This outcrop is the only one found in the Monument. Most of the lapilli measure close to one-half inch in diameter, and considerable search was necessary to find any as large as 1 inch or less than one-quarter inch in diameter. When loosely packed and in contact with a fine, ashy matrix, most of them approach the spherical; but in zones where they are more plentiful many are deformed owing to the close packing. The eastern boundary of the lens is obscured; but westward from the zone of the greatest number of accretionary lapilli, it is observed that they decrease in number gradually until finally only an occasional spherical lapilli can be seen in a matrix of light-gray ash. In no case was bedding noted.

The light-gray, poorly welded tuff of member 4 is incoherent at the top, becoming more coherent toward the base, with an even, aphanitic, very porous groundmass containing scattered phenocrysts of sanidine laths and rounded quartz grains. In the more-coherent basal portion thin, parallel lenses of whiter, more-porous material up to 7 cm long and 2 cm thick are noted.

The texture is uniform throughout this unit. A groundmass consisting of about equal parts of xenomorphic quartz and sanidine grains, never over 1 mm in diameter, and microcrystalline aggregates, probably devitrified glass, forms 95 per cent of the rock. Angular phenocrysts of sanidine and quartz, seldom larger than 3 mm in diameter and some showing absorption borders, make up the other 5 per cent of the rock. Magnetite as small grains sparsely scattered through the groundmass or as occasional phenocrysts is noted. Spherulitic and axiolitic structures are absent, and no orientation of the grains or microscopic eutaxitic structure can be seen. The material is highly porous throughout.

The phenocryst to groundmass ratio and the magnetite content increase near the base of the member. The appearance of the porous lenses of white material indicates that larger pumice fragments are present nearer the base, but small crystals, glass shards, and small pumice fragments make up most of the stratum.

The firmly welded lenses of grayish-red tuff exhibit eutaxitic structure parallel to the base of the lens, shown by bands of very vesicular, light-gray material in the more-dense, grayish-red matrix. The light-gray, vesicular bands appear to be flattened inclusions, and may be as much as 5 cm long and 5 mm wide. Phenocrysts of sanidine laths and rounded quartz grains are plentiful and generally haphazardly oriented, although occasionally a very rough layering is noticed, with the phenocrysts stringing out parallel to the long axes of the flattened, vesicular inclusions.

The groundmass, which forms 90 per cent of the rock, exhibits a texture unlike that of the light-gray ash. There is little evidence of crystal fragments, and much evidence that it is an originally vitric matrix, now largely devitrified. The texture is generally cryptocrystalline, but abundant spherulites and axiolites are present, some of the spherulites reaching a diameter of 0.8 mm. Good microscopic eutaxitic structure is observed in the parallelism of the axes of the axiolites and in strings of iron oxide grains, probably originally magnetite but now in large part altered to hematite. The microscopic eutaxitic structure is especially well developed between close-lying phenocrysts. Some of the spherulitic and axiolitic structures cut across the microscopic eutaxitic structure shown by the iron oxide grains; in other cases the iron oxide strings align themselves parallel with the radiating crystal needles of the spherulites. Occasional granular masses of xenomorphic quartz and sanidine are noted in the groundmass, with some grains up to 0.4 mm

in diameter. The groundmass is well compacted, few pores or vesicles being noted.

Outward from the hard red rock, into the gradational zone, axiolitic and spherulitic features become less common, oriented strings of hematite grains disappear, and the groundmass becomes more porous and less vitric.

The accretionary lapilli are light-gray spheres, about one-half inch in diameter. The exterior is rough where grains of sanidine and quartz extend beyond the softer, aphanitic, gray matrix. Where tightly packed the spheres become distorted and welded together. A few, when broken, show a concentric structure as if formed in layers around a nucleus, but the majority exhibit an even texture throughout. Although many were cut and dyed, by the technique Berry outlined (1928–1929, p. 582), only a few showed definite evidence of concentric lamination. The cementing matrix or ashy groundmass containing the lapilli differs from the lapilli only in being more porous and less coherent. On weathered surfaces the cementing matrix tends to wash out, and the lapilli stand out in relief.

The mineralogy of the accretionary lapilli is identical with that of the matrix, and only the textures differ. The sparsely scattered lapilli near the edge of the lens show a texture identical with that of the matrix, being softer and less coherent than those near the center of the lens. Nearer the center of the lens not only do the lapilli become more numerous and more coherent, but also they become changed in groundmass texture. The cryptocrystalline aggregates disappear and a xenomorphic, granular mass of sanidine and quartz takes their place. The xenomorphic grains average 0.3 mm in diameter, but some narrow crystalline units up to 1.5 mm in length are noted. The extinction of these xenomorphic grains tends to be undulatory. In some of the more-coherent lapilli a very broad and poor spherulitic texture is developed, with many of the elongated crystalline masses extending radially from the center. This spherulitic structure is modified by the phenocrysts and the mosaic structure of the xenomorphic, granular groundmass.

The fall of mud balls during volcanic eruptions has often been observed, and most authorities consider them to be due to aerial mixing of volcanic dust and moisture, although detailed ideas of origin differ. Wet particles of pumice or ash under the influence of surface tension would tend to coalesce to form a nucleus which would be tossed about by turbulent currents. A series of ascents and descents through layers containing varying amounts of moisture and ash would result in concentric layering of the nucleus.

The upper, ashy phase of member 4 is thought to be merely the upper, poorly welded portion of a typical welded-tuff unit. The upper deposits of ash were rather heterogeneous, containing lenses richer in vitric constituents than usual, and hence more likely to be welded into firm layers. The uppermost, dusty debris of the *nuée ardente* became involved with thunderstorm activity, and a thick but local layer of accretionary lapilli was formed.

It is also logical to consider this ashy section as formed by several small *nuées ardentes* capped by an ash shower which was involved with a thunderstorm. The thoroughly welded layers in the less coherent, ashy mass might then correspond to the hotter, lower portions of small *nuées ardentes*. Unfortunately the exposures are too few and the evidence insufficient to permit a completely satisfactory explanation.

Basal firmly welded phase.—The ashy, upper phase of member 4 gradually becomes more coherent and firmly welded toward its base until about 65 feet below the top of the formation it has become a pinkish-gray, firmly welded rock which will ring under strokes of the hammer. In addition, porosity decreases downward while the appearance of streaks of a porous, light-gray material leads to the development of eutaxitic structure. These streaks may be several centimeters long and 3–4 mm thick. They are actually disk-shaped, but on a broken surface of rock only two dimensions are usually noted. These streaks undoubtedly represent flattened masses of included lapilli.

Good vertical jointing in this rock leads to the formation of columns. Intersection of the joint sets forms a roughly square set of columns which weather to round or oval forms. Some tall, vertical pillars are found, but such development is minimized by an almost horizontal set of joints. The almost-horizontal joints actually are inclined at angles of 10°–15° in various directions. Many are only 4–5 feet

apart, and thus break the formation up into sheets. Superposition of the vertical upon the essentially horizontal jointing develops a series of blocks piled one upon the other inclined to their plane of horizontal contact so that there is a tendency for them to slip off and thus prevent development of tall, vertical piles or pillars.

The texture and mineralogy of this firmly welded phase are very similar to those of all the other firmly welded tuffs of the area. Quartz and sanidine phenocrysts up to 3 mm in diameter, mostly rounded and corroded but with occasional subhedral crystals, are embedded in a uniform, pinkish groundmass formed primarily of shards and shreds of firmly welded and largely devitrified glass which presents a general cryptocrystalline appearance but contains occasional larger grains or masses of xenomorphic quartz and sanidine. About 10–15 per cent of the rock is composed of phenocrysts, 85–90 per cent of groundmass. The pink color of the groundmass comes from many tiny grains of red iron oxide disseminated throughout. Some small, red, cryptocrystalline inclusions and the larger, porous, courser-grained, white inclusions are noted. The porous, white inclusions consist of xenomorphic quartz and sanidine grains, up to 0.5 mm in diameter, enclosing phenocrysts of corroded quartz and sanidine. Both axiolitic and microscopic eutaxitic structure are observed in the pink groundmass, but only occasionally is either well developed.

Member 5

In Bonita Canyon, directly above member 4, is found a layer of 30 inches of volcanic material which shows, in this short distance, all of the features observed in the thicker welded-tuff or ignimbrite units. A vertical section throught this unit shows:

Firmly welded, glassy base of member 6	
Very-light-gray, incoherent tuff	6 inches
Light-gray, rather coherent tuff	8 inches
Black to dark-gray, firmly welded tuff containing horizontally aligned, flattened, pinkish-gray to very-light-gray, porous inclusions in a dark, aphanitic groundmass	16 inches

The brittle, glassy base of member 5 differs from the base of the overlying member 6 only in being black to dark gray rather than grayish red. The darker color appears to be due partly to unaltered magnetite in the groundmass. In this dark, glassy groundmass are found flattened, very-light-gray, porous streaks aligned parallel to the base of the unit, some attaining a length of 5–6 cm. These appear to be flattened lapilli similar to those found in other welded-tuff units. The base of this thin welded tuff shows a good microscopic eutaxitic structure and as good flattening of the inclusions as does the base of the thick unit above. Apparently something other than the weight of a mere 14 inches of overlying ash caused the superior welding and the flattening of the inclusions in the base of this unit.

Marshall (1935, p. 339–340), Gilbert (1938, p. 1849), Cotton (1944, p. 200), and others who have examined welded tuffs consider that thick sections of material, as well as high temperatures, are necessary to cause the welding leading to a product that will ring under hammer strokes. The flattening of the inclusions and the development of microscopic eutaxitic structure in the groundmass of member 5 are most probably due to the vertical pressure from the overburden; and since an overburden of only a few inches of incoherent dust would be incapable of this, the 880 feet of the overlying member 6 must have been deposited soon after member 5 and before it had cooled appreciably. Many volcanologists have mentioned the insulating properties of the fine ash on the surface of the deposit left by a *nuée ardente*, and the high temperatures of the underlying material days or even weeks after the eruption. The great pressure of the overlying rock mass would flatten the hot fragments in the base of member 5 and more firmly weld those portions still hot enough to be welded. The overlying, comparatively cool ash would be unaffected.

Unfortunately member 5 could be studied in one outcrop only, namely the road cut in Bonita Canyon just beneath the rock formation known as the Chinese Boy. In other parts of the Monument where the base of member 6 is exposed, member 5 is missing. Evidently it is very limited in areal extent.

Member 6

General description.—Directly above the thin member 5 lies the thickest and most prominent welded rhyolite tuff of the entire Chiricahua section. Throughout most of its thickness this stratum is a light-brownish-gray rock showing prominent eutaxitic structure caused by a great many lenses of porous, very-light-gray pumice included in a dense, brownish-gray matrix. Phenocrysts of sanidine and glassy quartz are common.

Most of the surface rock of Chiricahua National Monument belongs to member 6. It can be seen at Massai Point and along the ridge road, and followed on the uplands west of Sugarloaf Mountain until it finally disappears under the alluvium of the Sulphur Springs Valley. This member reaches its maximum thickness of 880 feet in Bonita and upper Rhyolite canyons. Elsewhere in the Monument it is exposed at the surface, and erosion has stripped away portions of its upper part, thus making a complete section impossible to obtain. It thins steadily westward until, when last seen on the ridge north of the road opposite El Dorado School, it is less than 100 feet thick. The unusual and spectacular rock formations for which the Monument is famous are developed in member 6 and result from weathering guided by well-developed, vertical joints and the coarse eutaxitic structure.

Upper ashy phase.—The upper portion of member 6 consists of 20 feet of pinkish-gray rhyolite tuff containing many red cinders as inclusions and exhibiting good bedding locally. Good cross-bedding can be observed in places, and in certain localities the bedding appears curved as if the layers were fitted into a small stream channel. The bedding changes rapidly laterally, becoming indistinct in many places, and disappears downward into the transition zone beneath it. Red cinders and grains of quartz and sanidine several millimeters in diameter occur in streaks and layers in the very fine, gray matrix of this rock. The bedding appears to be due to reworking of the soft, ashy upper phase of the *nuée ardente* deposit by wind and stream action.

The matrix is extremely fine-grained. It is composed of a mixture of partially devitrified glass shards and grains of quartz, sanidine, and magnetite. Although an occasional feldspar lath is present, the mineral grains are generally xenomorphic, and no mineral grain exceeding 0.2 mm in diameter was found. The mineral grain to glass shard ratio is 35 per cent mineral to 65 per cent glass.

Basal firmly welded phase.—The ashy upper portion of member 6 becomes darker in its lower portions and grades into a light-brownish-gray, firmly welded tuff some 160 feet thick, which in turn grades into a grayish-red, very firmly welded phase which makes up the remaining 700 feet of the formation. Mineralogically the lower phases of this member are identical, differing only in color and texture. Throughout this entire thickness the rock consists of easily recognizable quartz and feldspar phenocrysts in an aphanitic groundmass.

Where exposed in Bonita Canyon the base of member 6 exhibits a very dense, glassy texture, and lies with knife-edge contact on the underlying member 5. At the mouth of Picket Canyon the base is again exposed, but here member 6 lies directly on member 1. Either the intervening members have not been deposited in this area, or if deposited have been removed by erosion. The basal 6 feet of member 6 at this outcrop contains many angular, roughtly flattened vesicles parallel lengthwise to the base. These vesicles may be several inches long and an inch or two high. The contact is irregular; and at the contact member 6 contains a concentration of spherulites and lithophysae, some as much as 6 inches in diameter. These spherulites resemble those found by Mansfield and Ross (1935, p. 320) in the welded tuffs of southeastern Idaho. Many of the spherulites and lithophysae are cut and partially disrupted by the angular vesicles.

Phenocrysts of rounded quartz grains and sanidine laths, reaching a maximum size of 3 mm in length or diameter and exhibiting corroded and embayed borders, and a few magnetite grains, up to 0.5 mm in diameter, make up 20–30 per cent of the rock. The groundmass consists of glass as shards, shreds, dust, and small pumice fragments, all of which may be extensively devitrified, along with broken fragments of feldspar and quartz and occasional

inclusions of red, cindery material of cryptocrystalline nature. The rock may be porous or dense, but commonly exhibits very good microscopic eutaxitic structure and also good axiolitic and spherulitic structure. The axiolitic structures parallel the microscopic eutaxitic structure, which the spherulitic structures often transect.

Although the welded tuffs at Chiricahua are composed of large crystals of feldspar and quartz embedded in a maze of minute, glass shreds, these glass shreds may not retain their vitreous characteristics. In many of the rocks the glassy nature is lost by devitrification although the form of the original glass particles may have been retained. Westerveld (1943, p. 211–212; 1947, p. 34) maintains that most welded rhyolite tuffs show partial or complete crystallization of the glassy groundmass, and that the axiolitic and spherulitic structures are due to the development of orthoclase or albite and tridymite. He suggests epigenetic crystallization effected by rising gases emitted by the still-hot particles in the lower levels immediately after emplacement of the deposit. He pictures this action as pneumatolytic, with vapors and/or solutions laden with silica and alkalies mineralizing the interstices between the glass and mineral particles and replacing the glass shards metasomatically. According to this concept, welding of the viscous glass shards is aided by cementation of the fragments by tridymite and alkali feldspar. He reports that in eastern California and in New Zealand pneumatolytic alterations are more strongly developed in the upper levels of the tuff masses.

The mineral matter in the spherulites, axiolites, and other devitrification or recrystallization phenomena found in the Chiricahua tuffs is considered to be quartz and sanidine. Because tridymite is said to develop in welded tuffs, the products of recrystallization were carefully analyzed. In addition to petrographic analyses, selected samples of member 6 were subjected to X-ray analysis, but no evidence of tridymite appeared. The feldspar can in some cases be definitely determined as sanidine, but in other cases the needles formed by the devitrification are so fine as to defy accurate determination. These feldspar needles have an index less than balsam, and might be albite or orthoclase; but, owing to the positive presence of sanidine in larger masses and the preponderance of K_2O over Na_2O in the chemical analysis of member 6, it is thought that the feldspar is sanidine containing a considerable quantity of the $NaAlSi_3O_8$ molecule.

Unusual features.—Certain features commonly attributed to welded tuffs are shown particularly well by member 6.

(1) A coarse eutaxitic or pseudo-bedded structure is outstanding. This structure is not so apparent in the light-brownish-gray transition phase of the unit, but as the rock assumes a grayish-red color below the upper 180 feet the eutaxitic structure becomes distinct. Maximum development of this feature is seen in Bonita Canyon near the base of member 6. The rock is made up of two distinctly different materials; pinkish-gray, porous, lens-shaped masses are embedded in a pale-red, stony matrix. The lenses are oriented parallel to the base of the rock, and may make up as much as 25 per cent or as little as 5 per cent of the rock mass. Ordinarily these lenses are no more than a few inches long and a fraction of an inch wide, but may reach a foot in length and 2 inches in width. Upon exposure to the atmosphere the porous lenses localize weathering, and parallel indentations or gouges form on the rock surface, giving it almost a bedded appearance.

Microscopic examination shows that both layers consist of 20–25 per cent phenocrysts. The groundmass of the lenses is porous and formed of 70 per cent xenomorphic quartz and sanidine grains along with a few sanidine laths, the grains or laths measuring up to 0.5 mm in diameter, and 30 per cent vitreous or cryptocrystalline material. The whole mass contains a light sprinkling of magnetite and hematite, but not enough to color it. The groundmass of the grayish-red, stony matrix is finer grained and far less porous. It is formed of only 10 per cent xenomorphic quartz and sanidine in grains large enough to allow their recognition, while the other 90 per cent consists of cryptocrystalline or vitreous material. The groundmass of the stony matrix contains more magnetite and hematite and exhibits very fine microscopic eutaxitic structure.

This texture probably formed in the following manner: the rock was composed of a mixture of fragments of porphyritic pumice, blocks

of rhyolite, red cinders, broken crystals of quartz and sanidine, and a great deal of fine, vitric material such as shards and shreds of glass. Magnetite and hematite were spread as phenocrysts and fine dust in the porphyritic pumice and rhyolite blocks and as grains and dust throughout the fine, vitric material. At the top of the tuff the porous pumice fragments and rhyolite blocks were very small and sparsely scattered through a great deal of very fine, very loosely packed, vitric material. The basal portion of the tuff was richer in lapilli, blocks, and pumice boulders. This is borne out by a progressive enrichment in gray, porous lenses, and an increase in the size of the lenses near the base of the tuff. With the increased pressure and more-thorough welding caused by greater overburden, the pumice fragments and rhyolite blocks are flattened and aligned parallel to the base; but they possess a stronger framework than the vitric dust, and hence offer greater resistance to complete collapse and complete welding. The loose, vitric material suffers a maximum of compaction and welding; the shards and shreds of glass are flattened and molded one to the other, bending around the solid phenocrysts. The dusty iron oxide, originally scattered uniformly through the mass, is concentrated as the mass collapses, thus giving increased pigment per unit of volume. It aligns itself parallel to the glass shreds and around the phenocrysts, producing the microscopic eutaxitic structure so typical of the grayish-red stony matrix of the rock. Some of the rare, red cindery inclusions and the more common, porous gray material were of more rigid construction than the smaller material in the stony matrix, and cuts along the Echo Canyon trail show eutaxitic structure bent about these rigid inclusions.

Gilbert (1938, p. 1833–1835) noted the heterogenous nature of the original tuff in the Bishop tuff of California, and describes pumice fragments as unoriented and very porous at the top but progressively flattened and aligned in the horizontal plane toward the base. The writer has observed that the gray, porous lenses (flattened pumice bombs and lapilli or blocks of rhyolite) show more advanced devitrification than the reddish groundmass. Gilbert (1938, p. 1850), on the other hand, states:

> "The crystalline tuff grades downward into the glassy type near the base of the formation. In this change the first appearance of the glass is in the larger fragments, lapilli of collapsed pumice, and the last appearance of glass is in the finest constituents. This indicates that the larger fragments crystallized less readily."

(2) An increasing amount of glass is noted in the groundmass toward the base of the unit, while the devitrified glass shows an increasing preponderance of weakly birefringent material over the recognizable zenomorphic grains of sanidine and quartz. Apparently crystallization in the glass has advanced much further in the porous, gray, upper tuff than in the more thoroughly welded and better-compacted reddish tuff toward the base.

Both Marshall in New Zealand and Gilbert in California noted this increase in glass near the base of the formation. Marshall (1935, p. 338) considered that the cold substratum would cool the base rapidly, while heated gases, emitted from the lower portion of the ignimbrite, would maintain the high temperature of the upper part. Gilbert (1938, p. 1850) also attributes the development of the crystallinity in the upper portion in part to rising gases without explaining the process. Marshall and Gilbert imply that the gases gain their heat from the lower part of the tuff, in which case this lower portion should be hotter than the upper.

As previously mentioned, Westerveld (1943, p. 211–212) ascribes recrystallization to vapors and solutions, laden with alkalies and silica, mineralizing the interstices between the glass particles, and also replacing the glass shreds metasomatically.

Formation of glass implies such rapid cooling of a liquid magma that migration of the ions is retarded and crystallization inhibited. This is particularly noted in acid lavas. Glass is a metastable material, however, and is likely to crystallize or devitrify with passage of time, especially if subjected to raised temperatures. Such raised temperatures seem to have existed, particularly in the porous lenses and in the upper portions of the tuff where maximum crystallization occurs. This might be due to the escape and reaction of some of the volcanic gases. These gases would naturally tend to be concentrated in the more permeable zones of the tuff. Also they tend to react most violently

in the very uppermost portions of lava masses or when discharged into the air. Their reaction might last for an appreciable time, and most of the energy would be freed in the upper portions of the tuff.

Kozu (1934) has observed fumarolic activity which continued for 6 weeks after the ejection of pumice flows of *nuée ardente* origin emitted from the crater at Komagatake in Japan. Day and Shepard (1913, p. 598), working on the volcanic gases set free at Kilauea, state:

> "Whatever may have been the previous opportunities for chemical readjustment among the gases as they rose in solution with the magma and were gradually set free with the diminishing pressure, they are still in process of reaction when discharged into the air."

T. A. Jaggar (1917, p. 214) made actual measurements on the lava temperature at Kilauea, and found that in lava fountains and domes where gas reactions were taking place the temperature was as high as 1350° C, while 3 feet below the surface it was only 750°–850° C.

Mansfield and Ross (1935, p. 312–314) suggest gas reactions to account for the widespread welding of tuffs in southeastern Idaho.

Metasomatic replacement and the addition of minerals between the shards could not have caused the welding and devitrification of the Chiricahua welded tuffs. In the first place, these would necessitate a much greater flow of vapors and solutions than could be supplied by the escape of the gases retained by the tuff after its deposition; and, in the second place, such methods should develop more thorough welding in the upper portion than in the lower since vapors and solutions from the lower portions would deposit their loads during the upward migration.

(3) Spherulitic and axiolitic structures are common; and in places another devitrification texture consists of small, needlelike microlites developing in the vitreous groundmass, oriented parallel to the microscopic eutaxitic structure.

(4) Vertical jointing is prominent in this member. The joint prisms are generally square or rectangular, and may be as much as 30 feet in diameter. When weathered they may stand as single columns over 150 feet high. Jointing is common in the well-consolidated, lower portions of all the welded tuff members in the Monument, but none is so outstanding as the jointing in this particular rock unit.

(5) At various localities in the Monument, but perhaps best shown on the Echo Canyon trail, this basal, firmly welded phase of member 6 develops cavernous rock hollows. The rocks involved have a resistant exterior, generally covered with desert varnish, which has been breached to form an opening leading to the cavernous interior. The cavity extends not only inward from the opening, but also upward and to both sides. The inner surface of the hollow is covered with crumbling scales of rock, and the floor with several inches of scales and sand, apparently debris which has dropped from the walls and the roof. The hollows range from recesses only an inch or two deep to caves large enough to hold several people.

The origin of these rock hollows seems to involve case-hardening of the exterior of the rock, along with granular disintegration and exfoliation within the boulder.

Chemical composition and classification.—Two complete rock analyses were run on selected samples of member 6 by Lois D. Trumbull at the Denver Rock Analysis Laboratory of the U. S. Geological Survey. The chemical analyses in weight per cent of the oxides and calculations of the normative minerals, according to the method of Cross, Iddings, Pirsson, and Washington, are given in Table 3.

If the weight percentages of the normative minerals are used in the Johannsen classification, the following results are obtained:

Sample 1—(116 E), tordrillite or leuco-soda-clase-rhyolite

Sample 2—(117 E), no name recommended.

The use of the weight percentages of the norm in applying the Johannsen classification is not completely satisfactory, but is more accurate than volume percentages of the mode in view of the large proportion of glass and cryptocrystalline material. Undoubtedly some of the soda would enter the orthoclase so that the calculation of the plagioclase is probably too high, and the plagioclase molecule might well be oligoclase rather than albite. These changes would place both samples in (126 E) where they would be termed leucorhyolites. The leucorhyolites are normal rhyolites with less than 5 per cent of dark minerals, and Johannsen

TABLE 3.—CHEMICAL ANALYSES AND CALCULATED NORMS FOR TWO SAMPLES OF MEMBER 6

	Sample 1*										Sample 2†									
	Wt. %	Mol.	pv or	pv ab	an	C	hm	pv by	Q		Wt. %	Mol.	fr	pv or	pv ab	an	hm	di	pv wo	Q
SiO_2	76.38	1.273	.312	.288	.006	....	....	.004	.663	SiO_2	74.55	1.242	....	.300	.300	.020	....	.008	.008	.606
Al_2O_3	12.47	.123	.052	.048	.003	.020	....	....	....	Al_2O_3	11.16	.110	....	.050	.050	.010	....	....	....	....
Fe_2O_3	1.56	.010	....	....	....	....	.010	....	....	Fe_2O_3	1.51	.009	....	....	....	....	.009	....	....	....
FeO	Tr.	....	....	....	....	....	....	....	....	FeO	.00	....	....	....	....	....	....	....	....	....
MgO	.15	.004	....	....	....	....	....	.004	....	MgO	.16	.004	....	....	....	....	....	.004	....	....
CaO	.15	.003	....	....	.003	....	....	....	....	CaO	1.53	.028	.006	....	....	.010	....	.004	.008	....
Na_2O	3.0	.048	....	.048	....	....	....	....	....	Na_2O	3.11	.050	....	....	.050	....	....	....	....	....
K_2O	4.85	.052	.052	....	....	....	....	....	....	K_2O	4.66	.050	....	.050	....	....	....	....	....	....
H_2O	.26	....	....	....	....	....	....	....	....	H_2O	.76	....	....	....	....	....	....	....	....	....
H_2O	.85	....	....	....	....	....	....	....	....	H_2O	1.15	....	....	....	....	....	....	....	....	....
TiO_2	.12	.001	....	....	....	....	....	....	....	TiO_2	.11	.001	....	....	....	....	....	....	....	....
P_2O_5	.01	....	....	....	....	....	....	....	....	P_2O_5	.02	.001	....	....	....	....	....	....	....	....
MnO	.05	.0005	....	....	....	....	....	....	....	CO_2	.04	.001	....	....	....	....	....	....	....	....
										SO_3	.54	.006‡	....	....	....	....	....	....	....	....
										Cl	.08	.001	....	....	....	....	....	....	....	....
										F	.49	.013	.013	....	....	....	....	....	....	....
										MnO	.12	.001	....	....	....	....	....	....	....	....
											99.99	....	....	....	....	....	....	....	....	....
										Less	0.23	....	....	....	....	....	....	....	....	....
Total.....	99.86	....	....	....	....	....	....	....	....	*Total*.....	99.76	....	....	....	....	....	....	....	....	....
Wt. %.....	....	....	28.91	25.15	0.83	2.04	1.60	0.40	39.78	*Wt. %*.....	....	....	1.01	27.80	26.20	2.78	1.44	0.93	0.93	36.36
						Total 98.71										*Total* 97.46				

* Very fresh sample from basal portion of member 6, just above Echo Park

† Fresh sample bearing a superficial coating of desert varnish; collected 200 feet higher in member 6 than sample 1

‡ Contains none of the Hauynite group, so thenardite is not calculated; it contains no FeO, so pyrite cannot be calculated

states (1932, p. 259) that an examination of Washington's Tables (1917) shows them to be the most common type of rhyolite in North America.

The close mineralogical relationship between all rhyolite members of the Rhyolite Canyon formation suggests a chemical composition for all the members similar to that of member 6.

Member 7

Directly above member 6 and separated from it by an erosional surface is found 10 feet of coherent tuff, deposited by an ash shower or by a small *nuée ardente*. This tuff is pinkish gray, weathering to pale yellowish brown. The exterior shows some case-hardening locally, and cavernous portions develop on the outcrop. Recognizable quartz and sanidine phenocrysts, some white crystalline inclusions, and many dark-reddish-brown to black, finely porous cinders are embedded in a gray, pumiceous groundmass. The reddish-brown cinders may be as much as 2 inches in diameter.

The red cinders are a finely porous mass of devitrified glass containing feldspar microlites and considerable magnetite in very fine grains. Alteration of the magnetite to red oxide gives the color.

The gray tuff contains corroded and rounded grains of quartz, laths of sanidine, and irregular grains of magnetite as phenocrysts. Some laths of feldspar reach a length of 7 mm, while the quartz and magnetite grains are much smaller. The ratio of phenocrysts to groundmass is about 5 per cent phenocryst to 95 per cent groundmass. The groundmass is composed of well-devitrified glass shards and shreds along with fragments of crystalline quartz and sanidine. The amount of crystalline material is high, averaging about 50 per cent of the groundmass; the crystalline grains in the groundmass are very small, 0.05 mm or less in diameter. It is difficult to determine whether the small crystalline grains are actually broken crystalline fragments included in the tuff or devitrification products of the glass. Perhaps both sources contribute these grains.

Member 8

Above member 7 is a welded rhyolite tuff 50 feet thick. This unit varies from top to bottom, as indicated below, each lithologic unit grading insensibly into the next.

Soft, pinkish-gray tuff	10 feet
Hard, compact tuff identical with above, but well consolidated	15 feet
Hard, compact, pale-brown rhyolite rich in phenocrysts	25 feet

The upper portion of this unit is composed of poorly welded, pinkish-gray, porous rock, containing recognizable phenocrysts of quartz and sanidine and inclusions of both pumice and a more solid rock composed chiefly of a crystalline mass of sanidine and quartz. None of the inclusions is larger than an inch in diameter, and they are very sparse; many are equidimensional, but some are flattened parallel to the base of the rock, which gives a very crude and intermittent eutaxitic structure. The groundmass is made up of very small glass fragments.

The upper portion of this rock grades imperceptibly down into the intermediate portion which is darker, much tougher, and more brittle. In many respects this part of the rock is similar to that above; and in both cases sanidine and quartz phenocrysts along with rock or pumice inclusions are set in a fine, gray groundmass.

The basal 25 feet of the unit is composed of a pale-brown, brittle rock. The poor horizontal or eutaxitic structure reaches its optimum development in the basal portion. This structure is due to horizontal streaks of light, porous material identified as large pieces of badly flattened pumice. Vertical jointing which is uncommon in the upper portions of this unit becomes common in the more brittle, basal portion.

About 2–3 per cent of the soft, upper portion of the unit is composed of phenocrysts of quartz, sanidine, and a few large magnetite grains. The quartz and sanidine commonly show marginal corrosion, and may reach a diameter of 3 mm. The groundmass shows a vitroclastic structure, consisting of loosely-packed glass shards and glass dust, along with pumice fragments and broken pieces of quartz, sanidine, and magnetite. Glass fragments vary from masses of intact, vesicular pumice to large shards to extremely fine dust particles. Some of the glass shards take on a typical, subtriangular shape, and may be as much as 0.07 mm long.

In addition to crooked, tubular vesicles in the pumice, loose packing of the fragments leaves many vesicles, some of which are as much as 0.5 mm in diameter; and thus a very loose, highly porous structure is developed. Much of the glass has begun to devitrify, giving aggregate polarization caused by the development of very tiny crystalline grains of what is probably a mixture of quartz and potash feldspar. Seventy-five to eighty per cent of the total rock is made up of glass or devitrified glass, while the rest consists of broken crystalline fragments or large phenocrysts.

Toward the base of the member the following progressive changes are noted.

(1) The sanidine and quartz phenocrysts become larger and more abundant. They make up 35 per cent of the volume, and phenocrysts 4 mm in diameter are not uncommon.

(2) Magnetite becomes more abundant. Many grains measure 2 mm in diameter, some altered to red oxide around the borders. The groundmass is colored reddish by many tiny specks of red iron oxide, perhaps alteration products of magnetite.

(3) Glass shards and dust with flattened, porous, crystalline masses and porous, pumice fragments are present, but the pumice fragments seem to be larger; and all have a strong tendency to be aligned in parallel planes, forming eutaxitic structure.

(4) Between close-lying phenocrysts there is dense, reddish glass showing no devitrification and exhibiting a microscopic eutaxitic structure.

(5) Although there is some aggregate polarization indicating devitrification in the glassy groundmass, in the lower part of the member there is far less than in the upper part of the stratum. The areas of chief devitrification appear to be in regions away from the phenocrysts. Good examples of axiolitic and poor examples of spherulitic structure are noted in the devitrifying glass.

(6) The porosity of the groundmass progressively decreases, and the rock becomes more firmly welded.

Member 9

General description.—Sugarloaf Mountain is capped by a 220-foot flow of rhyodacite which constitutes the youngest and uppermost member of the Rhyolite Canyon formation. It is black to medium dark gray when fresh, weathering to brownish gray. The texture is porphyritic, about 10 per cent phenocrysts to 90 per cent aphanitic groundmass, although the phenocrysts become more numerous in the uppermost 25 feet of the flow. The phenocrysts are chiefly plagioclase, and appear as white spots in the gray matrix. The rock becomes vesicular in the upper 25 feet, many of the vesicles being filled with chalcedony or containing spherulites of chalcedony. A faint flow texture, or at least a banding parallel to the base of the bed, can be seen both in the outcrops and in the thin sections.

Phenocrysts of plagioclase are very abundant, augite common, quartz, magnetite, and horneblende rare. Maximum size is reached in the plagioclase phenocrysts which occur as laths or tablets as much as 1 mm long. Four-sided, eight-sided, and rounded augite crystals from 1 mm to tiny grains are found. Large, corroded grains of plagioclase and augite, or aggregates of coarse-grained plagioclase and augite are common. These invariably exhibit heavily corroded and embayed borders, and appear to be inclusions. The plagioclase grains may be as much as 2.25 mm in diameter, while the aggregates or rock fragments are sometimes 5 mm across. Zonal structure in these large plagioclase grains is not uncommon. The groundmass exhibits a hyalopilitic texture, with needlelike microlites and skeleton crystals of plagioclase, microlites of sanidine, tiny round to square grains of augite, and small, irregular quartz grains embedded in a matrix of glass. The glassy matrix has devitrified in places, forming a cryptocrystalline mass. Crude flow texture is occasionally noted in the groundmass.

Constituents.—Plagioclase was found as large, corroded inclusions or as laths and microlites in the glassy matrix. Extinction angles and indices determined on fragments of both types of feldspar indicate that they have similar compositions. Indices of refraction on cleavage flakes gave 1.552 and 1.543 on (001), 1.548 and 1.543 on (010). This would indicate a composition near Ab_{68} An_{32}.

Upon calculation of the norm, 21.68 per cent standard orthoclase molecule is obtained; some of the microlites in the glassy matrix are probably sanidine, although the mineral could not be positively determined.

Colorless to pale-green, irregular grains or euhedral crystals of augite, either prismatic or four- and eight-sided when euhedral, are found. They may be as large, corroded inclusions, or as tiny, sharp grains in the glassy groundmass.

A complete rock analysis on a sample collected on the Sugarloaf Mountain trail about 150 feet below the top of member 1 was made by Lois D. Trumbull. This analysis and the calculation of the normative minerals, com-

TABLE 4.—CHEMICAL ANALYSIS AND CALCULATED NORM FOR MEMBER 9

	Wt. %	Mol.	ap	il	pv or	pv ab	an	mt	hm	di	hy	Q
SiO_2	62.55	1.042	....	....	.234	.366	.114	....	....	.020	.035	.273
Al_2O_3	16.04	.157	....	....	.039	.061	.057	....	....	....	....	.....
Fe_2O_3	3.75	.023	....	....	....	....	....	.012	.011	....	....	.....
FeO	1.58	.022	....	.010	....	....	....	.012	....	....	....	.....
MgO	1.82	.045	....	....	....	....	....	....	....	.010	.035	.....
CaO	4.32	.077	.010	....	....	....	.057	....	....	.010	....	.....
Na_2O	3.76	.061	....	....	....	.061	....	....	....	....	....	.....
K_2O	3.67	.039	....	....	.039	....	....	....	....	....	....	.....
H_2O+	.49	....	....	....	....	....	....	....	....	....	....	.....
H_2O-	.52	....	....	....	....	....	....	....	....	....	....	.....
TiO_2	.82	.010	....	.010	....	....	....	....	....	....	....	.....
CO_2	.01	....	....	....	....	....	....	....	....	....	....	.....
P_2O_5	.38	.003	.003	....	....	....	....	....	....	....	....	.....
MnO	.09	.001	....	....	....	....	....	....	....	....	....	.....
	99.80	1.480										
% *wts.*	....	....	1.01	1.52	21.68	31.96	15.85	2.78	1.76	2.16	3.50	16.38 = 98.50

The maximum diameter of the included grains is near 1.5 mm.

Some green, pleochroic laths of hornblende as much as 2 mm long are found, most commonly in the uppermost 25 feet of the flow, partially altered to chlorite.

Quartz has been observed as occasional phenocrysts of irregular size, but no more than 0.2 mm in diameter, or as small grains, with diameters 0.05 mm or less, associated with the feldspar needles and square grains of augite in the glassy groundmass.

Grains of magnetite, up to 1 mm in diameter, occur as phenocrysts, and a good deal of dusty magnetite is scattered throughout the groundmass.

Colorless to brown glass, with an index of refraction of 1.512, makes up a very large proportion of the rock. In much of the rock the glass has partially or wholly devitrified, but in the vesicular, upper portion of the flow no devitrification has taken place. According to George (1924, p. 368), an index of 1.512 indicates a glass of dacite, trachyte, or andesite composition.

Chalcedony appears to be secondary, deposited in the vesicular, upper part of the flow. It is generally seen as spherulites or spherulitic masses occupying the vesicles.

puted according to the method suggested by Cross, Iddings, Pirrson, and Washington, are given in Table 4. Weight percentages of normative minerals used in the Johannsen classification places the rock in subdivision (227 E) for which the recommended name is rhyodacite.

Origin.—Since member 9 lies on and parallel to a series of welded tuffs, it might itself be a welded tuff rather than a flow. Unfortunately the outcrop is limited to the very crest of Sugarloaf Mountain and is so covered with talus that adequate field study is difficult, thus necessitating heavy reliance upon a petrographic study of the rock.

Although the lower portion of member 9 is quite dense, it becomes vesicular toward the top. It does not, however, lose its coherency with an increase in porosity as does a welded tuff. The rock matter between the vesicles maintains its dense, brittle nature, indicating a vesicular structure resembling that which develops in the upper portion of a flow. No shards, pumice fragments, or vitroclastic texture are noted, and the typical microscopic eutaxitic structure of the welded tuffs is also missing. Microlites and skeleton crystals of plagioclase haphazardly oriented in the glassy groundmass bear evidence to crystallization in a coherent matrix rather than to a clastic ori-

gin. The rock is notably lacking in the inclusions of solid rock material, such as the cindery, red inclusions or the gray pumice common to the welded tuffs in this region. All of this evidence appears to rule out the pyroclastic origin necessary in a welded tuff, and to indicate solidification of a molten or semifluid stream.

Structure of Rhyolite Canyon Formation

Attitude of the Beds

The inclination of the welded tuffs is, in general, gentle and westerly. The strata form a broad, gently dipping, asymmetrical syncline plunging toward the west at about 3°. The local dip varies, depending upon the position of the strata with respect to the syncline and with respect to a fault zone trending southeast parallel to upper Bonita and Whitetail canyons. The axis of the syncline runs almost due west from Sugarloaf Mountain, giving rise to a very gentle, westerly dip in Bonita and Rhyolite canyons and intervening areas. To the north of this axis the dip becomes southwesterly, reaching angles of 15°–25° in North Bonita Canyon and West Whitetail Canyon. To the south of the axis the dip swings to the northwest, but is more gentle, usually no more than 10°.

Along the fault zone paralleling West Whitetail, upper Bonita, and Whitetail canyons strong anomalous dips appear. These are particularly noticeable along the road from Bonita Park to Massai Point where easterly dips of 30°–40° are noted. One quarter mile west from this road the normal, gentle westerly dip resumes. In this area of anomalous dips the joints, which are normally vertical, are inclined at various angles but are always perpendicular to the eutaxitic structure.

Faults

The welded tuffs are cut by a number of number of faults striking about S. 30°W. The fault planes are almost vertical, and the northeastern block is usually downthrown. The vertical movement on these faults tends to counteract the regional dip. The base of member 6 in upper Rhyolite Canyon has an elevation of 6100 feet, while 3 miles west at a point above Faraway Ranch it is at 5600 feet. Since the westerward dip of the beds is at 3°, the base of the formation should be at 5270 feet. Three faults are crossed during this traverse, and in each case the westerly block has been upthrown, causing the 330 feet gain in elevation.

Paralleling upper Bonita and Whitetail canyons, striking S. 20°–30° E., is the major fault zone which cuts both the welded tuffs and the underlying rocks. The anomalous dips along the road from Bonita Park to Massai Point are thought to be due to drag in this zone. In this instance the block northeast of the fault zone seems to have been upthrown.

Joints

Both Marshall (1935, p. 342) and Gilbert (1938, p. 1855) point to columnar jointing as a distinctive feature in welded tuffs, and attribute it to contraction in a cooling mass. When rupture takes place in the cooling and contracting mass three vertical fractures, making angles of 120° with each other, radiate out from numerous centers located on the horizontal plane. If these centers are evenly distributed, the fractures will bound hexagonal columns. While the columns are ideally hexagonal the fractures may be irregularly distributed, and three-, four-, or five-sided prisms may result. Each of these columns is a distinct entity, and the joints are short, ending at an intersecting joint within a few feet at most.

Upon first sight the vertically jointed rhyolites and some of the cliffs at Chiricahua appear to be similar to the jointed ignimbrites and cliffs described by Marshall. The similarity of the joints in the Chiricahua rhyolites to the columnar joints in flows and sills led Maxwell (1941, p. 22), who did the pioneer work in the area, to attribute the origin of the joints to contraction of the rhyolite on cooling.

Closer inspection, however, indicates that the joints bear no real similarity to contraction joints. The rock columns outlined by the jointing are generally four-sided and many are almost square in cross-section. Rectangular masses, roughly rounded by weathering, may be as much as 30 feet in diameter and stand as single pillars over 150 feet high. The columns are not bounded by irregularly distributed, short joints forming three- to six-sided prisms but by intersecting joint sets. These joints may

be traced for some distance, and may serve to bound several columns. In some localities one set of joints is better developed than the other, and tabular rock masses rather than columns are formed. The so-called "Chinese Wall" in lower Hunt Canyon is a notable example of this feature. In Rhyolite Canyon and on the flanks of Sugarloaf Mountain a sequence of strata revealing the contacts between members 5, 6, and 7 can be seen, and joints extend from one member into another without break and without change in pattern.

A great many bearings on joint directions were taken, and in most of the Monument two or three regular, well-developed sets of joints were present, along with minor joints whose bearings were so variable that no pattern could be determined for them. A study of aerial photographs indicated that the major joint sets were readily observed. Many gullies and tributaries were joint-controlled, and the vegetation was concentrated along the major joints. In certain areas the rock columns or tabular masses were easily observed in the photographs, and their bounding joints were easily plotted. The average bearings of the major joint sets plotted along with the major faults in the area helped reveal the origin of the joints.

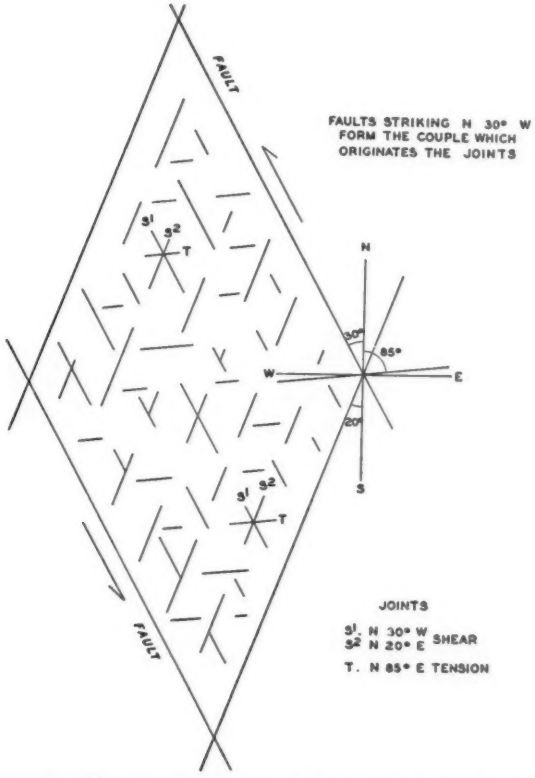

FIGURE 4.—APPLICATION OF A NORTHWEST-SOUTHEAST SHEAR DIAGRAM TO FAULTS AND JOINTS IN THE RHYOLITE CANYON FORMATION

The major joints in the welded tuffs of Chiricahua National Monument are vertical joints caused by a couple in the blocks between the normal faults. Two sets of shear joints and one set of tensional joints result. Figure 4 represents the faults and the three sets of joints resulting from the couple. Shear joints are represented by S^1 and S^2, the ten-

sional joints by T. The majority of the joints in the area correspond to the directions N. 30° W., N. 20° E., or N. 85° E., within limits of 10° east or west of the preferred bearing. The shear joints bearing N. 30° W. and paralleling the faults are usually the best developed, and are sometimes the only set that can be mapped from aerial photographs. The second set of shear joints bearing N. 20° E. is next in importance, while the tensional joints bearing N. 85° E. are well developed only in the extreme southeast and northwest portions of the area, although generally present throughout the Monument. It is common for only two, well-developed sets of joints to appear, but in many cases all three sets are well defined.

Origin

The name rhyolite comes from the Greek meaning "lava stream" or "torrent," indicating the origin from solidification of a stream of molten rock material. The name rhyolite tuff was applied to fragmental, volcanic deposits of rhyolite that had been compacted or cemented into a coherent rock. Such rhyolite masses exhibit certain characteristics indicative of their modes of origin. Most of the rhyolite masses of the Rhyolite Canyon formation are not solidified sheets or streams of molten rock, nor are they tuffs resulting from ash showers.

Rhyolitic lava is generally very viscous; hence, flows of rhyolite are apt to be tongue-like masses of small to moderate size, thick in the middle and thinning toward the edges where they congeal to form steep slopes. The steep edges and front break away in red-hot boulders as the lava moves. As the flow spreads over it this mass of debris is incorporated into the basal portion as accumulations of breccia. The upper surface of the flow is also apt to be rough, marked by the development of a mass of blocks.

Upon explosive eruption various types of magmatic or volcanic debris are formed. Pumice lumps, lapilli, and large amounts of ash from sand to dust grades are thrown out of the vent. This debris may be thrown and drifted by wind currents for many miles, settling over the country as a mantle of ash. Ash thrown out in such a manner may be, and usually is, comparatively cool when it settles out of the air. When consolidated this material is termed tuff or breccia, depending upon its grade size. The finer material may be found many miles from the vent. This material falls on all surfaces alike, and commonly follows, but modifies, the relief of the land. A tuff is usually loose, porous, friable, and soft, readily allowing the point of pick to penetrate the rock without fracturing it.

Extrusive rhyolite rocks which apparently have not been formed by streams or flows of liquid rock nor by the usual ash showers have been described from New Zealand, eastern California, Sumatra, and other localities. The rocks have been termed ignimbrite by Marshall (1935, p. 323), but they are usually termed welded tuff (Iddings, 1909, p. 331) in this country. Welded tuffs are thought to be due to eruptions of superheated gases, heavily charged with incandescent ash and volcanic sand which have been termed *nuées ardentes*, or glowing clouds, by Lacroix (1904, p. 203). This material is not rained down as from an ash shower but descends the mountain side like a hot avalanche. So much solid is suspended in the cloud that it becomes too dense to surmount obstacles and behaves rather like a liquid. Frank A. Perret (1937, p. 84) believes the mobility is due to subdivision of the lava into liquid particles which are enveloped and suspended in a highly-compressed gaseous atmosphere, caused largely by continuous vapor emission by the particles themselves. There is developed during the descent of the avalanche a violently expanding cloud of gas and ash, often referred to as a "great black cloud," which tends to hide the hot-sand avalanche beneath it.

Two processes have been postulated for induration of the debris left behind by the *nuées ardentes*. The fragments of incandescent material might well adhere and weld themselves together, especially if subjected to pressure from an overburden; or recrystallization under the influence of hot gases could bring about induration.

Westerveld (1943, p. 211–212; 1947, p. 34) and Fenner (1948, p. 883) emphasize the part played by recrystallization in the induration of the deposits of *nuées ardentes*. Fenner advocates using the term welded tuff only for deposits indurated primarily by heat, and the term sillar for deposits indurated by recrystallization. The

secondary minerals formed by recrystallization are said by Fenner to be tridymite and orthoclase or natrosanidine; and he writes that the recrystallization is due to pneumatolytic exhalations, but fails to mention their source. Westerveld attributes the formation of tridymite and albite in the welded tuffs of Sumatra to recrystallization of the glassy groundmass under the influence of gases rising from the lower levels of the tuff mass immediately after emplacement.

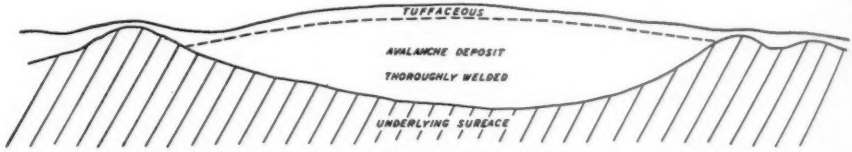

FIGURE 5.—CROSS SECTION OF A TYPICAL DEPOSIT OF *NUÉE ARDENTE* ORIGIN

Of the nine members comprising the Rhyolite Canyon formation seven exhibit all the characteristics typical of welded tuff. Induration of these seven members is thought to be due primarily to union of the glass shards by heat and pressure, and hence, they belong to the true class of welded tuffs as defined by Fenner.

The capping member 9 is a flow; member 7 might be due to an ash shower or to marginal deposition of the upper or "great black cloud" portion. Petrographic study of member 7 gave inconclusive evidence, and the outcrop area was too small to furnish adequate field evidence.

The deposits at Chiricahua suggest several eruptions of *nuées ardentes* piling up hundreds of feet of material. While several *nuées* laid down what might be termed a normal or typical kind of depositional unit, many variables are involved which may drastically modify this so-called typical unit. A typical unit of deposition consists of a lower firmly welded portion containing pumice and other rock inclusions of a coarse nature with eutaxitic structure developed by collapse of these coarse inclusions, overlain by an upper, less coherent portion, finer in grade size and with an even texture. In addition to the vertical gradation, there is also a gradation from the center toward the margins of the lens of welded tuff. A cross section of this typical deposit is shown in Figure 5.

The thoroughly welded portion of the deposit is lower in porosity, higher in specific gravity, and darker in color than the tuffaceous portion. It is generally richer in phenocrysts and inclusions, contains a higher proportion of glass in the groundmass, and exhibits microscopic as well as megascopic eutaxitic structure.

The two-fold nature of the typical welded tuff deposit is a natural outgrowth of the two-fold nature of the *nuée*: the hot avalanche moving along the ground carrying great blocks and incandescent fragments, and the great black cloud of hot dust and gas, towering thousands of feet above, carrying finer and cooler material. The major variables capable of modifying the typical deposit are (1) explosive power, temperature, size, composition of magma, and type of inclusions of the *nuée ardente*, (2) distance of the deposit from the vent or fissure, (3) rapidity of eruptions, and (4) character and conditions of the underlying surface.

Gradations might be expected between the typical *nuée* and the completely vertical, explosive activity which gives rise to the ash shower on the one hand, and between the *nuée* and true lava flows on the other. Perret (1937, p. 97) discussed modifications of the *nuée ardente* to some extent, dwelling particularly upon the block and ash flow type of *nuée* which contains lava of the weakest gas charge and forms deposits resembling the ordinary aa flow. Williams (1941, p. 279) states, "We can no longer doubt that between true lavas and flows of gas-glass-dust emulsion there are all gradations."

There is certain to be variation in temperature of the erupted material. The feeble type of *nuée* described by Perret is lacking in gas, and hence energy. In the debris left by such eruptions poor welding might result, even though the deposit were very thick; or the finer dust and ash might be thoroughly welded, while the

FIGURE 6.—SECTION THROUGH CHIRICAHUA NATIONAL MONUMENT FROM THE NORTHEAST CORNER TO BONITA CANYON NEAR RANGER HEADQUARTERS

pumice fragments and inclusions would be too cool and strong to collapse, and thus the eutaxitic structure would not be formed.

The mass of material emitted would certainly affect the resulting deposit, with heavy overburden as well as high temperature facilitating thorough welding and the development of distinct eutaxitic structure in the basal portions. A very small *nuée* might leave a deposit of such small size and low temperature that little welding would be possible, and hence it might be difficult to distinguish from an ash-shower deposit.

The distribution and size of the separate deposits studied at Chiricahua and the great area covered by welded tuffs in the Chiricahua Mountains would indicate more than one vent. The possibility of a number of vents scattered over a large area and penetrating country rock of different composition would introduce other variables, resulting in *nuées* formed from magmas of different composition, bearing different inclusions.

Both the size of the *nuée* and the distance it has traveled will affect the deposit. The extreme outer edge of the deposit would be due solely to the great black cloud in a very weakened form with no avalanche material present, and hence would be indistinguishable from an ash shower type of deposit.

The time interval between separate eruptions is important in controlling the type of deposits resulting from *nuée ardente* activity, as was pointed out by Gilbert (1938, p. 1858). If several flows followed one another very closely time might be insufficient for the fine material to settle out from the great black cloud, and the separate avalanche might deposit a considerable pile of material with or without distinct zones or surfaces of separation.

Both Marshall (1935, p. 338) and Gilbert (1938, p. 1858) point out that the character of the underlying surface would affect the deposition of the welded tuff. Large depressions would confine the flow, thus forming unusually thick deposits; while a cold surface or a water-saturated surface might develop a glassy, incoherent base, or develop secondary explosions. A hot underlying surface, such as newly deposited eruptive material, would aid in the welding of the lowermost layer of the deposit.

Considering all these variables, in addition to the tendency in volcanic eruptions to mix flows with explosive phenomena, one could readily predict the type of volcanic rock that would collect about vents with a pronounced leaning toward the expulsion of *nuées ardentes*. Such are the deposits found at Chiricahua National Monument, and a consideration of the variables mentioned will lead to an understanding of all the depositional and petrographic features noted in the Rhyolite Canyon formation.

Source of Material

The volcanic deposits at Chiricahua National Monument represent but a small portion of the volcanic rocks of the Chiricahua Mountains. The major tuff deposits of the Chiricahua Mountains lie to the south and west of the Monument. Little is known of the deposits of the main Chiricahua range, but the deposits of the Monument thin noticably to the west, indicating a source to the east. Some members thin to the south, but others thicken to the south, suggesting more than one vent to the east.

Maxwell (1941, unpublished report, Natl. Park Service, p. 19) suggested that the intrusive igneous mass extending southeast from Cochise Head to Maverick Peak might occupy the site of the vent that gave rise to the volcanic rocks of the Monument. However, a series of vents running S. 35° E. from Cochise Head, parallel to the prominent fault zone, might well have furnished the source for the rhyolites of the entire northern part of the Chiricahua Mountains. Little definite evidence is available, however, and without more information the location of the source of the volcanic activity can be only a matter for speculation.

Summary

The rocks cropping out in Chiricahua National Monument consist of the Lower Permian Chiricahua limestone, the basal portion of the Lower Cretaceous Bisbee group, basalt flows and rhyolite dikes of doubtful Cenozoic or Cretaceous age, and a thick sequence of predominately rhyolitic volcanic rocks with interbedded, lacustrine sedimentary rocks which

are thought to be Cenozoic, perhaps Miocene and younger.

The stratified rocks of the Monument dip westward, forming a monoclinal block which is broken along the crest of the Chiricahua range in this region by a fault zone striking S. 20°–30° E. The northeastern fault block has been upthrown and eroded, and the Paleozoic sedimentary rocks are exposed in contact with the thick, Cenozoic volcanic rocks in the southwestern block. The Cenozoic volcanics are cut by several normal faults striking S. 30° W., with the northeastern block generally downthrown. Owing to shear developed by movement along the normal faults, the blocks of volcanic rock lying between the normal faults have been broken into rectangular units by three sets of vertical joints.

The thick volcanic sequence of the Monument is divided into two natural subdivisions by an angular unconformity. The lowermost section has been termed the Faraway Ranch formation, and the uppermost the Rhyolite Canyon formation.

The Rhyolite Canyon formation consists of 1900 feet of stratified, volcanic rock, the major portion of which is made up of welded tuffs or ignimbrites which are the result of a series of volcanic eruptions of the *nuée ardente* type. Typical welded-tuff units consist of a rhyolite layer, grading from a light-gray, porous, loosely cohering, tuffaceous top down into a grayish-red, dense, coherent base which rings when struck with the hammer and exhibits a well-marked eutaxitic structure. The formation is capped by a flow of rhyodacite 220 feet thick which is underlain by eight parallel layers, all but one of which are certainly of *nuée ardente* origin. These strata generally exhibit the features listed as typical of a welded-tuff unit, but show occasional anomalies which can be traced to variables within the *nuée ardente* itself, the character of the underlying surface, the rapidity of eruption, or the distance from the vent. The thickness of each complete stratum of welded tuff is variable, reaching a maximum of 880 feet and a minimum of 2½ feet. A series of vents to the east of Chiricahua National Monument is considered a plausible source for the volcanic sequence.

Analysis of Characteristic Features of the Welded-Tuff Variety of Nuées Ardentes Deposits

According to the usage of Iddings (1909, p. 323) and Fenner (1948, p. 883) deposits of *nuées ardentes* are not always welded tuffs, but welded tuffs form from hot pumice and volcanic glass from a *nuée ardente* eruption of the Peléan or Katmain variety. A review of the literature, in particular articles by Lacroix (1930), Moore (1934), Mansfield and Ross (1935), Marshall (1935), Gilbert (1938), Williams (1941), and Westerveld (1943, 1947), reveals many identifying features typical of the welded-tuff deposits of *nuées ardentes*.

A study of the rhyolites at Chiricahua National Monument can help verify or modify these generalizations. Because deposits of *nuées ardentes* are gradational with those of ash showers and lava flows, exceptions will be found to all "typical" characteristics. Of 24 diagnostic features gained from the literature, 10 appear to be so generally true as to require little comment, while the others may be only locally true, or even contradictory, and hence require clarification and explanation.

It is generally true that:

(1) A brecciated base is wanting.

(2) A scoriaceous surface is lacking.

(3) The upper surface of the deposit approaches the horizontal plane. The lower surface is likewise very regular, showing little or no roughness such as that generally seen on the lower surface of a lava flow.

(4) There is no indication of mass flow.

(5) The rocks may contain inclusions, especially of fairly large pumice blocks. Chips and fragments of the older rocks of the region may be found in the tuff, but are not abundant.

(6) Pumice fragments, very porous and unoriented at the top of a welded tuff or ignimbrite, are progressively collapsed, flattened, and aligned in the horizontal plane toward the base.

(7) The material is restricted to an area which is smaller than the area which would correspond to its particle size if formed of ash shower or projected type of material.

(8) Though there is no scoriaceous structure, the specific gravity of the rock is low.

(9) Variation is rapid from tuff and breccia to a coherent, flowlike rock. This variation is related to a regular change in the individual sheets, both from top to bottom and from the middle toward the margins.

(10) The extent of the deposit is greater than that of volcanic avalanches.

Features which are only locally valid or contradictory, or which benefit by further clarification may be summarized as follows:

(1) The rock masses are coherent and quite solid, commonly ringing under the hammer.

This is characteristic only of the lower and thoroughly welded portion of the typical welded tuff deposit. The uppermost portion could be indistinguishable from an ash-shower tuff if the lower gradational contact were obscured. The outermost deposit of the *nuée ardente*, or the deposit of a very small *nuée* might likewise fail to become thoroughly welded.

(2) There is an increase in specific gravity from the top to the bottom of each formation or complete layer.

In the very thick layers studied at the Monument a constant specific gravity is obtained within a hundred feet or less of the top of the individual members, and no further change is noted. In the lower 780 feet of the very thick member 6 no change in specific gravity takes place. If the upper hundred feet were removed by erosion, the resulting deposit would show no variation from top to bottom.

(3) There is a marked gradational variation in porosity between the top and bottom of a layer of ignimbrite or welded tuff.

The porosity, like the specific gravity, tends to reach a fixed value in the upper 50–100 feet, and exhibits no further change.

(4) Microscopic eutaxitic structure is shown by the bending of viscous glass shreds about previously existing crystals.

This is not found in the upper 25–50 feet of incoherent tuff.

(5) Microscopic examination shows vitroclastic structure or recognizable shards of glass, fragments of bubble walls, pumice grains, and angular inclusions of rocks of different color or texture.

Vitroclastic texture and recognizable clastic fragments of glass are best seen in the upper, less coherent portion of the welded-tuff unit, and tend to disappear in the lower, more thoroughly welded tuff.

(6) The rocks show a streaky, varicolored banding or eutaxitic structure.

This is true only of the more coherent, lower portions of the welded-tuff unit, and not always there. Member 1 of the Rhyolite Canyon formation lacks this structure, and member 3 exhibits very little. Some of the thin welded-tuff members of southeastern Idaho fail to show this feature. However, at Chiricahua it is the general rule.

(7) There is a pronounced columnar structure, or, as stated by some writers, the rock shows pronounced prismatic jointing.

The terms columnar or prismatic structure and columnar or prismatic jointing, when applied to igneous rocks, commonly refer to joints or columns bounded by joints which have been formed by contraction of the cooling rocks. In many outcrops of welded tuff a prominent columnar structure is present, and seems to have been formed by contraction on cooling. The vertical jointing at Chiricahua which leads to the formation of the massive rock columns is, however, almost certainly of tectonic origin. Some of the thinner welded-tuff members of the Monument exhibit tectonic joint patterns which do not lead to the formation of rock columns and, hence, do not possess any type of columnar structure. It must be concluded that the development of prismatic jointing or columnar structure in welded tuffs is of local importance. A welded-tuff origin for volcanic strata is possible even though prominent columnar structure or prismatic jointing were missing.

(8) There is an absence of bedding, and no alignment of particles.

This contradicts number 6 in the list of features generally present. This concept was probably gained from a study of very thin deposits, for as the deposits increase in thickness a progressive flattening and alignment of the inclusions appears forming eutaxitic structure parallel to the base of the formation. Bedding is expressed not only by the several welded-tuff members which exhibit lenses or strata of similar lithology, but also by an imperfect, graded bedding noted within each member. In most welded-tuff members at

Chiricahua the base contains coarse inclusions, such as blocks and lapilli, which gradually give way to ash and dust toward the top. The top of the formation is poorer in phenocrysts of sanidine and quartz than is the underlying material.

(9) The rocks have a uniform and normally fine texture.

The texture varies from top to bottom of the individual deposits, and varies also with the number of inclusions found in the particular deposit.

(10) The material is unsorted, and shows no relationship between coarseness and the position of the source.

No specific information concerning the latter part of this statement was gained at Chiricahua, but a sorting was certainly noted. The welded-tuff members characteristically exhibit graded bedding if they are sufficiently thick, although this bedding is very crude. The graded bedding noted in the welded-tuff members at Chiricahua can be predicted from a consideration of the structure of the *nuée ardente*. All observers emphasize the hot-sand avalanche at the base and the black cloud above containing gases and hot dust.

(11) The material is derived from one magma and contains no extraneous matter, with the exception of carbonized vegetable remains.

The majority of the material is undoubtedly derived from one magma, but extraneous matter such as inclusions, in addition to vegetable remains, is not at all uncommon. Gilbert (1938, p. 1838–1839) points out that chips and fragments of nearly all the older rocks of the region may be found in the welded tuffs of eastern California, although stating that they are not abundant. The dense, dusky-red inclusions found in the welded tuffs at Chiricahua are never abundant but appear to be solid fragments of a foreign nature. The light-gray inclusions found in the dusky-red matrix of member 3 are likewise extraneous inclusions, and in places abundant.

(12) The material is found on ridges and slopes, as well as in valleys and flats.

Although this characteristic was originally set up merely to help differentiate deposits of *nuées ardentes* from those of mudflows, it is still stated as a general characteristic. It may be present as erosional remnants on ridges, but the fluidity of the *nuée* leads to channeling of the deposits, and hence they are most likely to be found in valleys and flats.

(13) A thin bed of extremely fine glass dust occurs below the formation in typical localities.

This is true only locally. Marshall (1935, p. 299) mentions it in New Zealand ignimbrites, and Williams (1941, p. 279) refers to it in the case of the Aso lavas of Kyusyu; no such deposit was found at Chiricahua National Monument. An underlying cold surface would probably be required for the quick chilling which would prevent welding and flattening of the pumice fragments.

(14) The borders of each shard are minutely recrystallized, and small pores between shards are lined with larger crystals; or the interstices between shards and the shards themselves may be permeated by secondary, pneumatolytic mineral growths. These crystals are tridymite and orthoclase, natrosanidine or albite, depending upon the composition of the original rock mass and its released gases.

Recrystallization is apparent in the welded tuffs at Chiricahua, but no tridymite was noted and the recrystallization is thought to be due to spontaneous crystallization or devitrification in glass aided by high temperatures rather than to pneumatolytic mineral growths. Pneumatolytic mineral growths appear to be a local phenomenon.

References Cited

Berry, J. Allan, 1928–29, The volcanic deposits of Scinde Island. With special reference to the pumice bodies called chalazoidites: New Zealand Inst. Trans. and Proc., v. 59, p. 571–608.

Cotton, C. A., 1944, Volcanoes as landscape forms: Wellington, Whitecombe and Tombs Ltd., 416 p.

Day, A. L. and Shepherd, E. S., 1913, Water and volcanic activity: Geol. Soc. America Bull. v. 24, p. 573–606.

Enlows, H. E., 1951, The igneous geology of Chiricahua National Monument, Arizona: Tulsa Geol. Soc. Digest, v. XIX, p. 105–107.

Fenner, Clarence N., 1948, Incandescent tuff flows in southern Peru: Geol. Soc. America Bull., v. 59, p. 879–893.

George, William O., 1924, The relation of the physical properties of natural glasses to their chemical composition: Jour. Geology, v. 32, p. 353–372.

Gilbert, Charles M., 1938, Welded tuff in eastern California: Geol. Soc. America Bull., v. 49, p. 1829–1861.

Iddings, J. P., 1909, Igneous rocks: N. Y., John Wiley and Sons, v. 1, 464 p.

Jaggar, T. A., Jr., 1917, Volcanologic investigations at Kilauea: Am. Jour. Sci., 4th ser., v. 44, p. 161–220.

Johannsen, A., 1932, A descriptive petrography of the igneous rocks: Chicago, University of Chicago Press, v. 2, 428 p.

Kozu, S., 1934, The great activity of Komagatake, in 1929: Tschermak's Mineralogische und Petrographische Mitteilungen, v. 45, p. 133–174.

Lacroix, A., 1904, La Montagne Pelée et ses eruptions: Paris, Acad. des Sciences, 662 p.

—— 1930, Remarques sur les materiaux de projection des volcans et sur la genese des roches pyroclastiques qu'ils constituent: Jubilee vol. centenaire de la Soc. Geol. de la France, v. 2.

Lasky, S. G., 1938, Geology and ore deposits of the Lordsburg mining district, Hidalgo County, New Mexico: U. S. Geol. Survey Bull. 885, 62 p.

Mansfield, C. R., and Ross, C. S., 1935, Welded rhyolitic tuffs in southeastern Idaho: Am. Geophys. Union Trans., 16th ann. mtg., p. 308–321.

Marshall, P., 1935, Acid rocks of the Taupo-Rotorua volcanic district: New Zealand Inst. Trans. and Proc., v. 64, p. 323–375.

Moore, Bernard N., 1934, Deposits of possible *nuée ardente* origin in the Crater Lake region, Oregon: Jour. Geology, v. 42, p. 358–375.

National Research Council rock-color chart committee, 1948, Rock-color chart: Washington, D. C., Nat. Research Council.

Perret, F. A., 1937, The eruption of Mt. Pelée 1929-1932: Carnegie Inst. Washington, 126 p.

Stoyanow, A. A., 1926, Kaibab fauna in southeastern Arizona: Amer. Jour. Sci., 5th ser., v. 12, p. 318–319.

Vogt, J. H. L., 1921, The physical chemistry of the crystallization and magmatic differentiation of igneous rocks: Jour. Geology, v. 29, p. 318–350.

Washington, H. S., 1917, Chemical analyses of igneous rocks: U. S. Geol. Survey Prof. Paper 99, 1201 p.

Westerveld, J., 1943, Welded rhyolitic tuffs or "ignimbrites" in the Pasoemah region, West Palembang, South Sumatra: Leidsche Geol. Meded., v. 13, p. 202–217.

—— 1947, On the origin of the acid volcanic rocks around Lake Toba, North Sumatra: Kon. Ned. Akad. v. Wet., Verh. (Tweede Sectie), DL. XLIII, no. 1, p. 1–52.

Williams, Howel, 1941, Calderas and their origin: Univ. Calif. Publ., Bull. Dept. Geol. Sci., v. 25, no. 6, p. 239–346.

Department of Geology, University of Tulsa, Tulsa 4, Okla.

Manuscript Received by the Secretary of the Society June 8, 1954

BULLETIN OF THE GEOLOGICAL SOCIETY OF AMERICA
VOL. 66, PP. 1247-1256, 1 FIG. 1 PL. OCTOBER 1955

PRECAMBRIAN MONAZITE AND ZIRCON FROM THE MOUNTAIN PASS RARE-EARTH DISTRICT, SAN BERNARDINO COUNTY, CALIFORNIA

BY HOWARD W. JAFFE

ABSTRACT

Age determinations were made of three monazite samples from carbonate rock and four zircon samples from the associated shonkinite of the Mountain Pass district, San Bernardino County, California. The determinations made by the alpha-counting and total-lead method gave an average age of 950 million years for monazite and 840 million years for zircon. One of the monazite samples contains 2.65 per cent thorium, 0.002 per cent uranium, and 0.1130 per cent lead, giving a maximum age of 955 million years uncorrected for original lead. The Pb^{208}/Th^{232} age of this monazite is 925 million years, based on an isotopic analysis of the monazite lead corrected for original lead by an isotopic analysis of galena lead from the same deposit. The monazite lead is 98.854 per cent radiogenic of which 98.342 per cent is Pb^{206} and 0.512 per cent is Pb^{207}. The isotopic composition of the galena lead is similar to that of Precambrian galena from other localities.

Optical properties of the monazite are: $\alpha = 1.779, \beta = 1.781, \gamma = 1.833$, 2V (calc.) = 26° (+), $r < v$, $Z \wedge c = 7°$, and $Y = b$. The density measured on the Berman microbalance is 4.98; the density calculated from the rule of Gladstone and Dale, $n - 1/d = K$, is 5.03. Other data include spectrographic and chemical analyses of the monazite.

CONTENTS

TEXT

	Page
Introduction	1247
Acknowledgments	1249
Location of monazite samples	1249
Separation and purification of monazite	1249
Optical properties and density of monazite	1249
Spectrographic and chemical analyses of monazite	1250
Isotopic analyses of galena and monazite	1252
Age of monazite from the Pb^{208}/Th^{232} ratio	1253
Age of monazite by the Larsen method	1253
Age determinations of zircon from shonkinite	1254
Petrographic relations of monazite and bastnaesite	1255
Geological significance	1256
References cited	1256

ILLUSTRATIONS

Figure	Page
1. Distribution of monazite and bastnaesite in the Sulphide Queen carbonate body, Mountain Pass, San Bernardino County, California	1248

Plate	Facing page
1. Monazite and bastnaesite in carbonate rock	1254

TABLES

Table	Page
1. Chemical analysis of monazite of sample SQ-81, Sulphide Queen carbonate body, Mountain Pass, California	1250
2. Isotopic abundance of lead from galena, SP-56, Sulphide Queen carbonate body, Mountain Pass, California	1251
3. Analytical data and age calculations for monazite of sample SQ-81, Sulphide Queen carbonate body, Mountain Pass, California	1251
4. Isotopic composition of lead from galena of different geological age calculated in atom per cent and with reference to Pb^{204} as 1.00	1252
5. Original lead in monazites	1253
6. Age determinations of monazite, Mountain Pass, California	1253
7. Modal analyses of shonkinite, sample NM-1, Mountain Pass, California	1255
8. Age determinations of zircon from shonkinite, sample NM-1, Mountain Pass, California	1255

INTRODUCTION

The geology of the Mountain Pass district is described by Olson *et al.* (1954). Carbonate-rich rocks, composed essentially of calcite, dolomite, barite, bastnaesite, and quartz, occur as veins and irregular bodies in foliated meta-

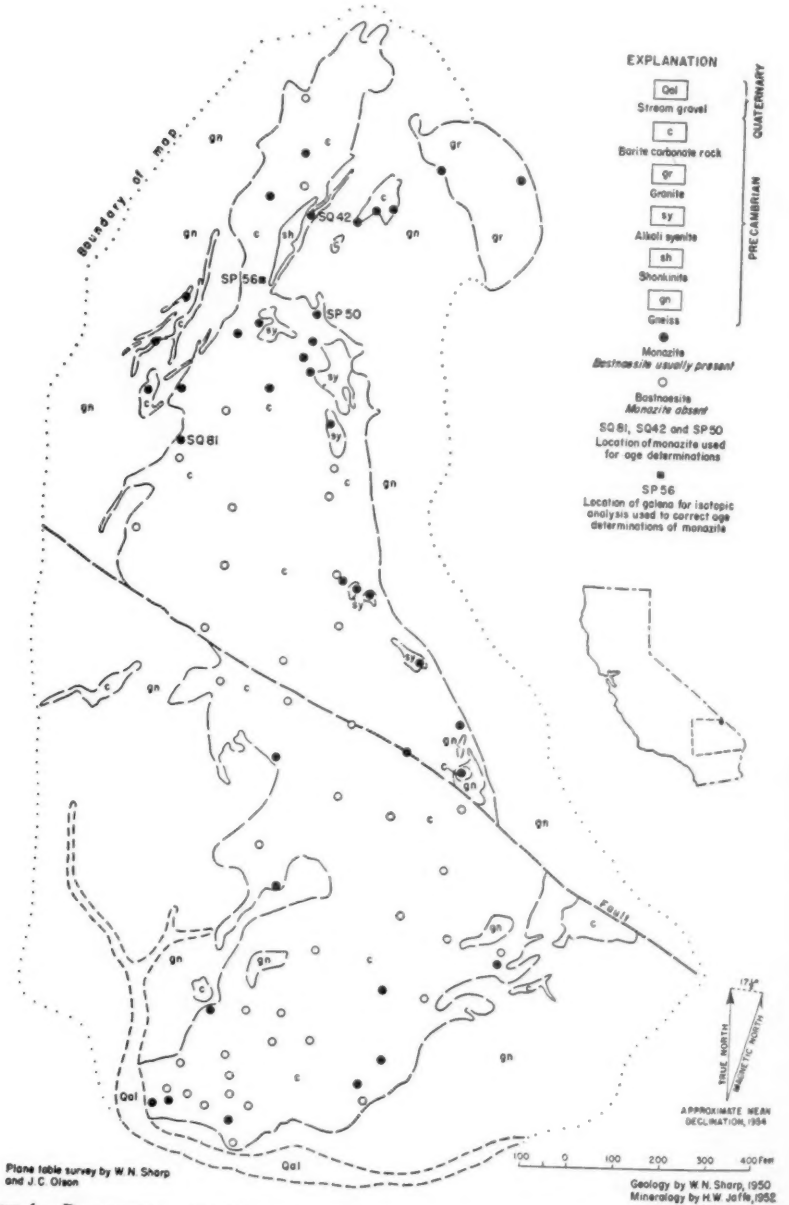

FIGURE 1.—DISTRIBUTION OF MONAZITE AND BASTNAESITE IN THE SULPHIDE QUEEN CARBONATE BODY, MOUNTAIN PASS DISTRICT, SAN BERNARDINO COUNTY, CALIFORNIA

With index map showing San Bernardino County and area mapped

morphic Precambrian rocks. The largest of the irregular carbonate-rich bodies, locally referred to as the Sulphide Queen (Fig. 1), contains calcite, barite, and bastnaesite throughout. Rocks in which dolomite is the principal carbonate occur as small inclusions at the border of the carbonate body near its contact with gneiss, and in satellitic stringers into the gneiss beyond the contact. Monazite shows the same peripheral distribution, for it occurs principally in the dolomite-rich rocks and to a lesser extent in calcite-rich rocks near the contact with gneiss (Fig. 1). Monazite also occurs in a few syenite inclusions near the border of the carbonate body, in granite outside the carbonate body, and in a small mica-rich carbonate-rock area between the granite and the carbonate body (Fig. 1).

Geologic relations alone date the carbonate rocks and the associated alkalic igneous rocks as pre-Tertiary. In order to establish the geologic age a detailed study was made of the accessory minerals in the carbonate-rich rocks and in the associated shonkinite and syenite. Age determinations were made of three samples of monazite from barite-carbonate rock and four samples of zircon from coarse-grained shonkinite. Zircon concentrated from the syenite was not used in this investigation because of contamination with barite.

The results of this investigation indicate that both the shonkinite and the carbonate rocks are late Precambrian. Determinations average 840 million years for zircon and 950 million years for monazite. The most reliable determination is believed to be the Pb^{208}/Th^{232} age, 925 million years, obtained from monazite of sample SQ-81.

Acknowledgments

The author is indebted to several colleagues in the U. S. Geological Survey for assistance throughout this investigation. W. T. Pecora coordinated the laboratory and field investigations and with D. R. Shawe, J. C. Olson, W. N. Sharp, and T. B. Nolan collected samples of monazite-bearing carbonate rock and shonkinite. D. F. Hewett generously supplied the author with several grams of monazite concentrate. L. R. Stieff and T. W. Stern provided valuable suggestions for preparation of lead from monazite and galena for isotopic analysis and for methods of calculation of isotopic data. H. J. Mela prepared the lead as the iodide for isotopic analysis. E. S. Larsen, Jr., W. L. Smith, David Gottfried, and George Hayfield advised and assisted the author in separating zircon from shonkinite.

Location of Monazite Samples

The location of the three specimens yielding monazite on which age determinations were made is shown in Figure 1. Samples SQ-81 and SP-50 are medium- to coarse-grained barite-carbonate rock composed essentially of calcite, barite, bastnaesite, parisite, phlogopite, monazite, galena, pyrite, quartz, and hematite. Sample SQ-42 is a fine- to medium-grained barite-carbonate rock containing dolomite rather than calcite as the dominant carbonate mineral.

Separation and Purification of Monazite

The monazite investigated was separated and purified from barite-carbonate rocks collected by D. F. Hewett, W. T. Pecora, D. R. Shawe, J. C. Olson, and W. N. Sharp. Several grams of 40–100-mesh monazite concentrate from sample SQ-81 were contributed by D. F. Hewett. Additional monazite was separated by the author from several hand specimens of sample SQ-81, collected by D. R. Shawe, sample SQ-42, collected by W. T. Pecora and J. C. Olson, and sample SP-50, collected by W. N. Sharp.

The monazite was concentrated by sizing on 65-, 100-, and 200-mesh sieves, heavy-liquid separation in methylene iodide, and magnetic separations on the Frantz isodynamic magnetic separator. Final concentrates of 18 grams, 4 grams, and 80 milligrams of monazite were obtained from samples SQ-81, SQ-42, and SP-50, respectively. Grain counts of the three concentrates indicated 99.+ per cent purity. The remaining trace impurity was phlogopite.

Optical Properties and Density of Monazite

Optical properties of monazite of sample SQ-81 are as follows:

$$\alpha = 1.779 \pm 0.002$$
$$\beta = 1.781 \pm 0.002$$
$$\gamma = 1.833 \pm 0.002$$
$$\gamma - \alpha = 0.054$$
$$Y = b$$
$$Z \wedge c = 7°$$
$$2V \text{ (calc.)} = 26°(+), r < v$$

TABLE 1.—CHEMICAL ANALYSIS OF MONAZITE OF SAMPLE SQ-81, SULPHIDE QUEEN CARBONATE BODY, MOUNTAIN PASS, CALIFORNIA

A. M. Sherwood and H. J. Rose, analysts

Oxide	Weight per cent	Mol. ratios	Oxygens	Metals	Cations to 8 oxygens	
Ce_2O_3	36.19	1102	3306	2204	1.04	
La_2O_3	19.65	0603	1809	1206	0.57	
Nd_2O_3	8.20	0244	0732	0488	0.23	
Pr_2O_3	2.94	0089	0267	0178	0.08	1.99
Sm_2O_3	0.85	0024	0072	0048	0.02	
ThO_2	3.01	0114	0228	0114	0.05	
PbO	0.12	0005	0005	0005	0.00	
P_2O_5	29.23	2059	10295	4118	1.94	2.00
SiO_2	0.70	0117	0234	0117	0.06	
Total	100.89					

Analytical notes:

(1) U = 0.002 per cent determined fluorimetrically by Frank Cuttitta

(2) Pb = 0.1130 per cent determined spectrographically by C. L. Waring

(3) Rare earths, other than cerium, were determined by spectrochemical analysis of the rare-earth precipitate

The density measured with the Berman microbalance is 4.98. The density calculated from the indices of refraction and the chemical analysis by the rule of Gladstone and Dale, $n - 1/d = K$, is 5.03. The specific refractive energies: $k_{P_2O_5} = 0.190$, $k_{ThO_2} = 0.12$, $k_{PbO} = 0.137$, and $k_{SiO_2} = 0.207$ are those given by Larsen and Berman (1934, p. 31). The value, $k_{(Ce,La,Nd,Pr,Sm)_2O_3} = 0.144$ was calculated by the author (Unpublished data) from artificial inorganic compounds and rare-earth minerals.

SPECTROGRAPHIC AND CHEMICAL ANALYSES OF MONAZITE

A semiquantitative spectrographic analysis, in per cent, of monazite of sample SQ-81 made by Helen Worthing of the Geological Survey is as follows:

10	*1–10*	*0.1–1*
Ce La P	Th Nd Pr	Sm Si Gd Pb

0.01–0.1	*0.001–0.01*	*0.0001–0.001*
Al Sr Ba Mg Y Eu Fe	Mn	Yb

A complete chemical analysis of the monazite is given in Table 1. The atomic ratios are in close agreement with the theoretical formula $(CePO_4)_2$, and confirm the coupled substitution of $Th^{+4}Si^{+4}$ for $Ce^{+3}P^{+5}$.

During the course of the investigation it was determined that the dithizone mixed-color method (Sandell, 1950, p. 393) for the determination of lead did not give consistent results. Thirteen determinations made by this method gave values for lead ranging from 0.0675 to 0.107 per cent with an average value of 0.0809 ± 30 per cent. Apparently the method is not applicable to the determination of lead in monazite because of the presence of a large amount of phosphorus. According to Sandell (1950, p. 389), the dithizone method fails in the presence of large amounts of calcium and phosphorus and may be expected to give low results because some of the lead is carried down by insoluble phosphates to produce an incomplete dithizone extraction. A more reliable method was required for an age-determination study. An unsuccessful attempt was made to determine lead in monazite by a polarigraphic method used and described by Smales (*in* Holmes, 1948, p. 120–124). No determination was reported by the analyst because the lead was lost in one of the many separation processes required by the method. A third chemical method for the determination of lead in monazite is being studied, and the results will be reported elsewhere. The method involves separation and determination of lead by a strontium-sulfate carrier-dithizone mixed-color method modified from Sandell (1950, p. 391–395).

A spectrographic method described by Waring and Worthing (1953, p. 827–834), previously used for the determination of small amounts of lead in zircon, was found to give

TABLE 2.—ISOTOPIC ABUNDANCE* OF LEAD FROM GALENA, SP-56, SULPHIDE QUEEN CARBONATE BODY, MOUNTAIN PASS, CALIFORNIA

	Lead (atom per cent)				
	204	206	207	208	Sum
Analysis 1	1.470	23.532	22.499	52.499	100.000
Analysis 2	1.463	23.594	22.475	52.468	100.000
Average	1.466	23.563	22.487	52.484	100.000
	Lead with Pb^{204} as 1.000				
Analysis 1	1.000	16.008	15.305	35.714	68.027
Analysis 2	1.000	16.127	15.362	35.863	68.352
Average	1.000	16.067	15.333	35.788	68.188

* Isotopic analyses were made by Mass Assay Laboratory, Carbide and Carbon Chemicals Co., Y-12 Area, Oak Ridge, Tennessee.

TABLE 3.—ANALYTICAL DATA AND AGE CALCULATIONS FOR MONAZITE FROM SAMPLE SQ-81, SULPHIDE QUEEN CARBONATE BODY, MOUNTAIN PASS, CALIFORNIA

Chemical determinations, in weight per cent: Pb*, 0.1130; U†, 0.002; Th‡, 2.65.

	Isotopic abundance of lead (atom per cent)§				
	204	206	207	208	Sum
Total Pb	0.016*8*	0.782	0.258	98.943	99.999*8*
Original Pb	0.016*8*	0.270	0.258	0.601	1.145*8*
Radiogenic Pb	.....	0.512	.....	98.342	98.854*0*
	Age calculations by Kulp nomographs (1953)				
	207/206	206/238	207/235	208/232	
Ratios	.....	0.332	.....	0.0470	
Age (M.Y.)	Future	1860	Future	925	
	Age calculations from Wickman's curves (1939)				
Ratios	.....	2.89^{10-1}	.....	4.19^{10-2}	
Age (M.Y.)	Future	1880	.....	925	

* Pb determined spectrographically by C. L. Waring

† U determined fluorimetrically by Frank Cuttitta

‡ Th determined colorimetrically by A. M. Sherwood

§ Isotopic analyses made by Mass Assay Laboratory, Carbide and Carbon Chemicals Co., Y-12 Area, Oak Ridge, Tennessee.

good precision for the determination of lead in monazite. Eight spectrographic determinations of lead in monazite of sample SQ-81 were made over a period of 2 years by C. L. Waring. These are as follows: Pb = 0.1110, 0.1080, 0.1120, 0.1140, 0.1130, 0.1160, 0.1140, and 0.1150, and average 0.1130 ± 5 per cent. Further evidence of an indirect nature supporting the spectrographic method is the agreement between ages determined on zircon and monazite samples separated from rocks whose geological age has been reasonably well established from paleontological and stratigraphic studies. Ages determined by the Larsen method, described by Larsen *et al.* (1952), depend on spectrographic lead determinations and would not be expected

TABLE 4.—ISOTOPIC COMPOSITION OF LEAD FROM GALENA OF DIFFERENT GEOLOGICAL AGE CALCULATED IN ATOM PER CENT AND WITH REFERENCE TO Pb^{204} AS 1.00

Locality	Lead				Sum	Geological age
	204	206	207	208		
(1) Mountain Pass, California*	1.47	23.53	22.50	52.50	100.00	Precambrian
	1.00	16.01	15.30	35.71	68.02	
(2) Mountain Pass, California*	1.46	23.59	22.48	52.47	100.00	Precambrian
	1.00	16.13	15.36	35.86	68.35	
(3) Broken Hill, N. S. W.†	1.47	23.64	22.66	52.23	100.00	Precambrian
	1.00	16.08	15.41	35.53	68.02	
(4) Tetreault mine, Canada‡	1.47	23.92	22.28	52.33	100.00	Precambrian
	1.00	16.27	15.16	35.60	68.03	
(5) Great Bear Lake, Canada†	1.48	23.59	22.66	52.27	100.00	Precambrian
	1.00	15.94	15.31	35.32	67.57	
(6) Nassau, Germany†	1.38	24.96	21.47	52.19	100.00	Carboniferous
	1.00	18.09	15.56	37.82	72.47	
(7) Clausthal, Germany‡	1.36	25.04	21.24	52.36	100.00	Carboniferous
	1.00	18.41	15.62	38.50	73.53	
(8) Alpine Trias, Austria‡	1.37	24.31	22.20	52.12	100.00	Triassic
	1.00	17.74	16.20	38.04	72.98	
(9) Rifle mine, Colorado§	1.38	26.10	20.97	51.55	100.00	Tertiary
	1.00	18.91	15.20	37.35	72.46	
(10) Cougar mine, Colorado§	1.36	25.90	21.05	51.69	100.00	Tertiary
	1.00	19.04	15.48	38.01	73.53	

* New data, Table 2, this paper
† Data from Nier (1938)
‡ Data from Nier *et al.* (1941)
§ Data from Stieff and Stern (1953)

to agree with the assigned geological ages if the lead determinations were in error. The agreement between the age determinations of zircon and monazite and the assigned geological age for rocks of diverse locality and geological age is supported by data of Chapman *et al.* (1954) for the Boulder batholith; Lyons *et al.* (in preparation) for the New Hampshire granites; Larsen *et al.* (1954) for the Idaho batholith; Yates *et al.* (in preparation), and Overstreet *et al.* (in preparation) for rocks of the western Piedmont.

The spectrographic lead determinations of monazite are believed more reliable than the dithizone lead determinations, and so are used exclusively in this report. The problems of wet-chemical determination of lead in monazite indicate the need for more precise methods. The entire question of the suitability of monazite and other thorium minerals as age indicators cannot be resolved unless the methods for the determination of lead can be improved.

ISOTOPIC ANALYSES OF GALENA AND MONAZITE

Isotopic analyses of the lead extracted from galena of sample SP-56 (Table 2) and from monazite of sample SQ-81 (Table 3) were made

at the Mass Assay Laboratory, Carbide and Carbon Chemicals Co., Y-12 Area, Oak Ridge, Tennessee. The galena is believed to be of the same geologic age as the monazite and its isotopic composition was used to correct the

TABLE 5.—ORIGINAL LEAD IN MONAZITES

Locality	Original Pb (ppm)	Total Pb (ppm)
(1) Mountain Pass, California	13	1130
(2) Front Range, Colorado*	19	1485
(3) Mount Isa, Queensland†	80	2850
(4) Huron Claims, Manitoba†	10	15240
(5) Las Vegas, New Mexico†	70	3720

* Data from George Phair (Personal communication)

† Data from Holmes (1948)

monazite for original lead (lead that crystallized with the monazite). The isotopic composition of the lead extracted from the galena shows it to be comparable to Precambrian lead from other localities. (*See* Table 4.)

AGE OF MONAZITE FROM THE Pb^{208}/Th^{232} RATIO

The age of the monazite from sample SQ-81, uncorrected for original lead, is calculated according to the formula derived by Keevil (1939, p. 214):

$$T = \frac{7.23\ Pb}{U + 0.322\ Th} \times 10^9$$

$$T = \frac{(7.23)(0.1130)}{0.002 + (0.322)(2.65)} \times 10^9 = 955 \text{ million years}$$

Corrected for original lead, the age of the monazite from Pb^{208}/Th^{232} ratio is equivalent to 925 million years using the curves of Wickman (1939, p. 6) or the nomographs of Kulp *et al.* (1953, p. 31–34) for the ratios obtained from the isotopic data given in Table 3. The age obtained from Pb^{208}/U^{238}, 1860–1880 million years, is considered unreliable in view of the extremely small amounts of uranium and Pb^{206} present in the sample. Ages from Pb^{207}/U^{235} and Pb^{207}/Pb^{206} cannot be calculated because of the absence of radiogenic Pb^{207} (Table 3). Inasmuch as 98.85 per cent of the total lead is radiogenic, of which 98.34 per cent is radiogenic Pb^{208} produced from Th^{232}, the thorium age is undoubtedly the only valid selection.

TABLE 6.—AGE DETERMINATIONS OF MONAZITE, MOUNTAIN PASS, CALIFORNIA

By the Larsen method of alpha counting and total lead

Sample	Th* (per cent)	U† (per cent)	α/mg/hr		Pb‡ (ppm)	Age (M.Y.)
			Calc.	Meas.		
SQ-81	2.65	0.002	2350	2200	1130	970
SQ-42	2.56	0.002	2270	2200	1145	990
SP-50	§	§	....	1190	550	890
					Average =	950

* Th determined by A. M. Sherwood

† U determined by Frank Cuttitta

‡ Pb determined by C. L. Waring

§ Not determined, insufficient material

AGE OF MONAZITE BY THE LARSEN METHOD

Age determinations were also made of monazite from samples SQ-42 and SP-50, in addition to SQ-81, by the alpha-counting and total-lead method devised by Larsen and described by Larsen *et al.* (1952, p. 1045–1052). The Larsen method is applicable to monazite as well as to zircon because the monazite also shows only small amounts of original lead. Other isotopic analyses of monazite lead shows that only 1–3 per cent of the lead is original (Table 5). The ages obtained from the three samples of Mountain Pass monazite by the Larsen method (Table 6) average 950 million years and are in good agreement with the 925 million years age obtained from the isotopic analysis of monazite of sample SQ-81.

Monazite was ground to minus-100-mesh grain size and mounted in small counting trays, 0.8 cm and 1.1 cm in diameter, requiring approximately 50 mg and 100 mg of sample, respectively. The alpha counts were made in the Geological Survey laboratory with the equipment used by E. S. Larsen, Jr., and his colleagues. The background counts range from 5 to 15 alpha counts per hour with the equipment in use daily. The alpha activity, measured in terms of α/mg/hr, was obtained experi-

mentally by the author, and lead was determined on 12 mg of the same sample by C. L. Waring using the spectrographic method described by Waring and Worthing (1953, p. 827–834). The absorption factor for thick-source alpha counting of monazite has been calculated by P. M. Hurley (personal communication, 1953) and varies with the amount of Th + U present. The absorption factor 0.382 was used for the Mountain Pass monazites ranging from 1 to 3 per cent Th + U. The age formula,

$$T_1 = \frac{c\ \mathrm{Pb}}{\alpha/\mathrm{mg/hr}},$$

where c is a constant equal to 2680 for U alone and 1980 for Th alone, is given by Larsen *et al.* (1952, p. 1049). Ages greater than 300 million years must be corrected for parent decay according to the formula,

$$T = T_1 - \tfrac{1}{2}(T_1^2 k)$$

where k is a decay constant based upon the thorium-uranium ratio (Keevil, 1939, p. 204–207). Monazite from Mountain Pass contains only traces of uranium (Table 6) and the constants $c = 1980$ and $k = 0.62 \times 10^{-4}$ were used in the age calculations. The alpha activity of a monazite may be calculated on the basis of 0.0884 Th + 0.362 U = α/mg/hr. The alpha activities of monazites from samples SQ-81 and SQ-42 are shown in Table 6. Inasmuch as the reproducibility of the alpha counting is ±5–10 per cent, the calculated and measured values for α/mg/hr (Table 6) are in good agreement. Only 80 mg of monazite from sample SP-50 was available, leaving insufficient material for chemical uranium and thorium determinations. If all the activity (1190 α/mg/hr) is due to thorium, the calculated percentage of thorium is 1.35. The analyzed monazites from Mountain Pass are all relatively low in activity. Monazites with lower thorium contents, however, have been recorded from Llallagua, Bolivia (Gordon, 1944, p. 330), where thorium could not be detected at all, and from Katanga, Belgian Congo, where thorium is 0.2 per cent (Palache *et al.* 1951, p. 694).

Age Determinations of Zircon from Shonkinite

Age determinations of four samples of zircon separated from the Mountain Pass shonkinite, sample NM-1, were made by David Gottfried and the author using the Larsen method. The shonkinite sample, NM-1, was collected by T. B. Nolan and W. T. Pecora. Three modal analyses of the shonkinite are given in Table 7. The selective concentration of apatite and zircon in the −100+200-mesh fraction of the rock is shown in column 3 of the table.

The zircon was concentrated by heavy-liquid separations of the −100+200-mesh fraction of the rock in bromoform and methylene iodide followed by passing of the heavy minerals through the Frantz isodynamic magnetic separator at different intensities. Four fractions of zircon were separated by slight variations in pitch, tilt, and magnetic intensity of the Frantz separator. The final concentrates were then carefully examined in the binocular microscope for trace impurities of sulfides which tend to concentrate with zircon in the least-magnetic fractions. Pyrite was removed by hand-picking each grain with a thinned camel's hair brush. It has been found that sulfides such as pyrite and molybdenite contain large amounts of lead. Inasmuch as the Larsen method of age determination is based upon total lead in zircon, it is essential to remove each grain of sulfide that

Plate 1.—Monazite and Bastnaesite in Carbonate Rock

Figure 1.—Optically Continuous Intergrowth of Bastnaesite and Parisite

Intergrowth is large, striated grain running east-west across center of photograph. Discrete grains of monazite are dark grains with high relief, lower right-hand corner of photograph. Matrix is twinned calcite in barite-carbonate rock SP-50. ×150; Plane-polarized light.

Figure 2.—Euhedral Crystals of Monazite in Barite-Carbonate Rock SP-50

Opaque grains are galena. ×250; Plane-polarized light.

Figure 3.—Prismatic Monazite, Twinned Calcite and Dolomite, Biotite, Barite (Bottom of Photograph), and Galena (Opaque Grains) in Carbonate-Rock Inclusion in Gneiss

×300; Plane-polarized light.

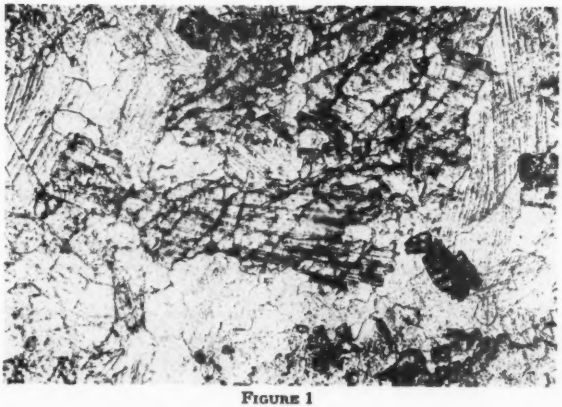

FIGURE 1

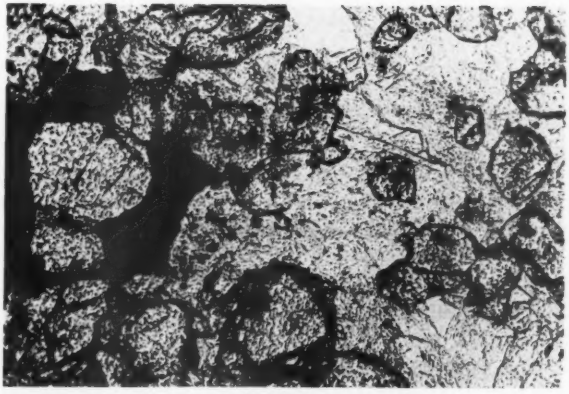

FIGURE 2

FIGURE 3

MONAZITE AND BASTNAESITE IN CARBONATE ROCK

may contribute contaminating lead in excess of the radiogenic lead in the zircon. The results of the age determinations of the four samples of zircon separated from the shonkinite are given

TABLE 7.—MODAL ANALYSES OF SHONKINITE, SAMPLE NM-1, MOUNTAIN PASS, CALIFORNIA

Modes determined by H. W. Jaffe

	1	2	3
Potash feldspar	34.9	44.6	35.6
Biotite	40.6	34.9	39.1
Augite	15.6	11.3	13.0
Crocidolite	0.4	0.4	
Altered olivine	1.5	3.4	3.5
Opaque	1.5	1.0	
Calcite	0.8	0.3	0.7
Apatite	4.7	4.1	8.0
Zircon	tr	tr	0.1
	100.0	100.0	100.0

(1) Volumetric mode of thin section of shonkinite, NM-1, cut parallel to the foliation

(2) Volumetric mode of thin section of shonkinite, NM-1, cut normal to the foliation

(3) Fragment analysis by grain counting of the −100 + 200 mesh fraction of shonkinite, NM-1, the sample used for separation of zircon for age determination

in Table 8, and the average is 840 million years, which compares favorably with the age of the monazite. In applying the formulas,

$$T_1 = \frac{c\ \text{Pb}}{\alpha/\text{mg/hr}}$$

and

$$T = T_1 - \tfrac{1}{2}(T_1^2 k),$$

the values 2400 and 1.42×10^{-4} are used for the constants c and k, respectively. This assumes slightly more thorium than uranium in the zircon samples, based upon analyses of other zircons by Larsen *et al.* (1952, p. 1049). Should the zircon activity be due entirely to thorium ($c = 1980$) or to uranium ($c = 2680$), which is unlikely, the age determinations would be subject to an error of 16 per cent. Thus far, no such zircons have been found by Larsen and his colleagues in their current investigations.

PETROGRAPHIC RELATIONS OF MONAZITE AND BASTNAESITE

More than 100 thin sections of the Sulphide Queen carbonate rock and associated alkalic igneous rocks were studied by the writer during an investigation of the mineralogy and geochemistry of the rare-earth deposits of the Mountain Pass district. Where monazite and bastnaesite occur together in the same thin section, they are rarely seen in contact (Pl. 1, fig. 1). Bastnaesite occurs in euhedral hexagonal plates and prisms, skeletal grains intergrown with calcite, optically continuous intergrowths with parisite (Pl. 1, fig. 1) in crystals with frayed, dirty margins, and occasionally in cryptocrystalline grains identifiable only by an X-ray diffraction pattern. Throughout most of the Sulphide Queen carbonate body, bastnaesite and calcite are so intimately associated in grain size and intergrowths that they appear to be of the same period of crystallization. Possible extensive plastic flow and recrystallization of calcite, however, may have obscured many early and significant features. Monazite occurs in euhedral crystals (Pl. 1, fig. 2) less than 10 mm in diameter, in prismatic grains (Pl. 1, fig. 3), and less commonly in tablets or needles forming radial clusters. The occurrence of monazite, unlike that of bastnaesite, is extremely sporadic both in hand specimen and in a single thin section. There is no convincing

TABLE 8.—AGE DETERMINATIONS OF ZIRCON FROM SHONKINITE, SAMPLE NM-1, MOUNTAIN PASS, CALIFORNIA

By the Larsen method of alpha counting and total lead

Sample	α/mg/hr*	Pb (ppm)†	Age (M. Y.)
Zircon-B	300	110	820
Zircon-C	600	210	790
Zircon-D	270	110	910
Zircon-M	1220	465	850
		Average =	840

* α/mg/hr determined by David Gottfried and H. W. Jaffe

† Pb was determined spectrographically by C. L. Waring

microscopic evidence for the replacement of bastnaesite by monazite or vice versa (Pl. 1, fig. 1). This suggests that the two minerals may be of the same general age of mineralization, with monazite forming until all available P_2O_5 is used up, and bastnaesite continuing to crystallize with calcite throughout the major part of the carbonate body.

Geological Significance

The age of 950 million years for monazite and 840 million years for zircon, both from rocks of the Mountain Pass rare-earth district, would support the conclusion that the alkalic rocks and associated rare-earth mineral deposits were introduced into metamorphic rocks in late Precambrian time. Such a petrogenetic province may have been more extensive in the Cordilleran region and could conceivably be exposed in the Precambrian terrane of other areas.

References Cited

Chapman, R. W., Gottfried, David, and Waring, C. L., 1954, Age of the Boulder batholith and other batholiths of western Montana: U. S. Geol. Survey Trace Elements Inv. Rept. 420, p. 8.

Gordon, S. G., 1944, The mineralogy of the tin mines of Cerro de Llallagua, Bolivia: Acad. Nat. Sci. Philadelphia Proc., v. 96, p. 330–332.

Holmes, Arthur, 1948, Monazite as a geological timekeeper: Royal Soc. Edinburgh Proc., v. 63, pt. 2, p. 115–124.

Keevil, N. B., 1939, The calculation of geological age: Am. Jour. Sci., v. 237, p. 203.

Kulp, J. L., Bate, G. L., and Broecker, W. S., 1953, Present status of the lead method of age determination: U. S. Atomic Energy Comm., NYO-6200, p. 31–34, and 1954, Am. Jour. Sci., v. 252, p. 345–365.

Larsen, E. S., Jr., and Berman, Harry, 1934, The microscopic determination of the nonopaque minerals: U. S. Geol. Survey Bull. 848, p. 30–32.

Larsen, E. S., Jr., Keevil, N. B., and Harrison, H. C., 1952, Method for determining the age of igneous rocks from the accessory minerals: Geol. Soc. America Bull, v. 63, p. 1045–1052.

Larsen, E. S., Jr., Gottfried, David, Jaffe, H. W., and Waring, C. L., 1954, Age of the southern California, Sierra Nevada, and Idaho batholiths (Abstract): Geol. Soc. America Bull., v. 65, p. 1277.

Nier, A. O., 1938, Variations in the relative abundances of the isotopes of common lead from various sources: Am. Chem. Soc. Jour., v. 60, p. 1573.

Nier, A. O., Thompson, R. W., and Murphey, B. F., 1941, The isotopic composition of lead and the measurement of geological time; III: Phys. Rev., v. 60, p. 115.

Olson, J. C., Shawe, D. R., Pray, L., and Sharp, W. N., 1954, Rare earth mineral deposits of the Mountain Pass district, San Bernardino County, California: U. S. Geol. Survey Prof. Paper 261.

Palache, Charles, Berman, Harry, and Frondel, Clifford, 1951, Dana's System of Mineralogy, v. 2: 7th ed., N. Y., John Wiley and Sons, p. 694.

Sandell, E. B., 1950, Colorimetric determination of traces of metals, Chemical analysis, v. 3: 2d ed., N. Y., Interscience Publishers, Inc., p. 111, 389, 391–395.

Stieff, L. R., and Stern, T. W., 1953, A preliminary determination of the age of some uranium ores of the Colorado Plateaus by the lead-uranium method: U. S. Geol. Survey Circ. 271, p. 19.

Waring, C. L., and Worthing, Helen, 1953, A spectrographic method for the determination of trace amounts of lead in zircon and other minerals: Am. Mineralogist, v. 38, p. 827–834.

Wickman, F. E., 1939, Some graphs for the calculation of geological age: Sveriges geol. Undersökning, ser. C, no. 427, fig. 1, p. 6.

U. S. Geological Survey, Geochemistry and Petrology Branch, Washington 25, D. C.

Manuscript Received by the Secretary of the Society January 27, 1955

Publication Authorized by the Director, U. S. Geological Survey

BULLETIN OF THE GEOLOGICAL SOCIETY OF AMERICA
VOL. 66, PP. 1257-1274, 8 FIGS., 4 PLS. OCTOBER 1955

EXPERIMENTAL DEFORMATION OF HASMARK DOLOMITE

BY JOHN HANDIN AND H. W. FAIRBAIRN

ABSTRACT

Jacketed cylindrical specimens of pure, homogeneous, anisotropic Hasmark dolomite have been deformed dry under a constant confining pressure of 5000 atm at a strain rate of 1 per cent per minute. Uniaxial compression and extension experiments were carried out on cylinders oriented parallel and perpendicular to the direction of the optic-axis maximum of the fabric, and tests were conducted at room temperature and at 300°C for each orientation. All tests ended in fracture along a shear surface inclined at about 60° to the least principal stress axis, at a strain of less than 10 per cent. The stress-strain curves obtained suggest (1) little or no strength anisotropy beyond the yield points, (2) little or no effect of temperature on strength or ductility, (3) a marked dependence of strength on normal stress.

The grain orientation of the deformed specimens was investigated by standard U-stage methods. After deformation at 300°C the principal visible change in the fabric is a moderate development of $\{02\bar{2}1\}$ twins. Measurements indicate that these have a negative[1] direction sense of gliding, thus conforming with the recent lattice analysis of Bradley *et al.* (1953) and the recent experimental work of Turner *et al.* (1954). Observed results compare favorably with predicted deformed fabrics based on the assumption of twin-glide on $\{02\bar{2}1\}$ in a negative sense, a mechanism further supported by lamellae-spacing index data. No unequivocal evidence for translation-glide on the base $\{001\}$ or for any other mechanisms was found. However, preliminary results of single crystal experiments confirm Johnsen's (1902) discovery of basal translation.

[1] After Turner *et al.* (1954, p. 482), the sense of shear is such that upper layers of the crystal lattice are displaced downwards from the upper end of the c_r axis.

CONTENTS

TEXT

	Page
Scope of investigation	1258
Acknowledgments	1258
Previous work	1258
Dolomite crystal lattice	1258
Selection and preparation of material	1260
Experimental work	1261
Apparatus	1261
Procedure	1262
Experimental results	1264
Grain-orientation studies	1264
General remarks	1264
Undeformed fabric	1265
Experiments favorable to development of *f* twins	1265
Experiments unfavorable to development of *f* twins	1266
Spacing-index data	1267
Predicted fabric changes	1268
General remarks	1268
Analytical methods	1268
Results	1269
Summary and conclusions	1271
References cited	1272

ILLUSTRATIONS

Figure	Page
1. Dolomite crystal lattice	1259
2. Orientation and marking of test specimens, and optic-axes fabric for undeformed *T* cylinder	1260
3. Schematic diagram of the triaxial testing apparatus	1261
4. Stresses in triaxial testing	1262
5. Stress-strain curves for Hasmark dolomite under 5000 atm confining pressure	1263
6. Lamellae spacing-index data for *T* and *I* cylinders compressed 9 per cent at 300°C	1267
7. Geometry of mechanical twinning on *f* $\{02\bar{2}1\}$	1269
8. Fabric diagrams	1270

Plate	Facing page
1. Recording and control panels	1260
2. Hasmark dolomite	1261
3. Diagrams for grain-orientation studies	1264
4. Predicted optic-axes fabrics of *T* cylinders homogeneously deformed by twinning on $\{02\bar{2}1\}$ in a negative direction sense	1270

mentally by the author, and lead was determined on 12 mg of the same sample by C. L. Waring using the spectrographic method described by Waring and Worthing (1953, p. 827–834). The absorption factor for thick-source alpha counting of monazite has been calculated by P. M. Hurley (personal communication, 1953) and varies with the amount of Th + U present. The absorption factor 0.382 was used for the Mountain Pass monazites ranging from 1 to 3 per cent Th + U. The age formula,

$$T_1 = \frac{c\ \text{Pb}}{\alpha/\text{mg/hr}},$$

where c is a constant equal to 2680 for U alone and 1980 for Th alone, is given by Larsen *et al.* (1952, p. 1049). Ages greater than 300 million years must be corrected for parent decay according to the formula,

$$T = T_1 - \tfrac{1}{2}(T_1^2 k)$$

where k is a decay constant based upon the thorium-uranium ratio (Keevil, 1939, p. 204–207). Monazite from Mountain Pass contains only traces of uranium (Table 6) and the constants $c = 1980$ and $k = 0.62 \times 10^{-4}$ were used in the age calculations. The alpha activity of a monazite may be calculated on the basis of 0.0884 Th + 0.362 U = α/mg/hr. The alpha activities of monazites from samples SQ-81 and SQ-42 are shown in Table 6. Inasmuch as the reproducibility of the alpha counting is ±5–10 per cent, the calculated and measured values for α/mg/hr (Table 6) are in good agreement. Only 80 mg of monazite from sample SP-50 was available, leaving insufficient material for chemical uranium and thorium determinations. If all the activity (1190 α/mg/hr) is due to thorium, the calculated percentage of thorium is 1.35. The analyzed monazites from Mountain Pass are all relatively low in activity. Monazites with lower thorium contents, however, have been recorded from Llallagua, Bolivia (Gordon, 1944, p. 330), where thorium could not be detected at all, and from Katanga, Belgian Congo, where thorium is 0.2 per cent (Palache *et al.* 1951, p. 694).

Age Determinations of Zircon from Shonkinite

Age determinations of four samples of zircon separated from the Mountain Pass shonkinite, sample NM-1, were made by David Gottfried and the author using the Larsen method. The shonkinite sample, NM-1, was collected by T. B. Nolan and W. T. Pecora. Three modal analyses of the shonkinite are given in Table 7. The selective concentration of apatite and zircon in the −100+200-mesh fraction of the rock is shown in column 3 of the table.

The zircon was concentrated by heavy-liquid separations of the −100+200-mesh fraction of the rock in bromoform and methylene iodide followed by passing of the heavy minerals through the Frantz isodynamic magnetic separator at different intensities. Four fractions of zircon were separated by slight variations in pitch, tilt, and magnetic intensity of the Frantz separator. The final concentrates were then carefully examined in the binocular microscope for trace impurities of sulfides which tend to concentrate with zircon in the least-magnetic fractions. Pyrite was removed by hand-picking each grain with a thinned camel's hair brush. It has been found that sulfides such as pyrite and molybdenite contain large amounts of lead. Inasmuch as the Larsen method of age determination is based upon total lead in zircon, it is essential to remove each grain of sulfide that

Plate 1.—Monazite and Bastnaesite in Carbonate Rock

Figure 1.—Optically Continuous Intergrowth of Bastnaesite and Parisite

Intergrowth is large, striated grain running east–west across center of photograph. Discrete grains of monazite are dark grains with high relief, lower right-hand corner of photograph. Matrix is twinned calcite in barite-carbonate rock SP-50. ×150; Plane-polarized light.

Figure 2.—Euhedral Crystals of Monazite in Barite-Carbonate Rock SP-50

Opaque grains are galena. ×250; Plane-polarized light.

Figure 3.—Prismatic Monazite, Twinned Calcite and Dolomite, Biotite, Barite (Bottom of Photograph), and Galena (Opaque Grains) in Carbonate-Rock Inclusion in Gneiss

×300; Plane-polarized light.

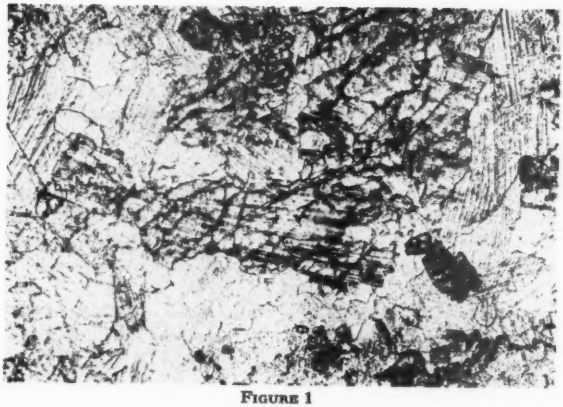

FIGURE 1

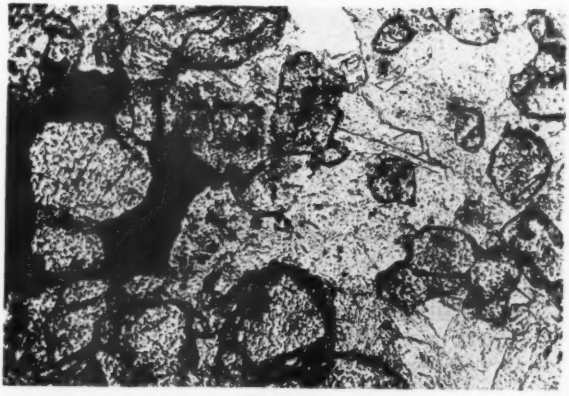

FIGURE 2

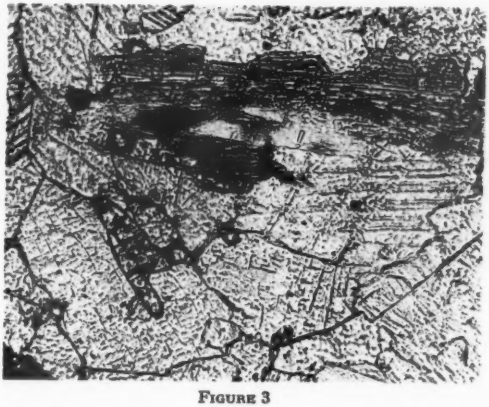

FIGURE 3

MONAZITE AND BASTNAESITE IN CARBONATE ROCK

may contribute contaminating lead in excess of the radiogenic lead in the zircon. The results of the age determinations of the four samples of zircon separated from the shonkinite are given in Table 8, and the average is 840 million years, which compares favorably with the age of the monazite. In applying the formulas,

$$T_1 = \frac{c\ \text{Pb}}{\alpha/\text{mg/hr}}$$

and

$$T = T_1 - \tfrac{1}{2}(T_1^2 k),$$

the values 2400 and 1.42×10^{-4} are used for the constants c and k, respectively. This assumes slightly more thorium than uranium in the zircon samples, based upon analyses of other zircons by Larsen *et al.* (1952, p. 1049). Should the zircon activity be due entirely to thorium ($c = 1980$) or to uranium ($c = 2680$), which is unlikely, the age determinations would be subject to an error of 16 per cent. Thus far, no such zircons have been found by Larsen and his colleagues in their current investigations.

TABLE 7.—MODAL ANALYSES OF SHONKINITE, SAMPLE NM-1, MOUNTAIN PASS, CALIFORNIA

Modes determined by H. W. Jaffe

	1	2	3
Potash feldspar	34.9	44.6	35.6
Biotite	40.6	34.9	39.1
Augite	15.6	11.3	13.0
Crocidolite	0.4	0.4	
Altered olivine	1.5	3.4	3.5
Opaque	1.5	1.0	
Calcite	0.8	0.3	0.7
Apatite	4.7	4.1	8.0
Zircon	tr	tr	0.1
	100.0	100.0	100.0

(1) Volumetric mode of thin section of shonkinite, NM-1, cut parallel to the foliation

(2) Volumetric mode of thin section of shonkinite, NM-1, cut normal to the foliation

(3) Fragment analysis by grain counting of the −100 + 200 mesh fraction of shonkinite, NM-1, the sample used for separation of zircon for age determination

PETROGRAPHIC RELATIONS OF MONAZITE AND BASTNAESITE

More than 100 thin sections of the Sulphide Queen carbonate rock and associated alkalic igneous rocks were studied by the writer during an investigation of the mineralogy and geochemistry of the rare-earth deposits of the Mountain Pass district. Where monazite and bastnaesite occur together in the same thin section, they are rarely seen in contact (Pl. 1, fig. 1). Bastnaesite occurs in euhedral hexagonal plates and prisms, skeletal grains intergrown with calcite, optically continuous intergrowths with parisite (Pl. 1, fig. 1) in crystals with frayed, dirty margins, and occasionally in cryptocrystalline grains identifiable only by an X-ray diffraction pattern. Throughout most of the Sulphide Queen carbonate body, bastnaesite and calcite are so intimately associated in grain size and intergrowths that they appear to be of the same period of crystallization. Possible extensive plastic flow and recrystallization of calcite, however, may have obscured many early and significant features. Monazite occurs in euhedral crystals (Pl. 1, fig. 2) less than 10 mm in diameter, in prismatic grains (Pl. 1, fig. 3), and less commonly in tablets or needles forming radial clusters. The occurrence of monazite, unlike that of bastnaesite, is extremely sporadic both in hand specimen and in a single thin section. There is no convincing

TABLE 8.—AGE DETERMINATIONS OF ZIRCON FROM SHONKINITE, SAMPLE NM-1, MOUNTAIN PASS, CALIFORNIA

By the Larsen method of alpha counting and total lead

Sample	α/mg/hr*	Pb (ppm)†	Age (M. Y.)
Zircon-B	300	110	820
Zircon-C	600	210	790
Zircon-D	270	110	910
Zircon-M	1220	465	850
		Average =	840

* α/mg/hr determined by David Gottfried and H. W. Jaffe

† Pb was determined spectrographically by C. L. Waring

microscopic evidence for the replacement of bastnaesite by monazite or vice versa (Pl. 1, fig. 1). This suggests that the two minerals may be of the same general age of mineralization, with monazite forming until all available P_2O_5 is used up, and bastnaesite continuing to crystallize with calcite throughout the major part of the carbonate body.

Geological Significance

The age of 950 million years for monazite and 840 million years for zircon, both from rocks of the Mountain Pass rare-earth district, would support the conclusion that the alkalic rocks and associated rare-earth mineral deposits were introduced into metamorphic rocks in late Precambrian time. Such a petrogenetic province may have been more extensive in the Cordilleran region and could conceivably be exposed in the Precambrian terrane of other areas.

References Cited

Chapman, R. W., Gottfried, David, and Waring, C. L., 1954, Age of the Boulder batholith and other batholiths of western Montana: U. S. Geol. Survey Trace Elements Inv. Rept. 420, p. 8.

Gordon, S. G., 1944, The mineralogy of the tin mines of Cerro de Llallagua, Bolivia: Acad. Nat. Sci. Philadelphia Proc., v. 96, p. 330–332.

Holmes, Arthur, 1948, Monazite as a geological timekeeper: Royal Soc. Edinburgh Proc., v. 63, pt. 2, p. 115–124.

Keevil, N. B., 1939, The calculation of geological age: Am. Jour. Sci., v. 237, p. 203.

Kulp, J. L., Bate, G. L., and Broecker, W. S., 1953, Present status of the lead method of age determination: U. S. Atomic Energy Comm., NYO-6200, p. 31–34, and 1954, Am. Jour. Sci., v. 252, p. 345–365.

Larsen, E. S., Jr., and Berman, Harry, 1934, The microscopic determination of the nonopaque minerals: U. S. Geol. Survey Bull. 848, p. 30–32.

Larsen, E. S., Jr., Keevil, N. B., and Harrison, H. C., 1952, Method for determining the age of igneous rocks from the accessory minerals: Geol. Soc. America Bull, v. 63, p. 1045–1052.

Larsen, E. S., Jr., Gottfried, David, Jaffe, H. W., and Waring, C. L., 1954, Age of the southern California, Sierra Nevada, and Idaho batholiths (Abstract): Geol. Soc. America Bull., v. 65, p. 1277.

Nier, A. O., 1938, Variations in the relative abundances of the isotopes of common lead from various sources: Am. Chem. Soc. Jour., v. 60, p. 1573.

Nier, A. O., Thompson, R. W., and Murphey, B. F., 1941, The isotopic composition of lead and the measurement of geological time; III: Phys. Rev., v. 60, p. 115.

Olson, J. C., Shawe, D. R., Pray, L., and Sharp, W. N., 1954, Rare earth mineral deposits of the Mountain Pass district, San Bernardino County, California: U. S. Geol. Survey Prof. Paper 261.

Palache, Charles, Berman, Harry, and Frondel, Clifford, 1951, Dana's System of Mineralogy, v. 2: 7th ed., N. Y., John Wiley and Sons, p. 694.

Sandell, E. B., 1950, Colorimetric determination of traces of metals, Chemical analysis, v. 3: 2d ed., N. Y., Interscience Publishers, Inc., p. 111, 389, 391–395.

Stieff, L. R., and Stern, T. W., 1953, A preliminary determination of the age of some uranium ores of the Colorado Plateaus by the lead-uranium method: U. S. Geol. Survey Circ. 271, p. 19.

Waring, C. L., and Worthing, Helen, 1953, A spectrographic method for the determination of trace amounts of lead in zircon and other minerals: Am. Mineralogist, v. 38, p. 827–834.

Wickman, F. E., 1939, Some graphs for the calculation of geological age: Sveriges geol. Undersökning, ser. C, no. 427, fig. 1, p. 6.

U. S. Geological Survey, Geochemistry and Petrology Branch, Washington 25, D. C.

Manuscript Received by the Secretary of the Society January 27, 1955

Publication Authorized by the Director, U. S. Geological Survey

BULLETIN OF THE GEOLOGICAL SOCIETY OF AMERICA
VOL. 66, PP. 1257-1274, 8 FIGS., 4 PLS. OCTOBER 1955

EXPERIMENTAL DEFORMATION OF HASMARK DOLOMITE

BY JOHN HANDIN AND H. W. FAIRBAIRN

ABSTRACT

Jacketed cylindrical specimens of pure, homogeneous, anisotropic Hasmark dolomite have been deformed dry under a constant confining pressure of 5000 atm at a strain rate of 1 per cent per minute. Uniaxial compression and extension experiments were carried out on cylinders oriented parallel and perpendicular to the direction of the optic-axis maximum of the fabric, and tests were conducted at room temperature and at 300°C for each orientation. All tests ended in fracture along a shear surface inclined at about 60° to the least principal stress axis, at a strain of less than 10 per cent. The stress-strain curves obtained suggest (1) little or no strength anisotropy beyond the yield points, (2) little or no effect of temperature on strength or ductility, (3) a marked dependence of strength on normal stress.

The grain orientation of the deformed specimens was investigated by standard U-stage methods. After deformation at 300°C the principal visible change in the fabric is a moderate development of $\{02\bar{2}1\}$ twins. Measurements indicate that these have a negative[1] direction sense of gliding, thus conforming with the recent lattice analysis of Bradley *et al.* (1953) and the recent experimental work of Turner *et al.* (1954). Observed results compare favorably with predicted deformed fabrics based on the assumption of twin-glide on $\{02\bar{2}1\}$ in a negative sense, a mechanism further supported by lamellae-spacing index data. No unequivocal evidence for translation-glide on the base {001} or for any other mechanisms was found. However, preliminary results of single crystal experiments confirm Johnsen's (1902) discovery of basal translation.

[1] After Turner *et al.* (1954, p. 482), the sense of shear is such that upper layers of the crystal lattice are displaced downwards from the upper end of the c_r axis.

CONTENTS

TEXT

	Page
Scope of investigation	1258
Acknowledgments	1258
Previous work	1258
Dolomite crystal lattice	1258
Selection and preparation of material	1260
Experimental work	1261
Apparatus	1261
Procedure	1262
Experimental results	1264
Grain-orientation studies	1264
General remarks	1264
Undeformed fabric	1265
Experiments favorable to development of *f* twins	1265
Experiments unfavorable to development of *f* twins	1266
Spacing-index data	1267
Predicted fabric changes	1268
General remarks	1268
Analytical methods	1268
Results	1269
Summary and conclusions	1271
References cited	1272

ILLUSTRATIONS

Figure	Page
1. Dolomite crystal lattice	1259
2. Orientation and marking of test specimens, and optic-axes fabric for undeformed *T* cylinder	1260
3. Schematic diagram of the triaxial testing apparatus	1261
4. Stresses in triaxial testing	1262
5. Stress-strain curves for Hasmark dolomite under 5000 atm confining pressure	1263
6. Lamellae spacing-index data for *T* and *I* cylinders compressed 9 per cent at 300°C	1267
7. Geometry of mechanical twinning on *f* $\{02\bar{2}1\}$	1269
8. Fabric diagrams	1270

Plate	Facing page
1. Recording and control panels	1260
2. Hasmark dolomite	1261
3. Diagrams for grain-orientation studies	1264
4. Predicted optic-axes fabrics of *T* cylinders homogeneously deformed by twinning on $\{02\bar{2}1\}$ in a negative direction sense	1270

Scope of Investigation

Deformed carbonate rocks are a familiar feature of many tectonic assemblages and have long attracted the attention of field geologists. In recent years considerable progress in structural interpretation has been made through studies of the microfabric (Sander, 1930; 1950). Fairbairn and Hawkes (1941) emphasized the development in several metamorphic dolomites of polysynthetic twinning on f $\{02\bar{2}1\}$ and suggested its importance for structural petrology. Laboratory deformation studies have lagged, although the experimental work of Griggs *et al.* (1951; 1953) has yielded a rich harvest of data for calcite. This paper reports the results of a joint investigation of the laboratory deformation of dry Hasmark dolomite under 5000 atm confining pressure at 20°C and at 300°C. The experimental work was done by Handin at the Houston laboratories of Shell Development Company. Fairbairn made the petrofabric studies at the Massachusetts Institute of Technology.

Acknowledgments

The authors wish to express their appreciation to D. V. Higgs who made the measurements for the lamellae spacing-index data; to R. A. Rowland for collecting the material used in these experiments; to J. H. Spotts who made the computations for the predicted fabric study; and to J. R. Sosoka who assisted with the experimental work. Thanks are due D. T. Griggs and F. J. Turner for their critical reading of the manuscript.

Previous Work

Experimental and petrofabric work on dolomite does not account for much of the literature of structural petrology. On the analytical side, the most recent paper (Ladurner, 1953) deals with the fabric of alpine-type dolomites, published as yet only as an extended summary, with no diagrams. Prior to this the only paper devoted mainly to dolomite orientation was that of Fairbairn and Hawkes (1941), which summarized older experimental work and offered a modest amount of new petrofabric data. It reported that the only successful deformation experiment on a dolomite crystal was made by Johnsen (1902), who produced, at room temperature and pressure, translation-slip on the base, with the direction of slip parallel to the edge between the base and the rhombohedral cleavage (T = $\{0001\}$, t = $[0001 : 10\bar{1}1]$). Repeated attempts failed to produce twin-slip on f $\{02\bar{2}1\}$, although this had been the major purpose of the experiments. This unexpected result, contrasting in every way with experiments under similar conditions on calcite (no translation-slip, easy twin-slip on e $\{01\bar{1}2\}$) gave added interest to the present experimental study. Independently, and at about the same time that our work was being done, Turner *et al.* (1954) also studied this aspect of the dolomite problem, and their results have been correlated with the writers'. Francis Birch and E. C. Robertson have tested still another dolomite at room temperature and under confining pressures to 25,000 atm and found the rock to be essentially brittle. No microscopic examinations were made of their deformed material (Personal communication, November 1953).

Dolomite Crystal Lattice

A common working hypothesis of the manner in which a single dolomite crystal deforms is needed to explain certain features of the strain data, predicted grain orientation, and U-stage measurements. A brief summary of the dolomite lattice is of considerable help.

Figure 1 is a section of a dolomite lattice, parallel to c_0, and normal to the e and f planes. The large circles represent Ca, the small circles Mg; the CO_3 planar groups are shown as lines only. The original lattice occupies the left side of the figure, and a unit rhomb, bounded on two sides by the f plane, is indicated by broken lines. The direction sense of the twinning on f as shown by the arrow (upper right) is such that upper layers of the crystal lattice are displaced downwards from the upper end of the c_0 axis. (This is the "negative" sense in the convention of Turner *et al.*, 1954, p. 482.) The corresponding twinned portion of the crystal includes a unit rhomb in its new position. The possibility of twinning in the reverse sense cannot be ruled out from considerations of symmetry alone.

Inspection of the lattice shows why twinning on e is unknown for dolomite. A unit rhomb in

the untwinned portion of the lattice at the *e* plane would from symmetry considerations be twinned with the direction sense indicated by the arrow (right center). For dolomite the energy requirements of this glide, involving sections between the basal plane *c* {0001} and the three rhombohedral cleavage planes *r* {10$\bar{1}$1} of the dolomite lattice and are not in the plane of the section. No other translation has ever been reported for dolomite.

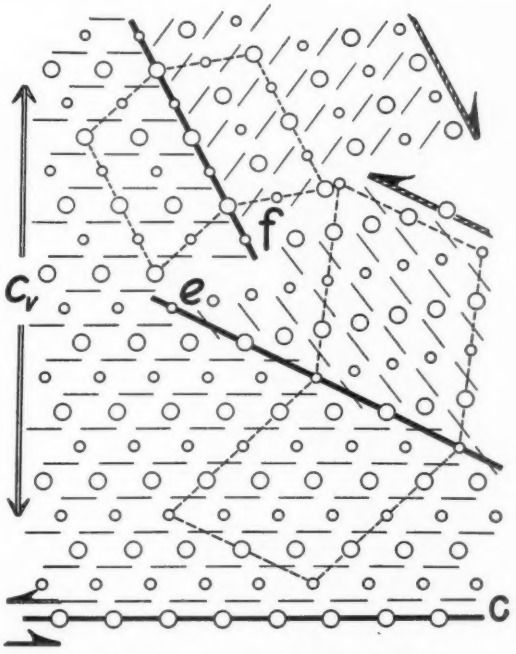

FIGURE 1.—DOLOMITE CRYSTAL LATTICE
Showing hypothetical mechanical twinning on $f\{02\bar{2}1\}$ and $e\{01\bar{1}2\}$ and translation on $c\{0001\}$; large circles, Ca; small circles, Mg; lines, CO_3

drastic rearrangement of Ca and Mg, would very probably be prohibitive. Also the Ca and Mg atoms are then not arranged in planes parallel to the base as seems to be required for dolomite. Bradley *et al.* (1953, p. 215) have discussed this briefly.

In addition to mechanical twin gliding, translation gliding must be considered. Basal slip in dolomite has been mentioned, and shown in Figure 1, where the glide plane *c* {0001} is normal to c_v and to the section of the lattice. The double arrow indicates that the motion of a layer of cations with respect to a layer of carbonate is relative and could proceed with equal facility in either direction sense. The three similar glide lines correspond to the three horizontal crystal axes a_1, a_2, a_3; they are the intersections between the basal plane *c* {0001} and the three rhombohedral cleavage planes *r* {10$\bar{1}$1} of the dolomite lattice and are not in the plane of the section. No other translation has ever been reported for dolomite.

Since dolomite offers the possibility of both twin-slip (on *f*) and translation-slip (on *c*) reorientation of deformed single grains should be considered. Where the deformation is characterized by a compression axis subparallel to c_v (Fig. 1) the first stage of the strain obviously should be confined to twin-slip on *f*, in a negative direction sense, since the resolved shear stress in the base is low. A completely twinned grain with a new c_v rotated about 54° from the original position of the optic axis (upper right section of Fig. 1) would not develop further *f* twins unless the compression axis were radically changed. However, the twinned grain would now be favorably oriented for translation-slip on *c*, and the ensuing external rotation would tend to restore the original orientation. The

entire cycle—twinning followed by translation—could now repeat if the deformation were large enough.

The degree to which this theoretical strain pattern is realized for single crystals is not at present known but is being investigated. The

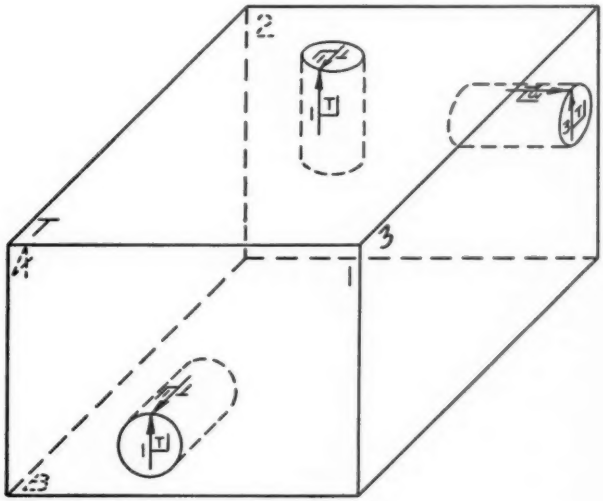

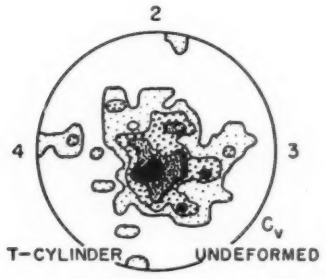

FIGURE 2.—ORIENTATION AND MARKING OF TEST SPECIMENS, AND OPTIC-AXES FABRIC FOR UNDEFORMED *T* CYLINDER
Contour interval 1, 3, 5, 7 per cent

Where the deformation is characterized by a compression axis at high angles to c_v (Fig. 1) it is clear that the first stage of the strain will be translation-slip on *c* even though the resolved shear stress coefficient is low, because twin-glide is impossible. If carried far enough, so that *c* rotates through a considerable angle, the grain might eventually be reoriented to permit twin-slip on *f*. This cycle could then repeat.

degree to which it conforms with actual deformation of a crystal aggregate will be recorded in the following pages.

SELECTION AND PREPARATION OF MATERIAL

Dolomite from the Hasmark formation was selected because (1) its overall grain size permits reliable U-stage analysis, and (2) its relatively uniform grain size gives optimum condi-

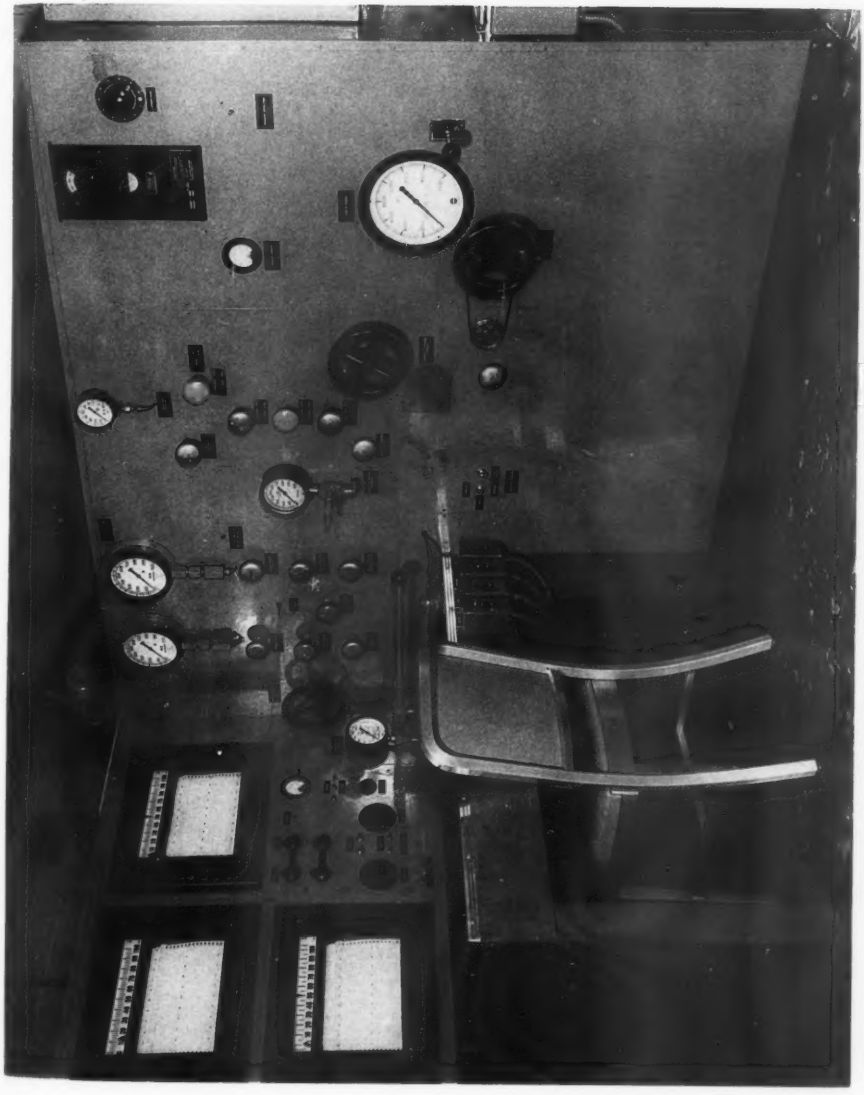

RECORDING AND CONTROL PANELS

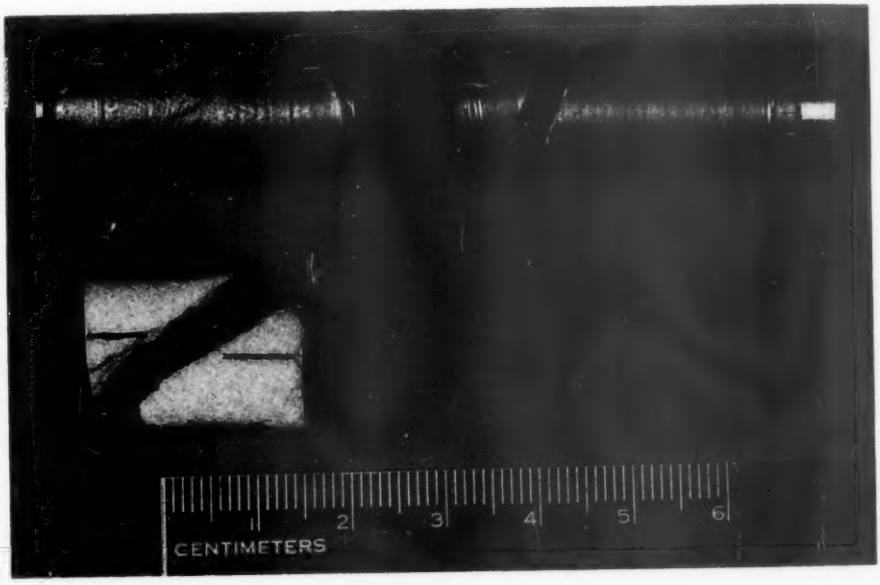

FIGURE 1

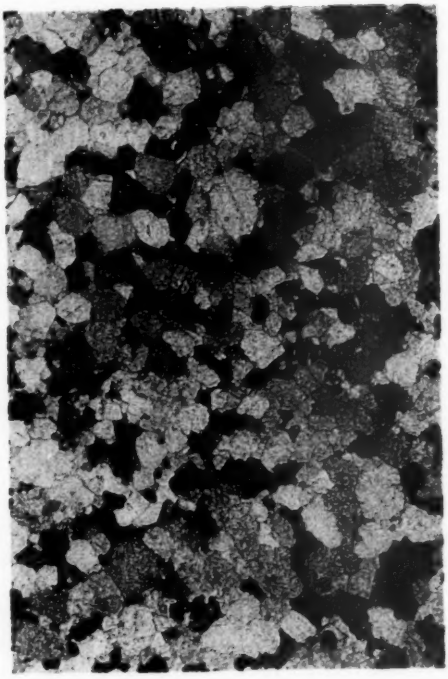

FIGURE 2

FIGURE 3

HASMARK DOLOMITE

tions for experimental work. The analysis of a specimen of the Hasmark by Fairbairn and Hawkes (1941) helped in planning experimental work.

tacts and have an average size of about 0.50 mm. Grains of quartz and muscovite comprise less than 1 per cent of the rock. Details of the grain orientation will be discussed.

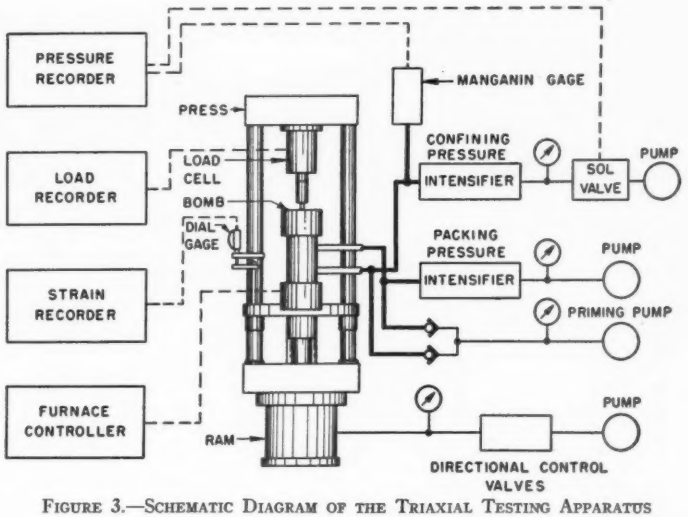

FIGURE 3.—SCHEMATIC DIAGRAM OF THE TRIAXIAL TESTING APPARATUS

Cylindrical specimens one-half inch in diameter and 1 inch long were cored from a geographically unoriented block of the nearly pure, highly anisotropic dolomite rock collected by Dr. R. A. Rowland from the Cambrian Hasmark formation at an abandoned mine near Philipsburg, Montana. Figure 2 shows the orientation of the cores relative to the optic-axes fabric of the rock and indicates the convention used in marking specimens. *T* cylinders are cut approximately parallel and *1* cylinders perpendicular to the optic axis maximum. A piece cut from the end of each core is retained for microscopic study of the undeformed material. Differential thermal, chemical, and X-ray spectrometer analyses all give results which are considered standard for dolomite.

The rock is coarse and even-grained. The grains are equidimensional with smooth con-

EXPERIMENTAL WORK

Apparatus

The triaxial testing equipment and techniques for making these deformation studies have been fully described elsewhere (Handin, 1953) and are only briefly reviewed here. Jacketed specimens were deformed dry under a nearly constant confining pressure of 5000 atm in the apparatus shown in the simplified schematic diagram of Figure 3. The recording and control panels can be seen in Plate 1.

Within the bomb a sample is surrounded by kerosene under pressure generated by an intensifier, measured by a manganin wire gage, and held constant to ±0.5 per cent. The pressures are indicated by a recorder-controller which actuates a solenoid-operated four-way valve in the low-pressure oil-supply line to the

PLATE 2.—HASMARK DOLOMITE

FIGURE 1.—DEFORMED SPECIMENS

On the left two broken in compression (one shown in its jacket); on the right one broken in extension; *compare* inclinations of fracture with those of Figure 4.

FIGURE 2.—PHOTOMICROGRAPH OF UNDEFORMED DOLOMITE

FIGURE 3.—PHOTOMICROGRAPH OF DOLOMITE COMPRESSED 9 PER CENT AT 300°C

double-acting intensifier. The specimen is attached to a piston which emerges from the bomb to bear against a load cell for externally measuring the differential force applied axially to the specimen by the ram of the press. The bomb is of conventional design except for a Harwood

Procedure

Stress-strain curves are derived by correcting recorded displacements for elastic distortion of the apparatus and converting to per cent strain, and by determining true stress from recorded values of force and computed cross-

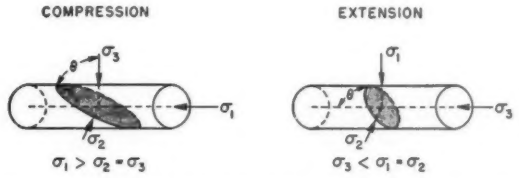

$\sigma_1, \sigma_2, \sigma_3$ ARE RESPECTIVELY THE MAXIMUM, INTERMEDIATE, AND MINIMUM PRINCIPAL STRESSES

ρgZ = VERTICAL PRESSURE = CONFINING (OVERBURDEN) PRESSURE, CONSTANT AT A GIVEN DEPTH, Z

$$\text{SHEAR STRESS} = \tau = \frac{\sigma_1 - \sigma_3}{2} \sin 2\theta$$

$$\text{NORMAL PRESSURE} = \sigma = \frac{\sigma_1 + \sigma_3}{2} + \frac{\sigma_1 - \sigma_3}{2} \cos 2\theta$$

FIGURE 4.—STRESSES IN TRIAXIAL TESTING

piston packing in which the moving piston passes through a thin-walled steel sleeve subjected externally to a separate pressure provided by the second intensifier. The radial elastic deformation of the sleeve controls the clearance around the piston. A slow leak is deliberately permitted to provide lubrication, and friction during free travel of the piston seldom exceeds 50 kg. A priming pump restrokes the intensifiers and fills both pressure systems so that the intensifiers need only compress the kerosene. A dial gage coupled to a potentiometer measures piston displacements. Measurements have a full-scale sensitivity of 0.1 per cent and an accuracy of 0.25 per cent.

The bomb can be heated by an external resistance furnace. The temperature is indicated and regulated by a Foxboro potentiometer-controller with a thermocouple in the wall of the bomb as a sensing element. The temperature difference, 15°C at 300°C, between this thermocouple and the specimen is known from an experiment made with a second thermocouple placed at the position of the center of a specimen, access being through a special hollow piston. The maximum temperature variation during an experiment is 2°C.

sectional areas of the specimen, assuming that the deformation is homogeneous and that no volume changes result from plastic flow. The rate of strain is maintained nearly constant at 1 per cent per minute. Since the equipment is designed for measuring large stresses and strains, the early, elastic part of the curves is not very accurate, and is adjusted so as to pass through the origin. (Young's modulus is about 10^6 kg/cm^2 at room temperature and atmospheric pressure.) The stress-strain curves of Figure 5 are the average of two or more runs for each orientation.

Tests were made on *T* and *I* cylinders (that is, parallel to and perpendicular to the optic-axes maximum) in compression and extension and at room temperature and 300°C, so that eight sets of curves were obtained. Figure 4 shows how two simple states of stress in the crust are simulated in an experiment. One principal stress, approximately vertical in the crust, is the overburden pressure; it is the liquid confining pressure in a test and therefore equal to the horizontal intermediate stress. In a compression test the other horizontal (axial) pressure, the greatest principal stress, exceeds the confining pressure, the least principal stress;

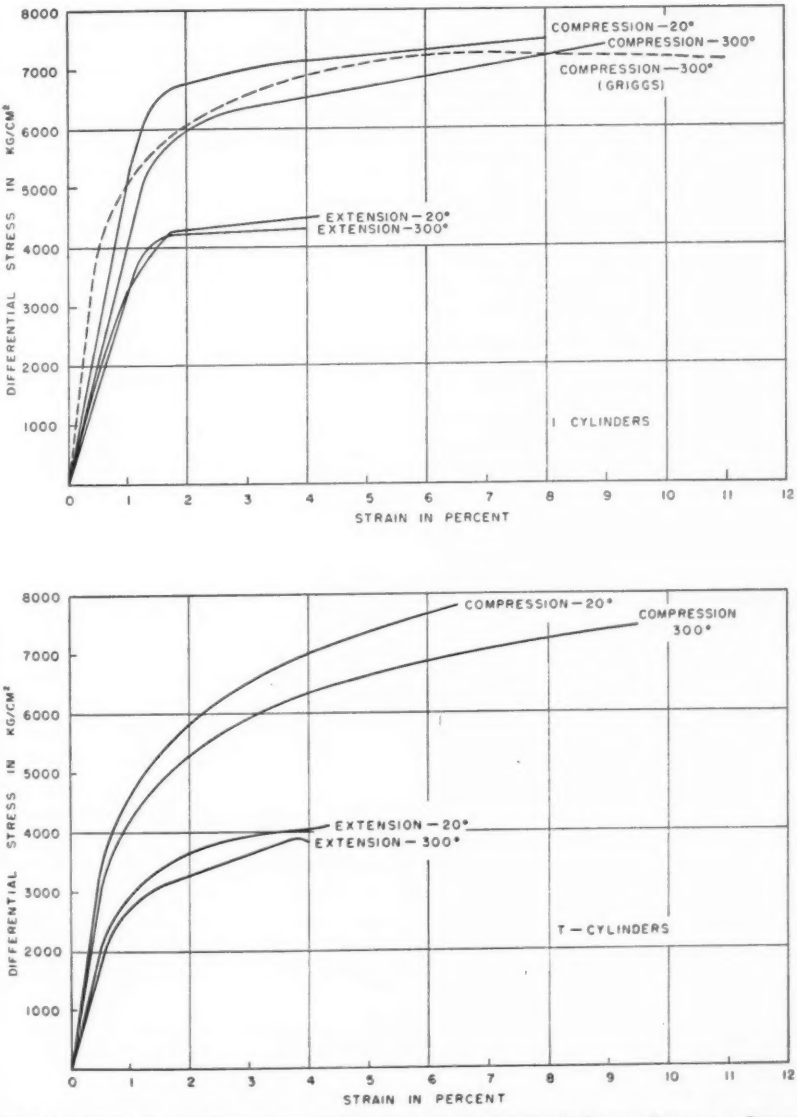

FIGURE 5.—STRESS-STRAIN CURVES FOR HASMARK DOLOMITE UNDER 5000 ATM CONFINING PRESSURE

and the specimen shortens and may fracture along a shear surface inclined at an angle of 45° or more to the direction of least pressure. In an extension test the greatest principal stress is vertical, the least horizontal, and the specimen elongates even though all the principal stresses are compressive. The maximum shear stress is one-half the difference between the maximum and the minimum pressures; that is, one-half the differential pressure. The normal pressure across any surface involves both the sum and difference, and is therefore greater for a compression test at any given confining pressure.

Experimental Results

The Hasmark dolomite was chosen for study because of its high degree of preferred orientation, and test specimens were oriented so as to take full advantage of the anisotropy (Fig. 2), the supposition being that, if mechanical twinning were an important deformation mechanism, then stress-strain curves might indicate a pronounced strength anisotropy. No data were available for dolomite, but the Yule marble (calcitic) tested under similar conditions and with about the same fabric anisotropy had strength differences of the order of 20 per cent (Griggs and Miller, 1951, Fig. 3). The curves presented in Figure 5 have very different yield points, but at a few per cent strain there is little or no strength anisotropy; that is, the difference in the magnitudes of the stress at a given strain, say 4 per cent, for a *T* cylinder and a *1* cylinder compressed at room temperature, or at 300°C, is about 3 per cent, which is less than the average deviation of 6 per cent for compression tests. The differences for the two orientations of extended cylinders is about 10 per cent, but the reproducibility of extension tests is poor, the average deviation being 12 per cent at room temperature and 15 per cent at 300°C. In view of the reproducibility of the experiments, the breaking strength of the rock is apparently largely independent of grain orientation. The dolomite is stronger and much less ductile than Yule marble under comparable experimental conditions (maximum plastic strain of about 9 per cent as opposed to 30 per cent or more).

Strength differences at 20°C and 300°C are much smaller than anticipated, about 10 per cent or less. For compression tests these differences, though small, are probably significant, but again the poor reproducibility of extension tests prohibits conclusions as to the effects of temperature, except that they must be small. (In the Yule marble work by Griggs *et al.*, 1953, p. 1329, a reduction in strength of 50 per cent is reported.)

Finally, the stress-strain curves indicate that all extension curves as a group are lower than all compression curves, regardless of orientation or temperature differences.

All the tests were terminated by shear fracture on surfaces inclined at about 60° to the least principal stress axis. Plate 2 shows the appearance of some typical deformed specimens. In extension tests initiation of shear led to immediate rupture of the jacket and consequent separation of the specimens. In compression tests, however, considerable motion on the shear surface, amounting probably to as much as several hundredths of an inch, occurred without breaking the jacket. Thus at least part of the difference in ductility between compressed and extended specimens is not real. There is suggestion of increased ductility at 300°C for compression but not for extension tests.

Because of the early fracture and the unexpected interrelationships among the stress-strain curves, it was questionable whether plastic flow (in the strict sense, slip on a multiplicity of closely spaced glide planes) was occurring at all. The photomicrograph of Plate 2 taken of a thin-section from a specimen compressed 9 per cent at 300°C shows, however, profuse development of $\{02\bar{2}1\}$ lamellae in contrast to only moderate twinning in the undeformed rock.

Griggs's curve for another dolomite (from the lower Cambrian near Dover Plains, New York) with a very different fabric tested at 5000 atm and 300°C is shown in Figure 5 for comparison. The curve is remarkably similar to ours, having a yield point intermediate between our curves for *T* and *1* cylinders, and emphasizes that the arrangement of grains in the dolomite aggregate has little effect on the stress-strain relations beyond the yield point.

Grain-Orientation Studies

General Remarks

The results of the grain-orientation study are given in Plate 3. Orientation diagrams relating to compression experiments are at the left, extension experiments at the right; between them are diagrams of undeformed dolomite. In addition, the plate is arranged so that those diagrams in the upper half are, with respect to the directions of compression and

Diagram 1 Orientation of differential pressure P with respect to fabric diagrams of Plate 3.

Diagram 10 Positions of optic axis c' and twin poles f' for untwinned grain relative to differential compression P; and twinned position c'' and f'' assuming $\{02\bar{2}1\}$ twinning in negative sense.

UNDEFORMED CYLINDERS

Diag.	Expt.	U-stage Data	Cylinder
4	147	200 c_v 0-1-3-5 %	z
15	102	82 c_v of twinned grains 0-3-5-8 %	T
20	102	160 c_v 0-1-3-5-7 % 25 f poles (filled circles)	T

EXPERIMENTS FAVORABLE FOR DEVELOPMENT OF f TWINS

	Diag.	Expt.	U-stage Data	Exptl. Data
Compression (T cylinders)	2	107	180 c_v (measured) 0-1-3-5 %	300°C 9.6% strain
	3	107	170 f poles of grains with measured axes (c_v) 0-1-3-4-5 %	300°C 9.6% strain
	8	107	c_v positions of 65 grains obtained by construction (2 per grain)	300°C 9.6% strain
	9	107	165 f poles of grains shown in diag. 8 0-1-3-5 %	300°C 9.6% strain
	7	108	100 c_v, without selection 0-1-3-5-7 %	20°C 6.2% strain
Extension (z cylinders)	5	150	200 c_v of untwinned grains 0-1-3-5 %	20°C 5.1% strain
	11	150	25 c_v (filled circles) of twinned grains 26 f poles (open circles)	20°C 5.1% strain
	6	144	170 c_v 0-1-3-5-7 %	300°C 3.4% strain

EXPERIMENTS UNFAVORABLE FOR DEVELOPMENT OF f TWINS

	Diag.	Expt.	U-stage data	Exptl. Data
Compression (z cylinders)	13	153	55 c_v of twinned grains 0-4-8-12 %	300°C 9.0% strain
	14	153	90 f poles 0-1-3-5 %	300°C 9.0% strain
	18	153	200 c_v of untwinned grains 0-1-3-5%	300°C 9.0% strain
	19	153	a axes (3 per grain) of 48 untwinned grains 0-2-4-6 %	300°C 9.0% strain
	12	141	170 c_v of untwinned grains 0-2-4-7-9 %	20°C 7.2% strain
	17	141	31 c_v of twinned grains	20°C 7.2% strain
Extension (T cylinders)	16	133	200 c_v 0-1-3-5 % 30 f poles (filled circles)	300°C 5.0% strain
	21	115	144 c_v 0-2-4-6 %	20°C 4.7% strain
	22	134	125 c_v 0-2-5-8 %	300°C 5.6% strain

COMPRE

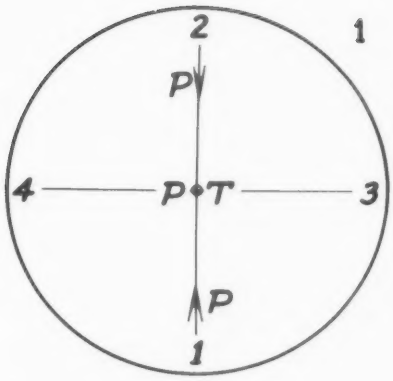

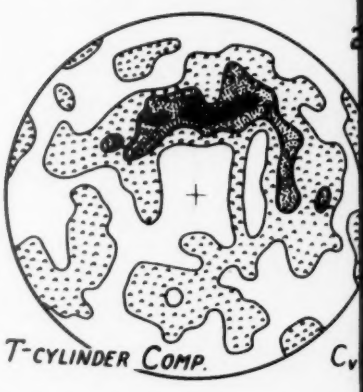

for
pres-
ing

Data
C rain
C rain
C rain
C rain
C rain
C rain
C rain

Data
C rain
C rain
C rain
C rain
ain
ain
ain
ain
ain

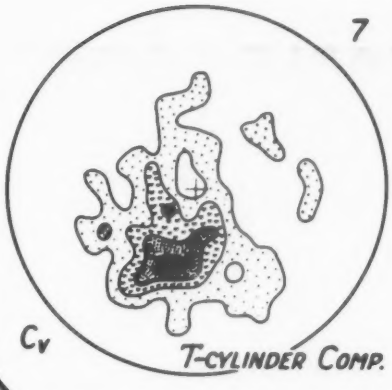

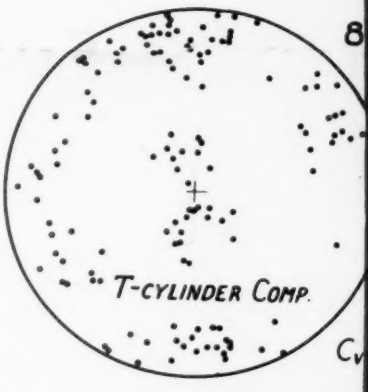

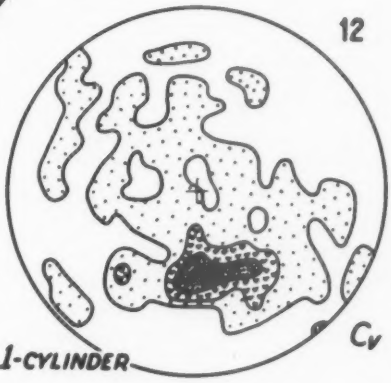

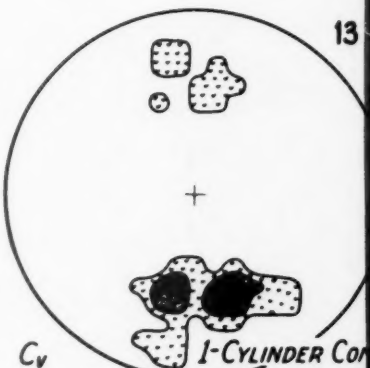

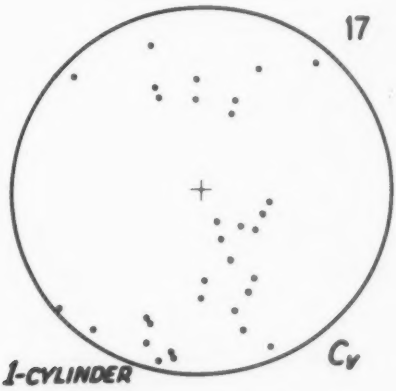

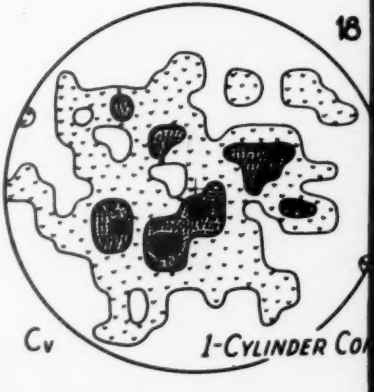

DIAGRAMS FO

COMPRESSION

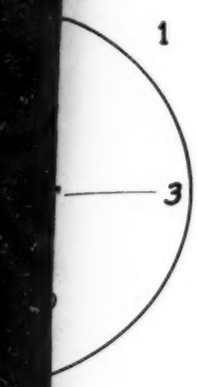

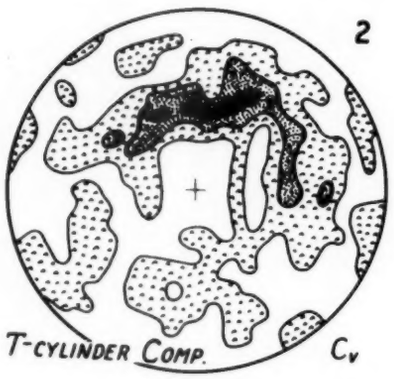

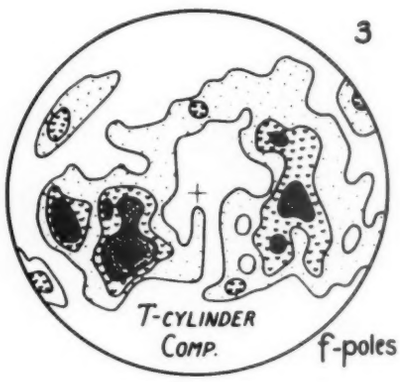

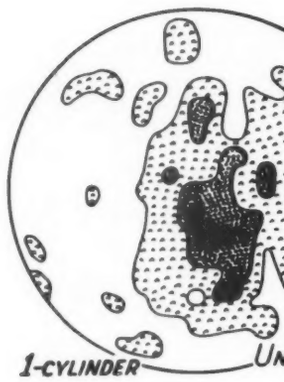

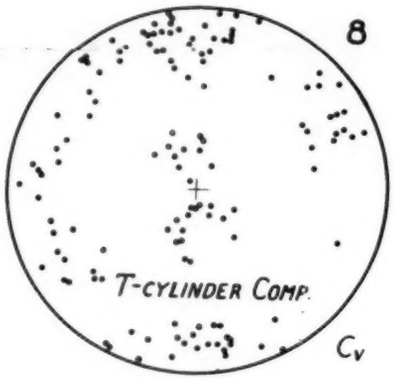

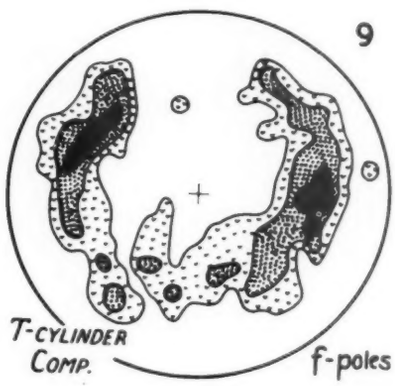

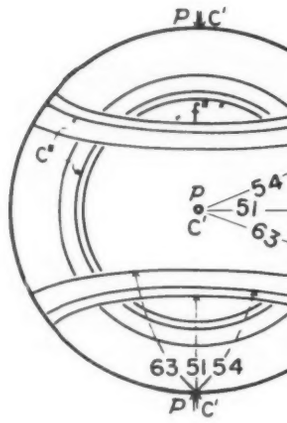

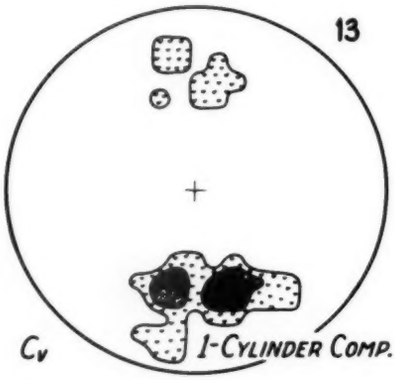

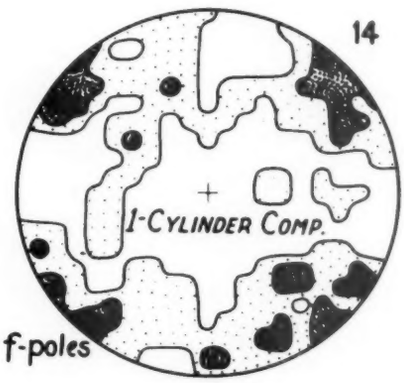

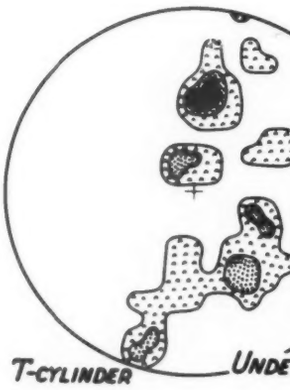

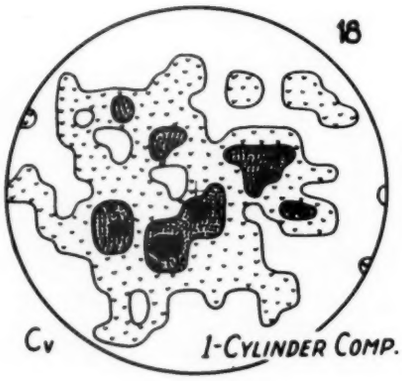

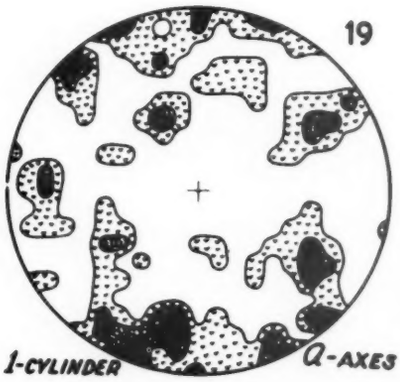

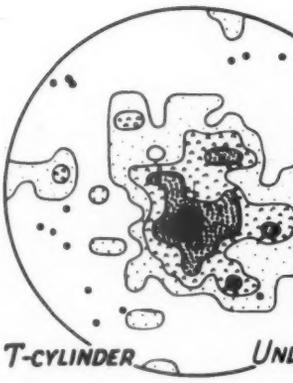

DIAGRAMS FOR GRAIN-ORIENTATION STUDIES

EXTENSION

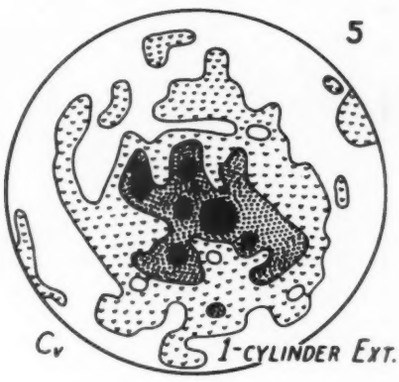

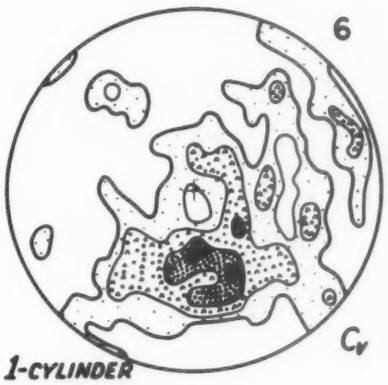

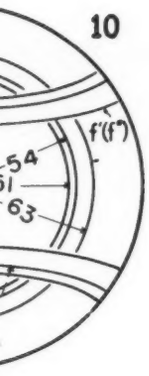

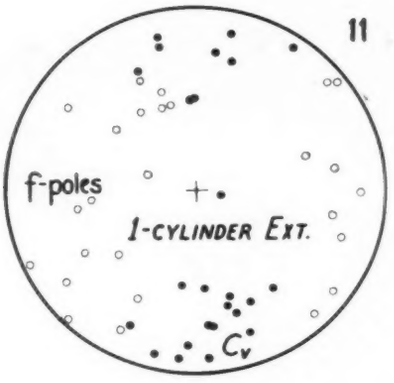

FAVORABLE FOR f-TWINS

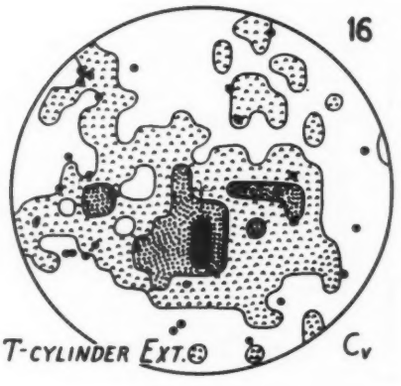

UNFAVORABLE FOR f-TWINS

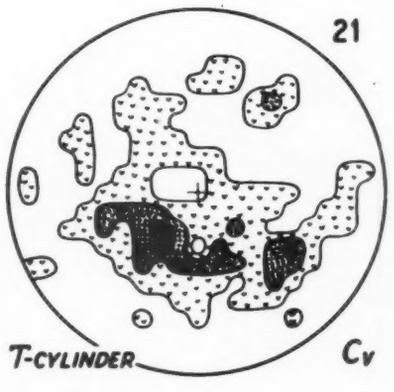

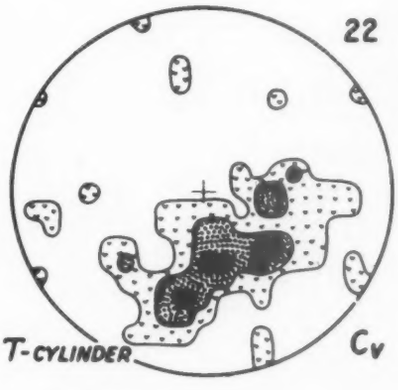

extension, favorably oriented for development of *f* twins; those in the lower half are unfavorably oriented. This is based on the assumption that the direction sense of twin gliding on *f* is negative as indicated on Figure 1. The diagrams are all in the same plane (parallel to *T* surface) irrespective of the orientation of the cylinder from which the thin sections were prepared (diagram 1). Cylinders of two orientations, perpendicular to each other, were investigated (Fig. 2). Since the compression (or extension) axis is always parallel to the cylinder axis, the *T*-cylinder diagrams in Plate 3 are correlated with compression (or extension) applied at the center, and the *l*-cylinder diagrams are correlated with compression (or extension) applied along a north-south line. (*See* diagram 1.) Additional information about individual diagrams is given in the explanation to Plate 3.

Undeformed Fabric

The undeformed dolomite fabric has a clear but poorly developed foliation (*s* surface) approximately parallel to the plane of the diagrams in Plate 3. Diagrams 4, 15, 20 show the c_v-axis orientation from both *T* and *l* cylinders. The grains show well-developed but not abundant twins, indicated by small filled circles (*f* poles) in diagram 20. The data required for the predicted fabric analysis are the crystallographic orientations of 100 representative grains in a section of the undeformed rock. For unique orientation of the space lattice, one element in addition to the optic axis must be located. Accordingly, positions of $\{02\bar{2}1\}$ lamellae and cleavages $\{10\bar{1}1\}$ were determined where possible. Grains in which *f* twin lamellae are visible have a restricted range of orientation as shown by comparing diagram 15 (optic axes of twinned grains) with diagram 20 (optic axes of all grains). For this reason the orientation of grains in the undeformed fabric (Fig. 8A; Pl. 4) were located by independent measurement by Mr. J. H. Spotts with reference to the optic axis and one or more cleavages $\{10\bar{1}1\}$. Every grain was measured in a random traverse until 100 with measurable cleavage were obtained. This fabric can be compared to that measured nonselectively (without regard to presence of lamellae or cleavage) shown in diagram 20. These are very similar and indicate that the rock is essentially homogeneous with regard to optic-axis orientation. No interpretation of the undeformed fabric is attempted since no field studies were made.

Experiments Favorable for Development of f Twins

If negative sense of slip on *f* is assumed, the preferred orientation pattern of the undeformed fabric is such that deformation by twin-glide on *f* is favored in compression experiments on *T* cylinders and in extension experiments on *l* cylinders. (*See* Fig. 1.)

Two compression experiments with *T* cylinders, at 20°C and 300°C, were made. The former (diagram 7) requires no discussion as there is no significant fabric change. The latter resulted in extensive development of *f* twins and possibly in some change in orientation of c_v. An idealized representation of reorientation by complete twinning is shown by diagram 10. If all the axes were originally concentrated in the center of the diagram at *C′*, then after complete twinning of the grains on *f′* (points on a circle 63° distant from *C′*) the reoriented axes *C″* would be on a circle 54° distant and the locus of poles to new twins *f″* would be a circle 51° distant. This reorientation would occur in response to pressure *P* parallel to *C′*, combined with a negative direction of slip. Another view, rotated 90°, is shown with *C′* and *P* parallel to a north-south diameter, and with the loci of *f′* and *f″* shown by arcs at the appropriate distances.

Diagram 2 for a *T* cylinder compressed 9 per cent at 300°C shows c_v axes of 180 grains in which the positions of optic axes could be measured directly. The c_v-axis pattern appears as a fairly distinct ring about 40° from the center of the diagram in contrast with the central maximum of the undeformed fabric (diagram 20) which suggests a tendency for an outward migration of c_v axes in response to the compression as predicted in diagram 10. However, the possibility cannot be overlooked that diagram 2 shows, in part at least, only an apparent fabric change because of the inherent selectivity of the measurements. That is, the optic axis cannot be directly measured in the most highly twinned grains, in which its original position would almost certainly be centrally located

(diagram 8); failure to measure it would, therefore, result in an apparent central void similar to that of diagram 2. Moreover, of all the grains of the original fabric (diagram 20), those least favorably oriented for twinning in compression would be located at the outskirts of the central maximum, which, owing to possible small translation shifts, corresponds roughly in position with the girdle of diagram 2. Measurement of *f* poles results in an incomplete girdle which straddles both the *f′* and *f″* circles of diagram 10. The fabric possibly includes both kinds of twin. Turner *et al.* (1954, p. 484) have been able to identify in some instances the two types, but similar attempts on our part have been unsuccessful.

In a number of grains it was not possible to obtain reliable axes measurements because of extensive twin development on two of the three possible *f* planes. However, measurements of pairs of *f* poles in such grains give, by construction, two possible axes positions per grain. Diagram 8 is a plot of these possible positions. If both lamellae lie in the original lattice, the constructed position of c_v must represent the original (untwinned) position. Since the resolved shear stress is highest for those grains with c_v subparallel to the compression axis, the centrally situated points (diagram 8) showing c_v of the most highly twinned grains, probably should be chosen as representing the actual positions of the optic axes. The peripheral concentration may possibly include some c_v axes in the twinned position, consistent with diagram 10, if one of the lamellae has developed in the new (twinned) lattice (*f″* of diagram 10).

In diagrams 5 and 6 (extension experiments on *1* cylinders) the direction of extension is north-south. Axes measurement of untwinned grains (diagram 5) shows no reorientation (compare with diagram 4). On the other hand twinned grains in this cylinder (diagram 11) show an axis pattern distinctly different from that of diagram 4. The shift from the central to the peripheral zone corresponds with diagrams 2 and 8 for compression.

Diagram 6 requires no comment, as the strain was small and no significant reorientation of axes has taken place.

In summary, *f* twins have been abundantly developed, especially by the compression experiments, and c_v has probably been generally reoriented as predicted. There is no unequivocal evidence of a translation-slip which could have succeeded the twinning stage, although some might have occurred.

Experiments Unfavorable for Development of f *Twins*

Compression of *1* cylinders and extension of *T* cylinders represent unfavorable conditions for *f*-twin development. It would be expected that deformation would be characterized by translation-slip on *c*, especially since the total strain (up to 9 per cent) is about the same as in the set of experiments favoring *f*-twin development.

Two compression experiments of this kind failed to give unequivocal evidence of translation-slip (diagrams 13, 14, 18, 19 and 12, 17). Diagram 18 of axes of untwinned grains is quite similar to diagrams 4 and 20 of the undeformed fabric, although the slightly greater scattering of the axes might be interpreted as the result of translation-slip. Construction of *a* axes (3 per grain) from a number of these untwinned grains likewise gives no clear evidence of a favored direction of slip in *c* (diagram 19). The criterion for translation-slip used by Turner *et al.* (1954), which is dependent on anomalously oriented twin lamellae, was also investigated but without success. It should be pointed out that the specimen orientations were chosen for this study with *f* twinning in mind. They are not favorable for basal translation, since the {0001} planes tend to lie nearly normal or nearly parallel to the stress axis, as do the optic axes, and so the resolved shear stress on the base is generally low, and rotations of the lattice would be relatively small.

A minor amount of twinning is developed by this experiment, but this is confined to grains having c_v axes nearly parallel to the direction of compression (diagrams 13, 14) and would be expected under such circumstances.

The second compression experiment using a *1* cylinder was carried out at room temperature and resulted in somewhat less strain than at 300°C. The diagrams (12, 17) add nothing to the discussion just given.

Three extension experiments on *T* cylinders give axes orientation (diagrams 16, 21, 22). The total strain is small (about 5 per cent), and

there is no clear evidence of reorientation of the axes (compare with undeformed fabrics—diagrams 4, 20).

l and a *T* cylinder, both compressed about 9 per cent at 300°C.

In the undeformed rock approximately 18

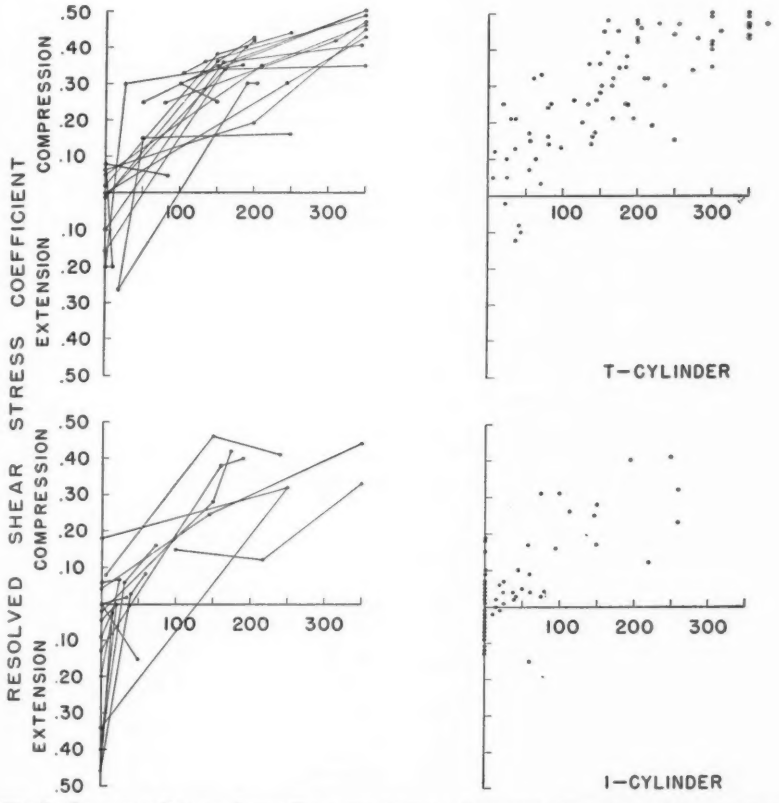

FIGURE 6.—LAMELLAE SPACING-INDEX DATA FOR *T* AND *l* CYLINDERS COMPRESSED 9 PER CENT AT 300°C
Left: spacing index vs. resolved shear stress coefficient for the three $\{02\bar{2}1\}$ planes for 15 grains; right: plot of plane with maximum index for each of 100 grains vs. stress

In summary, this group of experiments developed relatively few *f* twins. The thin sections show many fractures through the fabric. Positive evidence of translation-slip is lacking.

Spacing-Index Data

Since there is little or no development of lamellae in specimens deformed at room temperature or in any deformed in extension, spacing-index data were obtained only for a

per cent of all grains measured have one set of $\{02\bar{2}1\}$ lamellae developed; 10 per cent have two sets; and 2 per cent have all three sets. In the deformed *T* cylinders on the other hand, 38 per cent of all grains have one set of lamellae; 37 per cent have two sets; 18 per cent have three; and only 7 per cent have none. Moreover, the number of lamellae per set has greatly increased with compression; that is, the "spacing index," or number of lamellae per mm counted while viewed on edge (Turner and Ch'ih, 1951, p. 898) has increased from a mean

of less than 10 in the undeformed rock to more than 100 in the compressed *T* cylinder.

The relationship is consistent between the resolved shear-stress coefficient in the negative direction sense computed for an $\{02\bar{2}1\}$ plane and the value of the spacing index for that plane. A plot of the data for 15 grains of the *T* cylinder (Fig. 6) shows that the great majority (Fig. 6) suggests why this should be so. Most $\{02\bar{2}1\}$ planes have either a high resolved shear stress in the wrong sense (tension field) or a low stress in the postulated sense (compression field). For those few grains which are favorably of points lies above the zero stress line in the compression field; that is, the $\{02\bar{2}1\}$ planes are favorably oriented for twinning in compression if the direction sense is negative. Plots of the data for the other 85 grains of the 100 measured are not reproduced here, but the same trend is always indicated. For the three sets of lamellae of any one grain it is clear that the greater the resolved shear stress the more profuse the lamellae. If the sense of shear is positive for any set, the point representing that set is in the tension field, and no lamellae are developed. When those planes with the highest spacing index in each grain are plotted against resolved shear stress for all grains, the relationship still holds that the lamellae develop most profusely on planes of highest resolved shear stress (Fig. 6).

In the deformed *I* cylinder only about 30 per cent of the grains have lamellae, and the mean spacing index is about 25. A plot of data oriented for twinning in compression, the relationship again holds that the higher the stress the more profuse the lamellae. For many of the grains in this orientation all $\{02\bar{2}1\}$ planes are unfavorably situated for twinning; they are in the extension field and have no lamellae. This condition is not easily indicated in the diagram. Also, 350 is about the greatest number of lamellae that can be counted per mm, so the plots terminate at that value. Actually for high stresses in the favored field, the lamellae are spaced exceedingly closely, and their index may be 1000 or greater. Degree of deformation and hence, presumably, completeness of twinning are reflected in the number of very thin, closely spaced lamellae, and not in the broadening of relatively few lamellae.

Predicted Fabric Changes

General Remarks

An analytical method was successful in predicting rather closely the fabric changes accompanying the experimental deformation of Yule marble even with necessary simplifying assumptions (Handin and Griggs, 1951) and may be applied to dolomite as well as an additional indication of the mechanisms involved.

Only two mechanisms of plastic flow in dolomite had ever been demonstrated: translation gliding on the basal plane $\{0001\}$ and mechanical twin gliding on $\{02\bar{2}1\}$; it was assumed that only these two would operate. Since deformations were small in the experiments, and since Handin and Griggs (1951, p. 877–879) had shown that large plastic strains were required to produce significant fabric changes by translation gliding (which can only shift crystal elements as a result of slip-plane rotation accompanying shear), only the effects of twin gliding on $\{02\bar{2}1\}$ were considered.

Analytical Methods

The direction sense of mechanical twinning was uncertain at the time this study was undertaken, so both senses (Fig. 7) had to be considered. A negative sense seemed more likely in view of the results of Fairbairn and Hawkes (1941). Accordingly, the fabrics were derived on the assumption that changes accompanying deformation are due solely to twinning on $\{02\bar{2}1\}$ and, with one exception, are in a negative sense.

Figure 7 shows that the angle of shear, ψ, is 33° and that the optic axis moves through an angle θ of 54°. The shear $s = 2 \tan \psi/2 = 0.59$.

The procedures used in constructing the predicted fabrics are summarized here. (For details *see* Handin and Griggs, 1951.)

For each of the 100 representative grains in the undeformed fabric, the sense and magnitude of the resolved shear-stress coefficient were determined graphically for each of the three $\{02\bar{2}1\}$ planes and for the two stress orientations, parallel and perpendicular to the fabric maximum. Which twin plane would be operative was decided upon from these data and from the following assumptions, which ap-

peared to be valid in the Yule marble study:

(1) On the average, individual grains are subjected to the same stress field as the aggregate in bulk.

(2) The law of maximum resolved shear stress determines the operative glide plane.

(3) Twinning occurs on one and only one of the three possible planes. (Actually some grains are twinned on two or even three planes.)

It was further assumed that the deformation was "homogeneous" (Taylor, 1938, p. 319), that each grain deforms an amount equal to the specimen as a whole. Fabric changes were supposed to result only from the shift of the c_v axis by twinning, rotation of the active twin planes being ignored. Effects of any other mechanisms, accompanying twinning or occurring in grains which were not favorably oriented for twinning, were considered unimportant in reorienting optic axes.

The amount of deformation required for complete twinning of each grain was computed. Complete twinning of all grains of any orientation within the aggregate would require for dolomite an extension of 33 per cent or a compression of 24 per cent. A fabric for 5, 10, 15, and 20 per cent deformation was desired, so that to decide whether to plot the twinned or untwinned position or both of the c_v axes it was necessary to stipulate further: if a grain is two-thirds or more twinned, the twinned c_v axis only is plotted; if a grain is more than half but less than two-thirds twinned, both the original and twinned positions are plotted; and for grains less than half twinned, or with no plane on which twinning is possible, the untwinned position only is plotted.

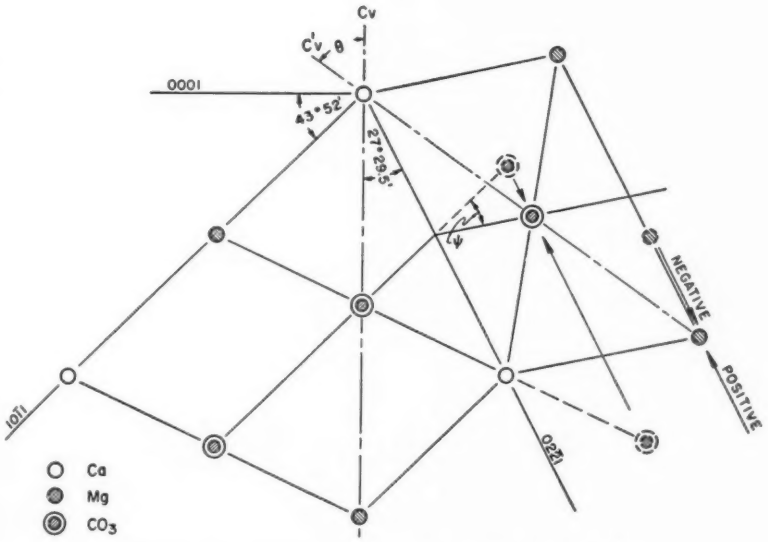

FIGURE 7.—GEOMETRY OF MECHANICAL TWINNING ON $f\{02\bar{2}1\}$
On $\{1\bar{2}10\}$ projection; ψ = angle of shear; θ = angle of shift of optic axis c_v

Results

With the convention adopted for plotting predicted fabrics, deformations of 20 per cent represent complete twinning in compression and nearly complete twinning in extension for all grains with at least one $\{02\bar{2}1\}$ plane oriented for twinning in the negative sense. Stages of the progress to this predicted maximum change are shown in Plate 4 for a T cylinder hypothetically deformed 5, 10, 15, and 20 per cent in compression and extension (countour inter-

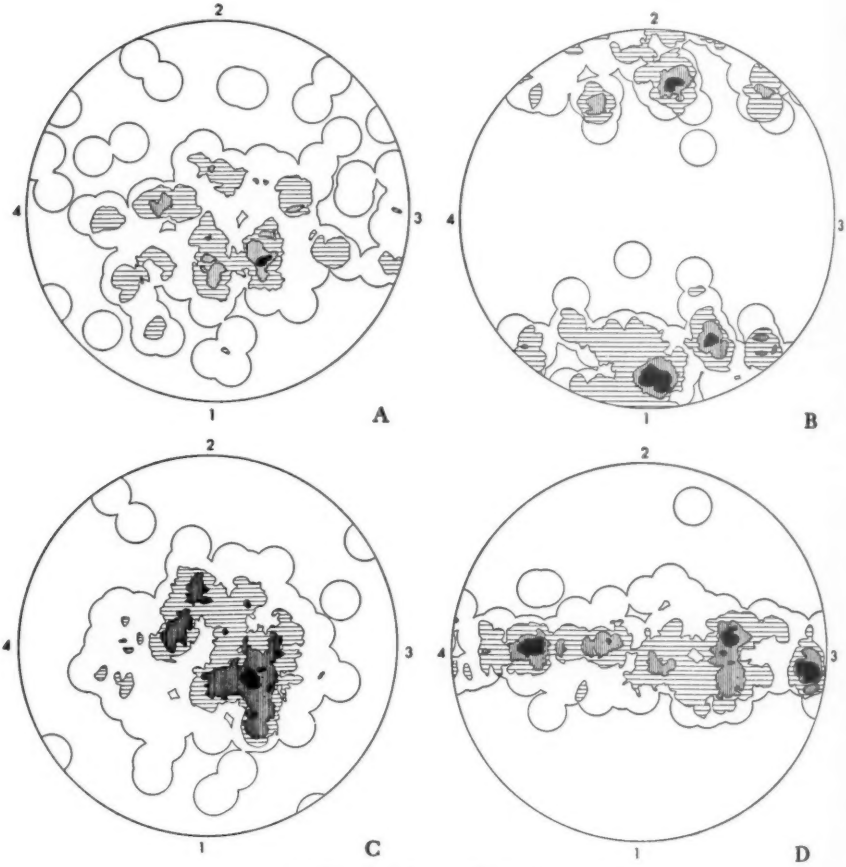

FIGURE 8.—FABRIC DIAGRAMS

A.—*T* section of a *T* cylinder of undeformed Hasmark dolomite; 100 optic axes measured at random; contour interval 1, 3, 5, 7 per cent

B.—*T* section of a *1* cylinder; 100 optic axes; predicted fabric for 20-per cent extension by mechanical twinning on $\{02\bar{2}1\}$; contour interval 1, 3, 5, 7 per cent

C.—*T* section of a *T* cylinder; 124 optic axes; predicted fabric for 20-per cent compression by mechanical twinning of $\{02\bar{2}1\}$ (positive sense); contour interval 1, 3, 5, 7 per cent

D.—*T* section of a *1* cylinder; 100 optic axes; predicted fabric for 20-per cent compression by mechanical twinning on $\{02\bar{2}1\}$; contour interval 1, 3, 5, 7 per cent

val 1, 3, 5, 7, per cent). Figure 8 shows the 20 per cent fabrics for *1* cylinders.

In both *T* and *1* cylinders under compression, the *c* axes migrate to form a girdle about the stress axis. For a *T* cylinder the axes move outward from the centrally situated maximum to form a peripheral girdle. The opposite was predicted and observed (Handin and Griggs, 1951, Pl. II; Turner and Ch'ih, 1951, Fig. 46) for Yule marble, as would be expected if the sense of twinning in dolomite is the reverse of that in calcite. (Although the mechanical twin planes are different, $\{01\bar{1}2\}$ in calcite and $\{02\bar{2}1\}$ in dolomite, both the shear and angle of optic-axis shift are very similar in the two minerals.)

For extensions the c_o axes are expected to become aligned with the stress axis. At 20 per cent deformation the result for a *T* cylinder (Pl. 4) is a sharpening of the central maximum

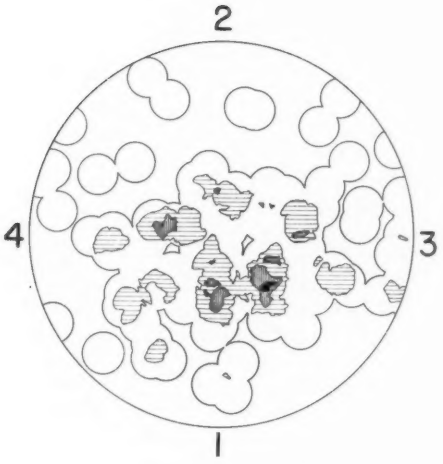

UNDEFORMED

PREDICTED OPTIC-AXES FABRICS OF T C

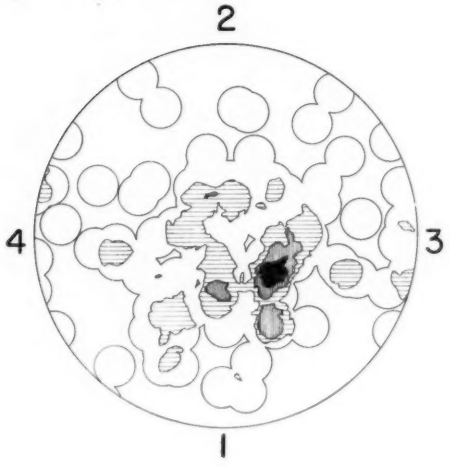

5 PERCENT

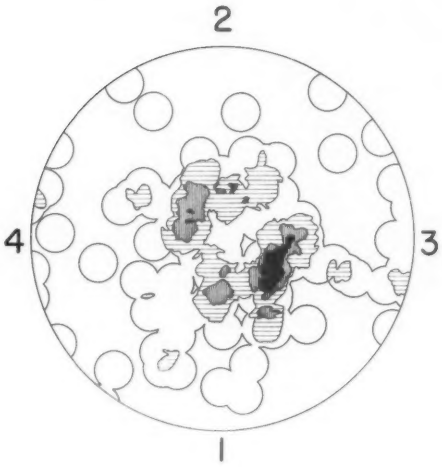

10 PERCENT

EXTEN

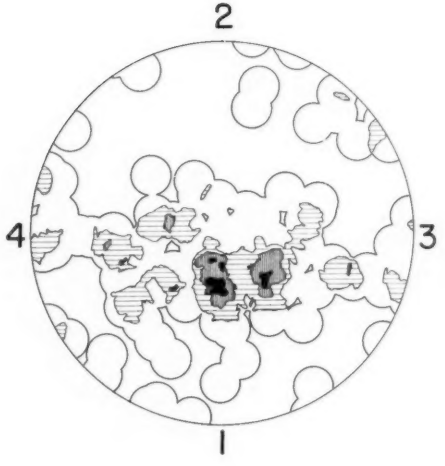

5 PERCENT

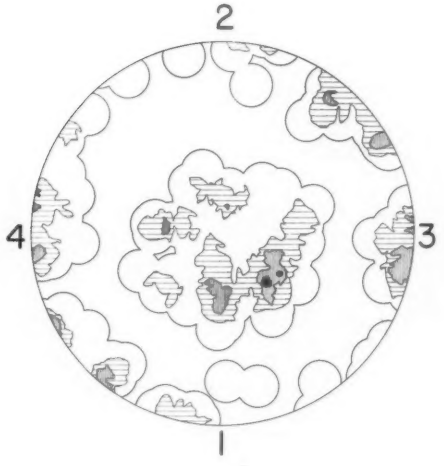

10 PERCENT

COMPRE

ABRICS OF T CYLINDERS HOMOGENEOUSLY DEFORMED BY TWIN

(Contour interval 1, 3, 5, 7 per cent)

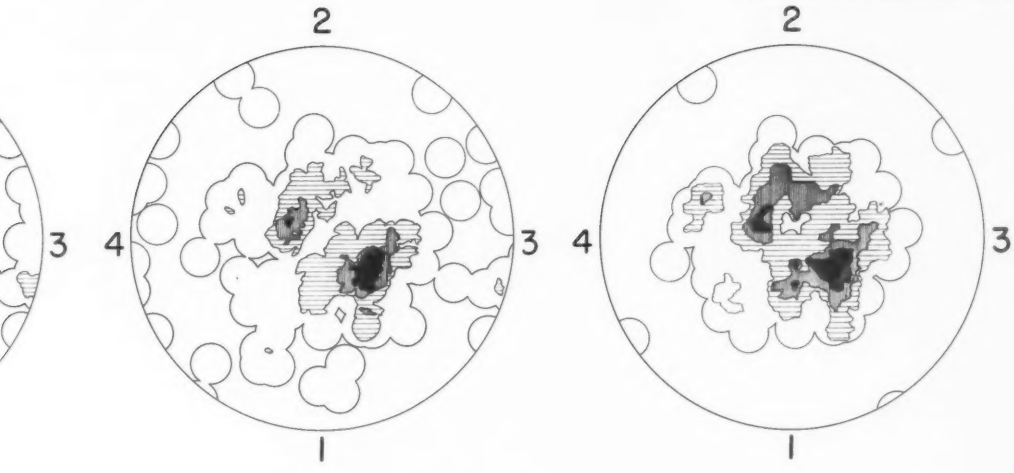

15 PERCENT 20 PERCENT

TENSION

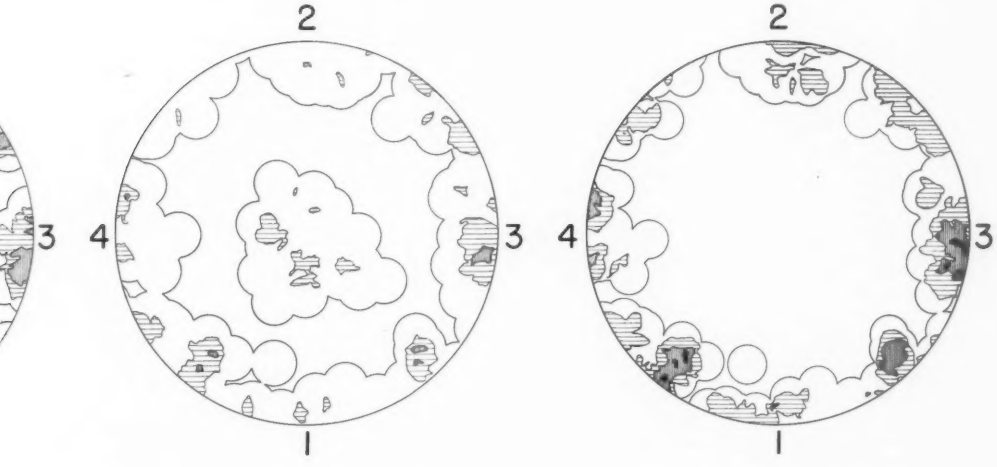

15 PERCENT 20 PERCENT

PRESSION

TWINNING ON $\{02\bar{2}1\}$ IN A NEGATIVE DIRECTION SENSE

and a cle
the revers
fabric for
One pr
show the
sense. C
change si
suming a
fabric of
This
twinning
anism in
should
10 per c
served cl
of the tw

Speci
Hasmar
under
tempera
extensio
rected
axes f
stress-s
yield
strengt
of grai
are affe
the ra
all con
extens
shear
60° to
about
cent i
in the
mater
substa
is rel
very
is alw
brittl
faces
least
is at
sion,
postp
hand
typic

and a clearing of the peripheral region, again the reverse of what happens to the Yule marble fabric for a similar deformation.

One predicted fabric is presented (Fig. 8) to show the results of twin gliding in the positive sense. Compression would produce a fabric change similar to that caused by extension assuming a negative sense, in other words to the fabric of calcite marble.

This analysis suggests that if mechanical twinning is an important deformation mechanism in dolomite, measurable fabric changes should occur even for deformations of about 10 per cent, and that the direction of the observed change should establish the correct sense of the twin-glide.

Summary and Conclusions

Specimens of pure, homogeneous, anisotropic Hasmark dolomite have been deformed dry under 5000 atm confining pressure at room temperature and at 300°C in compression and extension, and with the differential force directed parallel and perpendicular to the optic-axes fabric maximum. Evidence from the stress-strain relationship (Fig. 5) is that: (1) yield points are dependent, but ultimate strengths are largely, if not wholly, independent of grain orientation, (2) strength and ductility are affected little, if any, by temperature within the range of these experiments, (3) strength in all compression tests is greater than that in all extension tests, (4) all tests terminated in shear fracture on surfaces inclined at about 60° to direction of least pressure (Pl. 2) at about 9 per cent strain in compression, 5 per cent in extension. Behavior of the dolomite is in the transition from that of a typical "brittle" material to that characteristic of a "ductile" substance in that: (1) for brittle solids, strength is relatively insensitive to temperature, but very dependent upon normal pressure (which is always higher in a compression test); (2) brittle materials usually fracture on shear surfaces inclined at more than 45° to the axis of least pressure; (3) in these experiments ductility is at least in part actually greater in compression, which suggests that high normal pressure postpones loss of cohesion; (4) on the other hand, the shape of the stress-strain curves is typical of ductile solids—there is a straight elastic part, a well-defined yield point, considerable permanent deformation before fracture, and work-hardening.

No description of the differences in the stress-strain curves has been possible in terms of any particular deformation mechanism, but the fact that the yield points differ so greatly among specimens of different grain orientation strongly suggests that plastic flow involving crystallographic slip occurs during the early stages of the deformation. On the other hand, the lack of strength anisotropy in the later stages suggests that the macroscopic shear or "faulting" occurs then.

Grain orientation studies of the deformed specimens indicate:

(1) The original optic-axes fabric of the rock, characterized by a rather pronounced maximum normal to the foliation, is not much affected by any of the deformations at room temperature; nor is there an appreciable development of $\{02\bar{2}1\}$ lamellae (Pl. 3, diagrams 5, 7, 12, 20, 21).

(2) Compression at 300°C of specimens favorably oriented for twinning on $\{02\bar{2}1\}$ in a negative sense results in a profusion of lamellae and perhaps in a fabric change in which optic axes generally centrally situated in the diagram of the undeformed fabric are shifted outward to form a girdle about the axis of compression (Pl. 3, diagrams 2, 8).

(3) Extensions at 300°C of specimens favorably oriented for twinning, though only half as great as the compressions, do develop $\{02\bar{2}1\}$ lamellae and result in a minor reorganization of the c, fabric consistent with twinning in the negative sense (Pl. 3, diagram 6).

(4) Deformations at 300°C of specimens unfavorably oriented for $\{02\bar{2}1\}$ twinning yield a profuse development of lamellae, but only in relatively few grains whose optic axes presumably lie in the twinned position (Pl. 3, diagrams 13, 16, 18).

(5) Evidence for basal translation in the specimens is inconclusive, but neither are there results requiring that it be ruled out. The fact that no other glide systems, no pronounced cleavage or cataclasis, and no "recrystallization" were observed, makes it very likely that basal translation is operative, especially where f twinning is prohibited.

(6) Plots (Fig. 6) of lamellae-spacing index

vs. resolved shear-stress coefficient consistently show that lamellae develop most profusely parallel to $\{02\bar{2}1\}$ planes of highest-resolved shear stress in the negative sense. In most cases lamellae do not appear on planes with a low stress or with a high stress if the sense is positive.

Predicted fabrics (Fig. 8; Pl. 4) have been prepared for hypothetical deformations under the assumption that twinning on $\{02\bar{2}1\}$ is the only mechanism important to the reorientation of the c_v fabric. The predictions are:

(1) For compressions the optic axes migrate to form a girdle about the stress axis if the twin sense is negative, and align themselves parallel to the compression axis if the sense is positive.

(2) In extensions the reverse is indicated: for the negative direction sense, axes become aligned with the stress direction; for the positive sense a girdle would form about the axis.

(3) Although complete twinning would require a plastic strain of 20 per cent, significant fabric changes should result from a compression of the amount produced experimentally (9 per cent).

Conclusions resulting from the petrofabric work are:

(1) Plastic deformation at room temperature involves basal translation or some other mechanism undetermined in this study. There is little or no development of $\{02\bar{2}1\}$ twins or any other visible lamellae.

(2) Twinning occurs at 300°C if a twin plane is favorably oriented with respect to the applied force so that motion is in the negative sense. This is confirmed by the qualitative similarity of predicted and observed fabrics (compare especially Pl. 3, diagrams 2 and 8; Pl. 4 for 10 per cent compression) and by the lamellae-spacing index data (Fig. 6).

In a recent publication, Turner *et al.* (1954) report on a specimen of dolomite from Dover Plains, New York, deformed by compression under conditions comparable with the Hasmark experiments. The compression axis was at a considerable angle to the major axes concentrations in the undeformed rock, in contrast with the Hasmark fabric. Evidence of both *f* twins and $\{0001\}$ translation was obtained as would be expected from the relative attitudes of the compression axis and grain axes. This investigation, done independently and with different material, confirms the behavior of dolomite.

Preliminary results of experiments on dolomite single crystals, also at 5000 atm confining pressure, confirm Johnsen's discovery of $\{0001\}$ translation and indicate that at room temperature the critical resolved shear stress required for $\{02\bar{2}1\}$ twinning must be much greater than that needed for translation on the base. Conversely, calcite twins readily on $\{01\bar{1}2\}$ at temperatures ranging from room temperature to at least 500°C, which perhaps explains why polysynthetic twinning is rare in dolomite. Further work should definitely establish the twin sense in a single crystal and indicate effects of temperature.

Further work is planned on dolomite rock under conditions which may induce greater ductility (higher pressure, higher temperature, or both) so that larger fabric changes can be studied and the possibility of other deformation mechanisms can be investigated.

References Cited

Bradley, W. F., Burst, J. F., and Graf, D. L., 1953, Crystal chemistry and differential thermal effects of dolomite: Am. Mineralogist, v. 38, p. 207–217.

Fairbairn, H. W., and Hawkes, H. E., Jr., 1941, Dolomite orientation in deformed rocks: Am. Jour. Sci., v. 239, p. 617–632.

Griggs, D., and Miller, W. B., 1951, Deformation of Yule Marble: Part I—Compression and extension experiments on dry Yule marble at 10,000 atmospheres confining pressure, room temperature: Geol. Soc. America Bull., v. 62, p. 853–862.

Griggs, D., Turner, F. J., Borg, I., and Sosoka, J., 1951, Deformation of Yule Marble: Part IV—Effects at 150°C: Geol. Soc. America Bull., v. 62, p. 1385–1406.

Griggs, D., Turner, F. J., Borg, I., and Sosoka, J., 1953, Deformation of Yule marble: Part V—Effects at 300°C: Geol. Soc. America Bull. v. 64, p. 1327–1342.

Handin, J., 1953, An application of high pressure in geophysics: Experimental rock deformation: Am. Soc. Mech. Engineers Trans., v. 75, p. 315–324.

Handin, J. W., and Griggs, D., 1951, Deformation of Yule marble: Part II—Predicted fabric changes: Geol. Soc. America Bull., v. 62, p. 863–886.

Johnsen, A., 1902, Biegungen and Translationen: Neues Jahrb. Mineralog. Geol. Paleont., 1902, Bd. 2, p. 133–153.

Ladurner, J., 1953, Allgemeine Kennzeichnung ...

alpiner Dolomit-Tektonite: Anzeig. math.-naturw. Kl. Oesterr. akad. Wiss., no. 1, p. 1.

Sander, B., 1930, Gefügekunde der Gesteine: Springer, Vienna, 352 p.

Sander, B., 1950, Einführung in die Gefügekunde der geologischen Körper (pt. 2, die Korngefüge, p. 232–236): Springer, Vienna, 409 p.

Taylor, G. I., 1938, Plastic strain in metals: Inst. Metals Jour., v. 62, p. 307–324.

Turner, F. J., and Ch'ih, C. S., 1951, Deformation of Yule marble: Part III—Observed fabric changes due to deformation at 10,000 atmospheres confining pressure, room temperature, dry: Geol. Soc. America Bull., v. 62, p. 887–906.

Turner, F. J., Griggs, D. T., Heard, H., and Weiss, L. W., 1954, Plastic deformation of dolomite rock at 380°C: Am. Jour. Sci., v. 252, p. 477–488.

3737 Bellaire Boulevard, Houston 25, Texas; Department of Geology and Geophysics, Massachusetts Institute of Technology, Cambridge 39, Mass.

Manuscript Received by the Secretary of the Society, September 30, 1954

BULLETIN OF THE GEOLOGICAL SOCIETY OF AMERICA
VOL. 66, PP. 1275-1314, 25 FIGS., 4 PLS. OCTOBER 1955

EXPERIMENTAL STUDY OF THE STRENGTH OF ROCKS

BY EUGENE C. ROBERTSON

ABSTRACT

An experimental investigation of the homogeneous Solenhofen limestone and a number of other rocks was made to determine their their strengths while under moderate hydrostatic pressure at room temperature. The other rocks were fossiliferous limestone, shaly limestone, marble, granite, diabase quartzite, slate, soapstone, verde antique, and sandstone. The minerals tested were pyrite, quartz, microcline, and fluorite.

Three types of experimental procedures were used: compression of solid cylinders, crushing of hollow cylinders, and punching of disks. The specimens were all carefully shaped right circular cylinders, and during the tests were jacketed to prevent penetration by the pressure fluid. The hydrostatic pressures ranged from 1 atmosphere to 4000 kg/cm². Measurements were made to obtain strains and stresses developed in each specimen for deformation to the point of rupture or into the plastic range; the duration of the tests was 1–8 hours.

All rock specimens exhibited a range of elastic linearity of stress with strain. Under moderate hydrostatic pressures, the limestones and marbles could be made to flow plastically to large deformations, and some heating experiments on limestone demonstrated an increase of plasticity with heating. None of the silicate rocks and minerals exhibited any plastic behavior.

The experimental data were examined with reference to various criteria of failure. The maximum shear-stress criterion was found to be reliable in predicting the yield point for the limestones, and was found to be an approximate guide to failure of limestone by rupture.

The silicate rocks failed by rupture, and their rupture strength was increased by hydrostatic pressure. A rough, empirical criterion of failure was found for rupture of silicate rocks, namely, linearity of maximum shear stress with mean stress.

CONTENTS

TEXT

	Page
Introduction	1276
Acknowledgments	1277
Experimental results for limestones and marbles	1277
General testing procedure	1277
Accuracy of measurements	1278
Compression of solid cylinders	1279
Results from solid-cylinder compression tests on Solenhofen limestone	1279
Results from cyclic compression tests on solid cylinders of Solenhofen limestone	1281
Results from solid-cylinder compression tests on other limestones and marbles	1282
Compression of hollow cylinders	1283
Results from hollow-cylinder tests	1283
Punching of disks	1286
Results of heat and pressure studies	1287
Strength of limestone	1290
Definition of strength	1290
Symbols	1291
Stress distribution in the elastic range	1292
Stress distribution in the plastic range	1292
Criteria of failure	1294
Yield strength of limestone	1295
Rupture strength of limestone	1298
Conclusions on the strength of limestone	1300
Experimental results for silicate rocks and minerals	1301
Introduction	1301
Results from solid-cylinder compression tests	1301
Results from hollow-cylinder tests	1301
Application of criteria of failure to silicate rocks	1303
Rupture strength of silicate rocks	1305
Generalizations on rock strength	1307
Appendix 1: Descriptions of rocks and minerals	1309
Appendix 2: Density measurements	1312
References cited	1313

ILLUSTRATIONS

Figure	Page
1. Diagram of the external pressures on rock specimens in four experimental procedures	1277

Figure Page
2. Cross section of testing cylinder 1278
3. Stress-strain curves from axial-compression experiments on solid cylinders of Solenhofen limestone 1279
4. Cyclic-compression experiments on solid cylinders of Solenhofen limestone 1282
5. Stress-strain curves for solid cylinders of various marbles and limestones 1283
6. Complete stress-strain curves for solid cylinders of Solenhofen limestone, Danby marble, and Becraft limestone .. 1284
7. Hydrostatic pressure at failure vs. ratio of radii for three sizes of hollow cylinders of Solenhofen limestone 1284
8. Theoretical shearing surfaces in a hollow cylinder under external hydrostatic pressure 1285
9. Stress-strain curves from crushing experiments on hollow cylinders of Solenhofen limestone 1286
10. Stress-strain curves from punching experiments on disks of Solenhofen limestone 1287
11. Theoretical stress distribution in the wall of a hollow cylinder under external hydrostatic pressure 1293
12. Maximum shear stress vs. mean stress at the elastic limit, Solenhofen limestone. 1296
13. Maximum shear stress vs. mean stress at the elastic limit, Yule marble (Griggs and Miller, and Balsley) and Carrara marble (Adams and Bancroft) 1296
14. Maximum shear stress vs. mean stress at the elastic limit, marble (Karman and Boeker) 1297
15 Maximum shear stress vs. mean stress at the elastic limit, Danby marble and Rutland White marble 1297
16. Maximum shear stress vs. mean stress at rupture, Solenhofen limestone 1299
17. Maximum shear stress vs. mean stress at rupture, marble (Karman, Boeker, and Balsley) 1299
18. Mohr diagram of the results by Karman and by Boeker on rupture of marble ... 1300
19. Mohr diagram of the results on rupture of Solenhofen limestone 1300
20. Stress-strain curves from axial-compression experiments on solid cylinders of granite, slate, and pyrite 1302
21. Stress-strain curves from axial-compression experiments on solid cylinders of Blair dolomite 1302
22. Scatter diagram of rupture strength vs. ratio of radii for crusing tests of hollow cylinders of silicate rocks and minerals. 1303
23. Maximum shear stress vs. mean stress at rupture, various rocks and minerals 1304
24. Maximum shear stress vs. mean stress at rupture 1305
25. Comparison of rupture strengths and of yield strengths for crushing of hollow cylinders of the same ratio of radii 1308

Plate Facing Page
1. Solid cylinders of Solenhofen limestone 1280
2. Hollow cylinders of Solenhofen limestone .. 1281
3. Disks of Solenhofen limestone and heated and compressed hollow cylinders of Solenhofen limestone and Yule marble 1288
4. Solid and hollow cylinders of various silicate rocks and minerals 1289

TABLES

Table Page
1. Plastic deformation of hollow cylinders of Solenhofen limestone and Yule marble under heat and pressure 1290
2. Computed and observed tangential strains at inside surface of hollow cylinders at rupture 1294
3. Total axial stress and strain at rupture of solid cylinders of Solenhofen limestone .. 1298
4. Strength constant of Griffith criterion of failure from experiments on Solenhofen limestone 1301
5. Strength constant of Griffith criterion of failure from experiments on Barre granite 1303
6. Bridgman's shearing strengths for several rocks and minerals 1306

Introduction

This laboratory investigation was conducted to find some predictable regularity in the strength of fresh-rock specimens deformed to failure by fracture or plastic flow under hydrostatic pressures up to 4000 kg/cm², at room temperature, under pressures applied slowly and with no change of the chemical environment. Primarily, experiments were performed to examine the influence of the stress magnitude and orientation on strength, but exploratory work was also done to find the dependence of strength on stress rate and stress history, on heat, and on the type and physical character of the rocks.

F. D. Adams (1901; 1910; 1912; 1917) previously utilized the restraint of tightly fitted steel jackets to provide lateral pressure on specimens of many types of rocks. Karman (1911) and Boeker (1915) each studied the deformation of marble under hydrostatic pressure in various stress systems. Bridgman (1918; 1936; 1939; and miscellaneous data in numerous papers) has studied the strengths of rocks under low to very high hydrostatic pressure, principally by compression and shearing tests. Griggs (1936; 1939; 1940; Griggs *et al.*, 1951; 1953) is the principal modern worker in the study of rock deformation, especially of carbonate rocks and minerals. Balsley (1941) studied the strength of marble

by extension tests. Goguel (1943, Part II) has given a fairly complete analysis of the available experimental data, adding some work of his own. Handin (1953; Handin and Higgs, 1954) has given a review of recent literature and has begun a thorough study of deformation of dolomite. Joffe (1928) investigated the deformation of sodium chloride carefully.

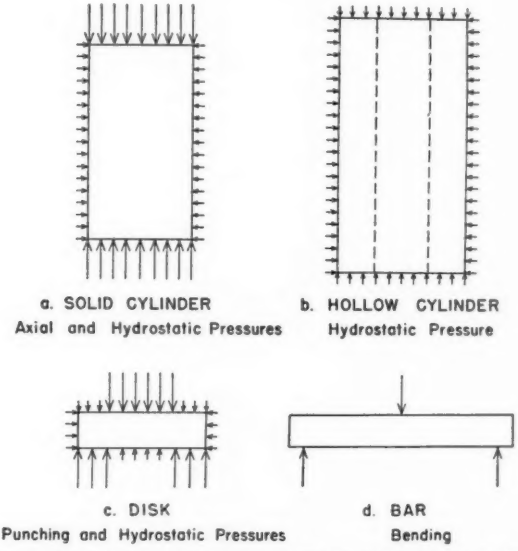

FIGURE 1.—DIAGRAMS OF THE EXTERNAL PRESSURES ON ROCK SPECIMENS IN FOUR EXPERIMENTAL PROCEDURES

In the experiments performed in this study, no tensional forces were applied; the forces were all compressive. Therefore, to avoid complication with signs of terms, the compressive stresses will be given as positive rather than negative.

The following are useful approximations:

$$1 \text{ ksc (kg/cm}^2) \cong 1 \text{ atmos} \cong 1 \text{ bar} \cong 15 \text{ psi (lb/in}^2) \cong 1 \text{ ton/ft}^2$$

1 mile depth $\cong$ 400 atmos

1 km depth $\cong$ 250 atmos

ACKNOWLEDGMENTS

Professor Francis Birch at Harvard University suggested to me the problem of finding an applicable criterion for failure in rocks, and he outlined the general and specific procedure involved in the solution of the problem. I acknowledge very gratefully Professor Birch's continued help and encouragement. The skillful machine work of Harold J. Ames with the help of L. Hammer and R. Hopewell was essential to the continuance of the investigation. Finally, I am indebted to the following men who have helped in various ways: R. K. Blumberg, P. H. Chang, C. Frondel, D. T. Griggs, H. E. McKinstry and E. Orowan.

EXPERIMENTAL RESULTS FOR LIMESTONES AND MARBLES

General Testing Procedure

Stress differences were developed within the specimens by applying hydrostatic pressure plus other loading on the external surfaces of the rock and mineral specimens. In each experiment, the difference between the stresses was increased until failure occurred. "Failure" signifies loss of strength both by breaking and by yielding. "Strength" is defined in Webster's New International Dictionary as "the quality of bodies by which they endure the application of force without breaking or yielding". In this

paper, rupture strength is the maximum stress difference at failure by breaking, and yield strength is the maximum stress difference at failure by yielding, assumed to occur at the elastic limit.

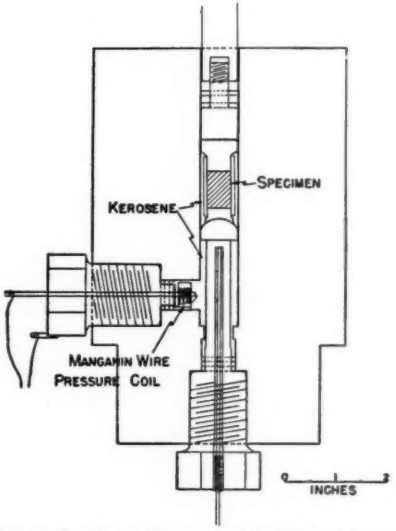

FIGURE 2.—CROSS SECTION OF TESTING CYLINDER

In one series of tests, solid cylinders of rock were compressed by hydrostatic pressure plus loading parallel to the cylinder axis (Fig. 1a). Another series of tests was made on hollow cylinders with closed ends; they were subjected only to hydrostatic pressure at the outside surfaces (Fig. 1b). Some punching experiments on disks of limestone under hydrostatic pressures were performed also (Fig. 1c). Only a few bending tests (Fig. 1d) at one atmosphere were performed. In almost all tests, the rate of loading was slow, at a rate of strain less than 1 per cent per half hour; and the length of the tests was from 1–8 hours.

A cross section of the steel testing cylinder used in most of the experiments is shown in Figure 2. The construction and use of high-pressure apparatus has been given in detail by Bridgman (for example, 1931, p. 30–77).

Hydrostatic pressure was built up in the pressure fluid in the testing chamber by advances of the piston driven by a hydraulic ram. The chamber was sealed against leaking at all openings by use of the Bridgman unsupported-area packing technique. The hydrostatic pressure was measured by balancing the change in the resistance of the manganin wire coil in the testing cylinder on a Carey-Foster bridge.

A device eliminating friction corrections in the measurement of the compressive force parallel to the axis of the steel testing cylinder was designed by Prof. Francis Birch; it is the bottom plug shown in Figure 2. The elastic strain of the hollow steel column of the plug was calibrated to give the compressive load on its top surface.

Accuracy of Measurements

Measurements in four categories were made at each change of conditions: time, hydrostatic pressure, axial pressure, and strain.

The room-temperature changes affected the precision of measurement of resistance by the Carey-Foster bridge so that the values of hydrostatic pressure were accurate only to plus or minus 25 ksc (kg/cm^2), although the sensitivity was 10 ksc.

Axial pressures measured by the strain of the bottom plug were accurate to plus or minus 50 ksc.

Rather uncertain corrections for strains in the packing and in the steel members to the measurements of shortening of solid cylinders and of punch penetration of disks reduced the accuracy of strains of the rock and mineral specimens considerably. The corrected total strain in the specimen was accurate only to within 10–20 per cent of its value, which precludes accurate computation of elastic constants; however, the reliability of the slope changes of the stress-strain curves was quite adequate for strength determinations. Longitudinal strains only were measured during the experiments; correction to the compressive stress was made for strains larger than a few per cent.

Each specimen was turned or ground to have a difference in diameter at all sections of less than 0.001 inch. The ends of the specimens were carefully ground to be perpendicular to the axes of the cylinders.

The well-known lack of homogeneity in rocks, and the anisotropy of minerals are complications in any study of their elastic properties,

although a statistical isotropy and homogeneity is approached in many fine-grained rocks, such as the lithographic limestone from Solenhofen, Bavaria, which was used for a majority of the tests. Solenhofen limestone has an extremely fine grain size (0.0002 inch), and a nearly random grain orientation is suggested by X-ray and physical-property tests.

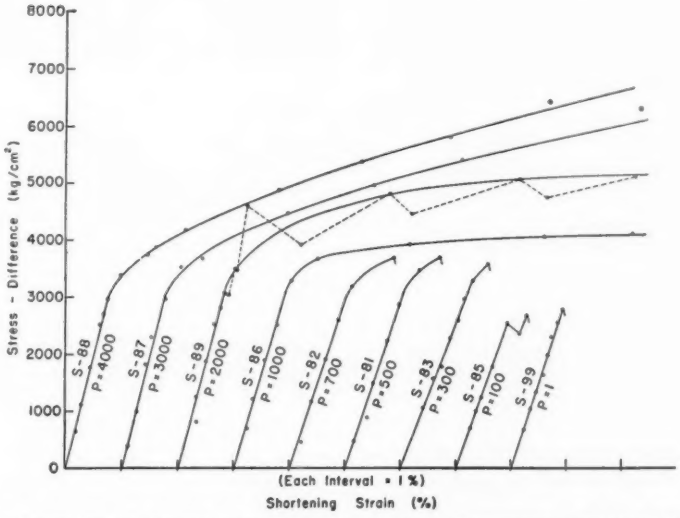

FIGURE 3.—STRESS-STRAIN CURVES FROM AXIAL-COMPRESSION EXPERIMENTS ON SOLID CYLINDERS OF SOLENHOFEN LIMESTONE

Each curve starts at zero strain; P = hydrostatic pressure in kg/cm.²

Compression of Solid Cylinders

The solid cylinders of rocks were all made ½ inch in diameter, and were ¾–1¼ inches long. Each specimen was mounted between two steel end plugs, and was jacketed with rubber tubing. Most of the experiments were done with solid end plugs (Pl. 1, fig. 2), which may have introduced certain irregularities in the stress distribution in the specimens, but the deformed specimens were quite symmetrical in appearance and consistent in strength. No lubrication was used between the steel end plugs and the specimen.

The advancing piston compressed excess of kerosene so that at contact with the end of the specimen the piston built up a hydrostatic pressure around the specimen. Thereafter, the piston produced both the hydrostatic and the differential axial pressures. A bleeder valve was used to remove kerosene, in order to maintain a constant hydrostatic pressure as the piston was advanced against the specimen. The piston was advanced intermittently, at about 5-minute intervals, each time increasing the stress difference about 200 ksc (kg/cm²), an average strain rate of about 0.02 per cent per minute in the elastic range. Testing was continued on each specimen well into the plastic range or to the rupture point.

Results from Solid-Cylinder Compression Tests on Solenhofen Limestone

The per cent decrease in length of the solid-cylinder specimens versus stress difference (total axial pressure minus hydrostatic pressure) in the cylinders are plotted in Figure 3. Within the limits of observation, the lower portion of all the curves is straight, and this justifies the application of Hooke's Law and elasticity theory to deformation below the elastic limit.

Specimens tested under hydrostatic pressures less than 1000 ksc show the abrupt termination of a rupture failure with a preceding, small

plastic flow. Specimen S-81 was shortened about 50 per cent and was considerably fractured, but nevertheless the interlocking fragments supported a compressive load greater than 1500 ksc for most of the deformation after the initial failure at 3740 ksc (Pl. 1, fig. 13). The four curves at the left in Figure 3 show considerable plastic deformation beyond the elastic limit. All specimens deformed plastically to a permanent set of more than 1 per cent were decreased slightly in density. (*See* Appendix 2.)

The dashed, zig-zag line for specimen S-89 is drawn to show how all the stress-strain curves (in solid lines in Fig. 3) were drawn in the plastic range. The peak points on the dashed line are stress-strain values after each increase of compressive stress, and the valley points are values after relaxation for at least 5 minutes. The solid line connects peak points. The high peak for S-89, which would fall on an extension of the elastic, straight-line portion of the curve, represents the stress-strain point achieved by applying additional compression suddenly, in about one second—almost an impact loading. This suggests that the limestone can withstand elastically an impact load much larger than the previously determined elastic limit. Metals also exhibit a higher elastic limit under impact loads. In the plastic range, the positions of the curves are strongly affected by the rate of application of stress, and the positions as plotted could be made to move upward considerably or downward slightly as the rate increases or decreases.

Rupture of limestone at low hydrostatic pressures seems to occur by a wedging action, (Pl. 1, figs. 7, 9), possibly formed by two sets of coalesced axial-radial and tangential-axial shears (Fig. 8c, a). (*See* Griggs, 1936, p. 552.)

The use of a jacket to prevent access of the pressure fluid into the pores of the specimen is very important in such testing as this. To confirm the difference in behavior, a test was made at 2700 ksc hydrostatic pressure of a cylinder of limestone with slots cut in its rubber jacket; the resulting rupture failure is shown in Figure 12 of Plate 1. Griggs (1936, p. 566–567) also found that penetration by the kerosene pressure fluid seems to weaken the limestone markedly beyond the elastic limit.

PLATE 1.—SOLID CYLINDERS OF SOLENHOFEN LIMESTONE

(Length of the scale bar is 1 cm.)

FIGURE 1.—SOLID-CYLINDER SPECIMEN ASSEMBLY WITH JACKET OF RUBBER TUBING AT TOP

FIGURE 2.—SOLID-CYLINDER SPECIMEN ASSEMBLY WITH SOLID END PLUGS

FIGURE 3.—S-SHAPE BUCKLING PRODUCED BY NONAXIAL LOADING

Spec. S-54; P_H = 1700 ksc; average shortening = 7.3%. $(\sigma_D)_{El\ Lim}$ = 3100 ksc.

FIGURE 4.—TENSION SIDE OF A BUCKLED SPECIMEN

(A piece of rubber is caught in a tension crack.) Spec. S-82; P_H = 700 ksc; average shortening = 12.0%; $(\sigma_D)_{Rup}$ = 3730 ksc.

FIGURE 5.—TANGENTIAL-AXIAL SHEAR LINES ON BULGED SURFACE

Spec. S-60; P_H = 500 ksc; permanent shortening = 3.5%; $(\sigma_D)_{Rup}$ = 3620 ksc.

FIGURE 6.—RUPTURE ALONG COALESCED TANGENTIAL-AXIAL SHEAR SURFACES

Spec. S-53; P_H = 170 ksc; rupture pressure uncertain.

FIGURE 7.—SPLITTING ACTION OF WEDGE IN BRITTLE RUPTURE

Spec. S-83; P_H = 300 ksc; shortening = 13%; $(\sigma_D)_{Rup}$ = 3610 ksc.

FIGURE 8.—DISPLACEMENT OF SKIN OF CYLINDER ALONG A TANGENTIAL-AXIAL SHEAR SURFACE

Spec. S-86; P_H = 1000 ksc; shortening = 16.3%; $(\sigma_D)_{El\ Lim}$ = 3100 ksc.

FIGURE 9.—WEDGE FAILURE IN BRITTLE RUPTURE

Spec. S-84; P_H = 300 ksc; shortening = 4%; $(\sigma_D)_{Rup}$ = 3600 ksc.

FIGURE 10.—PLASTICALLY DEFORMED SPECIMEN CHIPPED IN PREPARING IT FOR A SECOND TEST

Spec. S-88; P_H = 4000 ksc; shortening = 17.2%; $(\sigma_D)_{El\ Lim}$ = 2950 ksc.

FIGURE 11.—SIZE BEFORE DEFORMATION AND SIZE AFTER LARGE STRAIN INTO PLASTIC RANGE

Spec. S-89; P_H = 2000 ksc; shortening = 27.0%; $(\sigma_D)_{EL\ Lim}$ = 3100 ksc.

FIGURE 12.—RUPTURE OCCURRED BECAUSE SLOTS WERE CUT IN THE RUBBER JACKET TO PERMIT ACCESS OF KEROSENE PRESSURE FLUID

Spec. S-93; P_H = 2700 ksc; $(\sigma_D)_{Rup}$ = 3080 ksc.

FIGURE 13.—CYLINDER AFTER GREAT DEFORMATION AT A LOW CONFINING PRESSURE

Spec. S-81; P_H = 500 ksc; shortening = 53%; $(\sigma_D)_{Rup}$ = 3740 ksc.

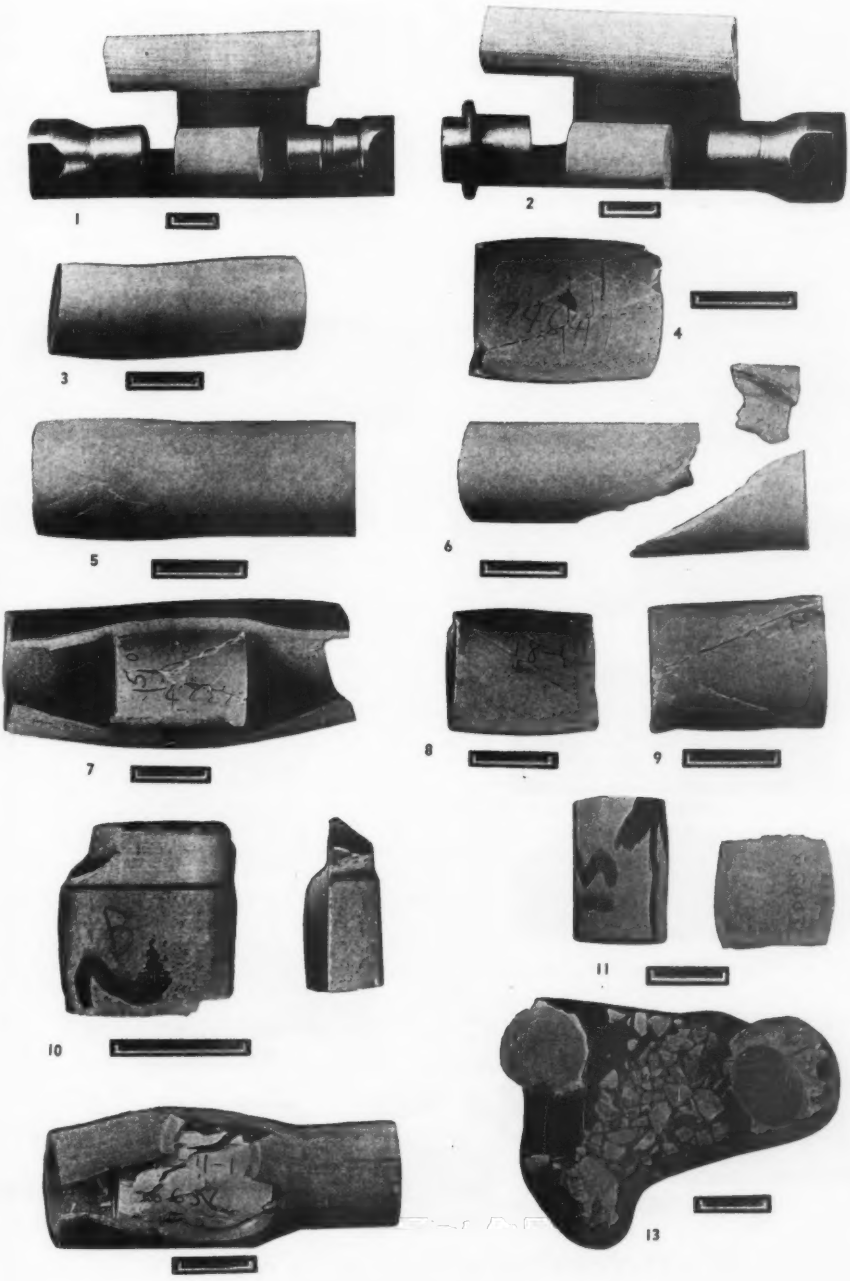

SOLID CYLINDERS OF SOLENHOFEN LIMESTONE

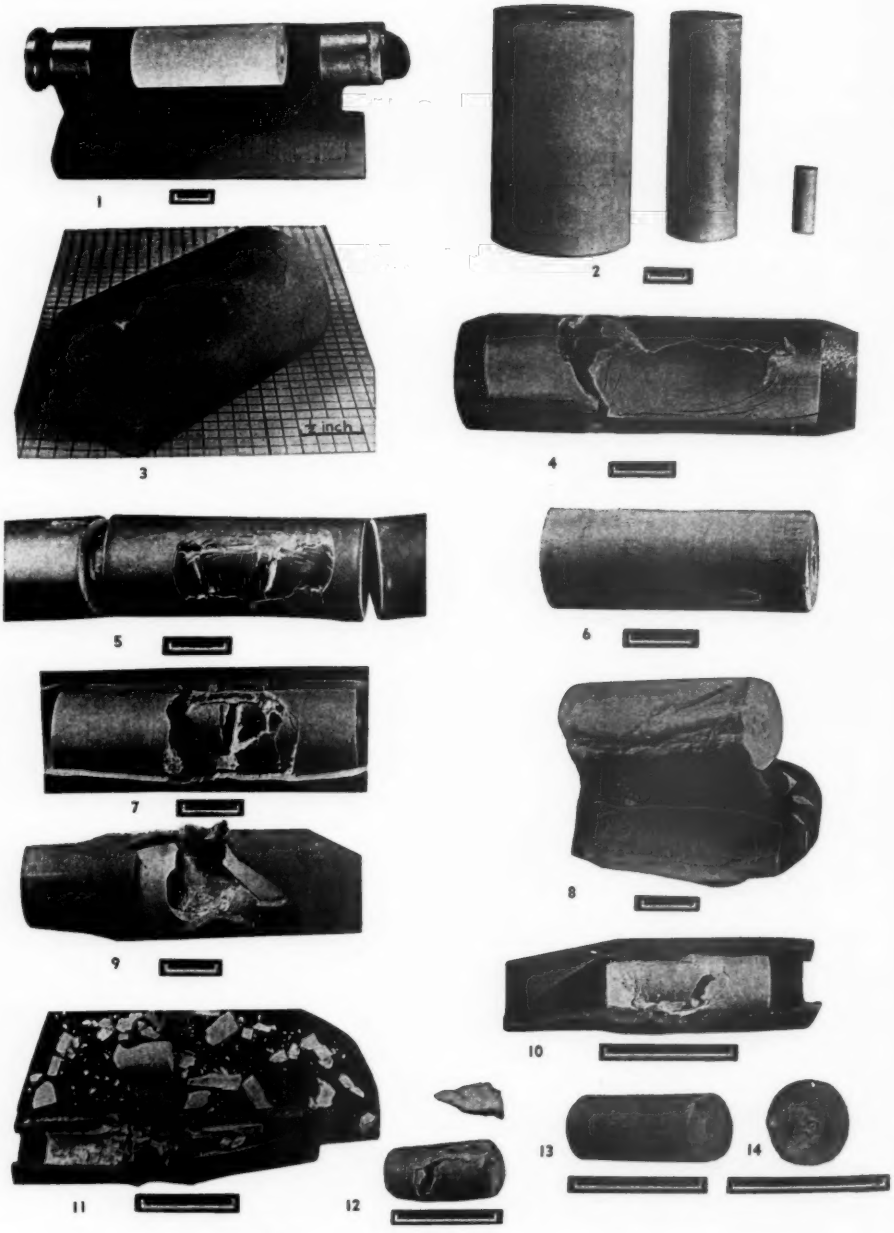

HOLLOW CYLINDERS OF SOLENHOFEN LIMESTONE

Results from Cyclic Compression Tests on Solid Cylinders of Solenhofen Limestone

In metals testing, the raising of the elastic limit (*i.e.*, raising the yield strength) by successive and increasing deformations of the piece into the plastic range is called strain hardening or work hardening. The metal is actually hardened by this processing, as well as strengthened. In testing limestone, a similar raising of the elastic limit was found, although there was no observable hardening of the limestone. It is suggested that the term, strain strengthening, may be more appropriate for this phenomenon in rocks, and it will be so used in this paper.

The limestone is strengthened (Fig. 4) while in the plastic condition, but within 24 hours after unloading loses its added yield strength, in contrast to the behavior of metals. By repeatedly loading and unloading solid cylinder S-128 (while under hydrostatic pressure during and between cycles) the yield strength was raised from 2800 ksc to 5100 ksc. (The total residual strain was 7 per cent.) Similar curves are given for S-124. The temporary nature of the strain strengthening is indicated by the fact that the elastic limits of the specimens when tested 24 hours and 64 days after removal from the press had both dropped back to 3100 ksc, although the succeeding plastic parts of the curves are steeper than in the first cycle.

Several other tests not shown in Figure 4 were made, which are relevant. The strength of a solid cylinder previously shortened 4 per cent and presumably strain strengthened under hydrostatic pressure was tested several months later at 1 atm, and its rupture strength was found to be much reduced; 1900 ksc instead of the usual 2800 ksc. Another cylinder, tested wholly in air, was loaded once to a stress of 1500 ksc, unloaded, and immediately reloaded to rupture failure; some plastic yielding

PLATE 2.—HOLLOW CYLINDERS OF SOLENHOFEN LIMESTONE

(Length of the scale bar is 1 cm.)

FIGURE 1.—HOLLOW-CYLINDER SPECIMEN ASSEMBLY WITH RUBBER JACKET BELOW

FIGURE 2.—THREE SIZES OF HOLLOW CYLINDERS TESTED, WITH OUTSIDE DIAMETERS: 1¼ INCHES, ⅝ INCHES AND 3/16 INCHES

FIGURE 3.—DIAGONAL VIEW OF A 1¼-INCH MEDIUM-WALLED CYLINDER

The hole was two-thirds full of clay to prevent complete collapse; spec. S-45; $\alpha = 2.52/1$; $(P_H)_{Rup} = 2400$ ksc.

FIGURE 4.—RUPTURE OF MEDIUM-WALLED CYLINDER ON A CURVED TANGENTIAL-RADIAL SHEAR SURFACE AT THE TOP AND HINGED ALONG THE BOTTOM

Spec. S-36; ⅝-in. dia.; $\alpha = 2.70/1$; $(P_H)_{Rup} = 2350$ ksc.

FIGURE 5.—RUPTURE FAILURE OF COPPER-JACKETED SPECIMEN

Spec. S-9; ⅝-in. dia.; $\alpha = 2.50/1$; $(P_H)_{Rup} = 1980$ ksc.

FIGURE 6.—PLASTIC FLOW OF A THICK-WALLED SPECIMEN

Spec. S-13; ⅝-in. dia.; $\alpha = 5.0/1$; $(P_H)_{Max} = 4500$ ksc.

FIGURE 7.—BRITTLE COLLAPSE OF A THIN-WALLED SPECIMEN

Spec. S-32; ⅝-in. dia.; $\alpha = 1.56/1$; $(P_H)_{Rup} = 1430$ ksc.

FIGURE 8.—EXFOLIATION OF HIGHLY DEFORMED CYLINDER

Spec. S-12; ⅝-in. dia.; $\alpha = 3.33/1$; $(P_H)_{Rup} = 3280$ ksc.

FIGURE 9.—RUPTURE OF CYLINDER CUT IN HALF ON A PLANE AT 45° WITH THE AXIS

Spec. S-70; ⅝-in. dia.; $\alpha = 2.56/1$; $(P_H)_{Rup} = 2310$ ksc.

FIGURE 10.—RUPTURE OF A SMALL MEDIUM-WALLED SPECIMEN

Spec. S-108; 3/16-in. dia.; $\alpha = 2.44/1$; $(P_H)_{Rup} = 3100$ ksc.

FIGURE 11.—BRITTLE FAILURE OF A SMALL THIN-WALLED CYLINDER

Spec. S-21; 3/16-in. dia.; $\alpha = 1.78/1$; $(P_H)_{Rup} = 1670$ ksc.

FIGURE 12.—RUPTURE OF A SMALL MEDIUM-WALLED CYLINDER

Spec. S-20; 3/16-in. dia.; $\alpha = 2.50/1$; $(P_H)_{Rup} = 3140$ ksc.

FIGURE 13.—SPALLING IN HOLE AND ELLIPTICAL CROSS SECTION AFTER FAILURE

Spec. S-64; 3/16-in. dia.; $\alpha = 3.61/1$; $(P_H)_{Max} = 5420$ ksc.

FIGURE 14.—SPALLING AND PLASTIC FLOW IN A THICK WALLED CYLINDER

Spec. S-109; 3/16-in. dia.; $\alpha = 3.57/1$; $(P_H)_{Max} = 4000$ ksc.

preceded the rupture, which occurred at 3100 ksc instead of 2800 ksc.

Two other cylinders were compressed into the plastic range, and while retaining the axial

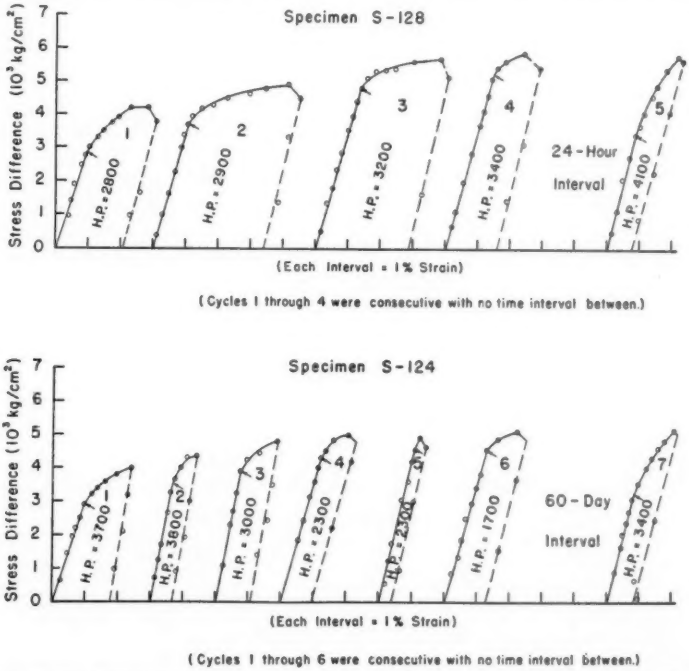

FIGURE 4.—CYCLIC-COMPRESSION EXPERIMENTS ON SOLID CYLINDERS OF SOLENHOFEN LIMESTONE

loads, the confining hydrostatic pressure on them was rapidly lowered from 3000 ksc to zero. Both cylinders ruptured at a stress difference of about 4300 ksc, while the falling hydrostatic pressure was still between 1000 and 2000 ksc. This high strength may be due in part to impact loading as well as to strain strengthening.

Considerable work needs to be done to evaluate the effects of cyclic testing (including the Bauschinger effect) and of the loading rate on the yield and rupture strengths of limestone. The qualitative work reported here indicates the variety and complexity of the results from such testing.

Results from Solid-Cylinder Compression Tests On Other Limestones and Marbles

The stress-strain curves of Figure 5 show the strengths at various hydrostatic pressures of various limestones and marbles. (*See* Appendix 1 for descriptions of carbonate rocks.) Most of the specimens of each rock were cut perpendicular to the foliation of the original block of rock; therefore, the strengths of the specimens cannot be considered as averages for the rocks, because both yield and rupture strengths differ in a foliated rock. As an example of the importance of foliation on strength, Griggs *et al.* (1951, Fig. 3) found a difference of 350 per cent in the yield strength in extension between two specimens of Yule marble oriented at 90° to each other with respect to the foliation.

The two marbles were considerably weaker than Solenhofen limestone. The Becraft limestone exhibited more coherence than the marbles but less than the Solenhofen limestone, possibly because of its coarse grain size and large fossil relicts. The shaly impurity in the New Scotland limestone seems to increase its rupture strength and increase its brittleness over the more pure carbonate rocks.

The experiment on Wm. Henry Bay marble was performed to examine the effect of the

relatively high porosity of the marble (5 per cent) and of its very crumbly character on its deformation. Specimen WHB-1 was compressed under a hydrostatic pressure of 3000 ksc to a termined by inspecting the specimen after each test; this method introduced some uncertainty in that the pressure at failure may have been heightened by strain strengthening since it had

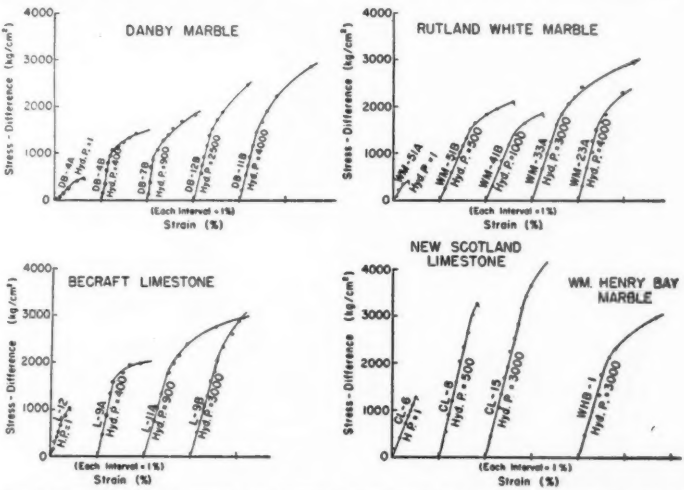

FIGURE 5.—STRESS-STRAIN CURVES FOR SOLID CYLINDERS OF VARIOUS MARBLES AND LIMESTONES
Each curve starts at zero strain; Hyd. P. = hydrostatic pressure in kg/cm².

longitudinal strain of 8 per cent at a stress difference of 5000 ksc. The density was increased in the test from 2.55 to 2.67, and the specimen was much less friable after the test.

The full extent of strain in the plastic range produced in several specimens of limestone and marble is shown in Figure 6. The curves show the large plastic deformation possible in carbonate rocks without rupture, when carried on at moderate hydrostatic pressures.

Compression of Hollow Cylinders

Most of the hollow cylinders were made with a ⅜-inch outside diameter, although some additional experiments were performed on 1¼-inch and 3/16-inch specimens of the Solenhofen limestone (Pl. 2). The size of the hole in the hollow cylinders was varied in each test series.

The hollow cylinders were subjected to hydrostatic pressure on the outside surface (Fig. 1b), the pressure being increased until failure occurred. The recognition of failure by rupture was by the sharp sound of the sudden collapse of the cylinder. Failure by plastic flow and spalling of thick-walled cylinders was determined to be bracketed by tests below and then above that pressure. However, these approximate results were checked by a series of tests by a procedure in which the strain at the inside surface was measured by the change in volume of the hole. The specimen was coupled to a long hollow steel stem which protruded through the bottom plug and was connected by hose to a manometer tube. Any bubbles of air entrapped in the measuring column were removed by flushing the column at the beginning of each experiment. The major source of error was from changes in position of the specimen relative to the manometer tube because of the compression of the rubber packing around the stem, but this displacement could be corrected adequately for strength determinations.

Results from Hollow-Cylinder Tests

The curves in Figure 7 are plotted from tests on the three sizes of hollow cylinders of Solenhofen limestone at failure. The curves show the relationship of rupture strength to wall thickness (related directly to hydrostatic pressure and ratio of radii respectively). There seemed to be a dichotomy of a total collapse failure for

radius ratios less than 3.0 and spalling failure for ratios greater than 3.0. The failure by spalling was a rupturing in a thin layer at the inside surface, accompanied by plastic deformation in a middle layer and by elastic strain in the outer part of the cylinder.

There is a very close agreement between the results for the 1¼-inch cylinders and the ⅝-inch cylinders. However, the 3/16-inch cylinders are apparently much stronger than the larger specimens, although all specimens were prepared and tested under similar conditions. Some experimental data on glass fibers (Griffith, 1920; Orowan, 1949, p. 198) indicate that fibers with very small diameters are stronger than large fibers. Griffith attempted to explain the discrepancy in strengths as due to fewer surface cracks about 2 microns long, on the smaller fibers. Recent experiments on glass (Preston, 1954) indicate that this widely accepted size effect on strength is incorrect; evidently systematic procedural errors account for the apparent difference in strength. The greater rupture strength of the small limestone

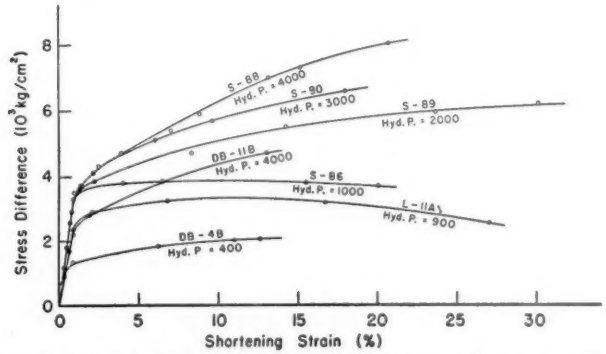

FIGURE 6.—COMPLETE STRESS-STRAIN CURVES FOR SOLID CYLINDERS OF SOLENHOFEN LIMESTONE, DANBY MARBLE, AND BECRAFT LIMESTONE

Stress difference was corrected roughly for increase in diameter by assuming no volume change with shortening.

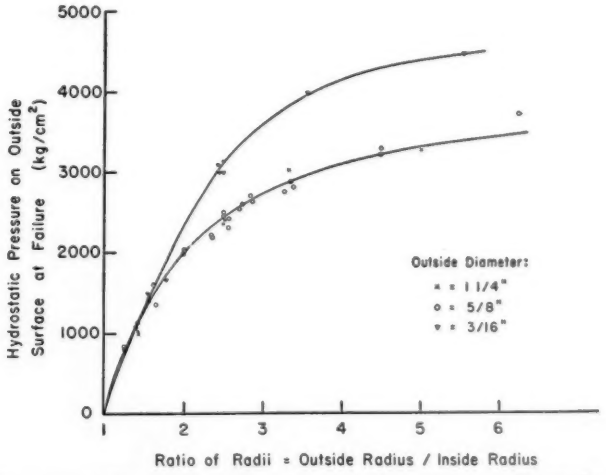
Hydrostatic Pressure on Outside Surface at Failure (kg/cm^2)
Ratio of Radii = Outside Radius / Inside Radius
Outside Diameter:
× = 1 1/4"
o = 5/8"
▾ = 3/16"

FIGURE 7.—HYDROSTATIC PRESSURE AT FAILURE VS. RATIO OF RADII FOR THREE SIZES OF HOLLOW CYLINDERS OF SOLENHOFEN LIMESTONE

cylinders may be due either to unrecognized differences in processing the cylinders or to fewer imperfections of gross dimension (e.g., bedding planes) than in the larger cylinders.

(Pl. 1, figs. 5, 8). Such helical shear lines (Lueder's lines) have been observed on solid cylinders in compression in the brittle failure of metals; to obtain this relation between the

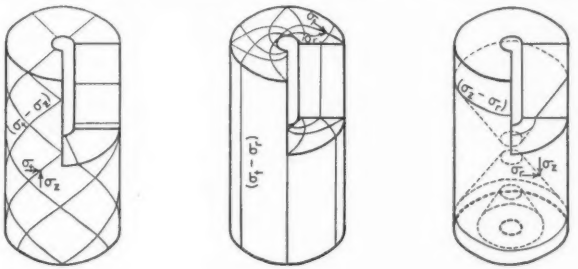
a. TANGENTIAL – AXIAL
$\sigma_1 > \sigma_t > \sigma_z$
$\tau_m = \frac{1}{2}(\sigma_1 - \sigma_z)$
b. TANGENTIAL – RADIAL
$\sigma_1 > \sigma_z > \sigma_r$
$\tau_m = \frac{1}{2}(\sigma_1 - \sigma_r)$
c. AXIAL – RADIAL
$\sigma_z > \sigma_1 > \sigma_r$
$\tau_m = \frac{1}{2}(\sigma_z - \sigma_r)$

FIGURE 8.—THEORETICAL SHEARING SURFACES IN A HOLLOW CYLINDER UNDER EXTERNAL HYDROSTATIC PRESSURE
After King, 1912, Figure 1.

A comparison of the theoretical and actual modes of yield failure is of interest here. Three families of theoretical elastic shearing surfaces can develop in a hollow cylinder depending on the three possible orientations of the principal stresses (Fig. 8). The maximum, intermediate, and minimum principal stresses each may have one of three orientations in cylindrical coordinates: axial, radial, and tangential or circumferential. By elasticity theory, the maximum shear surfaces are at 45° to the directions of the maximum and the minimum principal stresses, and on each of these surfaces there acts the appropriate maximum shear stress (equal to half the difference of the maximum and minimum principal stresses in any stress system).

In my experiments, actual fracture along which rupture occurred (even in the coarse-grained igneous rocks) resembled very closely the shape of the equiangular spiral of the tangential-radial shear surface shown in Figure 8b; the failure was a hinged "trap door" collapse (Pl. 2, figs. 3, 4). The axial-radial shear surface (Fig. 8c) was also observed at the ends of the "trap door" in some of the hollow cylinders. The tangential-axial shear surface (Fig. 8a) was seen on the surfaces of some solid cylinders stresses, the tangential stress may become relatively tensile in the outer skin owing to lateral expansion as the cylinder is shortened.

In Figure 9 are stress-strain curves for some hollow cylinders. There seems to be a marked yielding at the elastic limit, although the yield points chosen are somewhat arbitrary. The four curves at the left in Figure 9 are from tests of thick-walled specimens, (Pl. 2, fig. 6); the beginning of spalling was at the first large plastic strain (horizontal line on the curve). A perceptible surging of the kerosene in the manometer column occurred at the beginning of spalling, and therefore the spalling was not a release fracturing following the release of pressure. By continued application of hydrostatic pressure on a thick-walled cylinder, it could be closed down tightly on the spalled particles inside the cylinder, usually resulting in an elliptical cross section to the cylinder.

A series of tests were performed to determine the effect of a single plane of weakness in hollow cylinders on their strength, and incidentally to evaluate the importance of friction on such planes. Five hollow cylinders were cut in half along planes at 0°, 30°, 45°, 60°, and 90° to the axes of the cylinders. No sliding was observed on the planes, and no important

departure from the average strength of cylinders of this size nor from the usual tangential-radial surface of failure was found (Pl. 2, fig. 9).

Pictures of some of the deformed 1¼-inch and 3/16-inch specimens are shown in Plate 2.

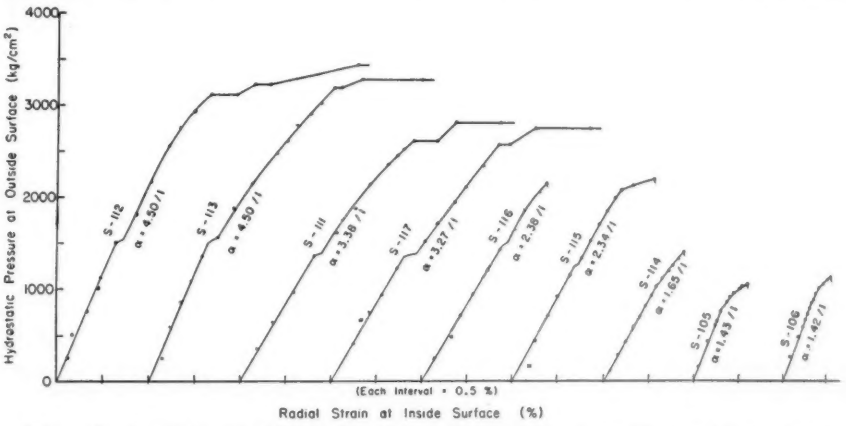

FIGURE 9.—STRESS-STRAIN CURVES FROM CRUSHING EXPERIMENTS ON HOLLOW CYLINDERS OF SOLENHOFEN LIMESTONE

Each curve starts at zero strain; α = ratio of radii = outside radius/inside radius.

The manner of failure was the same in all three sizes.

The type of material used for the jacket on the specimens did not seem to affect the strength of limestone, judging from the identical rupture strengths of copper-jacketed and rubber-jacketed hollow cylinders. However, Bridgman (1947b, p. 253) found that the "tensile" strength of glass under 25,000 ksc hydrostatic pressure was 11,000 ksc with rubber and 22,000 ksc with copper jackets.

Many experiments were done on hollow cylinders of Danby marble, Rutland white marble, Yule marble, calcite, New Scotland limestone, and Becraft limestone. Curves similar to those in Figures 7 and 9 were obtained from the data, but the results are only qualitative since the effect of rock foliation was not adequately accounted for.

Punching of Disks

The disks were all flat, solid cylinders, 5/8 inch in diameter and from 0.148 inch to 0.281 inch thick. The external pressure system is shown diagrammatically in Figure 1c, and the die and punch assembly is shown in Figure 1 of Plate 3. The diameter of the punch pin is 0.308 inch. The copper cups (at top in Pl. 3, fig. 1) were fitted over the steel pieces and were used to keep the kerosene from the disk; they were held tightly against the steel by the rubber jacket. The same instrumentation and the same method of producing hydrostatic pressure and axial loading as in the solid-cylinder tests were used.

Punching produces approximately a stress system of simple shear only. This simple stress configuration is made complex if the piece being punched is too thick, so most of the disks were made less than ¼ inch in thickness.

Solenhofen limestone was the only rock tested by punching, and the experimental data are reproduced in the curves in Figure 10. Hydrostatic pressure has a decided strengthening effect in punching tests. The pattern of rupture in the specimens shown in Figures 5 and 7 of Plate 3 consists of a circular sheared portion under the punch pin, and the radial cracks in the outer portion at about 45° or 90° intervals. For hydrostatic pressures above about 4000 ksc, the stress-strain curves for disks have elastic and plastic parts such as in the curves from solid-cylinder tests at high confining pressures. The maximum penetration of the punch in S-120 while under the maximum pressure was about 1/32 inch (Pl. 3, figs. 3, 4).

Results of Heat and Pressure Studies

A number of experiments were performed in which heat as well as pressure was applied to reconnoiter the effect of higher temperatures than 20° C on the strength of hollow cylinders of Solenhofen limestone and Yule marble. A large pressure vessel with an internal furnace was used, and the pressure fluid was nitrogen gas. The temperature was measured by a chromel-alumel thermocouple and was roughly controlled to within plus or minus 20° C. The cylinders of limestone and marble had about the same dimensions: 5/8 inch outside diameter, 1½ inches long, and ¼ inch inside diameter. The samples and steel end pieces were sealed in copper jackets.

The results of the heating experiments on hollow cylinders are listed in Table 1. The figures of the decrease in outside diameter in Table 1 were taken at the smallest diameter of the inevitably elliptical cross section which resulted from the plastic flow.

In specimens S-24 and S-10 (Pl. 3, figs. 10, 12, 13) the bore was closed down uniformly and completely for about half of the length (with a maximum 0.060-inch decrease in outside diameter), and in places the walls coalesced so well that only a trace of the hole remained. An increase in the density was found for a disk cut from the middle of S-10: the new density was 2.70, compared to the original of 2.61.

An attempt was made to cause failure in S-42 and S-43 by rupture by steadily increasing the hydrostatic pressure at constant temperature. For S-42 held at 400° C, rupture occurred at 3900 ksc after raising the pressure from 2000 ksc in a period of one hour. Specimen S-43 held at 500° C, merely closed down after raising the pressure from 2100 ksc to 5100 ksc in a period of 2 hours; the diameter of the inside hole changed from 0.26 inch to about 0.15 inch. The strength of the limestone was strikingly demonstrated by the extrusion of the low-carbon steel of the end plugs into the holes in the ends of the limestone cylinder (Pl. 3, figs. 11, 12).

The specimens may have had as much as ½ per cent water in the pores, which might have promoted plastic deformation by recrystallization, but this effect was not evaluated.

Three preliminary conclusions on the 12-hour (or longer) heating experiments can be made: the rate of plastic deformation increases with increasing temperature; at temperatures above 500° C, a pressure near or above that for rupture at 20° C will cause rapid, large plastic flow, but

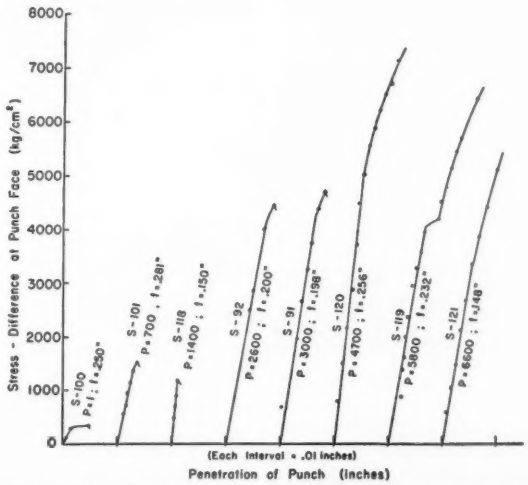

FIGURE 10.—STRESS-STRAIN CURVES FROM PUNCHING EXPERIMENTS ON DISKS OF SOLENHOFEN LIMESTONE
Each curve starts at zero penetration; P = hydrostatic pressure in kg/cm²; t = thickness of disk in inches.

without rupture; and at temperatures between 400° C and 500° C, plastic flow occurs, but rupture can be produced, although apparently only at a pressure at least 50 per cent higher than that for rupture at 20° C.

Griggs *et al.* (1951, Figs. 1, 2; 1953, Fig. 1) have recently completed a series of experiments on some oriented solid cylinders of Yule marble and single crystals of calcite deformed at room temperature, dry; at 150° C and 300° C, dry; and at 150° C and 300° C, with small amounts of water. In general, the yield strengths of the cylinders were lowered about 40 per cent by the heat and still further by the interstitial water. Although Griggs observed a lowering of the *yield* strength of Yule marble by heating, I observed a raising of the *rupture* strength of Solenhofen limestone by heating. Since concurrent strain measurements were not made in my experiments, the effect of the heat on the yield strength was not determined. At "blue heat" (about 300° C), the tensile (rupture) strength of some steel is raised 15 per cent over the strength at room temperature, although the strength falls off again as the temperature is further increased.

Separation of hydrostatic-pressure effects from heat effects on plasticity by recrystallization in Yule marble is difficult, but apparently there is an increase of recrystallization with increasing temperature (Griggs, Turner, Borg, and Sosoka, 1951, p. 1393–1394; 1953,

---

PLATE 3.—DISKS OF SOLENHOFEN LIMESTONE AND HEATED AND COMPRESSED HOLLOW CYLINDERS OF SOLENHOFEN LIMESTONE AND YULE MARBLE

(Length of scale bar is 1 cm.)

FIGURE 1.—SPECIMEN ASSEMBLY FOR PUNCHING TESTS ON DISKS

FIGURE 2.—CORE PUNCHED FROM A DISK

(The copper cups were also punched out.) Spec. S-92; P_H = 2600 ksc; t = 0.200 in.

FIGURE 3.—PUNCHED-OUT BULGE IN A DISK

Density was decreased 3.2%; spec. S-120; P_H = 4700 ksc; t = 0.256 in.

FIGURE 4.—PUNCHED DEPRESSION IN SAME DISK

Maximum penetration of punch = 0.025 in.; spec. S-120; P_H = 4700 ksc; t = 0.256 in.

FIGURE 5.—DISK TESTED IN AIR

Spec. S-100; P_H = 1 atmos.; t = 0.250 in.

FIGURE 6.—DEPRESSION PUNCHED IN A THIN DISK

Spec. S-121; P_H = 6600 ksc; t = 0.148 in.

FIGURE 7.—SPECIMEN BROKE BECAUSE OF THE WEAKENING EFFECT OF KEROSENE LEAKING PAST A COPPER CUP TO THE DISK, ALTHOUGH THE CONFINING PRESSURE WAS HIGH

Spec. S-102; P_H = 4000 ksc; t = 0.234 in.

FIGURE 8.—DEPRESSION PUNCHED IN A THICK DISK

Spec. S-119; P_H = 5800 ksc; t = 0.232 in.

FIGURE 9.—HOLLOW CYLINDER OF SOLENHOFEN LIMESTONE WHICH RUPTURED AT P_H = 3900 KSC AND T = 400° C

Test period = 1 hr.; spec. S-42; α = 2.40/1.

FIGURE 10.—HOLLOW CYLINDER OF SOLENHOFEN LIMESTONE SHOWING FLOW TOWARD THE HOLE

The end of the cylinder has been cut off where the closing down was almost complete. Spec. S-24; P_H = 2100 ksc; T = 700° C; α = 2.55/1; test period = 6 hrs.

FIGURE 11.—CLOSE-UP OF EXTRUDED STEEL PLUG AND END OF LIMESTONE CYLINDER

Spec. S-43; α = 2.40/1; $(P_H)_{Max}$ = 5100 ksc; T = 500° C; 3 test periods = 39 hrs. total.

FIGURE 12.—CROSS SECTIONS OF HOLLOW CYLINDER OF SOLENHOFEN LIMESTONE DEFORMED BY HEAT AND PRESSURE

Spec. S-10; α = 2.50/1; $(P_H)_{Max}$ = 2600 ksc; T = 600° C; test period = 3 hrs.

FIGURE 13.—CONICAL CUP, 3/16 INCH ACROSS AND 1/4 INCH DEEP

In end of same specimen—Spec. S-10.

FIGURE 14.—RUPTURED HOLLOW CYLINDER OF YULE MARBLE

Spec. YM-15; α = 2.38/1; $(P_H)_{Rup}$ = 1300 ksc; T = 300° C; test period = 2 hrs.

FIGURE 15.—HOLLOW CYLINDER OF YULE MARBLE FLATTENED (0.097 IN.) TO AN ELLIPTICAL CROSS SECTION

Spec. YM-14; α = 2.37/1; $(P_H)_{Max}$ = 2300 ksc; T = 400° C; test period = 20 hrs.

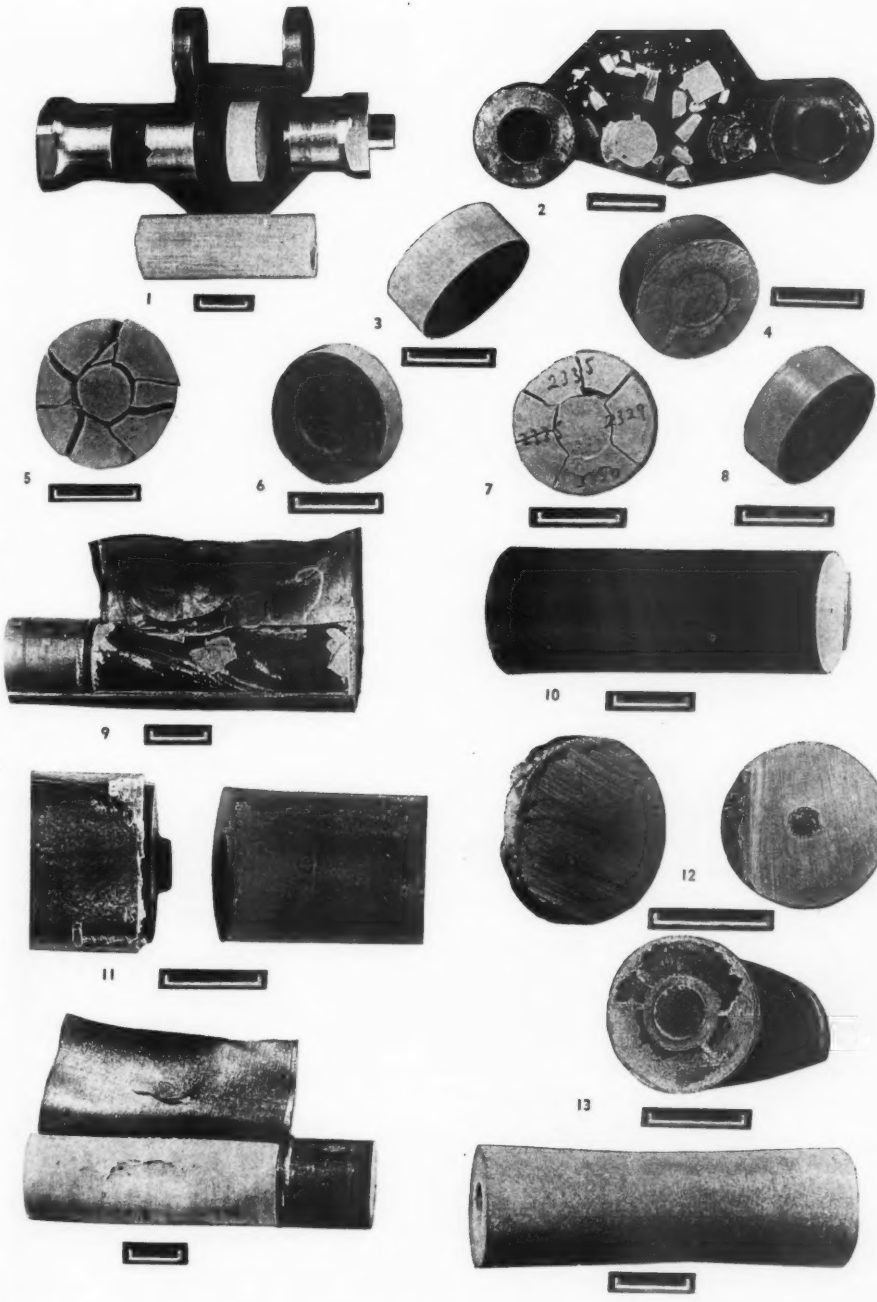

DISKS OF SOLENHOFEN LIMESTONE AND HEATED AND COMPRESSED HOLLOW CYLINDERS OF SOLENHOFEN LIMESTONE AND YULE MARBLE

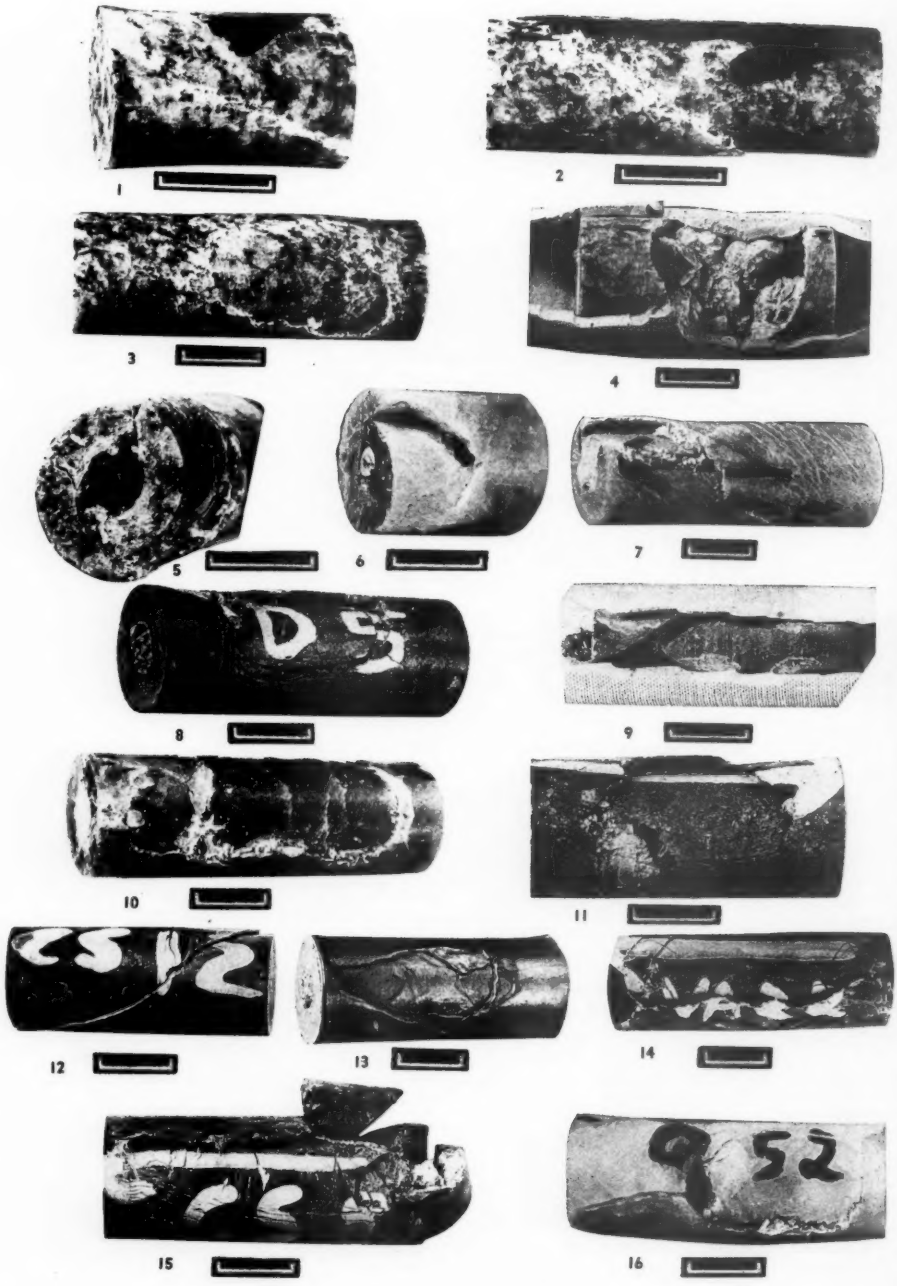

SOLID AND HOLLOW CYLINDERS OF VARIOUS SILICATE ROCKS AND MINERALS

p. 1341–1342). (Recrystallization may be characterized by healed glide and fracture planes in the marble grains.) The early heating experiments and microscope studes of Adams and Nicolson (1901) on solid cylinders of Carrara marble, support my observations that a minimum temperature of about 400° C is required to get plasticity by extensive recrystallization in short test periods. Increase of time under load and heat increases the amount of recrystallization of marble also (reported by all observers).

The possibility that the plastic flow might be aided by a polymorphic transition was considered, but it seems very unlikely. An approximate thermodynamic computation for the calcite-aragonite transformation shows that a mean pressure of about 10,000 ksc would be

---

PLATE 4.—SOLID AND HOLLOW CYLINDERS OF VARIOUS SILICATE ROCKS AND MINERALS

(Length of the scale bar is 1 cm.)

FIGURE 1.—RUPTURE ALONG A PLANAR SHEAR SURFACE OF A SOLID CYLINDER OF BARRE GRANITE
Angle with axis = 20°; spec. BG-17A; P_H = 500 ksc; $(\sigma_D)_{Rup}$ = 4350 ksc.

FIGURE 2.—RUPTURE ALONG A PLANAR SHEAR SURFACE AT 22° WITH CYLINDER AXIS IN A LONGER SPECIMEN OF BARRE GRANITE
Spec. BG-20; P_H = 550 ksc; $(\sigma_D)_{Rup}$ = 4800 ksc.

FIGURE 3.—RUPTURE ALONG "TRAP-DOOR" IN MEDIUM-WALLED HOLLOW CYLINDER OF BARRE GRANITE
Spec. BG-6; α = 3.19/1; $(P_H)_{Rup}$ = 3840 ksc.

FIGURE 4.—COLLAPSE OF THIN-WALLED HOLLOW CYLINDER OF CHELMSFORD GRANITE
Spec. C-1; α = 1.67/1; $(P_H)_{Rup}$ = 1950 ksc.

FIGURE 5.—END VIEW OF A TANGENTIAL-RADIAL SHEAR SURFACE, IN A HOLLOW CYLINDER OF BARRE GRANITE
Spec. BG-9; α = 1.90/1; $(P_H)_{Rup}$ = 2230 ksc.

FIGURE 6.—HELICAL SHEAR SURFACE IN A HOLLOW CYLINDER OF FLUORITE, CUT FROM A SINGLE CRYSTAL WITH THE AXIS PARALLEL TO AN A-AXIS
Spec. FT-15; α = 3.16/1; $(P_H)_{Rup}$ = 4450 ksc.

FIGURE 7.—RUPTURE AT THE END OF A HOLLOW CYLINDER OF MICROCLINE FELDSPAR
Spec. F-5; α = 3.18/1; $(P_H)_{Rup}$ = 3960 ksc.

FIGURE 8.—FAILURE OF A HOLLOW CYLINDER OF HOLYOKE DIABASE
Spec. D-5; α = 3.19/1; $(P_H)_{Rup}$ = 4410 ksc.

FIGURE 9.—DOUBLE-WEDGE SHEARING SURFACES (EACH AT 32° WITH AXIS) IN A SOLID CYLINDER OF PYRITE
Spec. P-2; P_H = 500 ksc; $(\sigma_D)_{Rup}$ = 5070 ksc.

FIGURE 10. "TRAP-DOOR" COLLAPSE OF A HOLLOW CYLINDER OF CHESHIRE QUARTZITE
Spec. CQ-22; α = 3.20/1; $(P_H)_{Rup}$ = 4750 ksc.

FIGURE 11.—COLLAPSE OF A HOLLOW CYLINDER OF COPPER ORE
Spec. CO-5; α = 3.15/1; $(P_H)_{Rup}$ = 4190 ksc.

FIGURE 12.—WARPED PLANE OF SHEARING, AT 16° TO 31° WITH THE AXIS OF A SOLID CYLINDER OF CAMBRIDGE SLATE
Spec. CS-12; P_H = 300 ksc; $(\sigma_D)_{Rup}$ = 5280 ksc.

FIGURE 13.—COPPER JACKETING DEPRESSED OVER "TRAP-DOOR" RUPTURE IN A HOLLOW CYLINDER OF SOAPSTONE
Spec. SP-1; α = 3.05/1; $(P_H)_{Rup}$ = 640 ksc.

FIGURE 14.—RUPTURE ALONG A TANGENTIAL-RADIAL SHEAR SURFACE IN A HOLLOW CYLINDER OF VERDE ANTIQUE ON THE SECOND TEST
In the first test there was a slight spalling for a hydrostatic pressure of 5620 ksc, which weakened the specimen. Spec. VA-22; α = 3.19/1; $(P_H)_{Rup}$ = 5000 ksc.

FIGURE 15.—SHEARING RUPTURE IN A HOLLOW CYLINDER OF CAMBRIDGE SLATE
Note tension cracks in the "hinge" at bottom. Spec. CS-8; α = 3.05/1; $(P_H)_{Rup}$ = 4670 ksc.

FIGURE 16.—SAW-TOOTH RIDGES ON THE TANGENTIAL-RADIAL SHEAR SURFACES OF A HOLLOW CYLINDER OF QUARTZ
Spec. Q-52; α = 3.19/1; $(P_H)_{Rup}$ = 8750 ksc.

required at 400° C to promote the inversion, and the pressure becomes higher with higher temperatures. (For recent experimental data on this system, *see* Jamieson, 1953.) Bridgman usage (Orowan, 1949, p. 186) as strength is usually applied only to ultimate resistance to rupture. As a geologic process, plastic flow is as important as fracturing in rocks.

TABLE 1.—PLASTIC DEFORMATION OF HOLLOW CYLINDERS OF SOLENHOFEN LIMESTONE AND YULE MARBLE UNDER HEAT AND PRESSURE

Specimen number	Ratio of radii	Hyd. press. (kg/cm²)	Temp. (°C)	Duration of experiment (hours)	Maximum decrease in O.D. (inches)	Normal rupture press. at 20°C* (kg/cm²)
S-10	2.50/1	2600	650°	3	.060	2400
S-24	2.55/1	2400	700°	2	.060	2450
S-34	2.40/1	1500	400°	20	<.001**	2350
		1700	400°	48	.002	....
S-25	2.35/1	1800	400°	50	.003	2300
S-42	2.40/1	2100	400°	56	.006**	2350
		3900 (Max.)	400°	1	Rupture	2500
S-43	2.40/1	1400	500°	20	<.001**	2350
		2000	500°	12	.016**	....
		5100 (Max.)	500°	7	.029	....
YM-15	2.38/1	1400	300°	2	Rupture	1350
YM-14	2.37/1	2100	400°	20	.097	1350
YM-16	2.40/1	600	400°	13	.001**	1400
		600	500°	12	.001**	....
		900	300°	12	.001**	....
		900	400°	12	.001**	....
		900	500°	12	.003**	....
		1100	400°	12	.002**	....
		900	400°	52	.002** (*Total* .013)	....

* Normal hydrostatic pressure at rupture taken from Figure 7 and Yule marble curves.
** Measurement made on outside of copper jacket.

(1939) found a transition in calcite (Phase I–Phase II) at 15,000 ksc at room temperature, but this inversion also is too high to be important here. The vapor pressure of CO_2 from $CaCO_3$ is less than 20 mm Hg, for temperatures below 600° C, so dissociation effects are not important in the recrystallization and plasticity.

STRENGTH OF LIMESTONE

Definition of Strength

The initiation of plastic deformation at the elastic limit or the yield point is the subject of considerable research by metallurgists, and the word strength is often applied by them to the maximum stress difference at the elastic limit, although there are objections to this

The change in property at the elastic limit from elastic to plastic is here termed yield strength; rupture strength designates strength at rupturing. Yield and rupture failure describe loss of strength by yielding and by rupturing; yield failure may be a less acceptable usage, but beyond the elastic limit, there is a failure to continue elastic deformation.

Yield strength may be defined as that stress difference a body is able to withstand without yielding plastically, and may be arbitrarily designated as the maximum stress difference at the elastic limit or proportional limit for constant experimental conditions. Rupture strength may be defined as the maximum stress difference a body is able to withstand prior to loss of cohesion by fracturing for constant experimental conditions; fracturing is conceived as the breaking process leading to rupture. In

this study, nearly constant experimental conditions were maintained as follows: room temperature, unvarying composition, fresh, homogeneous specimens with no recent strain history, and moderate strain rate—about 0.02 per cent per minute. To conform with general usage (especially tests in air) stress difference is used as the measure of yield strength and rupture strength because either strength was found in this study to be more or less predictable for any rock by the magnitude of the maximum shear stress (half the maximum stress difference) at failure.

Goranson (1940, p. 1032) has proposed that strength (*i.e.*, yield strength) be measured by extrapolation of stress difference for finite rates of creep to zero creep rate. However, theoretically (Freudenthal, 1950, p. 138) at a temperature above zero absolute, for a finite stress difference, the rate of plastic strain should always be greater than zero, and careful long-period measurement does show extremely small inelastic strain in limestone at stresses well below the elastic limit. On the other hand, for most substances under usual experimental conditions, the strain rate does seem to approach zero for finite stress differences, as demonstrated forcefully by the confidence placed in structural steel, brick, and other building materials. Creep of Solenhofen limestone in air (Griggs, 1939, p. 234–236, Fig. 4) with 1400 ksc compressive load showed a shortening of 0.02 per cent in a year and a half, which was extrapolated to give 0.05 per cent in one million years. Since determination of the yield strength at zero creep rate involves considerable experimental uncertainty, the short term elastic limit may be taken as an approximate lower limit of unrecoverable strain to fit Goranson's definition.

Jeffreys (1924, p. 111) stated that the strength (*i.e.*, yield strength) of a material may be called "the critical stress difference, above which the rate of change of shape does not decrease when the time of application of the stress increases". Even at high temperatures and pressures, limestone would not be the viscous nor perfectly plastic material suggested as necessary in Jeffreys' definition, and so this measure of yield strength does not seem practical.

Griggs defined his term, fundamental strength (1936, p. 564, 557), as the maximum differential stress a body will withstand for infinite time without failing by rupture or deforming continuously. This definition does not differentiate between yield strength and rupture strength, whereas it does seem that a distinction between the two is necessary to treat the two types of strength in rocks.

Symbols

The following symbols are used:

General

- r radius
- σ stress normal to a surface
- τ shear stress
- P pressure
- ϵ strain normal to a surface
- U displacement
- E Young's modulus
- G modulus of rigidity
- μ Poisson's ratio
- K constant

Subscripts

- z axial
- t tangential or circumferential
- r radial
- i inside surface
- o outside surface
- p punch face
- e elastic deformation
- s plastic deformation
- B elastic-plastic boundary

Particular

- σ_1 maximum principal stress
- σ_2 intermediate principal stress
- σ_3 minimum principal stress
- P_H hydrostatic pressure
- P_p pressure on punch face
- σ_D stress difference
- σ_m mean stress
- τ_M maximum shear stress
- t thickness of disks
- l, r initial length or radius
- l', r' final length or radius
- α ratio of outside radius to any radius in a hollow cylinder, $\frac{r_0}{r}$

Stress Distribution in the Elastic Range

The idealized distribution of stress in a solid cylinder in compression is simple (Fig. 1a): on any particle in the cylinder there is a hydrostatic pressure plus an axial compression. The total axial pressure on the ends of the cylinder produces the axial stress σ_a, and is the maximum principal stress, σ_1. The stresses on a plane perpendicular to σ_a are the tangential and radial stresses, which are equal to the hydrostatic pressure.

$$\sigma_r = \sigma_t = P_H = \sigma_3 = \sigma_3$$

The axial stress can be considered equal to the sum of the hydrostatic pressure and the stress difference.

Eq. 1 $$\sigma_a = \sigma_1 = \sigma_D + P_H$$

The maximum shear stress is given by

Eq. 2 $$\tau_M = \tfrac{1}{2}(\sigma_1 - \sigma_3) = \tfrac{1}{2}(\sigma_a - P_H) = \tfrac{1}{2}\sigma_D$$

The mean stress or mean pressure is one-third the sum of the principal stresses for all stress systems.

Eq. 3 $$\sigma_m = \tfrac{1}{3}(\sigma_1 + \sigma_2 + \sigma_3) = \tfrac{1}{3}(\sigma_a + 2P_H)$$

The longitudinal strain in the solid cylinders was a shortening.

Eq. 4 $$\epsilon_a = \frac{l - l'}{l}$$

In the hollow cylinders, there was a hydrostatic pressure on the outside surfaces (Fig. 1b) and zero pressure on the inside surface, and the expressions for the stresses are as follows (*see* Love, 1944, p. 145–146):

Eq. 5 $$\sigma_t = \sigma_1 = P_H \cdot \frac{r_o^2}{r^2} \cdot \frac{r^2 + r_i^2}{r_o^2 - r_i^2} = P_H \frac{\alpha_o^2}{\alpha_o^2 - 1} \cdot \frac{\alpha^2 + 1}{\alpha^2}$$

Eq. 6 $$\sigma_r = \sigma_3 = P_H \frac{r_o^2}{r^2} \cdot \frac{r^2 - r_i^2}{r_o^2 - r_i^2} = P_H \frac{\alpha_o^2}{\alpha_o^2 - 1} \cdot \frac{\alpha^2 - 1}{\alpha^2}$$

Eq. 7 $$\sigma_a = \sigma_2 = P_H \cdot \frac{r_o^2}{r_o^2 - r_i^2} = P_H \frac{\alpha_o^2}{\alpha_o^2 - 1}$$

Each principal stress is a function of hydrostatic pressure and wall thickness. With r_i constant, wall thickness varies directly with ratio of radii.

$$\Delta r = r_o - r_i = r_i(\alpha - 1)$$

The shear stress in a hollow cylinder is maximum at the inside surface, where $r = r_i$, and $\alpha = \alpha_i = 1$

Eq. 8 $$\tau_M = \tfrac{1}{2}(\sigma_{ti} - \sigma_{ri}) = P_H \frac{\alpha_o^2}{\alpha_o^2 - 1}$$

The mean stress has the same value throughout the cylinder and also is equal to the maximum shear stress.

Eq. 9 $$\sigma_m = P_H \frac{\alpha_o^2}{\alpha_o^2 - 1}$$

In the disk tests (Fig. 1c), the deformation by shearing, and the average shear stress on a cylindrical surface within the disk under the edge of the punch is assumed to be the maximum shear stress.

Eq. 10 $$\tau_M = P_p \frac{r_p}{2t}$$

The critical principal stresses are developed under the edge of the punch also.

Eq. 11 $$\sigma_1 = \frac{P_p r_p}{2t} + P_H$$

Eq. 12 $$\sigma_2 = P_H$$

Eq. 13 $$\sigma_3 = -\frac{P_p r_p}{2t} + P_H$$

The mean stress in the disk is equal to the hydrostatic pressure.

Eq. 14 $$\sigma_m = P_H$$

Stress Distribution in the Plastic Range

The stresses in the plastic range of deformation are assumed to have the same orientation as the stresses in the elastic range for the solid cylinder and disk tests, even though the plastic strains are not simply related to the stresses.

In a hollow cylinder with closed ends, under hydrostatic pressure on the outside surfaces, the mechanism of plastic deformation probably

occurs about as follows. The first plastic flow is at the inside surface, and as the hydrostatic pressure is increased, a thicker portion of the inside wall flows inward; as the outside pressure is further increased, the zone of plasticity widens into the wall of the cylinder. Outside this plastic zone, of course, the cylinder behaves elastically. In the actual tests, the widening of the plastic zone was interrupted by collapse in the thin- and medium-walled specimens and by spalling in the thick-walled specimens.

Eq. 19 $\sigma_{r\epsilon} = \sigma_3 = \frac{\tau_M}{\alpha^2}(\alpha^2 \ln \alpha_B^2 - \alpha_B^2 + \alpha^2)$

Eq. 20 $\sigma_{z\epsilon} = \sigma_2 = 2\mu\tau_M(\ln \alpha_B^2 + 1)$

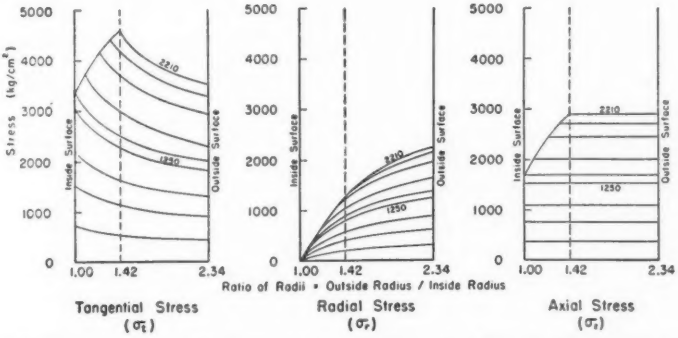

FIGURE 11.—THEORETICAL STRESS DISTRIBUTION IN THE WALL OF A HOLLOW CYLINDER UNDER EXTERNAL HYDROSTATIC PRESSURE

Beliaev and Sinitskii (1938) analyzed plastic flow in hollow cylinders; they assumed ideal plasticity, in which deformation is supposed to continue without increase of stress after reaching the yield point. They used Hencky's theory of plastic deformation in which the strain rate is not considered, and they assumed incompressibility in the plastic zone.

The stresses in the elastic and plastic zones in the wall of a closed hollow cylinder under external pressure is given by the following equations of Beliaev and Sinitskii. The maximum shearing stress is used to specify the condition for perfect plasticity.

Plastic zone:

Eq. 15 $\sigma_{t\epsilon} = \sigma_1 = 2\tau_M(\ln \alpha + 1)$

Eq. 16 $\sigma_{r\epsilon} = \sigma_3 = 2\tau_M \ln \alpha$

Eq. 17 $\sigma_{z\epsilon} = \sigma_2 = \tau_M(2 \ln \alpha + 1)$

Elastic zone:

Eq. 18 $\sigma_{t\epsilon} = \sigma_1 = \frac{\tau_M}{\alpha^2}(\alpha^2 \ln \alpha_B^2 + \alpha_B^2 + \alpha^2)$

At plastic-elastic boundary.

Eq. 21 $\sigma_{tB} = \sigma_1 = 2\tau_M (\ln \alpha_B + 1)$

Eq. 22 $\sigma_{rB} = \sigma_3 = 2\tau_M \ln \alpha_B$

Eq. 23 $\sigma_{zB} = \sigma_2 = \tau_M(2 \ln \alpha_B + 1)$

In order to demonstrate the differences in the stress distributions between the elastic range and the plastic range, the curves in Figure 11 were drawn from the data on specimen S-115. In the three diagrams, the wall of the inside surface is on the left and the wall of the outside surface is on the right. The ratio of outside to inside radius for this specimen was 2.34/1, and intermediate ratios (for radii within the cylinder wall) are plotted along the abscissa. The ordinate axis shows the sizes of the tangential, radial, and axial stresses in ksc (kg/cm²). The two numbers, 1250 and 2210, on the curves are the external hydrostatic pressures observed at the elastic limit of the inside surface and at rupture. The curves below the 1250 curves show the stress distributions for wholly elastic deformation, and the curves above for elastic and plastic deformation. The elastic-plastic boundary at rupture was calculated to be at a radius ratio of 1.42/1.

The plastic strain at the inside surface, as observed in each manometer tube test and as computed from the theory, is given in Table 2 to show at least a rough correspondence between

experiment and theory for hollow cylinders. The theoretical tangential strain for the plastic range at the inside surface is

Eq. 24 $$\epsilon_{si} = \frac{U_{si}}{r_i} = \tau_M \frac{\alpha_B^2}{2G}$$

and the observed strain is

Eq. 25 $$\epsilon_{si} = \frac{r_i - r_i'}{r_i}$$

TABLE 2.—COMPUTED AND OBSERVED TANGENTIAL STRAINS AT INSIDE SURFACE OF HOLLOW CYLINDERS AT RUPTURE

Specimen no.	Ratio of radii	Computed strain	Observed strain
S-106	1.42/1	.005	.006
S-105	1.43/1	.005	.006
S-114	1.65/1	.005	.009
S-115	2.34/1	.008	.013
S-116	2.38/1	.007	.014
S-117	3.27/1	.009	.020
S-111	3.38/1	.009	.021
S-112	4.50/1	.011	.017
S-113	4.50/1	.011	.021

The maximum shear stress in the cylinder at rupture is at the plastic-elastic boundary (Eqs. 21 and 22, also Fig. 13).

$$\tau_M = \tfrac{1}{2}(\sigma_{tB} - \sigma_{BB})$$

Eq. 26 $$= \tfrac{1}{2}[2\tau_M (\ln \alpha_B + 1) - 2\tau_M \ln \alpha_B]$$

$$= \tau_M$$

The mean stress is greatest at the plastic-elastic boundary.

Eq. 27 $$\sigma_{m_B} = \tau_m(2 \ln \alpha_B + 1)$$

Criteria of Failure

A criterion of failure (either rupture failure or yield failure) for a given material may be defined as a quantitative statement which should be usable for all stress systems to predict either rupture or yielding, for given conditions of temperature, physical and chemical environment, and time. (A criterion should predict failure for *all* materials for the given conditions, but no such generality is possible at the present time.) The criterion may be based on the strain or the stress condition. Most of the criteria discussed here are phenomenological; the Griffith criterion is mechanistic in that failure at flaws in a substance is the basis of analysis. Neither type of criterion takes into account time effects, such as rate of loading, length of time under load, or in general the history of loading. A brief recapitulation of the criteria is given here (for a detailed discussion *see* Nadai, 1933).

MAXIMUM PRINCIPAL-STRESS CRITERION: Failure occurs when the largest principal stress reaches a definite value, constant for a given material (Rankine and Lamé).

Eq. 28 $$|\sigma_1| = K$$

MAXIMUM STRAIN CRITERION: Failure occurs when the largest strain reaches a critical value, constant for a given material (St. Venant and Poncelet).

Eq. 29 $$|\epsilon_1| = K$$

MAXIMUM SHEAR-STRESS CRITERION: A stressed solid commences to flow plastically or to rupture when the maximum shear stress exceeds a limiting value, characteristic of the solid (Coulomb and Tresca).

Eq. 30 $$\tau_M = \tfrac{1}{2}\sigma_D = \tfrac{1}{2}(\sigma_1 - \sigma_3) = K$$

INTERNAL-FRICTION CRITERION: Failure occurs when the shear stress plus the stress due to internal friction on a failure plane reaches a value which is constant for a given substance. This is an extension of the maximum shear-stress rule based on the assumption that the resistance of a specimen to fracture on the surface of slip was influenced by the normal pressure on that surface (Navier).

Eq. 31 $$\tau_n + F_1\sigma_n = K_1$$

which can be expressed also as

Eq. 31a $$\sigma_1 - F_2\sigma_3 = K_2$$

where F_1 and F_2 are functions of the "coefficient of friction", ϕ, on the slip plane, n,

$$F_1 = \phi \quad \text{and} \quad F_2 = \frac{\sqrt{\varphi^2 + 1} + 1}{\sqrt{\varphi^2 + 1} - \phi}$$

and ϕ is related to the plane of fracturing by

$$\phi = \cot 2\theta$$

where θ is the angle between the maximum principal stress and the fracture plane.

MOHR CRITERION: Failure occurs at a maximum shear stress on a failure plane determined by some function of the normal stress on that plane, which is a generalization including the maximum shear stress and internal friction criteria (Mohr).

Eq. 32 $$\tau_M = f(\sigma_n)$$

Mohr showed that the envelope to the circles of the Mohr diagram expresses geometrically the interdependence of the shear stress and of the normal stress on the failure plane, and he suggested that the envelope is a function of the angle between the fracture plane and the principal stresses. (*See* Nadai, 1950, p. 94–108.)

STRAIN-ENERGY CRITERION: Failure occurs by yielding or rupture when a constant amount of distortional strain energy is stored in an element of volume (Von Mises and Beltrami).

The failure condition is usually expressed in terms of the stresses rather than the strains,

Eq. 33 $$(\sigma_1 - \sigma_2)^2 + (\sigma_1 - \sigma_3)^2 + (\sigma_2 - \sigma_3)^2 = 2K^2$$

Alternatively, this criterion was given a geometrical representation by Nadai (1950, p. 209–211), from which he obtains the name, octahedral shear stress.

Eq. 33a $$\tau_{oct} = \tfrac{1}{3}[(\sigma_1 - \sigma_2)^2 + (\sigma_1 - \sigma_3)^2 + (\sigma_2 - \sigma_3)^2]^{\frac{1}{2}}$$

The distortional strain energy criterion has been found applicable to the yielding of ductile metals.

GRIFFITH CRITERION: Failure by fracturing is caused by stress concentrations at the tips of an elongated crack when the work done by the external forces exceeds the elastic plus surface energies stored at the crack (Griffith, 1925). With tensile stresses regarded as positive:

If $(3\sigma_1 + \sigma_3) > 0$ rupture occurs when

Eq. 34a $$\sigma_1 = K$$

If $(3\sigma_1 + \sigma_3) < 0$ rupture occurs when

Eq. 34b $$(\sigma_1 - \sigma_3)^2 + 8K(\sigma_1 + \sigma_3) = 0$$

where K is the same constant in both equations.

WEIBULL CRITERION: This criterion is based on an assumed normal frequency distribution for rupture strengths, determined statistically from many experiments of one type on similar specimens (Weibull, 1939; Frankel, 1948). Since the stress function of strength must be found empirically for each stress system, this criterion is not general, and it will not be discussed.

Yield Strength of Limestone

The criteria may be applied to predict the yielding of limestone in the various stress systems. In this investigation, the beginning of plastic flow has been assumed coincident with yielding at the elastic limit, and in turn the elastic limit has been chosen arbitrarily to coincide with the proportional limit, that is, at the point on a stress-strain curve at which linearity of strain with stress ceases; and yield strength has been defined in terms of the elastic limit.

The maximum principal-stress rule does not apply in the solid cylinder case because of the linear increase of the total axial pressure with increase of hydrostatic pressure (Fig. 3; Eq. 1). The maximum strains differ with the various stress systems (Figs. 3, 9, 10), and no mutual regularity was found. The Griffith factor, K, can be shown to vary inversely with hydrostatic pressure for constant stress difference in the solid cylinder tests (Fig. 3; Eqs. 1, 34b), so the Griffith criterion does not apply.

The internal friction and Mohr criteria coincide with the maximum shear-stress rule for yielding at the elastic limit. In Figure 12 are plotted points at the elastic limit taken from the stress-strain curves for Solenhofen limestone (Figs. 3, 9, 10) and recalculated to maximum shear stress (Eqs. 2, 8, 10) and mean stress (Eqs. 3, 9, 14). The standard deviation of the mean value of maximum shear stress is about 100 ksc. An extension of the maximum shear line to the right in 12 could be made for mean stresses of 19,000 ksc and 23,000 ksc from additional tests on two solid cylinders of Solenhofen limestone. The maximum shear stress from both tests was 1800 ksc, plus or minus 300 ksc. The accuracy of these values in the high-pressure tests is rather low because of the uncertain friction corrections in the apparatus used (not described here).

The maximum shear stress is constant for each of the very different stress systems, and therefore this criterion of yield strength is valid for Solenhofen limestone over a large range of mean stress. The validity of the criterion is

enhanced by the coincidence of the theoretical surface of maximum shear stress (Fig. 8b) and the actual surface of fracture in the hollow cylinders, assuming that the fracturing was propagated without distortion from the elastic zone through the plastic zone. The mechanical restraints on the solid cylinders and disks modified their modes of failure.

A plot of octahedral shear stress for the same data as in Figure 12 does not give any closer distribution of points around a critical value than that shown for maximum shear stress. Therefore, in view of the approximately constant relation between maximum shear stress and octahedral stress, only the maximum shear stress need be discussed; also, the accuracy of the experimental data does not warrant separate analysis.

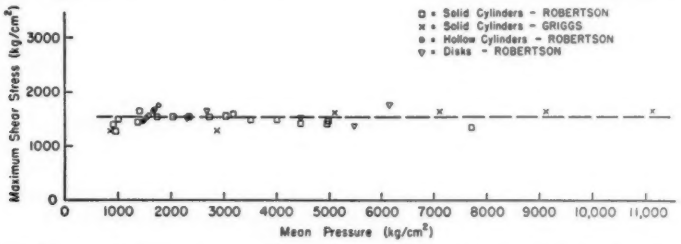

FIGURE 12.—MAXIMUM SHEAR STRESS VS. MEAN STRESS AT THE ELASTIC LIMIT, SOLENHOFEN LIMESTONE

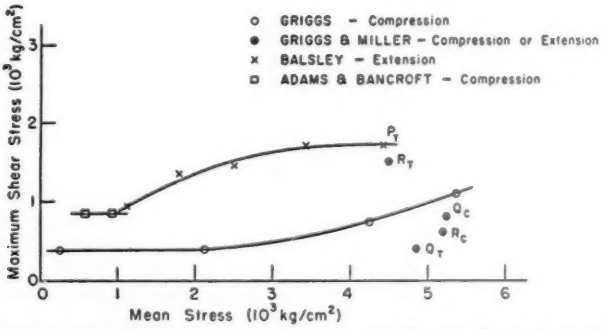

FIGURE 13.—MAXIMUM SHEAR STRESS VS. MEAN STRESS AT THE ELASTIC LIMIT, YULE MARBLE (GRIGGS AND MILLER, AND BALSLEY) AND CARRARA MARBLE (ADAMS AND BANCROFT)

The maximum shear-stress and the strain-energy criteria can be shown to be nearly equal in the numerical values of the yield condition. In the solid cylinder tests, the values of the principal stresses (Eq. 1) can be substituted in Equations 30 and 33a to give

$$\tau_{oct} = 0.94\,\tau_M$$

The same proportion between the values of the two criteria holds for any tension or compression tests and the punching tests on the disks for any hydrostatic pressure.

In the hollow cylinder tests (and for torsion tests), the values of the principal stresses (Eqs. 5, 6, 7) can be substituted in Equations 30 and 33a to give

$$\tau_{oct} = 0.82\,\tau_M$$

Although hydrostatic pressure has been used frequently for plotting of strength curves, mean stress is used here because it is a more general function.

Attempts to use the maximum shear-stress rule to evaluate all available reported tests on the strength of limestone or marble are given in Figures 13, 14, and 15; the points for the curves are computed from published and original data.

The circled-cross points in Figure 13 from Griggs and Miller (1951, Fig. 3) from tests on jacketed solid cylinders, bring out the anisotropy of strength caused by foliation. The lowest point, Q_T, represents an extension test in which

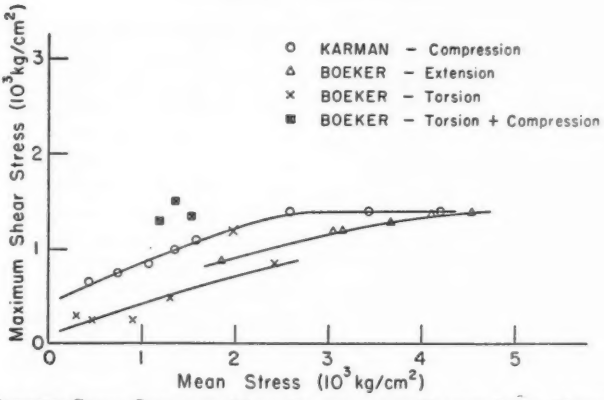

FIGURE 14.—MAXIMUM SHEAR STRESS VS. MEAN STRESS AT THE ELASTIC LIMIT, MARBLE (KARMAN AND BOEKER)

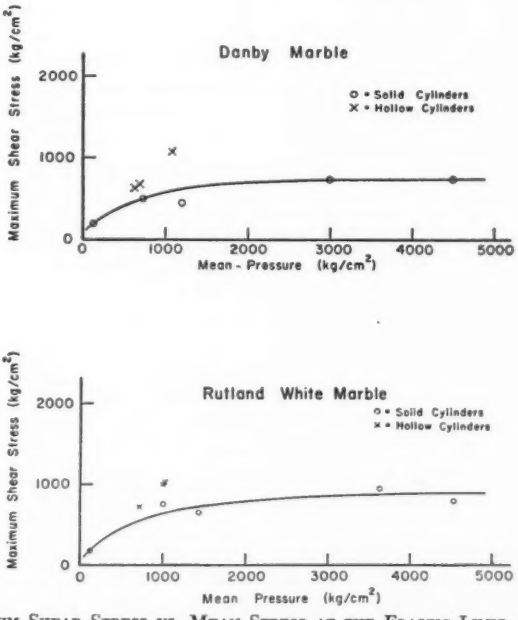

FIGURE 15.—MAXIMUM SHEAR STRESS VS. MEAN STRESS AT THE ELASTIC LIMIT, DANBY MARBLE AND RUTLAND WHITE MARBLE

the foliation of the specimen was perpendicular to a "tension" stress. The strongest orientation was that of P_T (Balsley, 1941, Fig. 6), perpendicular to R and to Q. Obviously, the yield strength of Yule marble depends on the orientation of the marble foliation and on the stress system used.

The curve in Figure 13 from Balsley's (1941, Fig. 4) experiments on jacketed, solid cylinders in extension approaches a limiting value of 1700 ksc which might be a limiting yield strength of the Yule marble for usual, room-temperature conditions. The curve from Griggs' (1936, Fig. 5) compression tests on an unknown marble may not be reliable because the solid cylinders were not jacketed. The two points from Adams

and Bancroft (1917) were obtained after recomputing their results on cylinders of Carrara marble in compression using tightly fitted steel jackets for lateral restraint.

TABLE 3.—TOTAL AXIAL STRESS AND STRAIN AT RUPTURE OF SOLID CYLINDERS OF SOLENHOFEN LIMESTONE

Specimen no.	Hydrostatic pressure	Total axial stress	Total axial strain
S-99	1 ksc	2800 ksc	.0034
S-55	1	2640	—
S-85	100	2670	.0092
S-83	300	3610	.0156
S-81	500	4240	.0168
S-82	700	4430	.0185

Curves of maximum shear stress drawn from curves and tables of the experimental results of Karman (1911) and Boeker (1915) on marble are shown in Figure 14. The test pieces in all cases were cylindrical and were jacketed with brass. The limiting value of the maximum shear stress at the elastic limit from Karman's compression tests is about 1400 ksc, and several points from Boeker's experiments approach the same limiting value. The torsion test point at 1200 ksc shear and 2000 ksc mean stresses is from the second cycle of a torsion experiment (the first cycle being at 850 ksc shear and 2420 ksc mean stress), which indicates that the marble was strain strengthened by the first cycle.

Curves of maximum shear stress versus mean stress at the elastic limit from solid- and hollow-cylinder experiments on Danby and Rutland White marbles are shown in Figure 15. Most of the cylinders of these marbles were oriented with the cylinder axes parallel to the plane of the foliation. The tests for strain data on the Becraft and the New Scotland limestones were too few to be conclusive.

Rupture Strength of Limestone

The quantitative analysis of the failure by rupture of a semiductile material like limestone is complicated by the plastic deformation that precedes the rupture.

Only the solid cylinders subjected to hydrostatic pressure less than 1000 ksc failed by rupture. Those tested at higher hydrostatic pressures deformed plastically with no important loss of cohesion for large strains and supported an increasing compressive load. The disk tests which resulted in rupture were those under hydrostatic pressures less than 3000 ksc; disks under higher hydrostatic pressures flowed. All hollow cylinders ruptured or spalled at well-defined hydrostatic pressures which varied regularly with wall thickness.

The maximum principal-stress (Eq. 28) and the maximum-strain (Eq. 29) criteria are not constant for solid-cylinder tests and so are not applicable (Table 3).

In order to try out the criteria of failure with the hollow-cylinder data, the principal stresses (Eqs. 15–23) had to be determined, and to do that a value of the shear-stress condition for perfect plasticity had to be found. A value of 1700 ksc was determined by curve-fitting; this value was substantiated roughly by comparison of observed positions with computed positions of the elastic-plastic boundary at rupture.

The curves of maximum shear stress versus mean stress at rupture for Solenhofen limestone are plotted in Figure 16. Only data from specimens which actually ruptured are plotted. Since the thick-walled hollow cylinders did not rupture completely, they are not plotted. There is a limiting value of the maximum shear stress of about 1900 ksc.

The curves for marble in Figure 17 are values of maximum shear and mean stresses at rupture computed from published results. It may be significant that there is an apparent limiting range (2000–3000 ksc) of maximum shear stress for all stress systems. The extension tests of Boeker and of Balsley are in close agreement, perhaps owing to the high hydrostatic pressures used. From the rupture data for Danby and Rutland White marbles and Becraft limestone, maximum shear stress at rupture approached but is less than that for Solenhofen limestone; New Scotland limestone was considerably stronger.

In order to test the Mohr (Eq. 32) and internal-friction (Eq. 31) criteria, a Mohr circle diagram from the experimental results of Karman and of Boeker (his extension tests only) is given in Figure 18; and Figure 19 is the diagram from my experiments on Solenhofen limestone. In both figures, only the data from speci-

mens which ruptured completely are plotted. If the Mohr criterion (or the internal-friction criterion) were valid, the envelope curves above the circles would be superimposed for all stress systems on a given material. Although unfortunately not plotted on Figure 18, it is evident from Figure 17 that a Mohr envelope of Boeker's torsion plus compression tests would lie much above the two envelopes shown. Boeker (1915) did his experiments to test the Mohr criterion, and he concluded that the Mohr criterion without correction did not satisfy both sets of data. Figure 19 suggests a similar conclusion.

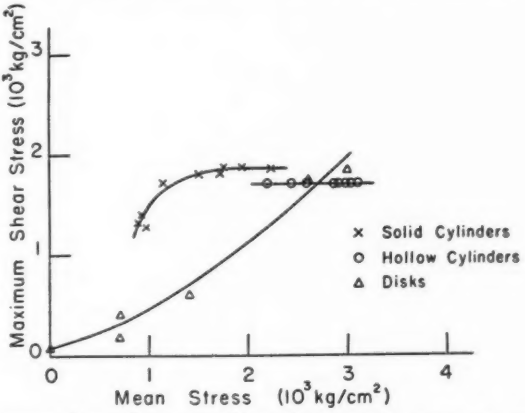

FIGURE 16.—MAXIMUM SHEAR STRESS VS. MEAN STRESS AT RUPTURE, SOLENHOFEN LIMESTONE

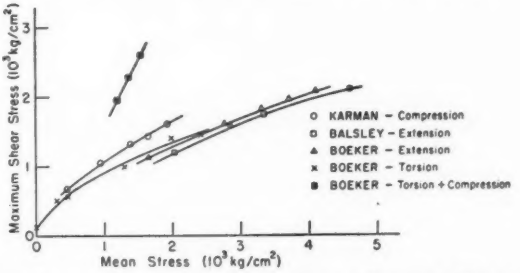

FIGURE 17.—MAXIMUM SHEAR STRESS VS. MEAN STRESS AT RUPTURE, MARBLE (KARMAN, BOEKER, AND BALSLEY)

Professor E. Orowan suggested that tension or bending tests on the limestone should be made as a check on the Griffith theory. (The check of the theory is in the comparison of the constant, K, found from a stress system in which Equation 34a applies with the K from a system in which Equation 34b applies.) Four rectangular bars of Solenhofen limestone were tested in an experimental set-up like that suggested diagrammatically in Figure 1d. The static load on a pan suspended from the middle of the bar was increased until the bar broke; there was no confining pressure.

A comparison of the rupture data from experiments on solid and hollow cylinders and on disks (using Eq. 34b) with the bending tests (using Eq. 34a) is made in Table 4. The values of the constant K, computed from the bending tests are listed with the values of K from the other tests. The values for K are scattered with some concentration between 300 and 400 ksc; there is a large variation of K with hydrostatic pressure in the disk tests. More experimental work is necessary to test this criterion thoroughly for rupture in Solenhofen limestone.

Conclusions on the Strength of Limestone

Limestone acts as a brittle material at low hydrostatic pressures and as a ductile material at high hydrostatic pressures. The boundary of hydrostatic pressure between the two types of behavior depends on the stress system involved: it is 1000 ksc for compression of solid cylinders, 3000 ksc for punching of disks, and about 6000 ksc for extension of solid cylinders.

The yield strength of Solenhofen limestone is nearly constant at 3200 ksc for mean pressures up to 23,000 ksc. The marble used by Karman and Boeker had an upper limit of the maximum shear stress at the elastic limit for their several stress systems of 1400 ksc. The upper limit of the maximum shear stress for Yule marble is about 1700 ksc. Generalizing, the yield strength of any fairly pure limestone or marble seems to have a consistent upper limit of about 3400 ksc for the nearly constant laboratory conditions, room temperature, slow strain rate, and constant chemical environment.

Rupture occurred in my experiments on Solenhofen limestone for limiting values of the maximum shear stress of 1700 to 1900 ksc. For marbles tested by Karman, Boeker, Balsley, and Griggs in compression, torsion, and extension, rupture occurred over a range of limiting maximum shear stress around 2000 ksc. In terms of stress difference, the limiting rupture strength of limestone and marble is about 4000 ksc for the nearly constant laboratory conditions.

The observed and theoretical rupture strengths of ionic crystals differ markedly. Polanyi (1921) and Zwicky (1923) determined for sodium chloride a theoretical tensile strength by rupture of about 10,000 ksc; the measured strength is about 50 ksc. Frankel's approximation (Orowan, 1940, p. 12) for shear strength

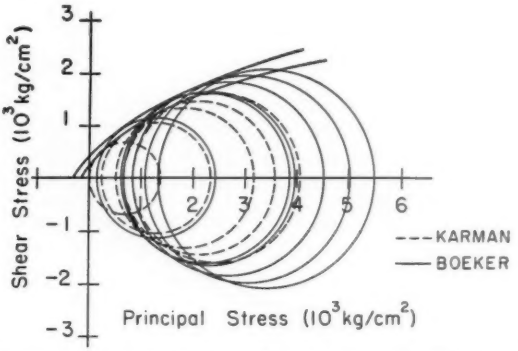

FIGURE 18.—MOHR DIAGRAM OF THE RESULTS BY KARMAN AND BY BOEKER ON RUPTURE OF MARBLE

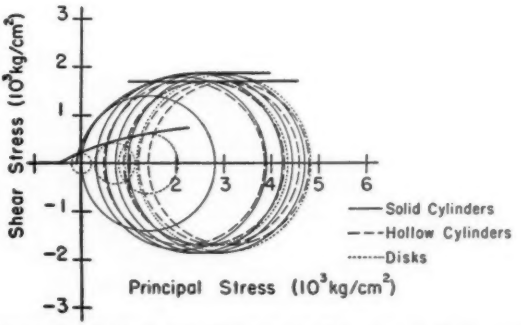

FIGURE 19.—MOHR DIAGRAM OF THE RESULTS ON RUPTURE OF SOLENHOFEN LIMESTONE

of ionic crystals is:

Eq. 35 $$\tau_N = \frac{G}{2\pi}$$

For limestone this expression gives a theoretical maximum shear stress of about 40,000 ksc, which is 20 times the limiting stress I observed. Bridgman's shearing test on Solenhofen limestone (Birch *et al.*, 1942, p. 127) shows that the shearing stress at the knee of his curve is about 7000 ksc for a hydrostatic pressure of about 30,000 ksc. It is possible that Bridgman was testing at least approximately the atomic forces holding welded calcium carbonate grains together.

TABLE 4.—STRENGTH CONSTANT OF GRIFFITH CRITERION OF FAILURE FROM EXPERIMENTS ON SOLENHOFEN LIMESTONE

Specimen type	Specimen no.	Hydrostatic pressure (ksc)	K (ksc)
Bar (Bending)	S-95	1	380
	S-96	1	400
	S-97	1	420
Solid cylinder (Compression)	S-99	1	350
	S-85	100	230
	S-83	300	390
	S-81	500	370
	S-82	700	340
	S-86	1000	300
Hollow cylinder (Compression)	All	—	400
Disk (Punching)	S-100	1	0
	S-101	700	60
	S-118	1400	70
	S-92	2600	290
	S-91	3000	280

EXPERIMENTAL RESULTS FOR SILICATE ROCKS AND MINERALS

Introduction

An attempt was made to determine some regularity in the strengths of silicate rocks and minerals. The same experimental techniques used in testing solid cylinders and hollow cylinders of limestone (Figs. 1a, 1b) were employed on twelve igneous, sedimentary, and metamorphic rocks, and on four minerals. The problems engendered by such physical characteristics as foliation, grain size, mineralogic and chemical composition, porosity, and moisture content were not evaluated.

Results from Solid-Cylinder Compression Tests

The stress-strain curves from experiments on igneous rocks are uniform in being elastic almost to the point of rupture. Furthermore, the effect of hydrostatic pressure seems to be the same for each rock: a marked increase in strength occurs with increasing hydrostatic pressure. The sedimentary and metamorphic rocks and the minerals tested all behaved in much the same way. Since these rocks are all brittle under the nearly constant laboratory conditions used, only their rupture strengths could be investigated.

Stress-strain curves from tests on solid cylinders of Barre granite, Cambridge slate, and pyrite are shown in Figure 20. (*See* Appendix 1 for rock descriptions and symbols.) The increase in the rupture strength with increasing hydrostatic pressure is obvious. Planar shear surfaces at angles less than 45° to the cylinder axis seem common to all specimens, with wedging failure in some specimens (Pl. 4, figs. 1, 2, 9, 12).

In view of the plasticity of limestone and marble, a series of experiments on solid cylinders of dolomite was performed for a large range of hydrostatic pressure (Fig. 21). Unlike limestone, the Blair dolomite is brittle, although for very high hydrostatic pressure evidence of plastic flow was observed; the permanent set in BD—6 was 0.8 percent. The rupture of the other specimens was typically brittle, a wedging and planar shearing failure.

Results from Hollow-Cylinder Tests

Owing to limitations in the strength of the apparatus, it was not possible to break solid cylinders of silicate rocks at hydrostatic pressures higher than about 1000 ksc (kg/cm²). Decreasing the size of the specimen to cause rupture would introduce inhomogeneities from the individual mineral grains. To obviate this problem, most of the tests were run on hollow cylinders, since higher stress differences could be attained. One test was made on each rock using the manometer tube to measure the strain at the inside surface. The mode of failure of the medium-walled hollow cylinders (Pl. 4), as in the limestones and marbles, was along the theoretical tangential-radial shear surface (Fig. 8b); the thin-walled cylinders disintegrated upon collapse.

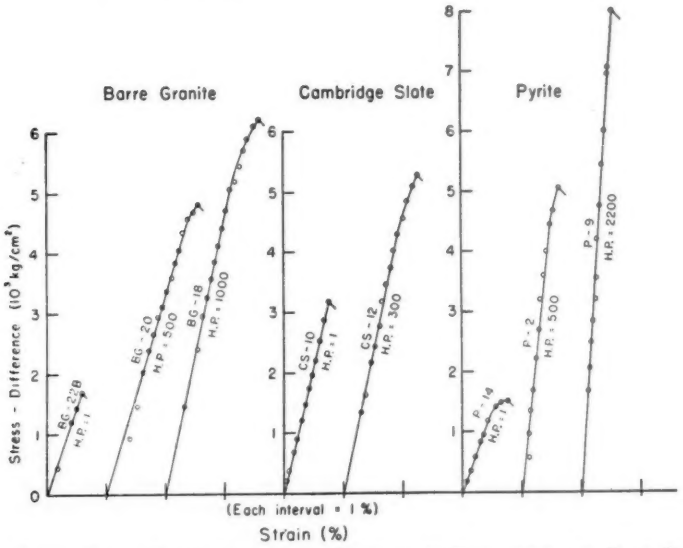
Barre Granite
Cambridge Slate
Pyrite
Stress - Difference (10^3 kg/cm^2)
BG - 22B H.P. = 1
BG - 20 H.P. = 500
BG - 18 H.P. = 1000
CS - 10 H.P. = 1
CS - 12 H.P. = 300
P - 14 H.P. = 1
P - 2 H.P. = 500
P - 9 H.P. = 2200
(Each interval = 1 %)
Strain (%)

FIGURE 20.—STRESS-STRAIN CURVES FROM AXIAL-COMPRESSION EXPERIMENTS ON SOLID CYLINDERS OF GRANITE, SLATE, AND PYRITE

Each curve starts at zero strain; H.P. = hydrostatic pressure in kg/cm^2.

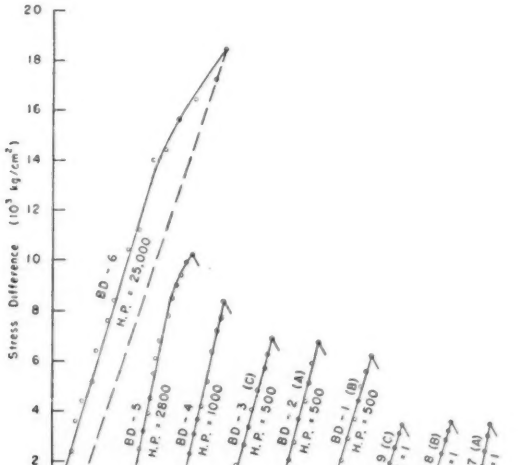
Stress Difference (10^3 kg/cm^2)
BD - 6 H.P. = 25,000
BD - 5 H.P. = 2800
BD - 4 H.P. = 1000
BD - 3 (C) H.P. = 500
BD - 2 (A) H.P. = 500
BD - 1 (B) H.P. = 500
BD - 9 (C) H.P. = 1
BD - 8 (B) H.P. = 1
BD - 7 (A) H.P. = 1
Each Interval = 1% Strain

FIGURE 21.—STRESS-STRAIN CURVES FROM AXIAL-COMPRESSION EXPERIMENTS ON SOLID CYLINDERS OF BLAIR DOLOMITE

Letters A, B, and C refer to three mutually perpendicular axes.

The hollow cylinders of the sedimentary and metamorphic rocks and of the minerals ruptured like the igneous-rock cylinders, and in fact all these geologic materials had about the same rupture strength (Fig. 22), although sandstone (GS and RS), soapstone (SP), and quartz (Q) are important exceptions.

Strain data from the manometer tests on the

hollow cylinders showed good agreement with the theoretical strains for all rocks except microcline and red sandstone, which may be explained by erratic errors in the apparatus.

cylinder tests, and so the Griffith criterion is not applicable to silicate rocks. Bridgman (1947a, p. 257–258) pointed out that Griffith's concept of microscopic failure by intensified

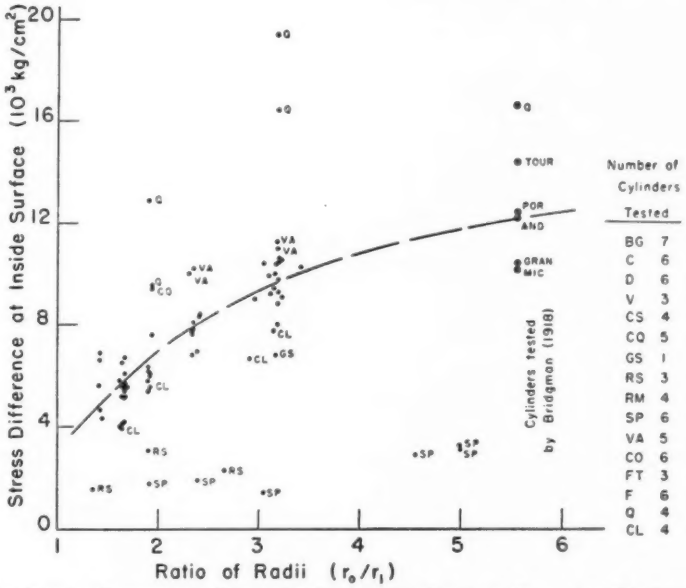

FIGURE 22.—SCATTER DIAGRAM OF RUPTURE STRENGTH VS. RATIO OF RADII FOR CRUSHING TESTS OF HOLLOW CYLINDERS OF SILICATE ROCKS AND MINERALS

Application of Criteria of Failure to Silicate Rocks

The most significant difference in behavior between the limestone and the silicate rock specimens is the complete lack of any important plastic flow phenomena in the silicate rocks. This thoroughly brittle behavior at room temperature of the silicate rocks and minerals is a marked feature of these materials for moderate hydrostatic pressures.

The usefulness of the criteria of failure can be tested for prediction of rupture of silicate rocks. The maximum principal-stress (Eq. 28) and maximum principal-strain (Eq. 29) criteria do not apply to rupture of silicate rocks, because these quantities increase with increasing hydrostatic pressure (Fig. 20). As for the Griffith criterion, values of K from the solid-cylinder and hollow-cylinder experiments on Barre granite are listed in Table 5; the value of K for granite in tension is 50 ksc. With increasing hydrostatic pressure, K increases linearly in the hollow-

TABLE 5.—STRENGTH CONSTANT FROM GRIFFITH CRITERION OF FAILURE FROM EXPERIMENTS ON BARRE GRANITE

Specimen no.	Max. prin. stress (ksc)	Min. prin. stress (ksc)	K (ksc)
Solid cylinders			
BG-22B	1700	0	210
BG-17B	4500	500	400
BG-20	5150	550	470
BG-18	6100	1000	460
Hollow cylinders			
BG-3	3800	0	480
BG-4	3600	0	460
BG-1	4400	0	540
BG-9	5200	0	640
BG-10	5000	0	620
BG-6	7000	0	880
BG-5	7600	0	960

stresses in cracks is oversimplified for the macroscopic, average nature of stress and strain.

The Mohr, internal-friction, and maximum shear-stress rules for failure (Eqs. 30, 31, 32) do not apply to these silicate rocks as found from Mohr circle plots of the rupture data. The Mohr circles for stresses at rupture for hollow cylinders are mutually tangent at the origin, although of increasing diameter (an increasing function of wall thickness), and no common envelope can be drawn between circles from hollow-cylinder and solid-cylinder data.

An effort was made to find a functional relationship between the maximum stress difference (rupture strength) and any other parameter in order to predict the rupture strength of the silicate rocks. A fairly satisfactory relation was found, which affords a rough approximation and which is given by a direct proportionality between maximum shear stress (half the maximum stress difference) and mean stress.

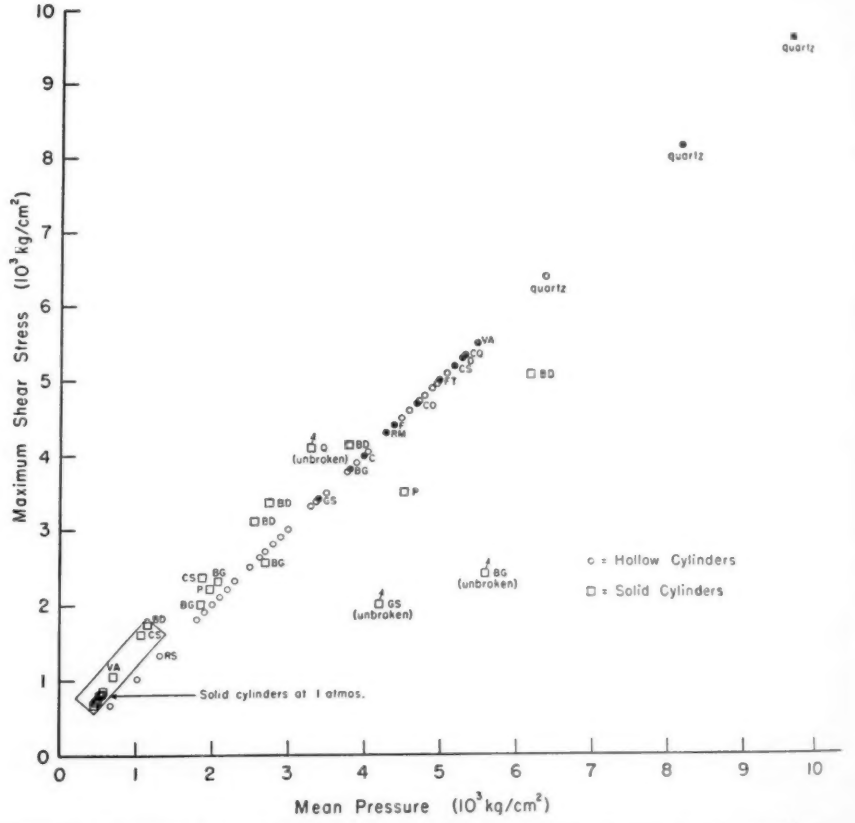

FIGURE 23.—MAXIMUM SHEAR STRESS VS. MEAN STRESS AT RUPTURE, VARIOUS ROCKS AND MINERALS

Eq. 36 $$\tau_M \cong \sigma_M$$

Certain mathematical errors are inherent in this approximation for certain stress systems. In Bridgman's "pinching-off" tests, in which the radial and tangential pressures on a solid cylinder are equal and the axial stress is zero, the approximation reduces to an identity in which the ratio τ_M/σ_m becomes 0.75 instead of 1.00. In axial tension or compression tests *in air*, the approximation reduces to another iden-

tity in which τ_M/σ_m becomes 1.50 instead of 1.00; however, for lateral pressures greater than zero, the identity need not hold.

Figures 22 and 23 strongly suggest that for the well-indurated rocks and for certain minerals the rupture strength of each is a function

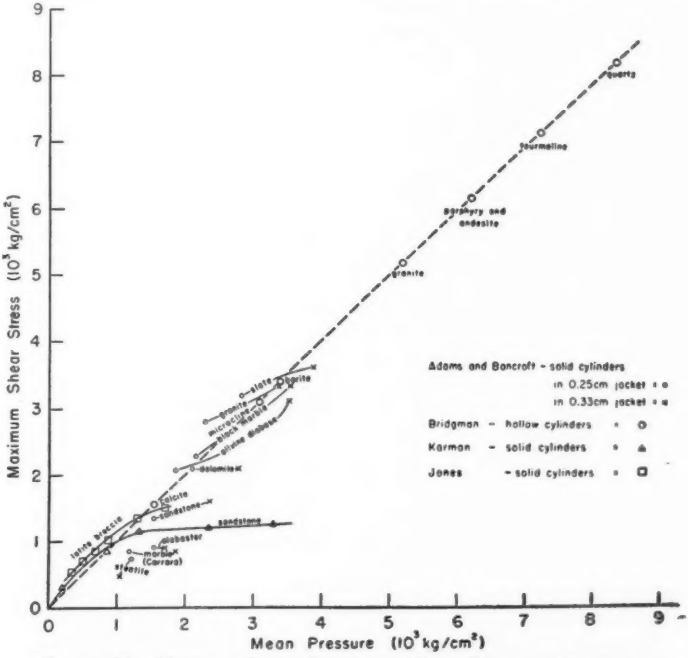

FIGURE 24.—MAXIMUM SHEAR STRESS VS. MEAN STRESS AT RUPTURE

From Experiments by Adams and Bancroft, Karman, Bridgman, and Jones on various rocks and minerals.

Rupture Strength of Silicate Rocks

A composite plot of data from all rocks and minerals I tested is given in Figure 23, which shows the apparent relation at rupture between the two parameters, τ_M and σ_m (Eq. 36). This equality is overemphasized for hollow cylinders in the straight line of Figure 23 because they are equal only according to first-order elasticity theory (Eqs. 8, 9); and the analysis used for the hollow-cylinder case cannot be applied too closely to rocks, because the elasticity of rocks is inexact compared to the mathematical model. (Circles for a radius ratio of about 3.2/1 are blackened in Figure 23.)

For all the variety of geologic materials in Figure 23 none of the rocks and minerals exhibits the limiting rupture strength preceding plasticity found in the experiments on limestone.

of the magnitudes of the stresses but not of the stress system nor of the composition of the rock. This is only tentative, in view of the scatter of the points in Figures 22 and 23, and should be used only as a first, rough outline of the behavior of these rocks.

Quartz is extraordinarily strong. The experiment represented in Figure 23 by the solid-cylinder point at shear stress 4100 ksc and mean stress 3300 ksc was run at a hydrostatic pressure of 600 ksc, and a maximum stress difference of 8200 ksc was reached without breaking the cylinder. In Bridgman's (1941, p. 468–469) last-reported compression test on a solid cylinder of quartz, the sample ruptured at a maximum shear stress of 20,000 ksc and mean stress of 37,000 ksc, which is a point well below the 45° line.

The results of tests on various rocks and min-

erals taken from the literature are shown in Figure 24, including the work of Karman (1911), of Bridgman (1918), of Jones (1945), and of Adams and Bancroft (1917). (New stress-strain curves for the rocks studied by Adams and Bancroft were plotted after recomputing the numerical data given. The pronounced yielding at the elastic limit was assumed to occur at the beginning of rupture of the sample which was much below the elastic limit for the steel jacket. The accuracy of the value of the lateral pressure of the jacket is difficult to appraise but it may be as good as plus or minus 100 ksc.)

TABLE 6.—BRIDGMAN'S SHEARING STRENGTHS FOR SEVERAL ROCKS AND MINERALS

Mineral or rock	Shearing strengths (kg/cm²)				
(confining pressure—kg/cm²)	10,000	20,000	30,000	40,000	50,000
Anorthite	2200	7700	11,000	14,000	14,000
Augite	1100	3000	6300	10,000	13,000
Basalt glass	3000	7600	13,000	14,000	17,000
Bronzite	1800	3400	9000	13,000	16,000
Cassiterite	1600	5100	8300	10,500	12,500
Cuprite	2200	6200	8200	9400	10,300
Diopside	2500	5900	9000	12,000	14,000
Garnet	....	....	....	....	15–19,000
Hematite	2300	6900	10,900	14,000	16,700
Hornblende	1100	3100	6400	10,000	13,000
Obsidian	3900	8000	12,000	14,000	15,000
Opal	3600	7100	10,000	12,000	18,000
Quartz	....	....	....	....	14,500
Pyrite	2300	6300	9700	11,500	12,500
Pyroxenite	2800	6400	9000	12,000	14,000
Sericite	....	....	....	....	13,000
Sillimanite	2100	6100	10,100	11,200	11,800
(Predicted strength)	(3300)	(6700)	(10,000)	(13,300)	(16,700)

The curve of points for tests on volcanic breccia by Jones (1945) shows a falling off like the sandstone of Karman, and like the Blair dolomite in Figure 23. The decrease in rupture strength as the mean stress is increased may mean that these materials will deform plastically at room temperature if the hydrostatic pressure is high enough.

Bridgman (1935; 1936; 1937) measured the shearing stress directly in his shearing experiments; and the principal stresses for his stress system are related as follows.

$$\sigma_1 > \sigma_2 = -\sigma_3$$

Substituting in Equation 36,

Eq. 36a $$\tau_M \cong \tfrac{1}{6}(\sigma_1 + \sigma_2 - \sigma_3) \cong \tfrac{1}{6}\sigma_1$$

The maximum principal stress, σ_1, was that of the pressure across the disk of the specimen. The relationship expressed by Eq. 36a holds fairly well for Bridgman's shearing data as listed in Table 6, (taken from Table 9-7 Birch *et al.*, 1942, p. 126–128) especially at the higher confining pressures. Bridgman's data fit the empirical relation (Eq. 36) surprisingly well for such very high pressures. Evidently the powders (used to make up Bridgman's disks for shearing) of these rocks and minerals act like solid specimens with regard to strength at these high confining pressures.

Equation 36 may also be restated in terms of a hydrostatic pressure and the maximum shear stress in systems where two of the principal stresses are equal and less than the third (as in the solid cylinder compression tests).

$$\sigma_1 > \sigma_2 = \sigma_3 = P_H$$

then

$$\tau_M \cong \tfrac{1}{6}[(\sigma_1 - \sigma_3) + \sigma_2 + 2\sigma_3]$$

Eq. 36 b $$\tau_M \cong 3\,P_H$$

or

$$\sigma_D \cong 6\, P_H$$

The fit of the data from solid cylinder tests to Equations 36 and 36b can be seen in Figures 23 and 24.

For the extension-stress system, in which two principal stresses are equal and greater than the third:

$$\sigma_1 = \sigma_2 = P_H > \sigma_3$$

Substituting in Equation 36,

$$\tau_M = \tfrac{1}{3}[-(\sigma_1 - \sigma_3) + \sigma_2 + 2\sigma_1]$$

Eq. 36 c $$\tau_M \cong \tfrac{3}{5} P_H$$

or

$$\sigma_D \cong \tfrac{6}{5}\, P_H$$

The stress situation at rupture given by Equation 36c would be realized when the "tensile" stress difference was about equal to the hydrostatic pressure. Very few extension tests on brittle rocks have been made. However, there are a few tests on silicate materials which may be inspected. Bridgman (1947a, p. 250) found the rupture of Pyrex glass under a hydrostatic pressure of 27,000 ksc to occur at a "tensile" stress difference of 24,500 ksc, which agrees roughly with the prediction of Equation 36c. However, for synthetic sapphire, the stress difference at rupture was about one-fifth the hydrostatic pressure of 27,400 ksc; and for pipestone and for sodium chloride, the stress difference at rupture was about one-sixtieth of the hydrostatic pressure of 27,400 ksc. Boeker's and Balsley's extension tests on marble showed the stress difference at rupture to be about half the hydrostatic pressure.

The results of the "pinching-off" tests may be tried as an extension stress system by assuming Equation 36c to apply for small σ_3 greater than zero. Rupture of Pyrex glass rods by "pinching-off" occurs at a hydrostatic pressure of about 1600 ksc (P. W. Bridgman, personal communication), which is about equal to its maximum observed tensile strength in air; however, the strength of glass in both types of tests is notoriously variable. Richart, Brandtzaeg, and Brown (1928) found that concrete cylinders "pinched-off" at a hydrostatic pressure about equal to the compressive strength of the concrete in air, which might be taken as the maximum possible tensile strength of concrete, although extremely difficult to attain with the usual tension techniques.

Although there seems to be some experimental support for Equation 36 and its derivations, it is evident that this criterion of failure by rupture is empirical and only approximate. It does bring out an apparent dependence of strength on the sum of the stresses for silicate rocks.

Generalizations on Rock Strength

Strength (both yield and rupture) is an average, macroscopic property of materials, and for this reason only reasonably homogeneous materials tested in the same manner give reproducible strengths. Solenhofen limestone is remarkably uniform and isotropic for a rock and does give consistent yield and rupture strength results, but a moderate change in the testing conditions was found to change both strengths considerably. The yield and rupture strengths of a substance are affected by several factors: stress conditions, temperature, composition, chemical environment, physical character, deformation history, and strain rate.

Both yield and rupture strengths of rocks are defined and can be predicted in terms of stress differences but the sum of the stresses seems to be an independent factor in affecting strength. Hydrostatic pressure causes brittle limestone to become ductile, and it raises the rupture strength of silicate rocks markedly. Mean stress is a more general stress function and may be more significant than hydrostatic pressure for geologic processes near the surface of the earth.

Although the yield strength of limestone is constant for the standard conditions of this study, it is lowered by heating. The yield strength of Yule marble was found by Griggs *et al.* (1951, Fig. 1; 1953, Fig. 1) to be about 2500 ksc at 20° C and about 1000 ksc at 150° C and at 300° C. The values are for marble specimens in one orientation under hydrostatic pressure of 10,000 ksc.

Rupture in limestone on the other hand, seems to be deferred by heating in that there is a promotion of ductility in the limestone (Table 1). By analogy it may be postulated that heating will promote plasticity in silicate rocks, and Griggs (1954) has reported it in preliminary results for several silicate rocks.

A comparison of stress-strain curves of hollow cylinders of carbonate and silicate rocks and minerals is given in Figure 25, showing either yield strengths or rupture strengths. The

Yield and rupture strengths are sensitive to perfection and type of crystal structure, and to the state of aggregation of the mineral grains in a rock. All inhomogeneities in a rock grading

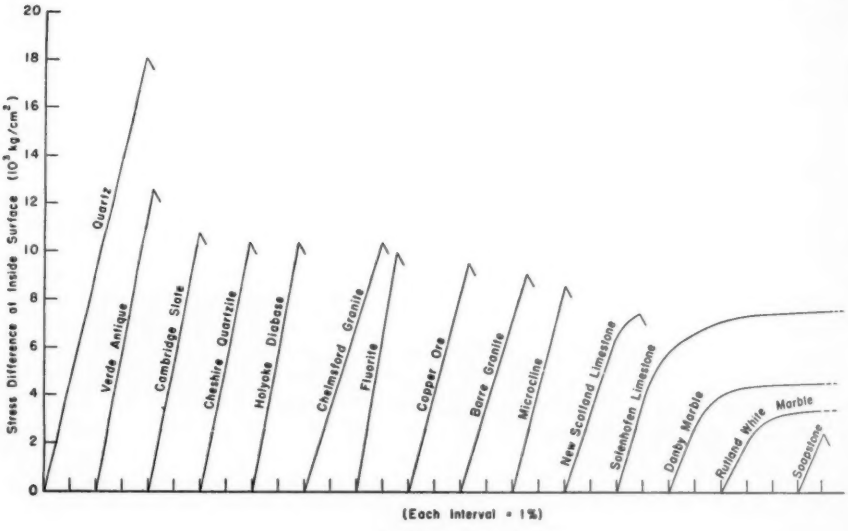

FIGURE 25.—COMPARISON OF RUPTURE STRENGTHS AND OF YIELD STRENGTHS FOR CRUSHING OF HOLLOW CYLINDERS OF THE SAME RATIO OF RADII
Curves were estimated from results on cylinders of nearest sizes.

contrast in behavior of the limestones and marbles with the silicate rocks and minerals is obvious, and the uniformity of rupture strengths of the silicate rocks is indicated (also Fig. 22).

The chemical environment is important, as shown by the experiments of Griggs (1940) on the deformation of gypsum under dry and under wet conditions, and the experiments of Joffe (1928) on salt under dry and wet conditions. Their results show that the effects of water on rupture strength may be due to chemical causes (e.g., recrystallization) or to physical causes (e.g., mechanical weakening) or both. The presence of water seems to strengthen salt by recrystallization, but it weakens gypsum mechanically. Mechanical weakening was shown in the variation of Young's modulus with moisture content by Delaney (1940); the modulus was halved by soaking a slab of soapstone in water, and the modulus came back as the slab dried out.

from imperfections inside mineral grains to inter-granular pores, and to foliations and joints, determine the effects of physical character on strength, and in general each imperfection weakens the rock. There is no reliable means at the present time of measuring the state of imperfection of a rock, so this is empirical and *a priori* reasoning.

The history of deformation (indicated by folding, jointing, and faulting) obviously affects the present rupture strength of a large mass of rock. Strain-strengthening effects from a history of cyclic deformation seem to be important in determining the yield strength of limestone but have not been studied adequately for limestone nor at all for silicate rocks.

A fast rate of loading causes the yield strength of limestone to be raised considerably, although it relaxes quickly.

An exponentially diminishing strain rate occurs in laboratory creep tests of limestone

(Griggs, 1939) for a static stress difference below the yield strength. However, creep of carbonate or silicate rock in the earth under a stress difference less than the yield or rupture strength cannot be evaluated very well in the laboratory, since the experiments are concerned with such minute time periods compared to geologic time. Bridgman (1936, p. 666) commented on this dilemma and on time effects in general, saying:

> "... I think we should not be frightened by the bogy of even geological time, but in our speculations freely use such concepts as shearing strength, admitting that the apparent strength in 10 million years may be a little lower than for laboratory experiments, or the strength for 100 million years a little lower than for 10 million, and also recognizing that the difference between geological and laboratory behavior may be a strong function of the material."

Appendix 1: Descriptions of Rocks and Minerals

Carbonate Rocks

(L) *Becraft limestone.*—The blocks of the Becraft limestone were obtained from a quarry at Alsen, New York. The rock is highly fossiliferous, the fossils in white calcite being clearly outlined in the reddish matrix, but thoroughly cemented into the matrix. It is a fairly pure limestone of early Devonian age. All test cylinders were cut with axes noraml to the bedding of the limestone.

(BD) *Blair dolomite.*—"Blair" is the local name for a dolomite from the Millville quarry at Martinsburg, West Virginia. The rock is a fine-grained, pure calcium-magnesium carbonate. Cylinder axes were cut in three perpendicular directions, (A, B, and C in Fig. 21).

(DB) *Danby marble.*—"Danby" is the trade name of the marble quarried at Danby, Vermont. The marble is a medium-grained (0.1 mm) white calcite marble, and is quite pure calcium carbonate; the impurities are 0.1 per cent Al_2O_3 plus Fe_2O_3, and 0.4 per cent MgO. The Danby marble is quarried from the Beldens formation of middle Ordovician age (Chazy). All test cylinders were cut with axes subparallel to the foliation.

(CL) *New Scotland limestone.*—The New Scotland limestone blocks were also obtained from the quarry at Alsen, New York. The fine-grained dark-gray New Scotland limestone is shaly. The argillaceous content is of the special mixture which makes the limestone a natural cement rock, and which accounts for the quarrying activity. An approximate chemical analysis of this early Devonian rock is 20 per cent SiO_2, 2 per cent Al_2O_3, 1 per cent MgO, 5 per cent FeO, and 72 per cent $CaCO_3$. The cylinders for test specimens were cut with axes normal to the bedding of the limestone.

(WM) *Rutland White marble.*—The name, "Rutland White", is the trade name of the Vermont Marble Co. for a high-grade statuary marble, quarried at West Rutland, Vermont. The impurities in the medium-grained marble are 0.1 per cent Al_2O_3 plus Fe_2O_3, and 0.3 per cent MgO. The Rutland marble is also taken from the Beldens formation. Axes of cylinders for testing were drilled in three directions.

(S) *Solenhofen limestone.*—The Solenhofen limestone has been considered one of the finest lithographic stones available. The original source of the limestone was Solenhofen, Bavaria. It is a buff-colored, extremely fine-grained (0.005 mm) limestone of fairly high purity. In addition to $CaCO_3$, the limestone contains 0.2 per cent Al_2O_3, 0.3 per cent FeO, 0.6 per cent MgO, 0.1 per cent K_2O and Na_2O, and 0.2 per cent H_2O at 100° C and 0.7 per cent H_2O at more than 100° C. The age is Jurassic. The test cylinders were cut in three orthogonal directions, but the orientation with respect to the original bedding is unknown.

(WHB) *William Henry Bay marble.*—The Wm. Henry Bay marble specimen was obtained from an outcrop in a small inlet of the same name, off the Lynn Canal and about 20 miles south of Haines, Alaska. The marble is a white, medium-grained (0.5–1.5 mm) rock. Chemical analyses of a marble which is presumed to be the same formation indicated that the Wm. Henry Bay marble is quite pure calcium carbonate. The age can only be tentatively set as early Paleozoic. The attitude of any foliation is not known.

(YM) *Yule marble.*—The Yule marble used was obtained from a quarry in Gunnison County, Colorado. The rock is a medium-grained, white marble of nearly pure calcium carbonate. The clear ellipsoidal grains form a granoblastic fabric. The age is Mississippian. Test cylinder axes were shaped in three perpendicular directions at odd angles with the foliation.

Igneous Rocks

(BG) *Barre granite.*—The Barre granite was obtained from the Rock of Ages quarry near Barre, in north central Vermont. The rock is medium- to coarse-grained (feldspar phenocrysts up to 5 mm in diameter) and medium gray in color. It contains orthoclase and microcline (about 45 per cent), light smoky quartz (about 25 per cent), oligoclase, plagioclase (about 20 per cent), biotite and some

muscovite (about 10%.) with small amounts of pyrite, magnetite, sphene, epidote, zircon, and rutile. The chemical composition is about 70 per cent SiO_2, 15 per cent Al_2O_3, 2.5 per cent FeO and Fe_2O_3, 1 per cent MgO, 2 per cent CaO, 5 per cent Na_2O, and 4 per cent K_2O. Test cylinders were cut with axes normal to the foliation of the granite.

(C) *Chelmsford granite.*—The blocks of Chelmsford granite were obtained from the quarry at West Chelmsford, Massachusetts. The rock is fine- to medium-grained and light gray. It is composed of microcline, quartz, and oligoclase, plagioclase, minor muscovite, and a little biotite, with accessories of magnetite, apatite, zircon, fluorite, and calcite. Test cylinders were shaped with axes normal to the foliation of the granite.

(D) *Holyoke diabase.*—The Holyoke diabase blocks were obtained from a quarry near Westfield, Massachusetts. The diabase is a dark-gray, very dense, fine-grained rock with broad conchoidal fracture; it is composed essentially of a network of elongate plagioclase feldspar and shapeless augite masses. The diabase sheet presumably was deposited in Jurassic-Triassic time. The test cylinders were all cut with axes normal to the layering of the diabase, and parallel to the hexagonal jointing.

(V) *Vinal Haven diabase.*—The diabase obtained from Vinal Haven, Maine, is a fine- to medium-grained, very dense, dark-grayish-green rock. It is composed of essential labrodorite plagioclase and minor diopside and olivine with accessory magnetite and biotite. An approximate chemical analysis of the diabase is 48 per cent SiO_2, 18 per cent Al_2O_3, 1 per cent Fe_2O_3, 7 per cent FeO, 9 per cent MgO, 12 per cent CaO, 3 per cent Na_2O, and 0.3 per cent K_2O. The orientation of the test cylinders with respect to the geologic occurrence is not known.

Sedimentary and Metamorphic Rocks

(CS) *Cambridge slate.*—The large specimens of Cambridge slate were obtained from an abandoned quarry beside the Mystic River in Somerville, Massachusetts. The rock is called an argillite, and is a massive rock with fairly widely spaced jointing. It is late Pennsylvanian. The axes of most of the specimen cylinders were perpendicular to the bedding.

(CQ) *Cheshire quartzite.*—Several large stream bounders of the Cheshire quartzite were obtained just east of Rutland, Vermont. The quartzite is a massive, light-brown rock, somewhat pocked by weathering. It is composed of medium-grained equidimensional, interlocking quartz grains. It is a basal lower Cambrian formation. The relative attitude of cylinders and bedding is unknown.

(GS) *Green sandstone.*—The test pieces of "green sandstone" were obtained from diamond-drill cores taken in the hills to the southeast of the Catskill Mountains. The rock is an olive-gray sandstone with an argillaceous cement; it is not limy; it is a slightly indurated, medium-grained massive rock. It is from the middle Ordovician Hudson River sandstone formation. Most of the cylinders were made with axes normal to the bedding.

(RS) *Red sandstone.*—The "red sandstone" also is from the middle Ordovician Hudson River formation. It is a fine-grained, red, argillaceous sandstone; it is not limy. Test cylinders were cut from diamond-drill cores, and their axes were normal to the bedding.

(RM) *"Red marble".*—"Red marble" is the trade name for a variegated, red and white shaly limestone, imported from Italy. The contorted patterns in the fine-grained rock are distinctive. The axes of the test cylinders were all in the same direction, but their orientation to the original bedding is not known.

(SP) *Soapstone.*—The trade name of the soapstone is "Albarene stone", which is obtained from a quarry in Virginia. It is a dark-green talc schist of fine grain size. It contains about 50 per cent talc, 20 per cent chlorite, 15 per cent calcite and dolomite, 10 per cent serpentine, and 5 per cent magnetite and pyrite. Cylinder axes were perpendicular to a fairly distinct foliation.

(VA) *Verde antique.*—The name, verde antique, is applied to a decoration stone, which is mostly dark-green serpentine with white calcite streaks. The blocks were originally obtained from a quarry at Roxbury, Vermont. The quarry is in a dike of ultramafic rock originally composed of olivine and pyroxene, but altered to serpentine with some talc, calcite, brucite, hematite, amphibole, and magnetite. An approximate chemical composition of the verde antique (free of calcite) is 30 per cent SiO_2 8 per cent Fe_2O_3, 2 per cent Al_2O_3, 40 per cent MgO, 20 per cent H_2O. The axes of all test cylinders of the rock were in the same orientation, but the relationship to the attitude of the body in the quarry is unknown.

Miscellaneous Minerals

(CO) *Copper ore.*—The sulfide copper ore originally was obtained from Butte, Montana. The ore is a coarse-grained (2–5 mm) aggregate consisting predominantly of pyrite with some bornite, chalcocite, and quartz. The block of ore is massive and has no apparent foliation or lineation although there are a few vugs.

(FT) *Fluorite.*—The brown fluorite was obtained

from Clay Center, Ohio. It occurs as a massive aggregate of large (about 1-inch diameter) crystals of fluorite with some euhedral celestite crystals (½ inch long) intergrown. One hollow cylinder was made from a single crystal of purple-tinted fluorite from Cumberland, England; the axis of the cylinder was cut parallel to an a-axis.

(F) *Microline.*—A large single crystal of microcline which was originally obtained from Delaware County, Pennsylvania, was used to make up the test pieces. The crystal is closely intergrown with perthite lamellae. The test cylinders were all cut with axes parallel to the c-axis.

(P) *Pyrite.*—The pyrite specimen used for making up test pieces was obtained from Bingham, Utah. The specimen was an intergrowth of four large (about 2 inches on a side) cubic crystals of pyrite. Test cylinder axes were at odd angles to the crystals, and each cylinder included at least parts of two of the crystals.

(Q) *Quartz.*—A large single crystal of quartz which came from Brazil, was used for test specimens. The crystal has a few phantom growth planes and is considerably twinned (Dauphine). Test cylinders were cut with axes parallel both to c-axis and to an a-axis.

APPENDIX 2: DENSITY MEASUREMENTS

Rock type	Specimen type	Specimen no.	Density	Method of volume determination	Amount of perm. strain (per cent)
Solenhofen limestone	Solid cyl. (Before testing)	S-a	2.605	Micrometer measurement	
		S-b	2.600		
		S-c	2.604		
		S-d	2.597		
		Average	2.601		
Solenhofen limestone	Solid cyl. (After testing)	S-63	2.574	Micrometer measurement	2.2
		S-52	2.580		3.6
		S-68	2.577		3.0
		S-66	2.606		0.42
		S-67	2.606		0.55
Solenhofen limestone	Solid cyl. (After testing)	S-66	2.612	Water displacement	0.42
		S-67	2.610		0.55
		S-68	2.592		3.0
		S-87	2.550		8.7
		S-88	2.489		17.2
		S-90	2.506		15.1
Solenhofen limestone	Disk (After testing)	S-119	2.624	Water displacement	
		S-120	2.567		
		S-121	2.617		
Danby marble	Solid cyl. (Before testing)	DB-14B	2.702	Water displacement	
		DB-12A	2.707		
		Average	2.705		
Danby marble	Solid cyl. (After testing)	DB-11B	2.650	Water displacement	12.0
		DB-12B	2.678		8.0
Rutland White marble	Solid cyl. (Before testing)	WM-33B	2.698	Water displacement	
		WM-41A	2.691		
		Average	2.695		
Rutland White marble	Solid cyl. (After testing)	WM-23A	2.706	Water displacement	2.1
		WM-33A	2.685		7.1
		WM-41B	2.711		0.9
Wm. Henry Bay marble	Solid cyl. (Before testing)	WHB-2	2.48	Water displacement	
		WHB-3	2.61		
		Average	2.55		
Wm. Henry Bay marble	Solid cyl. (After testing)	WHB-1	2.67	Water displacement	7.2

Note: The degree of accuracy of the measurements of density is about ±.005, although given to the third place.

References Cited

Adams, F. D., and Nicolson, J. T., 1901, An experimental investigation into the flow of marble: Royal Soc. London Phil. Trans., ser. A, v. 195, p. 363–401.

—— 1910, An experimental investigation into the action of differential pressure on certain minerals and rocks, employing the process suggested by Professor Kick: Jour. Geology, v. 18, p. 489–525.

—— 1912, An experimental contribution to the question of the depth of the zone of flow in the earth's crust: Jour. Geology, v. 20, p. 97–118.

Adams, F. D., and Bancroft, J. A., 1917, Internal friction during deformation and relative plasticity of rocks: Jour. Geology, v. 25, p. 597–637.

Balsley, J. R., 1941, Deformation of marble under tension at high pressure: Am. Geophys. Union Trans., v. 22, p. 519–525.

Beliaev, N. M., and Sinitskii, A. K., 1938, Stresses and strains in thick-walled cylinders in the elastic-plastic state: Izvestia Ak. Nauk, SSSR, No. 2, p. 3–54. (Free translation by Grad. Div. App. Math., Brown Univ., 1947, for Taylor Model Basin, Contract No. bs-34166, U.S. Navy.)

Birch, F., Schairer, J. F., and Spicer, H. C. (editors), 1942, Handbook of physical constants: Geol. Soc. America Spec. Paper No. 36, 325 p.

Boeker, R., 1915, Die Mechanik der bleidbenden Formänderung in kristallinisch auf gebauten Körpern: Forschungsarbeiten V. D. I., No. 175, p. 1–51.

Bridgman, P. W., 1918, Failure of cavities in crystals and rocks under pressure: Am. Jour. Sci., 4th ser., v. 45, p. 243–268.

—— 1931, The physics of high pressures: N. Y., Macmillan Co., 398 p.

—— 1935, Effects of high shearing stress combined with high hydrostatic pressure: Phys. Rev., v. 48, p. 825–847.

—— 1936, Shearing phenomena at high pressure of possible importance for geology: Jour. Geology, v. 44, p. 653–669.

—— 1937, Shearing phenomena at high pressures, particularly in inorganic compounds: Am. Acad. Arts Sci. Proc., v. 71, p. 387–460.

—— 1939, The high pressure behavior of miscellaneous minerals: Am. Jour. Sci., v. 237, p. 7–18.

—— 1941, Explorations toward the limit of utilizable pressure: Jour. Applied Physics, v. 12, p. 461–469.

—— 1947a, Effect of hydrostatic pressure on fracture of brittle substances: Jour. Applied Physics, v. 18, p. 246–258.

—— 1947b, Fracture and hydrostatic pressure: Am. Soc. Metals Trans., v. 39, p. 246–261.

Delaney, J. P., 1940, Variation of elastic constants with moisture in soapstone: Am. Geophys. Union Trans., v. 21, p. 696–698.

Frankel, J. P., 1948, Relative strengths of portland cement mortar in bending under various loading conditions: Am. Concrete Inst. Jour., v. 20, p. 21–32.

Freudenthal, A. M., 1950, The inelastic behavior of engineering materials and structures: N. Y., John Wiley & Sons, Inc., 587 p.

Goguel, J., 1943, Introduction à l'Etude Mecanique des deformations de l'Ecorce Terrestre: Ministère Prod. Indus. et Comm. Memoir, 514 p.

Goranson, R. W., 1940, "Flow" in stressed solids: an interpretation: Geol. Soc. America Bull., v. 51, p. 1023–1034.

Griffith, A. A., 1920, The phenomena of rupture and flow in solids: Royal Soc. London Phil. Trans., ser. A, v. 221, p. 163–198.

—— 1925, The theory of rupture: 1st Internat. Cong. Applied Mechanics Proc., Delft, (1924), p. 55–63.

Griggs, D. T., 1936, Deformation of rocks under high confining pressures: Jour. Geology, v. 44, p. 541–577.

—— 1939, Creep of rocks: Jour. Geology, v. 47, p. 225–251.

—— 1940, Experimental flow of rocks under conditions favoring recrystallization: Geol. Soc. America Bull., v. 51, p. 1001–1034.

Griggs, D. T., and Miller, W. B., 1951, Deformation of Yule marble: Part I, Compression and extension experiments on dry Yule marble at 10,000 atmospheres confining pressure, room temperature: Geol Soc. America Bull., v. 62, p. 853–862.

Griggs, D. T., Turner, F. J., and Durrell, C., 1954, Deformation of Rocks at 500° C, 5000 atmospheres pressure: Geol. Soc. America Bull., v. 65, p. 1258.

Griggs, D. T., Turner, F. J., Borg, I., and Sosoka, J., 1951, Deformation of Yule marble: Part IV —Effects at 150° C: Geol. Soc. America Bull., v. 62, p. 1385–1406.

—— 1953, Deformation of Yule marble; Part IV—Effects at 300° C: Geol. Soc. America Bull., v. 64, p. 1327–1342.

Handin, J., 1953, An application of high pressure in geophysics: Experimental rock deformation: Am. Soc. Mech. Engineers Trans., v. 75, p. 315–324.

Handin, J., and Higgs, D. V., 1954, Experimental deformation of dolomite single crystals: Geol. Soc. America Bull., v. 65., p. 1263.

Jamieson, J. C., 1953, Phase equilibrium in the system calcite-aragonite: Jour. Chemical Physics, v. 21, p. 1385–1390.

Jeffreys, H., 1924, The Earth: London, Cambridge Univ. Press, 278 p.

Joffe, A. F., 1928, The physics of crystals: N. Y., McGraw-Hill Book Co., 198 p.

Jones, V., 1945, Tensile and triaxial compression tests of rock cores from the passageway to Penstock Tunnel N-4 at Boulder Dam: U.S. Bur. Reclam., Lab. Rept., No. Sp. 6, 14 p.

Karman, Th. von, 1911, Festigkeit versuche unter allseitigem Druck: Zeit. des Ver. deut. Ing., v. 55, p. 1749–1757.

King, L. V., 1912, On the limiting strength of rocks under conditions of stress existing in the earth's interior: Jour. Geology, v. 20, p. 121–126.

Love, A. E. H., 1944, A treatise on the mathematical theory of elasticity, 4th Ed.: N. Y., Dover Publ., 643 p.

Nadai, A. L., 1933, Theories of strength: Am. Soc. Mechanical Engineers Trans., v. 55, p. 123.

—— 1950, Theory of flow and fracture of solids: N. Y., McGraw Book Co., 572 p.

Orowan, E., 1940, Problems of plastic gliding: London Phys. Soc., v. 52, p. 8–22.

—— 1949, Fracture and strength of solids: London Phys. Soc., Reports on Progress in Physics, v. 12, p. 185–232.

Polanyi, M., 1921, Über die Natur des Zerreissvorganges: Zeit. Physik, v. 7, p. 323–327.
Preston, F. W., 1954, The shoe on the other foot: Am. Ceramic Soc. Bull., v. 33, p. 355–358.
Richart, F. E., Brandtzaeg, A., and Brown, R. L., 1928, A study of failure of concrete under combined compressive stresses: Univ. of Ill. Eng. Exp. Sta. Bull., No. 185, 102 p.
Weibull, W., 1939, A statistical theory of the strength of materials: Ing. Svetenskaps Acad., Hand. No. 151, 153 p.
Zwicky, F., 1923, Die Reissfestigkeit von Steinsalz: Phys. Zeit., v. 24, p. 131–137.

Dunbar Laboratory, Harvard Univ., Cambridge 38, Mass.
Manuscript Received by the Secretary of the Society March 16, 1954.
Paper No. 136 Published under the Auspices of the Committee on Experimental Geology and Geophysics and the Division of Geological Sciences at Harvard University

Short Notes

BULLETIN OF THE GEOLOGICAL SOCIETY OF AMERICA
VOL. 66, PP. 1315-1316 OCTOBER 1956

PONY-CHERRY CREEK AGE RELATIONS IN SOUTHWESTERN MONTANA

BY ROLLAND R. REID

Attention is called to a misinterpretation of earlier work by Scholten *et al.* (1955, p. 350). This misinterpretation, if allowed to stand, would serve to further an idea based on shaky evidence—that Cherry Creek gneiss is younger than Pony gneiss.

They state:

"Farther east, Tansley *et al.* (1933, p. 10) found boulders of Pony gneiss in a schist at the base of the Cherry Creek. This relationship would suggest two periods of pre-Beltian metamorphism, one before and one after the Cherry Creek group."

This implies that the base of the Cherry Creek is known and that the "boulders of Pony gneiss in a schist" were observed in place. Tansley *et al.* (1933, p. 10) reads as follows:

"No unconformity has been found between the Pony and Cherry Creek groups. However, several lines of evidence point to the existence of such a stratigraphic break. In several places boulders were seen which contain unoriented inclusions of gneiss lying in a gneissic or schistose matrix. The best example of this feature is a large boulder, about 15 feet in diameter, in the South Boulder Creek valley, about 3 miles above the Mammoth mine. . . . An angular fragment of gneiss, about 2 feet across, is surrounded by a matrix of schist. . . . Its banding lies at a sharp angle to that of the enclosing quartz-biotite schist."

Tansley *et al.* considered the foliated matrix in the boulders to be Cherry Creek and the enclosed gneiss fragments to be Pony. It seems clear from the above-quoted paragraph that the boulders are not in place. In view of the fact that South Boulder Creek valley is a glacial valley, the boulder 3 miles above the Mammoth mine may have been transported for a considerable distance. This is significant when one considers the lithologic similarity of the Pony and Cherry Creek rocks; the boulder may have been transported to its present site from an area of Pony gneiss. Perhaps it should be emphasized that float boulders were used as evidence for an unconformity.

The weakness of this sort of evidence is emphasized in recent work in the Pony area by the present writer for the Montana Bureau of Mines and Geology. He has observed the same structure as that described by Tansley *et al.* *in place* in the rocks mapped by them as Pony gneiss (unoriented inclusions of gneiss lying in a gneissic or schistose matrix). The locality is near the Mammoth mine.

This kind of evidence could be used to show (in the manner of Tansley *et al.*) that the Pony gneiss is younger than the Cherry Creek gneiss; in the present writer's opinion, it reopens the question of age relations between the Pony and the Cherry Creek.

REFERENCES CITED

Scholten, Robert, Keenmon, K. A., Kupsch, W. O., 1955, Geology of the Lima region, southwestern Montana and adjacent Idaho: Geol. Soc. America Bull., v. 66, p. 345–404.

Tansley, Wilfred, Schafer, P. A., and Hart, L. H., 1933, A geological reconnaissance of the Tobacco Root Mountains, Madison County, Montana: Mont. Bur. Mines Geology Mem. 9, 57 p.

GEOLOGY DEPARTMENT, MONTANA SCHOOL OF MINES, BUTTE, MONTANA

MANUSCRIPT RECEIVED BY THE SOCIETY, MAY 23, 1955

BULLETIN OF THE GEOLOGICAL SOCIETY OF AMERICA
VOL. 66, PP. 1317-1318 OCTOBER 1955

PONY–CHERRY CREEK AGE RELATIONS IN SOUTHWESTERN MONTANA—A REPLY

BY ROBERT SCHOLTEN

Reid's correction of the record is highly appreciated. His comments touch upon two separate but related questions: the age relation between the Pony and Cherry Creek groups, and the position of the major unconformity in the pre-Beltian sequence found by him and Tansley *et al.*

That such a break exists seems clear from the occurrence of unoriented gneissic inclusions ("angular fragments" rather than boulders, to acknowledge an earlier error) in a schistose or gneissic matrix. Whether or not these occurrences are found *in situ* does not affect the validity of the statement quoted by Reid to the effect that two periods of pre-Beltian metamorphism are suggested.

The conclusion by Tansley *et al.* that this unconformity separates the Cherry Creek from the Pony and indicates a greater age for the Pony hinges on the question of whether the matrix was correctly identified as Cherry Creek and the inclusions as Pony. There is no doubt that many isolated occurrences of schist or gneiss are difficult to identify with confidence as Pony or Cherry Creek, and this applies with even greater force to transported boulders. Reid's find of unoriented gneissic inclusions in place is interesting, but until further mapping has established the complete definition and detailed areal distribution of the two units in this vicinity the evidence cannot be construed as disproving the age relation postulated by earlier workers.

In the absence of evidence in the Lima region, described in the paper to which Reid makes reference, conclusions regarding the age relation between the Pony and Cherry Creek groups had to be based on work done by others, including E. Wm. Heinrich, elsewhere in southwestern Montana. According to Heinrich (Pre-Beltian geology of Montana, manuscript, 1953) the present status of knowledge based on regional studies is as follows: (1) there are two main mappable units of metamorphic rocks in the pre-Beltian complex of southwestern Montana; (2) one of these units is the Cherry Creek group, which can be correlated widely on lithological grounds by virtue of its distinctive quartzites and marbles intercalated with gneisses and schists; (3) the other unit consists dominantly of gneisses of various types, and this unit includes the Pony as well as groups of similar metamorphic rocks in other isolated pre-Beltian outcrop areas; these groups are not only difficult to correlate from one area to another but do not necessarily represent time equivalents; (4) in several areas structural evidence indicates that these dominantly gneissic units (Pony equivalents (?) and others) are older than Cherry Creek rocks.

DEPARTMENT OF GEOLOGY, THE PENNSYLVANIA STATE UNIVERSITY, UNIVERSITY PARK, PA.
MANUSCRIPT RECEIVED BY THE SECRETARY OF THE SOCIETY, JUNE 29, 1955

BULLETIN OF THE GEOLOGICAL SOCIETY OF AMERICA
VOL. 66, PP. 1319-1324, 1 FIG., 2 PLS. OCTOBER 1955

PERMIAN GLACIATION IN NORTHERN MEXICO?

BY WILLIAM E. HUMPHREY

"*Las Uvas district.*—The Las Uvas section is dominantly brown weathered shale, with secondary fissility, which is marked wherever laminae, or intercalated thin quartzitic sandstones, are present. Interbedded with laminated shales or thin sandstone beds are thick non-laminated shales containing unsorted pebbles, cobbles and boulders of various rocks (Pl. 9, fig. 1). Black, dense limestone fragments might be thought to represent lenticular lime facies in the shale, but it would be impossible thus to account for associated large boulders of red granite, pegmatite, porphyry, and gneiss. Thin sections of pebbles show cataclastic pulverization, and a composition differing radically from the granodiorite intrusive to the south. Moreover, the igneous types represented cannot be derived from that intrusive body, for, as already shown, the beds associated with these conglomerates are older than the granodiorite. The types of igneous material are unlike anything observed in place in the Acatita-Las Delicias area, and were probably derived from the borderland of the geosyncline in which the Las Uvas sediments were deposited. Somewhat similar beds are found in La Difunta district near Puerto de las Sardinas, and to explain these, King[5] suggests local uplift during the Permian. This would not account, however, for the lack of stratification in the shaly matrix, the apparent lack of sorting, and the presence of granitic and gneissic material in Las Uvas district. The conglomerates are associated with a notable thickness of slate whose secondary cleavage shows indistinct laminae, but the banding is not like that of varved clays. The origin of these beds is still problematical; the readiest answer, that they may be tillites, would emphasize too greatly the lack of stratification, and imply supporting criteria that were not observed. Yet the occurrence of the unsorted conglomerates in beds of probable Permian age in an area which lies in latitude 26½ degrees north[6] gives them particular significance, in view of the widespread interest in former glacial periods."

On purely structural considerations Kelly considered that the conglomeratic beds at Las Uvas were older than the beds to the south (*i.e.*, Cañón Grande and La Difunta). According to Teodoro Díaz (Personal communication) and Kellum *et al.* (1936, p. 975), the Paleozoic sediments along the east side of the Acatita Valley are more metamorphosed than are the Permian strata on the Difunta flank in the Las Delicias area. Whatever their age may be, they are probably not older than Pennsylvanian since Kelly (1936, p. 1018) reported fusulinids common in the limestone pebbles of the conglomerates. Unfortunately these forms apparently have not been determined.

King (1944, p. 21) disagreed with Kelly's suggestions and discussed the significance of the material below the *Perrinites* zone as follows:

(p. 9) "... The conglomerates in this part of the section may either result from the breaking up of Pennsylvanian or basal Permian (Wolfcamp) limestone beds as a consequence of uplift immediately following their deposition, and redeposition of their fragments in the adjacent sea, or they may be basal deposits of a succeeding epoch of deposition."

(p. 21) "Kelly (1936, p. 1017–1019) noted the large boulder size, the unstratified matrix, and the lack of sorting in the conglomerates below the *Perrinites* zone near the Puerto de las Sardinas and near Las Uvas and Acatita farther north-northwest. He suggests the possibility that they may be tillites. The writer has no additional information to contribute regarding the deposits themselves but doubts their glacial origin. As indicated above, present evidence suggests that these beds are of Wolfcamp or early Leonard (early Permian) age. If so, they are contemporaneous with highly fossiliferous deposits of limestone and shale 260 to 300 miles farther north, in Texas and New Mexico. The faunas of the lower Permian of Texas are closely allied with those of the same age in the Eastern Hemisphere, and our present knowledge suggests that the connection between the Texas and Eurasian seas in Permian time was by way of the Coahuila Permian geosyncline. It is difficult to conceive of migration of these organisms through a basin of cold water, or to believe that glaciation could have occurred 300 miles south of an area where limestone was being deposited. The writer, therefore, seeks a tectonic cause for the boulder beds."

(p. 27) "Late Pennsylvanian (?) limestones, possibly in part of reef origin, were deposited simultaneously with products of volcanic activity. Coarse detritus from these and older rocks was deposited in the western part of the area either contemporaneously with the reefs or as a clastic wedge on the flank of a pre-Leonard uplift. The coarseness and unsorted character of the boulder conglomerates deposited at this time indicate that the boulders must have been transported by unusual processes."

Whatever the age and correlation of the coarsely clastic sections below the *Perrinites* zone on the Difunta flank near Puerto de las Sardinas and of those of the Acatita Valley at Cañón Grande and Las Uvas and however their peculiar lithologic characters may be interpreted, a repetition of similar lithologies well up in the documented Permian sequence in the Arroyo de la Difunta and in the Arroyo Colorada on the Difunta flank of the Las

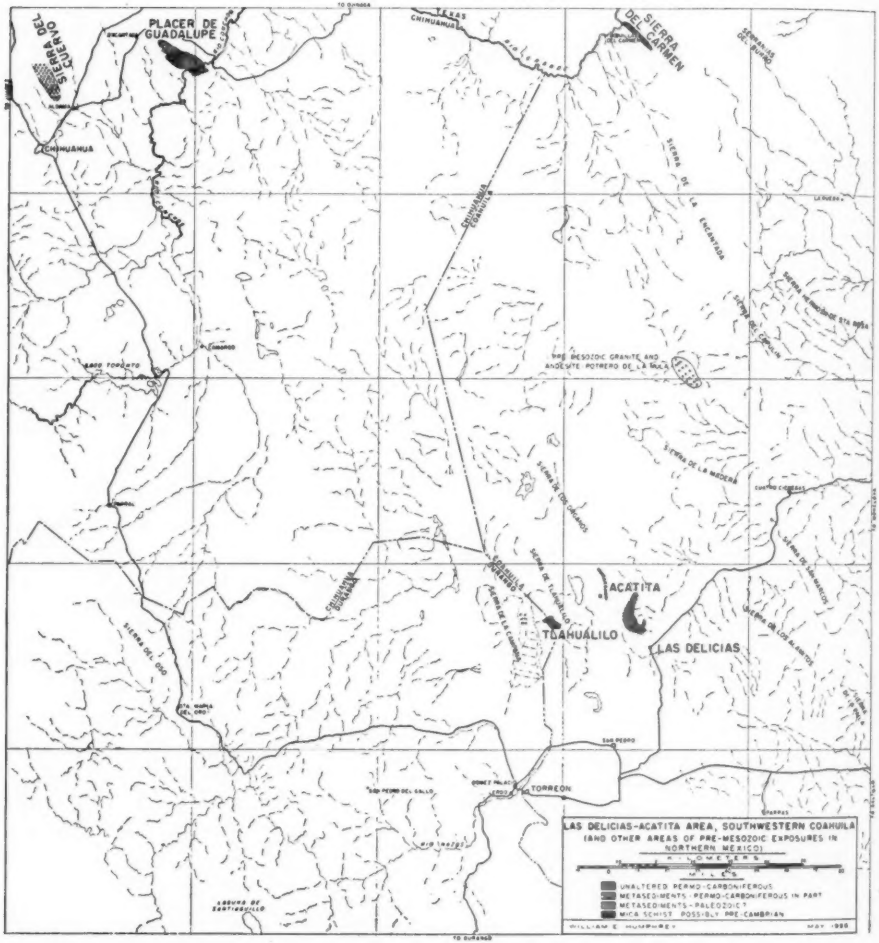

FIGURE 1.—INDEX MAP OF LAS DELICIAS-ACATITA AREA, SOUTHWESTERN COAHUILA

Delicias area was noted by the writer and is here illustrated (Pls. 1, 2).

On King's map (1944, Pl. 3), above and below the contacts of the *Timorites* shale zone, King shows "Brown igneous rock" and "Lava and Graywacke", respectively. In his section (1944, p. 13–15, p. 19), the *Timorites* zone is described as bounded above by "Gray-brown porphyritic lava" and below by "black shale with streaks of buff limestone and graywacke . . . ", followed by "Dark gray-brown lava flows and graywacke alternating with about 30% dark-gray shale. . . ." In the reconnaissance of Arroyo la Colorada and Arroyo de la Difunta, these intervals were observed to consist largely of alternating thin beds of shales and siltstone with interbedded intervals of varvelike, highly banded and laminated clay shales and siltstones and considerable intercalations of massive conglomeratic shales (boulder clays). Varvelike clay shales and silty breaks are found stratigraphically above the zone of *Waagenoceras* and below the zone of *Timorites* in the Arroyo de la Difunta (Pl. 2, fig. 1). A belt of boulder clay 4–6 m thick, also in the Arroyo de la Difunta, is stratigraphically

below the zone of *Timorites* and possibly in the upper part of the zone of *Waagenoceras* (Pl. 1, fig. 2). Figure 2 of Plate 2 shows the relative size of a large acid intrusive igneous boulder in another belt of boulder clay some distance stratigraphically *above* the zone of *Timorites* in the Arroyo la Colorada.

The observations and photographs on which the present note is based were made by the writer during a brief reconnaissance into the Paleozoic area near Las Delicias in southwestern Coahuila, México. The purpose of this visit, made in company of Ingeniero Teodoro Díaz of Petróleos Mexicanos toward the end of 1954, was to determine whether or not an excursion to that area could be conveniently carried out as part of the program of the Twentieth International Geological Congress, to be held in México, D. F., México, from September 4 to 11, 1956. Although because of difficult access the proposed excursion to Las Delicias will not form part of the 1956 Congress activities, observations made during the visit are believed to be of interest as they bear on this classical northern Mexico locality.

Permission of Petróleos Mexicanos and of DeGolyer and MacNaughton to publish this paper is gratefully acknowledged.

The Las Delicias area is of interest because, besides being *prima facie* evidence for an early Mesozoic positive element in north Mexican paleogeography (Böse, 1921; 1923; Kellum, Imlay, and Kane, 1936), it exhibits one of the thickest and best-documented marine Permian sections known from North America (King *et al.*, 1944). The Permian area of Las Delicias was first reported by Erich Haarmann (1913) and subsequently was studied by Emil Böse (1921), Robert E. King (1934), William A. Kelly (1936), and again by King and his collaborators (1944). The Permian rocks are best exposed on both flanks of a large, northeast-trending syncline in an area about 20 km northwest of the Hacienda de las Delicias. The western limb of the synclinal structure, named Difunta flank by King after good development along the Arroyo de la Difunta and from the locality of the same name, exhibits the thickest and most fossiliferous section (Pl. 1, fig. 1). According to King, the sequence there has an incomplete thickness of more than 10,844 feet (3305.2 m). It may be summarized, from top to bottom, as follows:

Difunta flank; Las Delicias, Coahuila (after R. E. King, 1944).

Unit	*Thickness (Feet)*	*(Meters)*
1. Brown igneous rock and graywacke.....	1080	(329.1)
2. *Kingoceras* zone. Concretionary shale.....	220	(67)
3. Brown igneous rock. Sill?.....	675	(205.7)
4. *Timorites* zone. Black concretionary shale...	558	(173)
5. *Parafusilina rothi* zone. Black shale with limestone, lava, and graywacke interbedded....	410+	(124.9+)
6. *Waagenoceras* zone. Limestone, shale, graywacke, and lava followed below by alternating shale and lava with thin beds of limestone.....	2385+	(726.9+)
7. Lava?, diabase sill, and some thin beds of shale.....	3075	(937.2)
8. *Perriniles* zone. Concretionary shale.....	710	(216.4)
9. Clastic sediments with coarse conglomeratic layers.....	1183	(360.5)
Total thickness.....	10844+	(3305.2)+

The conglomerates of the thick clastic section of Unit No. 9 below the *Perriniles* zone were described by King (1944, p. 15) as being interbedded with graywackes and shales; as lenses within an interbedded shale and graywacke unit; and as "well cemented conglomerate containing many igneous pebbles and cobbles of blue limestone." No conglomerates other than those from Unit No. 9 were described by King in his detailed measured section for the Difunta flank (1944, p. 13–15).

About 6.5 km north and west of the westernmost limit of King's Difunta section (A-A′ of his map, 1944, Pl. 3), Kelly (1936, p. 1018) described the following incomplete section from the north wall of Cañón Grande, an eastward-heading drainage on the east side of the Acatita Valley and about 5 km southeast of Acatita Ranch. This section (also reproduced

by King *et al.*, 1944, p. 17) is, from top to bottom, as follows:

Cañón Grande, Acatita, Coahuila (after W. A. Kelly, 1936)

Unit	Thickness (Feet)	(Meters)
1. Alternating beds of sandstone and dense gray-green shale	22	(6.7)
2. Concealed	40	(12.1)
3. Limestone	2	(0.6)
4. Partly laminated, dense hard gray siliceous shale, breaking into rhombic and irregular fragments	42	(12.8)
5. Concealed, probably shale	225	(68.5)
6. Concealed in part; possibly conglomerate like that below	40	(12.1)
7. Conglomerate, consisting of black limestone and chert fragments of irregular sizes interbedded in shale matrix. Large crinoidal columnals and specimens of Fusulinidae are common in the limestone pebbles	35	(10.6)
8. Concealed, probably shale	250	(76.2)
9. Conglomerate, black limestone fragments in shale matrix, like that of overlying beds	20	(6.0)
Total	676	(206.0)

The conglomerates of this sequence were tentatively correlated by both King (1944, p. 18) and by Kelly (1936, p. 1019), on the basis of lithologic similarities, with Unit No. 9 of King's Difunta flank section. They were further tentatively correlated by both workers with still more coarsely clastic sections near Las Uvas, about 20 km northwest of Cañón Grande and also on the east side of the Acatita Valley. The lithologies of the Las Uvas sequence were described by Kelly (1936, p. 1017) as follows:

The lithology of the belts of boulder clays on the Difunta flank above the *Waagenoceras* zone is very similar to that described by Kelly for the Las Uvas section in the Acatita Valley. Well-rounded pebbles, cobbles, and boulders of various dimensions (up to 100 cm + greatest diameter) of intrusive and extrusive igneous rocks and dark-gray to black limestones are scattered through a nonlaminated and massive matrix of dark clay shale. Sorting is practically nonexistent, and the coarse detritals appear to have been dumped into a sedimentary environment in which thin-bedded, laminated, and banded clay shales and siltstones were being deposited. No striated cobbles or boulders were observed during a hasty search. Within the clay matrix of the boulder conglomerate (Pl. 1, fig. 2) small nodules and concretions of dark-gray, brown-weathering limestone contain *Waagenoceras* sp. and other ammonoids.

Indistinct laminae were mentioned by Kelly (1936, p. 1017) as characterizing thick slates associated with the boulder clays in the Las Uvas section although he stated that the banding was not like that of varved clays. The clay shales and siltstones (Pl. 2, fig. 1) are definitely like varved clays. The color banding of light brown and dark brownish gray is not necessarily related to abrupt and obvious changes in lithology although such changes may be casually related to the banding. The banded silty clay shales illustrated are intercalated in an overall associated sequence consisting of thin alternations of siltstones and silty shales.

To the writer, the only satisfactory explanation for the unusual sedimentation of the boulder clays would be one in which the large rounded fragments of exotic materials must be assumed to have been rafted from their place of origin to the site of deposition in the north Mexican Permian sea. Such rafting could have been accomplished only by ice or by floating, river- and current-borne islands. Supporting evidence of banded clay shales and thin siltstones which conceivably may represent varve

PLATE 1.—EXPOSURES IN LAS DELICIAS AREA, COAHUILA

FIGURE 1.—DIFUNTA FLANK; EAST-DIPPING MARINE PERMIAN SECTION OVERLAIN WITH DISCORDANCE BY LOWER CRETACEOUS GYPSUM AND LIMESTONE

FIGURE 2.—EXPOSURE OF BOULDER CLAY BELOW THE ZONE OF *Timorites* AND POSSIBLY IN THE UPPER PART OF THE ZONE OF *Waagenoceras*

Note east-dipping contact with underlying concretionary shale at right. Arroyo de la Difunta.

FIGURE 1

FIGURE 2

EXPOSURES IN LAS DELICIAS AREA, COAHUILA

FIGURE 2

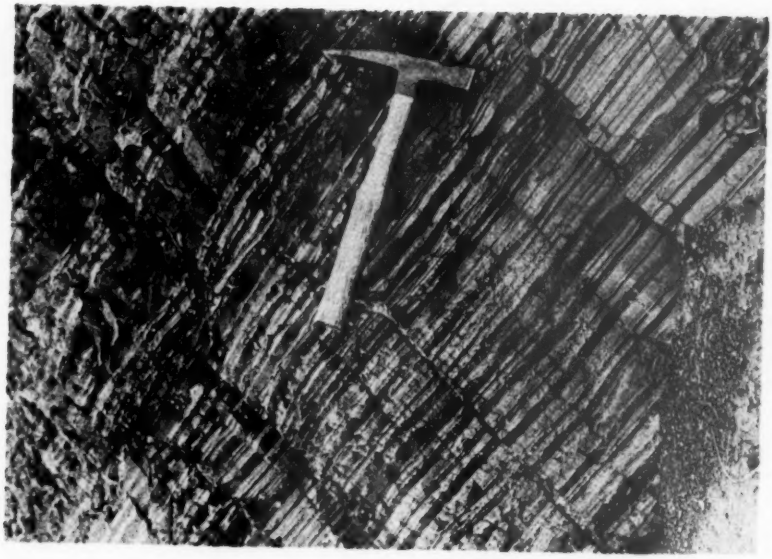

FIGURE 1

EXPOSURES IN LAS DELICIAS AREA, COAHUILA

deposits would tend to strengthen the hypothesis for ice-borne transport of the coarse materials. An appeal to turbidity currents for the transport of the coarse detritals does not seem justified from the observed character of the sedimentation nor from the stratigraphic succession. King (1944, p. 21) objected to Kelly's suggestion that the conglomeratic shales below the *Perrinites* zone might be tillites on the basis that "It is difficult to conceive of migration of these organisms (marine lower Permian faunas) through a basin of cold water, or to believe that glaciation could have occurred 300 miles south of an area where limestone was being deposited." Nevertheless, Pennsylvanian tillites have been described by Heim (1945) from the Province of San Juan, Argentina, as intercalations in marine shaly sediments characterized by abundant remains of widely known brachiopods, gastropods, bryozoans, and crinoids. According to Heim these Carboniferous Argentine tillites grade into conglomeratic shales, the erratic cobbles and boulders of which may be striated and polished. Furthermore, these and other marine glacial deposits seen by the writer in southern Buenos Aires Province in Argentina are remarkably like the conglomeratic shales of the Las Delicias area in Coahuila. Whether or not erratic-strewn glacial ice might enter a sea within 300 miles of an area where limestone was being deposited might be answered in Southwest Africa where limestone intercalations are not uncommon within the demonstrated glacial and glacio-marine deposits in the Dwyka Series of the lower part of the Karroo (Reed, 1949, p. 189). Moreover the conglomeratic shales of the Las Delicias-Acatita area, as well as similar lithologies associated with admitted glacial deposits of Upper Paleozoic age in southern South America, South Africa, Australia, and India need not represent true glacial till. If they were of glacio-marine origin, they might be thought of as subaqueous till or tillites representing localized dumping from disintegrating current-borne blocks of floating ice or as material from the melting aprons of valley or piedmont glaciers which may have debouched into the sea. Such conditions need not have presented any serious barriers to the migration of marine faunas nor should they necessarily have affected chemical or organic deposition of calcium carbonate in a relatively isolated area some distance away, where climatic and environmental conditions may have been considerably different.

References Cited

Böse, Emil, 1921, On the Permian of Coahuila, Northern Mexico: Am. Jour. Sci., 4th ser., v. 1, p. 187–194.

——, 1923, Vestiges of an ancient continent in Northern Mexico: Am. Jour. Sci., 5th ser., v. 6, 4 figs., p. 127–136, 196–214, 310–337.

Haarmann, Erich, 1913, Geologische Streifzüge in Coahuila: Zeitschrift d. deutsch. geol. Gesellschaft, Bd. 65, Monatsb. 1, p. 18–47.

Heim, Arnold, 1945, Observaciones tectónicas en Barreal, Precordillera de San Juan: Universidad Nacional de la Plata, Museo de la Plata, Revista (Nueva Serie), Sección Geológica, Tomo 2, no. 16, p. 267–285, 10 figs.

Kellum, L. B., Imlay, R. W., and Kane, W. G., 1936, Relation of structure, stratigraphy, and igneous activity to an early continental margin: Geol. Soc. America Bull., v. 47, p. 969–1008, 3 pl., 3 figs.

Kelly, William A., 1936, Geology of the mountains bordering the Valley of Acatita and Las Delicias: Geol. Soc. America Bull., v. 47, p. 1009–1038, 13 pl., 2 figs.

King, Robert E., 1934, The Permian of southwestern Coahuila: Am. Jour. Sci., 5th ser., v, 27, p. 98–112, 4 figs.

King, Robert E., *et al.*, 1944, Geology and paleontology of the Permian area northwest of Las Delicias, Coahuila, Mexico: Geol. Soc. America Special Paper 52, 172 p., 45 pls., 29 figs.

Reed, F. R. C., 1949, The geology of the British Empire: London, Edward Arnold & Co., 764 p., 26 figs.

De Golyer and MacNaughton, Inc., Mexico, D.F., Mexico

Manuscript Received by the Secretary of the Society, May 25, 1955

Plate 2.—EXPOSURES IN LAS DELICIAS AREA, COAHUILA

Figure 1.—Varvelike, Banded Clays and Siltstones, Below the Zone of *Timorites* and Stratigraphically Above the Zone of *Waagenoceras*, Arroyo de la Difunta

Figure 2.—Large Acid Igneous Boulder in Conglomeratic Clay Shale, Stratigraphically Above the Zone of *Timorites*, Arroyo la Colorada

BULLETIN OF THE GEOLOGICAL SOCIETY OF AMERICA
VOL. 66, PP. 1325-1328 OCTOBER 1955

USE OF INDICATORS IN THE DETERMINATION OF ICE-MOVEMENT DIRECTIONS IN ALBERTA

BY C. P. GRAVENOR AND L. A. BAYROCK

Introduction

An indicator is usually defined as an erratic which, by its unusual characteristics, can be traced to its original limited outcrop area. Although indicators may not have travelled in a straight line from their place of origin to their present resting place they nevertheless give a good clue to the general ice direction in a given area.

Little is known about ice directions in Alberta. Striae have not been found on the soft Cretaceous sediments which underlie central Alberta, and other glacial forms, such as flutings and drumlins, are quite rare. If reliable indicators could be found they would supply needed information on glacial directions in Alberta.

Rutherford (1928) described two occurrences of bituminous sandstone in the Edmonton district which undoubtedly were derived from the McMurray tar sands (Fig. 1). If the bituminous sandstone came from the eastern side of the McMurray tar sands outcrop, then the direction of ice movement would be S. 25°–35° W., and, if it came from the west side, S. 15°–20° W. Dr. C. R. Stelck, of the University of Alberta, has informed the writers that he has found heavy oil-impregnated dolomite erratics at Pouce Coupe, British Columbia, which probably came from Pine Point on the south side of Great Slave Lake where oil-impregnated Presqu'ile dolomite outcrops (Fig. 1). This dolomite indicator gives an ice-movement direction of S. 28° W. Glacial flutings in the Red Deer district of Alberta give ice directions of S. 25°–40° W (Fig. 1).

From the above evidence it would appear that the general ice direction in central and northern Alberta is about S. 30° W. If this general direction is correct, then it is reasoned that the Athabasca sandstone, which outcrops on the south side of Lake Athabasca, should have contributed to the drift of central Alberta. An examination of samples of this sandstone suggests that it has sufficient peculiar characteristics to make it a good indicator.

Description of Athabasca Sandstone Samples

Specimens of Athabasca sandstone in the Geology Department at the University of Alberta show that it is a white, fine- to medium-grained sandstone with reddish color bands. The color bands do not necessarily follow the bedding and in some instances resemble diffusion bands. The sandstone varies from friable to well cemented; the cement is silica. The individual grains are generally subrounded to rounded.

An examination of the heavy minerals of the Athabasca sandstone by J. B. Mawdsley (1954, manuscript) shows that tourmaline is the dominant heavy mineral and makes up 40–80 per cent of the suites. Minor heavies include zircon, garnet, rutile, and magnetite. In one sample all the tourmaline grains had conspicuous overgrowths. Although brown, green, pink, and blue tourmalines are present, all the overgrowths are colorless and developed in optical continuity with the original grains. The overgrowths show jagged ends (Pl. 1), which would indicate that they grew within the sandstone. Notwithstanding the fact that authigenic tourmaline is fairly common (Krynine, 1946), it offers an added method by which indicators of Athabasca sandstone could be identified.

Athabasca Sandstone Indicators

Athabasca sandstone indicators in central Alberta have been found at Warburg, Elk Island, Youngstown, Coronation, and Veteran (Fig. 1). All these indicator pebbles are composed of white sandstone and show reddish color banding. Heavy minerals were separated

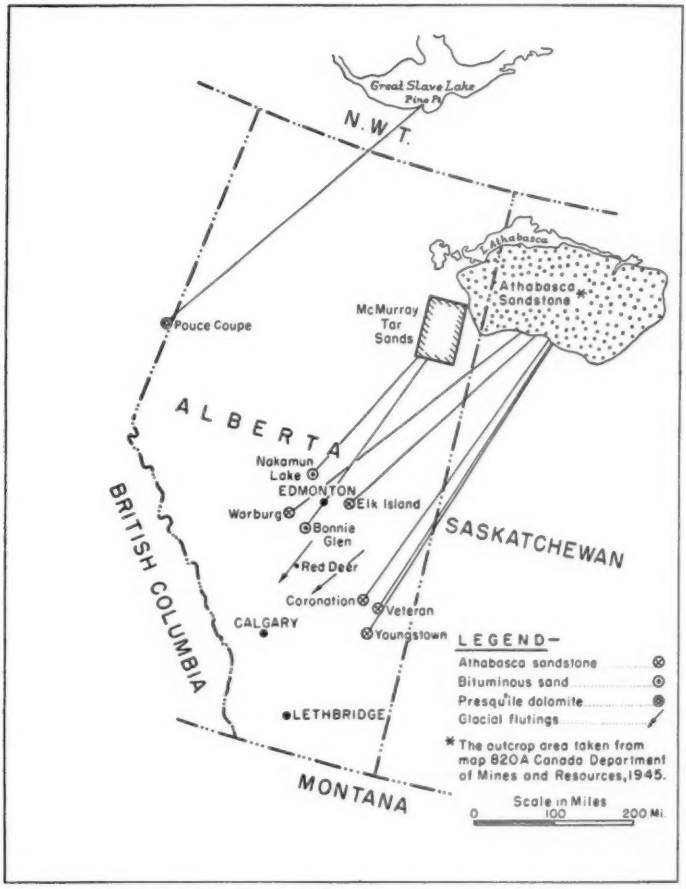

FIGURE 1.—LOCATION OF INDICATORS AND OUTCROP AREAS

from the indicator samples, and it was found that the heavy-mineral suites are essentially the same as those described from the Athabasca sandstone. The tourmalines found in the indicators are similar in color to those of the Athabasca sandstone, and in all cases they have overgrowths of clear tourmaline (Pl. 1). The macroscopic and microscopic similarities between the indicators and the Athabasca sandstone would seem to justify the conclusion that the indicators have been derived from the Athabasca sandstone.

PLATE 1.—TOURMALINE SHOWING OVERGROWTHS

FIGURE 1

From an Athabasca sandstone sample

FIGURE 2

From an indicator of Athabasca sandstone found at Warburg, Alberta

FIGURE 3

From an indicator of Athabasca sandstone found at Coronation, Alberta

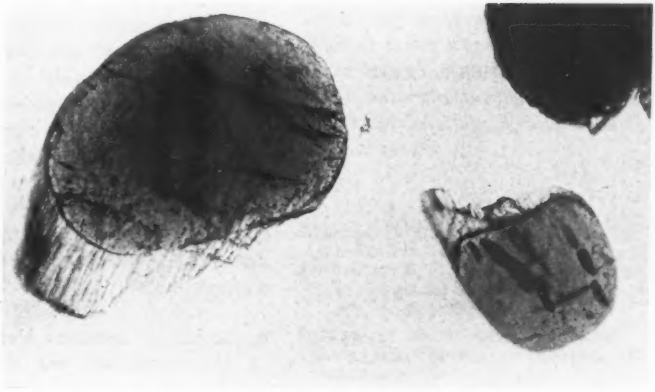

FIGURE 1

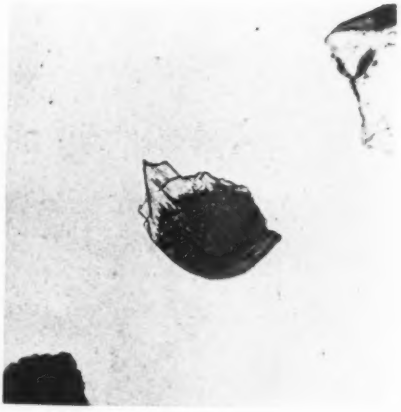

FIGURE 2

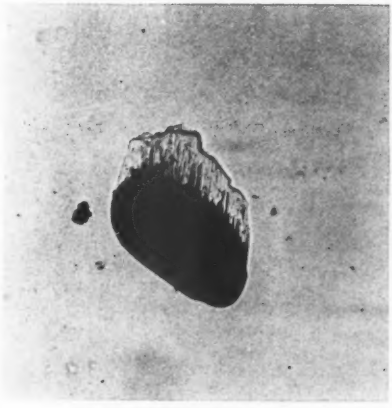

FIGURE 3

TOURMALINE SHOWING OVERGROWTHS

Conclusions

The three indicators—Athabasca sandstone, McMurray tar sand, and Presqu'ile domomite —all demonstrate that the ice-movement direction in central and northern Alberta was southwesterly. Lines drawn from the present location of the indicators to various parts of the original outcrop area give slightly different directions of ice movement; this is especially true of the Athabasca sandstone which has the largest outcrop area of any of the source rocks. In general, however, the ice direction was about S. 20°–35° W.

The writers draw attention to the use of heavy minerals in the identification of indicators. In many cases the more common rocks such as sandstones could be used as indicators if some peculiarity could be found by which they could be identified with certainty. While it is not suggested that an examination of the heavy minerals offers positive identification it nevertheless supports the identification and would certainly be valuable in the case of negative results.

References Cited

Krynine, P. D., 1946, The tourmaline group in sediments: Jour. Geology, v. 54, p. 65–87.

Rutherford, R. L., 1928, Two interesting boulders in the glacial deposits of Alberta: Jour. Geology, v. 36, p. 558–563.

University of Alberta, Edmonton, Alberta: Research Council of Alberta, Edmonton, Alberta

Manuscript Received by the Secretary of the Society, June 6, 1955